SELF-ASSEMBLY AND CHEMO-LIGATION STRATEGIES FOR POLYMERIC MULTI-RESPONSIVE MICROGELS

A Dissertation
Presented to
The Academic Faculty

by

Zhiyong Meng

In Partial Fulfillment
of the Requirements for the Degree
Doctor of Philosophy in the
School of Chemistry and Biochemistry

Georgia Institute of Technology
August 2009

SELF-ASSEMBLY AND CHEMO-LIGATION STRATEGIES FOR POLYMERIC MULTI-RESPONSIVE MICROGELS

Approved by:

Dr. L. Andrew Lyon, Advisor
School of Chemistry and Biochemistry
Georgia Institute of Technology

Dr. Victor Breedveld
School of Chemical and Biomolecular Engineering
Georgia Institute of Technology

Dr. Mohan Srinivasarao
School of Polymer, Textile, Fiber Engineering
Georgia Institute of Technology

Dr. Uwe Bunz
School of Chemistry and Biochemistry
Georgia Institute of Technology

Dr. David Collard
School of Chemistry and Biochemistry
Georgia Institute of Technology

Date Approved: June 11, 2009

Dedication to
My Wife and Daughter, My Parents and Brother

ACKNOWLEDGEMENTS

I would like to thank my advisor Professor Louis Andrew Lyon for his continuous support and encouragement during my research in his laboratory. Mentored by Professor Lyon, I could be able to view polymer science in a broader perspective. I could also independently develop my own ideas on research while getting suggestions from him. Furthermore, he also gave me constructive suggestions on my career development and family life. To me, Professor Lyon is not only an academic mentor, but also a friend in life.

I would also like to thank all members in the Lyon group: Dr. Ashlee St. John Iyer, Michael Smith, Grant Hendrickson, Toni South, Dr. Jongseong Kim, Dr. Bart Blackburn, Dr. Neetu Singh, Dr. Saetbyul Justin, Dr. Jonathan McGrath, and Dr. Courtney Sorrel. I further extend my thanks to Professor Victor Breedveld and Professor Mohan Srinivasarao for their great and stimulating suggestions on my research. Furthermore, I would like to thank Professor Nils Kröger, Dr. Robert Braga, and Dr. Leslie Gelbaum for granting me access to their Zetasizer, FTIR, and NMR facilities, respectively. I also thank Jae Kyu Cho, Qiang Luo, Kewei Xu, Yanfeng Chen, Yaru Shi, Xinming Qian, Honghui Lv, Chun Huang, Yanrong Shi, Xuan Zhang, Yadong Zhang, Rongwei Zhang, and Shaobo Pan for their friendship and help when I study in Georgia Institute of Technology.

Last but not lease, I would like to thank my parents, Zhaochen Meng, Shulian You, my brother, Zhiping Meng, my wife, Qing Ye, and my daughter, Haiyi Meng, for love and support they provided.

TABLE OF CONTENTS

LIST OF TABLES

Page

LIST OF FIGURES AND CHARTS

Page

LIST OF SCHEMES

LIST OF ABBREVIATIONS

AAc	Acrylic acid
AFM	Atomic force microscopy
AmF	5-Aminofluorescein
ATR	Attenuated total reflection
AzF	5-Azidofluorescein
AzHPMA	3-Azido-2-hydroxypropyl methacrylate
APS	Ammonium pefsulfate
BIS	*N,N'*-Methylene bisacrylamide
CTMRA	5/6-Carboxyl tetramethylrhodamine
DLS	Dynamic light scattering
DLVO	Dejaguin-Landau-Verwey-Overbeek
DVB	Divinyl benzene
DWS	Diffusing wave spectroscopy
EDC	1-[3-(Dimethylamino)propyl]-3-ethylcarbodiimide hydrochloride
EGDMA	Ethylene glycol dimethacrylate
EMCCD	Electron multiplying charge-coupled device
FCC	Face-centered-cubic
FITC	Fluorescein isothiocyanate
FPTU	Fluorescein propary thiourea
FTIR	Fourier-transform infrared
GMA	Glycidyl methacrylate
HCP	Hexagonal close packing

HEMA	Hydroxyethyl methacrylate
LbL	Layer-by-layer
LCST	Lower critical solution temperature
LDE	Laser Doppler electrophoresis
LYC	Lucifer yellow cadaverine
MMA	Methyl methacrylate
MAC	Magnitude cantilever excitation
MAAc	Methacrylic acid
MRJ	Maximally randomly jammed
MSD	Mean square displacement
NHS	*N*-Hydroxysuccinimide
NIPAm	*N*-Isopropylacrylamide
NMR	Nuclear magnetic resonance
NVP	*N*-Vinyl-2-pyrrolidone
PA	Propargyl acrylate
PALS	Phase analysis light scattering
PAm	Propargyl amine
PCS	Photon correlation spectroscopy
pAAc	Poly(acrylic acid)
PEG	Poly(ethylene glycol)
pHEMA	Poly(hydroxyethyl methacrylate)
pMAAc	Poly(methacrylic acid)
pNIPAm	Poly(*N*-isopropylacrylamide)
pNIPAm-AAc	Poly(*N*-isopropylacrylamide-*co*-acrylic acid)
pSt	Polystyrene

PTMRC	5/6-Propargyl tetramethylrhodamine carboxamide
RCF	Radical centrifugal force
RCP	Random close packing
SAM	Self-assembled monolayer
SANS	Small-angle neutron scattering
SDS	Sodium dodecyl sulfate
SGR	Soft glass rheology
St	Styrene
TMRC	Tetramethylrhodamine-5,6-carboxamide cadaverine
VA	Vinyl acetate
VIm	1-Vinylimidazole
VPT	Volume phase transition
VPTT	Volume phase transition temperature
VPy	4-Vinyl pyridine

LIST OF SYMBOLS

A	Measured baseline in DLS
β	Coherent factor of DLS detection
d	Dimensionality of space
D	Translational self-diffusion coefficient
$F(q,\tau)$	Dynamic structural factor
Φ	Volume fraction
G'	Storage modulus
G''	Loss modulus
$g(r)$	Radial distribution function
$G^{(2)}(\tau,\theta)$	Intensity-intensity autocorrelation function
$g^{(1)}(\tau,\theta)$	Electric field time correlation function
I	Scattered light intensity
k_B	Boltzmann constant
λ	Wavelength of irradiation
λ_0	Wavelength of irradiation in vacuum
η_s	Intrinsic viscosity of solvent
n	Refractive index
ppm	Part per million
q	Scattering vector
θ	Scattering angle
τ	Lag/relaxation time
σ	Hydrodynamic diameter

r	Center-to-center distance among nearest particles
R_h	Hydrodynamic radius
T	Absolute temperature
Γ	Relaxation rate
wt%	Weight percent
ζ	Zeta potential

SUMMARY

Microgels are sub-micron to micron-size polymeric particles swollen by a good solvent, sometimes also called hydrogel microparticles or microspheres if swollen in water. In contrast to the behavior of hard spheres, microgels behave more like soft spheres due to both steric repulsion of dangling chains tethered on their rough surface and electrostatic repulsion of charges, which could be compressed by imposing high concentration of microgels (osmotic deswelling) or higher ionic strength (compression of electric double layers). Among all microgels investigated nowadays, poly(*N*-alkylacrylamide), especially poly(*N*-isopropylacrylamide) (pNIPAm), microgels are one of the most extensively studied microgel particles due to their volume phase transition (VPT) at lower critical solution temperature (LCST). By incorporation of pH-responsive monomer, such as acrylic acid (AAc), copolymeric pNIPAm-AAc microgels further demonstrate multi-responsivity to temperature, pH, and ionic strength. A temperature-programmed polymerization protocol is proposed for the synthesis of large pNIPAm-AAc microgel particles with a hydrodynamic diameter of 2~5 μm. To observe the phase behavior of pNIPAm-AAc microgel dispersions, pNIPAm-AAc dispersion at various pH values and concentrations was allowed to age and undergo phase transition in closed system. Immediately after preparation of concentrated pNIPAm-AAc dispersions in closed system, the average hydrodynamic diameter is smaller than the unperturbed diameter due to osmotic deswelling effect. During the aging process, pNIPAm-AAc microgel particles swell while their dynamics slow down. (Sometimes the particle size in aged dispersions is even larger than the unperturbed size!) If the effective volume

fraction of pNIPAm-AAc microgel particles reaches a critical value (~40 %), the local and global crystallization of particles are observed. If the effective volume fraction of pNIPAm-AAc dispersions is beyond packing limit (~0.74), the compressed particles are observed in the crystalline and/or glassy phase, indicating the softness of pNIPAm-AAc microgels. The formation of crystalline phase should follow a nonergodic path in which microgel particles swell to the extent that they build up weak attractive interaction to allow them to associate while maintaining the opportunity of rearrangement to minimize local Gibbs free energy. The age-dependent thermostability of pNIPAm-AAc microgel dispersions suggests strong attractive interactions evolve between particles during crystallization. The attractive interactions are probably due to the multiple hydrogen bonding between amide and/or carboxylic acid groups on the dangling chains tethered on rough surfaces of pNIPAm-AAc microgel particles.

Finally, to introduce multiple biological "handle"s on the microgel particles for biomedical applications, the Cu(I)-catalyzed azide-terminal alkyne 1,3-dipolar cycloaddition, also called Sharpless-Meldal "click" reaction, is used to functionalize pNIPAm-AAc microgel particles. Glycidyl methacrylate (GMA) and propargyl acrylate (PA) are used to copolymerize with NIPAm and AAc to form multi-responsive microgels with "clickable" azido and acetylene groups respectively. "Clickable" fluorescent dyes are used to demonstrate the clickability of those microgels and epifluorescence microscopy is used to imaging the fluorescent particles after click reactions. Similarly, multi-functional thin films made of those clickable microgels could be fabricated via centrifugal deposition.

CHAPTER 1

MICROGELS: SYNTHESIS, SELF-ASSEMBLY, AND PHASE BEHAVIOR

The intention of this chapter is to introduce the preparation, self-assembly and phase behavior of stimuli-responsive microgel dispersions. First, the historical development of hydrogel (macrogel) and microgel materials will be briefly summarized. Furthermore, the advantages of stimuli-responsive microgels over their macroscopic counterpart in fundamental research and industrial applications will be demonstrated. Then the synthetic protocols of microgels, including (co)polymerization and cross-linking of reactive micelles, will be presented. "Clickable" stimuli-responsive microgels will also be introduced as a novel functionalization approach for biomedical applications. Finally, the physical aging and phase behavior of microgel dispersions will be briefly overviewed. Note that a myriad of studies related with microgels have been performed, so I will only cite the most important articles and reviews relevant to my research, which are biased by my perspective and by no means exhaustive and complete.

1.1 Hydrogels versus Microgels

1.1.1 Hydrogel and Stimuli-Responsive Hydrogels

Hydrogels are chemically or physically cross-linked organic or inorganic polymers which are capable of swelling in water while maintaining their integrity without dissolution in aqueous phase.[1] Physical cross-linking points are those non-covalently connected polymeric chains as a result of reversible sol-gel transition, such as physical entanglement, hydrogen bonding, hydrophobic interactions, coordination bonds, and electrostatic interactions.[2] Chemical cross-linking points are introduced via either cross-linker or chain transfer, which are covalent bifurcations connecting at least three

polymeric chains.[3] In addition, "sliding gel" offers another topology containing movable cross-linking points along the connected polymeric chains.[4,5]

In fact, the term "hydrogel" was introduced to describe water-borne inorganic polymers such as silica gel[6,7] and iron oxide gel.[8] In early 1960s, the first organic polymeric hydrogels, poly(hydroxyethyl methacrylate) (pHEMA),[9] were proposed by Wichterle[10] for biomaterial applications. Hydrogels based on pHEMA demonstrated supreme biocompatibility within the biological environment in that they meet the following criteria: desirable water content, inert to biological process, and permeable for metabolites.[10,11] Similarly, poly(vinyl alcohol) (pVA)[12] and poly(*N*-vinylpyrrolidone) (pNVP)[13] hydrogels were prepared as biomaterials as well. Many comprehensive reviews are available for synthesis and applications of polymeric hydrogels.[3,9,11,14-16] In addition to polymeric hydrogels, natural[1,17,18] and biohybrid[1,19] hydrogels were also developed for biomedical and pharmaceutical applications.[2,18,20] Although aforementioned hydrogels are biocompatible, most of them are not responsive to the milieu where they are applied.

The development of stimuli-reponsive polymer hydrogels, such as poly(acrylic acid) (pAAc),[21,22] poly(methacrylic acid) (pMAAc),[23,24] poly(*N*-isopropylacrylamide) (pNIPAm),[25,26] poly(ethylene oxide)-poly(propylene oxide)-poly(ethylene oxide) (poloxamer),[27] poly(ethylene oxide)-poly(L-lactic acid)-poly(ethylene oxide) (PEO-PLLA-PEO),[28] and poly(vinyl pyridine) (pVPy),[29] offers the pH- and thermo-responsivity, sometimes called "intelligence",[30] to polymeric hydrogels. However, the thermodynamic stimuli-responsivity of microgels can not be confused with human intelligence (the ability to learn or understand or to deal with new or trying situation, from "Merrian-Webster Online"). I therefore will only use "responsive", instead of "intelligent", microgels in this dissertation. The response mechanism is based upon the chemical structure of the polymeric network, especially the functional groups on the side chains. For ionic gels containing weakly acidic pendent groups, such as pAAc and pMAAc, polymeric network swell as the pH of the external solution increases due to the

electrostatic repulsive interaction between negative charges on side chains and the osmotic pressure increased within the networks as a result of deprotonation of acidic groups.[22] For temperature-responsive hydrogels, mostly based upon pNIPAm and its derivatives, they undergo a volume phase transition (collapse or shrinkage) when environment temperature is above their lower critical solution temperature (LCST) due to the broken hydrogen bonding between amide and structured water concurrent with the onset of hydrophobic interactions between pendent isopropyl groups.[31] Stimuli-responsive hydrogels have broad-spectrum applications in tissue engineering,[18,32-40] diagnosis,[41] drug delivery,[14,20,28,34,42,43] and biomaterials,[2,18,20,36,42,44] which has been extensively reviewed. Hydrogels are sometimes classified as "macrogels" if the solvent for swelling the polymer network is not emphasized.

1.1.2 Microgels and Stimuli-Responsive Microgels

When hydrogels are confined into a spherical space with a diameter ranging from 100 nm to 10 μm, those hydrogel particles are called microgels,[45-52] or μ-gels.[46] Microgels should be distinguished from dendrimers[53-55] and star polymers[56-58] because the size of cores of both dendrimers and star polymers is ignorable compared with that of microgel. Scheme 1.1 shows the topological difference between microgel, dendrimer and star polymer.

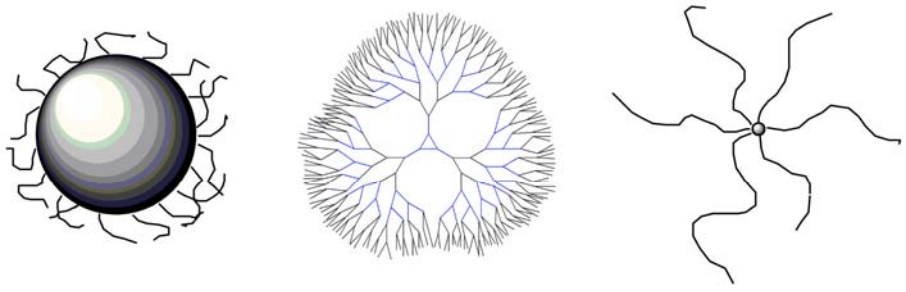

Scheme 1.1 Topological differences between microgel, dendrimer and star polymer.

Actually, microgels represent the structures intermediate between branched polymers and macroscopically cross-linked networks in that their overall dimensions are comparable with those of high-molecular-weight linear polymers with internal structures resembling typical networks.[46] Without cross-linking, polymeric chains in microgels would dissolve in solvent molecularly due to the dominance of polymer-solvent interaction over polymer-polymer interactions; microgels rely on the cross-linking to maintain their dimension stability and integrity.[48] Inside the microgel particles, polymeric chains are cross-linked chemically and/or physically, and microgels are swollen by water due to their hydrophilicity. However, the border between hydrogel and microgel is sometimes blurred because porous polymeric hydrogel is composed of microgels via interconnection or self-assembly.[59]

Historically, Elford first coined "microgel" for his membrane filtration study on Nitrocottons in 1930;[60] and Staudinger first synthesized microgels using styrene cross-linked by divinylbenzene in 1935.[61] The term "microgel" was initially inspected by Baker in 1949.[45] Furthermore, Shashoua classified microgels as the third topology of polymer chains, whereas the other two are linear and branched polymers.[62] Obviously, Shashoua missed macroscopically cross-linked gels in his classification of polymer topology.[63] Microgels are traditionally obtained by emulsion polymerization with micelles stabilized by emulsifiers as the loci of particle growth.[45,64-67] Polymeric microgels swollen by their corresponding monomers were also called latices.[68] However, in early 1970s, Dunn,[69] Kotera,[70] and Ottewill[71] suggested that hydrophobic monomers, i.e. vinyl acetate[69] and styrene,[70,71] could polymerize in water to form polymeric latices at elevated temperature without surfactant, which since then has been termed "surfactant-free emulsion polymerization".[68] The majority of microgel prepared before 1986 are hydrophobic microgels, such as polystyrene (pSt)[64,70,71] and poly(methyl methacrylate) (pMMA),[72] they are stabilized via surface charge or hydrophilic coating in aqueous phase.[68,70-72]

In 1986, hydrophilic thermoresponsive microgel composed of poly(*N*-isopropylacrylamide) (pNIPAm) was synthesized by Pelton via surfactant-free radical precipitation polymerization of NIPAm and cross-linker, *N,N'*-methylene bisacrylamide (BIS), in aqueous phase.[73] Because the polymerization temperature (~70 ºC) is much higher than the lower critical solution temperature of linear pNIPAm (~32 ºC), growing pNIPAm radicals would self-collapsed to form a globule as a precursor particle (precipitation) into which NIPAm monomers could be further incorporated.[51] Furthermore, residual sulfate groups from the decomposition of persulfate initiators are tethered on the surface of pNIPAm microgels, electrostatically stabilizing growing particles.[51,63] Note cross-linker is not required to form pNIPAm-based microgel particles. Due to the possible chain transfer from isopropyl or amide groups on NIPAm segments, the cross-linker-free pNIPAm-based microgels were also prepared by Frisken and co-workers,[74-76] and we will use those squishy particles for ultrathin films in Appendix C. The pNIPAm-based microgels are the most extensively explored examples of stimuli-responsive microgels because they have been prepared as bio/chemo-sensor,[41,77,78] drug delivery carriers,[79-81] and colloidal crystals.[82-86] The incorporation of charged monomers, such as acrylic acid (AAc),[87] methacrylic acid (MAAc),[88] imposes both pH- and ionic strength-responsivity to microgels. The chemical structures of NIPAm, AAc and BIS are shown in Scheme 1.2.

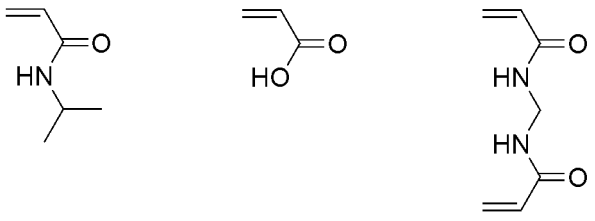

NIPAm AAc BIS

Scheme 1.2 The chemical structure of monomers NIPAm, AAc and cross-linker BIS.

As shown in Section 1.1.1, macroscopic hydrogels are useful as biomedical devices for drug delivery[2,14,16] and tissue engineering,[18] however, they are fairly difficult

to characterize using common techniques for linear polymers. The molecular weight of macroscopic hydrogels is not available, and therefore they are assumed an infinite molecular weight. Also, the macroscopic nature of networks renders the quantitative measurement of topological features of hydrogels notoriously difficult.[47] Limited by diffusion, the volume phase transition (VPT) of hydrogels is fairly slow.[88] In comparison with their macroscopic counterparts, stimuli-responsive microgels have definite size and molecular weight,[46,47,49,51,63] which are easily obtained by dynamic light scattering[47,89,90] and static light scattering,[47] respectively. Furthermore, the fast kinetics of volume phase transition of microgels enables them appropriate for fundamental studies[47,49] and biomedical applications.[88] Therefore, the preparation and phase behavior of stimuli-responsive microgel dispersions will be extensively discussed in this dissertation.

1.2 Synthesis and Modification of Microgels

1.2.1 Polymerization

Microgel particles are synthesized by either polymerization or cross-linking of reactive micelles.[46] The commonly adopted approach for microgel synthesis is (co)polymerization of vinyl monomers with cross-linker.[48,68] Polymeric microgels could be divided into two categories: hydrophobic microgels and hydrophilic microgels. As mentioned in Section 1.1.2, hydrophobic microgels, such as polybutadiene[45] and polystyrene[61] microgels, are earliest examples of microgels dispersed in organic solvent. The common monomers for hydrophobic microgels are butadiene,[45] styrene (St),[66,67,70,71,91,92] methylmethacrylate (MMA),[72,93,94] and vinyl acetate (VA),[69] whereas the common cross-linkers are divinyl benzene (DVB) [61,62,64] and ethylene glycol dimethacrylate (EGDMA).[93] The free-radical[66,71] and anionic[95] emulsion polymerization techniques were employed to prepare hydrophobic microgels in aqueous and organic medium, respectively. Due to the large difference between the refractive indices of

hydrophobic microgels and that of aqueous medium, van der Waals interactions between hydrophobic microgels are major driving force for the irreversible aggregation or coagulation of microgels, thereby reducing the yields. To enhance the colloidal stability and improve the yields, electrostatic[70,71] or steric[72] or electrosteric[96] stabilization due to surfactants and/or electric charges must be conferred to hydrophobic microgels. Hydrophobic microgels, or more traditionally latices, such as polystyrene[62] (pSt) latices, were therefore mostly obtained via emulsion polymerization in the presence of ionic surfactants. To improve the stability of latices, the polymerizable surfactant, such as sodium 9-acrylamidostearate, was introduced to immobilize surfactant on the surface of latices.[67] On the other hand, the surfactant-free emulsion polymerization was developed to maintain the colloidal stability of hydrophobic microgels while eliminating the troublesome removal of surfactant from latices after polymerization.[70,71] It is believed that surface-tethered sulfate anion (SO_4^-) from the decomposition of aqueous initiator, such as potassium persulfate (KPS) or ammonium persulfate (APS), stabilize hydrophobic latices electrostatically. For further details on the preparation and characterization of hydrophobic microgels, the readers are referred to these review articles.[48,49,63,68]

In contrast to hydrophobic microgels, hydrophilic microgels can stabilize themselves without external charge or agents due to steric stabilization from their dangling hydrophilic chains tethered on particle surface.[97] One of the most important hydrophilic microgels is thermoresponsive pNIPAm-based microgels.[31,49-51] Other common monomers for thermoresponsive microgel were summarized by Pelton.[51] It is well known that *N*-alkylacrylamide, especially *N*-isopropylacrylamide (NIPAm), could form thermoresponsive linear polymers,[98,99] which undergo a "coil-to-globule" transition at temperature higher than lower critical solution temperature (LCST) via expelling structured water molecules due to the dominance of polymer-polymer interaction (hydrophobic interaction) over polymer-water interaction (hydrogen bonding).[31] Inspired

by the collapse of pNIPAm chains at temperature higher than their LCST as nuclei for microgel growth, Pelton et al. used NIPAm as monomer to synthesize spherical hydrophilic thermoresponsive pNIPAm microgels.[73] The mechanism for the preparation of pNIPAm-based microgels via persulfate-initiated surfactant-free radical precipitation polymerization is shown in Scheme 1.3.

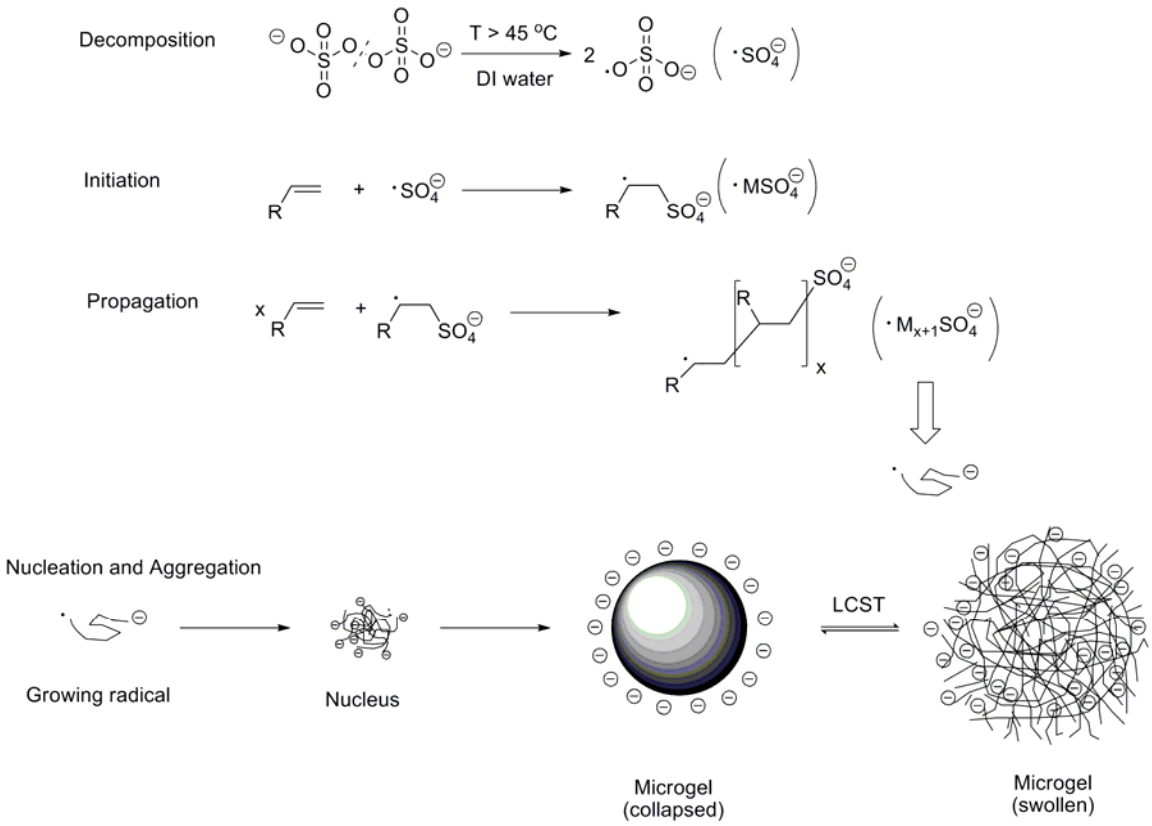

Scheme 1.3 Mechanism for the preparation of pNIPAm-based microgels via the surfactant-free radical precipitation polymerization. Note: 1. For the convenience, only head-to-tail addition is assumed in the scheme, however, head-to-head and tail-to-tail addition can not be excluded in principle. 2. Cross-linkers are not shown in the scheme, however, cross-linkers are incorporated in the pNIPAm chains to form branched polymers since initiation stage. 3. As shown in the text, at elevated polymerization temperature, most of tangling pNIPAm chains collapse onto the pNIPAm particle surface, only negative charges on surface-tethered sulfate groups decomposed from persulfate stabilize particles from further aggregation.[71,100] Whereas temperature cross-over the LCST, microgels become swollen stabilized via electrosteric mechanism.[51]

In addition to thermoresponsivity, pH- and ionic strength-responsivity could be introduced to microgel systems via copolymerization of NIPAm with acidic or basic

monomers. Thus the surfactant-free radical copolymerization of NIPAm with functional monomers, such as acrylic acid (AAc),[87,90,101-103] methacrylic acid (MAAc),[88,104-106] glycidyl methacrylate (GMA),[107-110] and 4-vinylpyridine (VPy),[111,112] in aqueous phase were used to form functional microgels.[50,73,87,88,97,101,113] If polymerized in aqueous phase, the multi-vinyl cross-linkers, such as *N,N'*-methylene bisacrylamide[62,73] (BIS) and ethylene glycol dimethacrylate (EGDMA),[93] were used to create network structure whereas ionic surfactants, such as sodium dodecyl sulfate (SDS),[62] are sometimes used for the stabilization of microgels and size control.[114-116] In this dissertation, one-pot surfactant-free radical precipitation copolymerization of NIPAm and AAc at fixed or ramped temperature will be presented and discussed in Chapter 2 and 3, respectively. We have noticed that the polymerization temperature played a crucial role in the determination of particle size if other parameters, such as NIPAm/AAc/BIS/APS ratio and total monomer concentration, are fixed. The increase of synthesis temperature leads to the decrease of the size of pNIPAm-AAc microgels with higher yields, which agrees well with the literature.[71,100]

In addition to one-pot copolymerization, microgels with "core-shell"[90,117,118] topology were also prepared via two-step "seed-feed" polymerization.[90] Almost all kinds of functional groups could be incorporated into microgel particles by one-pot copolymerization, two-step "seed-feed" polymerization, and post-functionalization.[50] For instance, the copolymerizations of NIPAm with other functional monomers were developed to incorporate biomolecule-reponsivity to microgel particles.[41,78,119,120] In addition to random copolymeric microgel particles, microgels with controlled spatial distribution of functionalities were prepared as Janus particles[121] via either microfluics[122] or Pickering emulsion[123] techniques. Furthermore, "patchy" particles was proposed as a model for precise spatial control of functionalities on microgels.[124] The hybridization of microgel particles with metal nanoparticles,[125] metal oxide,[126] metal sulfide,[127] and semiconductors[127] were performed for the application of microgels in diagnostics,

imaging and microreactors.[127] As for copolymerization and hybridization, readers are referred to Chapter 2, Section 2.1 for more details.

1.2.2 Cross-Linking of Reactive Micelles

In addition to (co)polymerization approach, cross-linking of reactive micelles in nano-/micro-meter size range could also give rise to microgels. Core cross-linked star (CCS) microgels[128,129] are one type of these microgels. Their rheological properties could be adjusted by tuning the softness, i.e. the arm number and length of CCS microgels.[130] Shell cross-linked microgels[131] are the other type of these microgels. Both core and shell cross-linked microgels could be obtained by cross-linking micelles formed by self-assembly of diblock copolymers,[132,133] such as polystyrene-b-poly(4-vinylpyridine) (PSt-b-PVP)[134] and polyethyleneoxide-b-polybutadine.[132] Various cross-linking techniques were reviewed, including photo-cross-linking,[134] chemical coupling,[135] polyelectrolyte complexation.[131]

1.2.3 "Clickable" Microgels

As shown in previous sections, the functionalization of pNIPAm-based microgels has several available routes, such as one-pot[73,87] or two-step "seed-feed"[90] copolymerization of monomers with functional groups and post-modification of microgels via functional transformation.[78,119] The important aim for functionalization is to add stimuli-responsivity to pNIPAm-based microgels.[87,88] For instance, the copolymerization of AAc,[87] MAAc,[88] 4-vinylpyridine (VPy)[111,112] with NIPAm adds both pH- and ionic strength- responsivity to microgels, as we already discussed. Furthermore, the stimuli-responsivity[87,89,113] and drug loading capability[136] enables pNIPAm-based microgels an appropriate candidate as targeted drug delivery vehicle[79,137-139] if microgels are equipped with ligands such as folate[79] to locate and bind tumor cells and with poly(ethylene glycol) (PEG) to suppress non-specific protein binding (non-fouling).[140-143]

Importantly, targeted drug delivery vehicles can often require the presence of multiple different chemical handles for the immobilization of both therapeutic drugs and targeting biomolecules.[80,138] However, the synthesis of such vehicles can be compromised when the targeting moieties possess functionalities that are cross-reactive or do not permit controlled, high-yield coupling to the microgel carrier. To circumvent this problem, the chemical handles should possess chemical orthogonality: not only be chemically inert to common functionalities and reactions in biological environments, but also react rapidly with complementary functionalities under ambient conditions and in aqueous media without interference from other functional groups. Bioorthogonal "click" reactions,[144,145] especially Cu(I)-catalyzed azide-terminal alkyne 1,3-dipolar cycloadditions,[146-148] meet the above criteria and therefore represent a good choice for functionalization of microgel particles.

"Click chemistry", a modular reaction performed in benign solvent (water) with high yields and tolerance to O_2 and H_2O, and yielding easily isolated product with no or inoffensive byproduct, was first proposed by Sharpless et al. in 2001.[145] All available "click" reactions are summarized by Sharpless et al.,[148] of which the most extensively investigated reaction is Cu(I)-catalyzed azide-terminal alkyne 1,3-dipolar Huisgen cycloaddition discovered by Sharpless and Meldal independently in 2002,[146,147] yielding 1,4-disubstituted 1,2,3-triazole. The original version of azide-alkyne 1,3-dipolar Huisgen cycloaddition was performed at elevated temperature with slow kinetics and 1,4- and 1,5-adduct,[149] whereas the Cu(I)-catalyzed "click" version of Huisgen cycloaddition gives rise to stereospecific 1,4-adduct at room temperature with fast kinetics.[146] In fact, water is employed as the solvent for click chemistry not only for environmental friendliness but also because water is the best heat-tank for handling enormous heat output by click reaction especially in large scale.[148] Yet another benefit of water is that water prevents interference from protic functional groups, like hydroxyl, amino, carboxy groups, which are ubiquitous in biomolecules.[148] Furthermore, thermodynamic reactivity and kinetic

stability of azide and terminal alkyne afford the unique orthogonality of Cu(I)-catalyzed 1,3-dipolar cycloaddition to most functional groups.[150] For instance, azides and alkynes are essentially inert to most biological and organic conditions, including highly functionalized biological molecules, molecular oxygen, water, and the majority of common reaction conditions in organic synthesis.[148,150] Finally, the key difference between original Huisgen version and Sharpless-Meldal variant of 1,3-dipolar cycloaddition (click reaction) is the introduction of Cu(I) as catalyst in click chemistry. In contrast to the concerted mechanism in Huisgen thermal 1,3-dipolar cycloaddition, Sharpless-Meldal Cu(I)-catalyzed 1,3-dipolar cycloaddition is supposed to follow a stepwise mechanism shown in Scheme 1.4.[146,150]

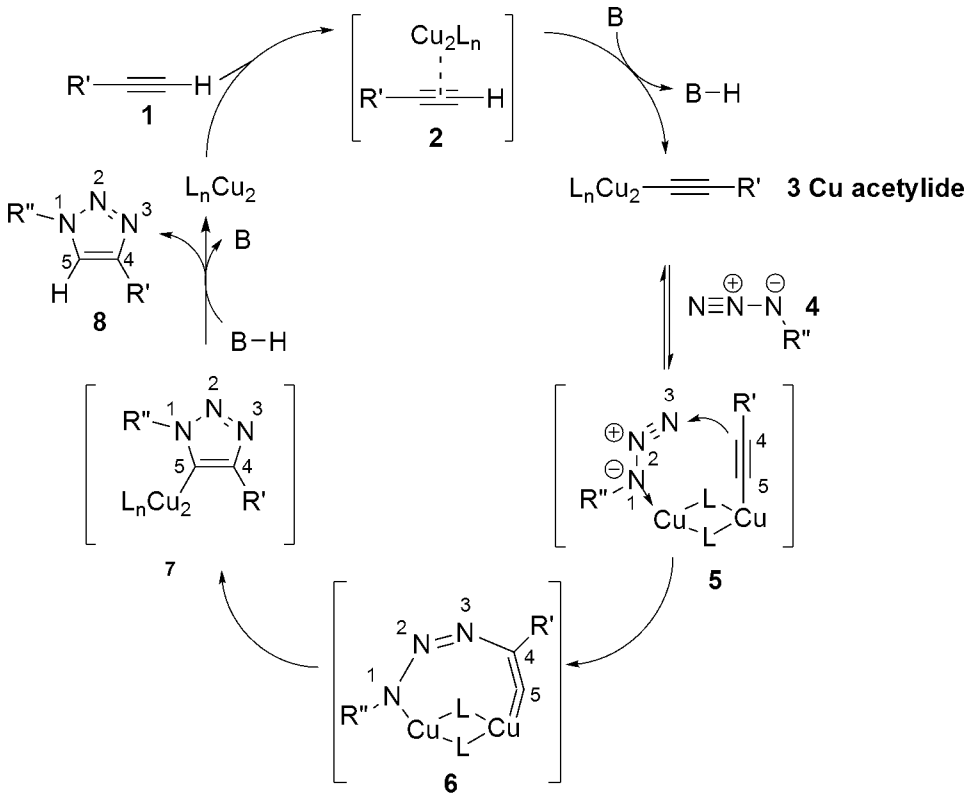

Scheme 1.4 Proposed mechanism of Cu(I)-catalyzed azide-terminal alkyne 1,3-dipolar cycloaddition. The stepwise catalytic cycle start from the formation of Cu(I)-acetylide **3** via a π complex **2** from the addition of Cu(I) catalyst on terminal alkyne **1**. Following the formation of the active copper acetylide species **3**, azide displacement of one ligand generates a copper acetylide-azide complex, such as the dicopper species **5.**

Complexation of the azide activates it toward nucleophilic attack of acetylide carbon C(4) at N(3) of the azide (numbers based on traditional triazole nomenclature), generating metallocycle **6**. This metallocycle **6** positions the bound azide properly for subsequent ring contraction by a transannular association of the N(1) lone pair of electrons with the C(5)–Cu π* orbital to form triazole copper derivative **7**. Protonation of triazole-copper derivative **7** followed by dissociation of the product **8** ends the reaction and regenerates the Cu(I) catalyst. Note B in the above mechanistic diagram denotes some sorts of base in reaction mixture.

Inspired by the bioorthogonality and biocompatibility of "click chemistry", many investigators have tried to prepare "clickable" particles via either one-pot copolymerization[151] or post-modification[152,153] of particles for fundamental studies. Click reactions has also been executed on the microgel particles[151,152,154-157] and biological nanoparticles.[158,159] However, none of those clickable particles are pNIPAm-based microgels, and none of those synthetic protocols could yield azido-containing particles in one-pot approach. In this dissertation, a one-pot multi-feed synthesis for azido- or alkynyl-containing pNIPAm-based microgels and the click reaction between microgels and fluorophores with complementary functionalities will be presented in Chapter 6.

1.3 Aging and Phase Behavior of Microgel Assemblies

1.3.1 Self-Assembly of Microgels

The self- or directed-assembly of microgels have been extensively reviewed.[160-167] Self-assembly[168] is the thermodynamically controlled association of entities at all length scales,[169] from small molecules[170] to polymers[171] and nanoparticles,[172,173] into structurally well-defined, stable aggregates through non-covalent interactions, including van der Waals interactions,[174] π–π stacking,[175] electrostatics,[176] metal coordination,[177] hydrophobic interactions,[178] and hydrogen bonding.[179] Microgels could self-assemble to form wires, [123] sheets, [180,181] and lattices[167,182,183] in one-, two-, and three-dimensional space, respectively. For instance, Janus microgel particles could form short wires via electrostatic interactions.[123] Microgel thin films could be obtained by layer-by-layer (LbL)

adsorption of microgels and/or linear polymers on the substrate.[162,167,182] In addition to colloidosomes,[184,185] microgels could self-assemble into colloidal crystals in 2-D[77] and 3-D space.[186,187] Asher et al. used pNIPAm colloidal crystals embedded in bulk hydrogels for optical switching.[186] Richtering et al. prepared pNIPAm-AAc microgel colloidal crystals and used shift factor to estimate the effective volume fractions at freezing and melting point of microgel dispersions.[83] Hellweg[84] and Hu[188] have shown that pNIPAm microgels could crystallize at appropriate volume fractions. Lyon[82,85,86,189-191] et al. have shown that pNIPAm-based microgels could self-assembled into colloidal crystals at appropriate pH and volume fractions. All the above mentioned work laid out a solid base for the investigation I conducted in my dissertation. The pNIPAm-AAc microgel dispersions are allowed to self-assemble in a closed 3D space to form colloidal crystals,[86] in which self-assembly is not only a thermodynamic phase behavior but also a kinetic process dictated by aging phenomena.[192]

1.3.2 Aging of Microgel Dispersions

Physical aging is a continuous dynamic evolution process wherein the rheological and mechanical properties of nonergodic disordered systems, i.e. glasses and polymers, change with time.[193] Thus, response functions that characterize equilibrium properties behave in an unusual manner. If the response functions are measured over a short period of time they sample the quasi-equilibrium properties over the measurement period; however, they can vary substantially if measured at a series of different periods of time, as the material will relax or age to a new metastable state.[194]

As for spherical particles, Grier et al. examined the impact of gravity on the aging of colloidal suspensions and spontaneous stratification after aging.[195] To eliminate the effect of gravity, Cipelletti et al. use multi-speckle dynamic light scattering to measure the dynamic structure factors $F(q,\tau)$[196] of colloidal fractal gels formed by aggregation of polystyrene (pSt) spheres suspended in a buoyancy-matching mixture with volume

fractions $10^{-4} < \Phi < 10^{-3}$. Along with aging, Cipelletti et al. found that a complete decay of $F(q,\tau)$ and a 2-order increase of the characteristic relaxation time τ, indicating a colloidal synerisis due to strong van der Waals attraction on pSt colloids. Furthermore, Schurtenberger et al. used diffusing-wave spectroscopy (DWS)[197] to investigate the sol-gel transition of concentrated suspensions of pSt spheres in buoyancy-matching mixture, and noticed that a dramatic change of the particle dynamics from a diffusion to subdiffusion arrested mode at the gel point.[198] The physical origin of these aging behaviors is that the relaxation rate decreases with the age of the sample, and thus the time scale of the relaxation is itself a function of the age.[199]

In addition to spherical particles, discoid particles such as laponite were used as models for studying the aging of colloidal glasses and gels. Bonn et al. used rheology to monitor the aging-induced transition from colloidal fluid to colloidal "Wigner" glass of highly charged laponite particles at very low volume fractions in ultrapure water.[200] Bonn et al. noticed that the storage modulus *G'* is lower than loss modulus *G"* immediately after sample preparation, indicating a diffusive fluid-like behavior; but with aging over hours, $G' >> G"$, showing a viscoelastic solid behavior. Furthermore, they use multi-speckle diffusing wave spectroscopy (DWS) to observe the decay of autocorrelation function $G^{(2)}(q,\tau)$, the first decay corresponding to the fast diffusion within the cage formed by surrounding particles (fast β-relaxation) whereas the second decay indicating the escape from the cage (α-relaxation). Knaebel and Abou[199,201] studied more concentrated laponite suspensions and find similar aging behavior in colloidal glasses.

In contrast to spherical hard particles, microgel dispersions, such as pMAAc and pNIPAm particles, can be fluid-like immediate after preparation even at very high volume factions due to osmotic de-swelling.[192] Cloitre et al. have studied the rheological behavior of concentrated poly(methacrylic acid) (pMAAc) microgel dispersions at different ages below the yield point. The concentrated polyelectrolyte microgel dispersions show history-dependent strain recovery, indicating aging occurs due to the

frustration and cooperative relaxation of steric constraints between interlocked neighboring particles.[202] Furthermore, van den Ende et al. investigated the aging phenomena of pNIPAm microgel dispersions,[203] and they found that the linear viscoelasticity of microgel colloids could be fitted by soft glass rheology (SGR)[204] model quantitatively.[205] Also, van den Ende et al. confirmed that the glass transition for microgel dispersions approach hard sphere limit, $\Phi_G \sim 0.58$, as particles get harder.[206] In addition to rheology and dynamic light scattering techniques, Maske et al. used video microscopy to investigate the aging temperature in colloidal glass.[207] Because of the larger microgel particle size (~1.5 μm) and advantages of real-time observation of microgel dynamics, we have used video microscopy to observe the evolution of concentrated pNIPAm-AAc microgel dispersions instead of using mechanical perturbation. It is noticed that pNIPAm-AAc particles deswell upon preparation freshly due to osmotic deswelling effect.[208-211] However, along with aging of microgel dispersions, pNIPAm-AAc microgels slowly swell and self-assembled into crystalline phase.[86,192]

1.3.3 Phase Behavior of Microgel Dispersions

The phase behavior of colloidal dispersions have been extensively investigated and reviewed.[83,86,192,196,212-217] The spherical colloidal particles could be categorized to several types: hard spheres, soft spheres, hard sticky spheres and soft sticky spheres. The simplest colloidal system contains only one component, which is hard-sphere dispersion in liquid media. Hoover and Ree theoretically determined the freezing and melting points of hard-sphere dispersions by equating the free energy of the fluid phase and that of the solid phase via Monte Carlo approaches.[218] At freezing the volume fractions of the co-existing fluid and solid phases were found to be $\Phi_F = 0.494 \pm 0.002$, whereas at melting the volume fractions of the co-existing fluid and solid phases were found to be $\Phi_M = 0.545 \pm 0.002$. Furthermore, Finney indicated that a more appropriate glass transition

point would be the volume fraction of random close packing (RCP), $\Phi_{RCP} = 0.637 \pm 0.001$.[219-221] Recently, Torquato argued that maximally random jammed (MRJ) state is a more mathematically precise definition for random close packing, with a corresponding volume fraction of $\Phi_{MRJ} \approx 0.64$.[222] All the above packing volume fractions should be lower than the volume fractions of closest packing, i.e. face-centered-cubic (FCC) packing or hexagonal-cubic packing (HCP), with a volume fraction of $\Phi_{FCC} = \Phi_{HCP} = 0.7405$ ($\pi/\sqrt{18}$). Along with the theoretical investigation, experimental studies were also conducted on hard-sphere model. Pusey and van Megen used poly(12-hydroxystearic acid) (pHSA)-stabilized poly(methyl methacrylate) (pMMA) colloidal particles in decalin-CS_2 mixture solvent to form a refractive index-matching dispersions for the systematic study of their phase behavior, and found that the freezing, melting and glass transition are all in reasonably good agreement with the theoretical predictions.[223] Soft spheres are regarded as spheres with long-range interactions; their phase behavior is dependent upon the interaction function form. For instance, for inverse power potential, the phase diagram was illustrated by Hoover,[224] whereas for star polymers, the phase diagram was much more complicated.[212] By adding free non-adsorbing polymers, short-range depletion interactions are introduced into colloidal particles, which was sometimes termed "stickiness".[225-229] The phase behavior of colloidal dispersions have been extensively studied and reviewed.[196,213,230-234] The canonical volume fraction for crystallization and glass transition will be compared with our effective volume fraction of pNIPAm-AAc microgels in phase behavior studies in this dissertation.[192]

Microgels, as convenient model for soft spheres, can not only adapt their interaction potential but also change their size by tuning the number density of microgels in dispersion due to osmotic deswelling.[209] Furthermore, with the inherent thermoresponsivity, pNIPAm-based microgels could change their size by tuning temperature without changing number density.[190,214,217] Richtering first reported the phase behavior of pNIPAm microgel dispersions, where he used rheological measurement to

determine the phase behavior of microgel dispersions and found that, by using shift factor deducted from Batchelor variation of Einstein equation,[235] crystallization start at $\Phi_{eff,F} \approx$ 0.59 and melting start at $\Phi_{eff,M} \approx 0.61$. The much higher crystallization volume fraction indicates the softness, or the deswellability of microgels.[83] Furthermore, the phase studies were actually focused on the crystallization of microgel particles under specific conditions. Hellweg used small-angle neutron scattering (SANS) and video microscopy to observe the colloidal crystals of pNIPAm microgels, giving a melting temperature for pNIPAm crystal at ~26 ºC.[84] Wu and Hu illustrate the correlation between the interaction potential and phase behavior of pNIPAm microgels.[214,215] Lyon group start to focus on the crystallization of pNIPAm-based microgels in 2000, originally using pNIPAm colloidal crystal as a potential candidate of photonic crystal.[82,85] After that, Lyon group pay much more attention on the thermodynamic and dynamic mechanism for the colloidal crystallization of pNIPAm-based microgels in closed system. We have investigated the role of volume fraction, obtained from shift factor via rheological studies, on the crystallization and melting of pNIPAm[217] or pNIPAm-AAc[190] colloidal crystals. Furthermore, we start to test the pH-responsivity of pNIPAm-AAc colloidal crystallization.[86] In addition to crystallization, we have also observe the heat-induced melting of colloidal crystals. In contrast to the melting of pNIPAm colloidal crystals at 26 ºC[215,217] (lower than VPTT of pNIPAm microgels), pNIPAm-AAc colloidal crystals show an unusual thermostability up to 40 ºC[86] (higher than VPTT of pNIPAm-AAc microgels), which provide an indirect evidence for the net attractive interaction evolved during the aging-convoluted crystallization process.[192] Finally, we expand the pH from 3.0 up to 6.0 and obtained the whole phase diagram of pNIPAm-AAc microgel dispersions, which definitely cover both crystallization and glass transition.[192]

REFERENCES

(1) Peppas, N. A.; Hilt, J. Z.; Khademhosseini, A.; Langer, R. Hydrogels in biology and medicine: From molecular principles to bionanotechnology, *Adv. Mater* **2006**, *18*, 1345-1360.

(2) Hoffman, A. S. Hydrogels for biomedical applications, *Adv. Drug Deliv. Rev.* **2002**, *54*, 3-12.

(3) Roorda, W. E.; Bodde, H. E.; Deboer, A. G.; Junginger, H. E. Synthetic hydrogels as drug delivery systems, *Pharm. Weekbl. Sci. Ed.* **1986**, *8*, 165-189.

(4) de Gennes, P. G. Sliding gels, *Physica A* **1999**, *271*, 231-237.

(5) Okumura, Y.; Ito, K. The polyrotaxane gel: A topological gel by figure-of-eight cross-links, *Adv. Mater.* **2001**, *13*, 485-487.

(6) van Bemmelen, J. M. Die absorption. 7. Abhandlung: Die einwirkung von höheren temperaturen auf das gewebe des hydrogels der kieselsäure, *Z. Anorg. Chem.* **1902**, *30*, 265-279.

(7) Foote, H. W.; Saxton, B. The effect of freezing on certain inorganic hydrogels, *J. Am. Chem. Soc.* **1916**, *38*, 588-609.

(8) Otto, R. Über das eisenoxyd und seine hydrate, *Ber. Dtsch. Chem. Ges.* **1901**, *34*, 3417-3430.

(9) Montheard, J. P.; Chatzopoulos, M.; Chappard, D. 2-Hydroxyethyl methacrylate (HEMA): Chemical properties and applictions in biomedical fields, *J. Macromol. Sci. Rev. Macromol. Chem. Phys.* **1992**, *C32*, 1-34.

(10) Wichterle, O.; Lim, D. Hydrophilic gels for biological use, *Nature* **1960**, *185*, 117-118.

(11) Ratner, B. D.; Hoffman, A. S. *Synthetic hydrogels for biomedical applications*; In *Hydrogels for Medical and Related Applications : A Symposium*; Andrade, J. D., Ed.; American Chemical Society: Washington, DC, 1976, p 1-36.

(12) Bray, J. C.; Merrill, E. W. Poly(vinyl alchohol) hydrogels for synthetic articular-cartilage material, *J. Biomed. Mater. Res.* **1973**, *7*, 431-443.

(13) Davis, T. P.; Huglin, M. B.; Yip, D. C. F. Properties of poly(*N*-vinyl-2-pyrrolidone) hydrogels crosslinked with ethyleneglycol dimethacryalte, *Polymer* **1988**, *29*, 701-706.

(14) Kim, S. W.; Bae, Y. H.; Okano, T. Hydrogels: Swelling, drug loading, and release, *Pharm. Res.* **1992**, *9*, 283-290.

(15) Kim, S. W. Hydrogels as drug delivery systems, *Pharm. Int.* **1983**, *4*, 90-91.

(16) Corkhill, P. H.; Hamilton, C. J.; Tighe, B. J. The design of hydrogels for medical applications, *Crit. Rev. Biocompat.* **1990**, *5*, 363-436.

(17) Amiya, T.; Tanaka, T. Phase transitions in cross-linked gels of natural polymers, *Macromolecules* **1987**, *20*, 1162-1164.

(18) Lee, K. Y.; Mooney, D. J. Hydrogels for tissue engineering, *Chem. Rev.* **2001**, *101*, 1869-1879.

(19) Ruel-Gariepy, E.; Leroux, J. C. In situ-forming hydrogels - review of temperature-sensitive systems, *Eur. J. Pharm. Biopharm.* **2004**, *58*, 409-426.

(20) Peppas, N. A.; Bures, P.; Leobandung, W.; Ichikawa, H. Hydrogels in pharmaceutical formulations, *Eur. J. Pharm. Biopharm.* **2000**, *50*, 27-46.

(21) Park, H.; Robinson, J. R. Mechanisms of mucoadhesion of poly(acrylic acid) hydrogels, *Pharm. Res.* **1987**, *4*, 457-464.

(22) Gil, E. S.; Hudson, S. A. Stimuli-reponsive polymers and their bioconjugates, *Prog. Polym. Sci.* **2004**, *29*, 1173-1222.

(23) Brazel, C. S.; Peppas, N. A. Synthesis and characterization of thermo- and chemomechanically responsive ooly(N-isopropylacrylamide-co-methacrylic acid) hydrogels, *Macromolecules* **1995**, *28*, 8016-8020.

(24) Zhang, J.; Peppas, N. A. Synthesis and characterization of pH- and temperature-sensitive poly(methacrylic acid)/poly(N-isopropylacrylamide) interpenetrating polymeric networks, *Macromolecules* **2000**, *33*, 102-107.

(25) Dong, L. C.; Hoffman, A. S. *Thermally reversible hydrogels: Swelling characteristics and activities of copoly(N-isopropylacrylamide-acrylamide) gels containing immobilized asparaginase*; In *Reversible Polymeric Gels And Related Systems*; Russo, P. S., Ed.; American Chemical Society: Washington, D.C. , 1987; Vol. 350, p 236-244.

(26) Beltran, S.; Baker, J. P.; Hooper, H. H.; Blanch, H. W.; Prausnitz, J. M. Swelling equilibria for weakly ionizable, temperature-sensitive hydrogels, *Macromolecules* **1991**, *24*, 549-551.

(27) Malmsten, M.; Lindman, B. Self-assembly in aqueous block copolymer solutions, *Macromolecules* **1992**, *25*, 5440-5445.

(28) Jeong, B.; Bae, Y. H.; Lee, D. S.; Kim, S. W. Biodegradable block copolymers as injectable drug-delivery systems, *Nature* **1997**, *388*, 860-862.

(29) Li, J.; Khan, I. M. Highly conductive solid polymer electrolytes prepared by blending high-molecular-weight poly(ethylene oxide), poly(2-vinylpyridine or 4-vinylpyridine), and lithium perchlorate, *Macromolecules* **1993**, *26*, 4544-4550.

(30) Chen, G. H.; Hoffman, A. S. Graft-copolymers that exhibit temperature-induced phase-transitions over a wide-range of pH, *Nature* **1995**, *373*, 49-52.

(31) Schild, H. G. Poly(*N*-isopropylacrylamide): Experiment, theory and application, *Prog. Polym. Sci.* **1992**, *17*, 163-249.

(32) Drury, J. L.; Mooney, D. J. Hydrogels for tissue engineering: scaffold design variables and applications, *Biomaterials* **2003**, *24*, 4337-4351.

(33) Varghese, S.; Elisseeff, J. H. *Hydrogels for musculoskeletal tissue engineering*; In *Polymers for Regenerative Medicine*; Springer-Verlag Berlin: Berlin, 2006, p 95-144.

(34) Barcili, B. Hydrogels for tissue engineering and delivery of tissue-inducing substances, *J. Pharm. Sci.* **2007**, *96*, 2197-2223.

(35) Brandl, F.; Sommer, F.; Goepferich, A. Rational design of hydrogels for tissue engineering: Impact of physical factors on cell behavior, *Biomaterials* **2007**, *28*, 134-146.

(36) Fedorovich, N. E.; Alblas, J.; de Wijn, J. R.; Hennink, W. E.; Verbout, A. J.; Dhert, W. J. A. Hydrogels as extracellular matrices for skeletal tissue engineering: state-of-the-art and novel application in organ printing, *Tissue Eng.* **2007**, *13*, 1905-1925.

(37) Nicodemus, G. D.; Bryant, S. J. Cell encapsulation in biodegradable hydrogels for tissue engineering applications, *Tissue Eng. B Rev.* **2008**, *14*, 149-165.

(38) Nisbet, D. R.; Crompton, K. E.; Horne, M. K.; Finkelstein, D. I.; Forsythe, J. S. Neural tissue engineering of the CNS using hydrogels, *J. Biomed. Mater. Res. B* **2008**, *87*, 251-263.

(39) Nuttelman, C. R.; Rice, M. A.; Rydholm, A. E.; Salinas, C. N.; Shah, D. N.; Anseth, K. S. Macromolecular monomers for the synthesis of hydrogel niches and their application in cell encapsulation and tissue engineering, *Prog. Polym. Sci.* **2008**, *33*, 167-179.

(40) Jia, X. Q.; Kiick, K. L. Hybrid Multicomponent Hydrogels for Tissue Engineering, *Macromol. Biosci.* **2009**, *9*, 140-156.

(41) Ulijn, R. V.; Bibi, N.; Jayawarna, V.; Thornton, P. D.; Todd, S. J.; Mart, R. J.; Smith, A. M.; Gough, J. E. Bioresponsive hydrogels, *Mater. Today* **2007**, *10*, 40-48.

(42) Bromberg, L. E.; Ron, E. S. Temperature-responsive gels and thermogelling polymer matrices for protein and peptide delivery, *Adv. Drug Deliv. Rev.* **1998**, *31*, 197-221.

(43) Qiu, Y.; Park, K. Environment-sensitive hydrogels for drug delivery, *Adv. Drug Deliv. Rev.* **2001**, *53*, 321-339.

(44) Jeong, B.; Kim, S. W.; Bae, Y. H. Thermosensitive sol-gel reversible hydrogels, *Adv. Drug Deliv. Rev.* **2002**, *54*, 37-51.

(45) Baker, W. O. Microgel, a new macromolecule: Relation to sol and gel as structural elements of synthetic rubber, *Ind. Eng. Chem.* **1949**, *41*, 511-520.

(46) Antonietti, M. Microgels - Polymers with a special molecular architecture, *Angew. Chem. Int. Ed. Engl.* **1988**, *27*, 1743-1747.

(47) Antonietti, M.; Bremser, W.; Schmidt, M. Microgels: model polymers for the crosslinked state, *Macromolecules* **1990**, *23*, 3796-3805.

(48) Funke, W.; Okay, O.; Joos-Muller, B. Microgels - Intramolecularly crosslinked macromolecules with a globular structure, *Adv. Polym. Sci.* **1998**, *136*, 139-234.

(49) Saunders, B. R.; Vincent, B. Microgel particles as model colloids: theory, properties and applications, *Adv. Colloid Interface Sci.* **1999**, *80*, 1-25.

(50) Kawaguchi, H. Functional polymer microspheres, *Prog. Polym. Sci.* **2000**, *25*, 1171-1210.

(51) Pelton, R. Temperature-sensitive aqueous microgels, *Adv. Colloid Interface Sci.* **2000**, *85*, 1-33.

(52) Das, M.; Zhang, H.; Kumacheva, E. Microgels: Old materials with new applications, *Ann. Rev. Mater. Res.* **2006**, *36*, 117-142.

(53) Tomalia, D. A.; Naylor, A. M.; Goddard, W. A. STARBURST DENDRIMERS - MOLECULAR-LEVEL CONTROL OF SIZE, SHAPE, SURFACE-CHEMISTRY, TOPOLOGY, AND FLEXIBILITY FROM ATOMS TO MACROSCOPIC MATTER, *Angew. Chem. Int. Ed. Engl.* **1990**, *29*, 138-175.

(54) Frechet, J. M. J. Functional polymers and dendrimers: Reactivity, molecular architecture, and interfacial energy, *Science* **1994**, *263*, 1710-1715.

(55) Bosman, A. W.; Janssen, H. M.; Meijer, E. W. About dendrimers: Structure, physical properties, and applications, *Chem. Rev.* **1999**, *99*, 1665-1688.

(56) Halperin, A.; Tirrell, M.; Lodge, T. P. Tethered chains in polymer microstructures, *Adv. Polym. Sci.* **1992**, *100*, 31-71.

(57) Grest, G. S.; Fetters, L. J.; Huang, J. S.; Richter, D. *Star polymers: Experiment, theory, and simulation*; In *Advances in Chemical Physics, Vol XCIV*; John Wiley & Sons Inc: New York, 1996; Vol. 94, p 67-163.

(58) Inoue, K. Functional dendrimers, hyperbranched and star polymers, *Prog. Polym. Sci.* **2000**, *25*, 453-571.

(59) David, G.; Simionescu, B. C.; Albertsson, A. C. Rapid deswelling response of poly(N-isopropylacrylamide)/poly(2-alkyl-2-oxazoline)/poly(2-hydroxyethy l methacrylate) hydrogels, *Biomacromolecules* **2008**, *9*, 1678-1683.

(60) Elford, W. J. Structure in very permeable collodion gel films and its significance in filtration problems, *Proc. Roy. Soc. B* **1930**, *106*, 216-228.

(61) Staudinger, H.; Husemann, E. Über hochpolymere verbindungen, 116. Mitteil.: Über das begrenzt quellbare poly-styrol, *Ber. Deuts. Chem. Ges.* **1935**, *68*, 1618-1634.

(62) Shashoua, V. E.; Beaman, R. G. Microgel: An idealized polymer molecule, *J. Polym. Sci.* **1958**, *33*, 101-117.

(63) Murray, M. J.; Snowden, M. J. The preparation, characterisation and applications of colloidal microgels, *Adv. Colloid Interface Sci.* **1995**, *54*, 73-91.

(64) Cragg, L. H.; Manson, J. A. Normal and cross-linked polystyrene 2. Viscosity behavior of polystyrene cross-linked in emulsion polymerization, *J. Polym. Sci.* **1952**, *9*, 265-278.

(65) Manson, J. A.; Cragg, L. H. Normal and cross-linked polystyrene 1. Huggins' k' as a measure of nonlinearity, *Can. J. Chem.* **1952**, *30*, 482-496.

(66) Woods, M. E.; Dodge, J. S.; Krieger, I. M.; Pierce, P. E. Monodisperse latices I. Emulsion polymerization with mixtures of anionic and nonionic surfactants, *J. Paint Tech.* **1968**, *40*, 541-548.

(67) Greene, B. W.; Sheetz, D. P.; Filer, T. D. In situ polymerization of surface-active agents on latex particles I. Preparation and characterization of styrene/butadiene latexes, *J. Colloid Interface Sci.* **1970**, *32*, 90-95.

(68) Hearn, J.; Wilkinson, M. C.; Goodall, A. R. Polymer latices as model colloids, *Adv. Colloid Interface Sci.* **1981**, *14*, 173-236.

(69) Dunn, A. S.; Chong, L. C.-H. Application of theory of colloid stability and the problem of particle formation in aqueous solution of vinyl acetate, *Br. Polym. J.* **1970**, *2*, 49-59.

(70) Kotera, A.; Furusawa, K.; Takeda, Y. Colloid chemical studies of polystyrene latices polymerized without any surfaceactive agents. I. Method for preparing monodisperse latices and their characterization, *Kolloid-Z. Z. Polym.* **1970**, *239*, 677-681.

(71) Goodwin, J. W.; Hearn, J.; Ho, C. C.; Ottewill, R. H. The preparation and characterisation of polymer latices formed in the absence of surface active agents, *Br. Polym. J.* **1973**, *5*, 347-362.

(72) Antl, L.; Goodwin, J. W.; Hill, R. D.; Ottewill, R. H.; Owens, S. M.; Papworth, S.; Waters, J. A. The preparation of poly(methyl methacrylate) latices in non-aqueous media, *Colloids Surf.* **1986**, *17*, 67-78.

(73) Pelton, R. H.; Chibante, P. Preparation of aqueous lattices with *N*-isopropylacrylamide, *Colloids Surf.* **1986**, *20*, 247-256.

(74) Gao, J.; Frisken, B. J. Cross-linker-free N-isopropylacrylamide gel nanospheres, *Langmuir* **2003**, *19*, 5212-5216.

(75) Gao, J.; Frisken, B. J. Influence of secondary components on the synthesis of self-cross-linked N-isopropylacrylamide microgels, *Langmuir* **2005**, *21*, 545-551.

(76) Gao, J.; Frisken, B. J. Influence of reaction conditions on the synthesis of self-cross-linked N-isopropylacrylamide microgels, *Langmuir* **2003**, *19*, 5217-5222.

(77) Tsuji, S.; Kawaguchi, H. Colored thin films prepared from hydrogel microspheres, *Langmuir* **2005**, *21*, 8439-8442.

(78) Kim, J.; Nayak, S.; Lyon, L. A. Bioresponsive hydrogel microlenses, *J. Am. Chem. Soc.* **2005**, *127*, 9588-9592.

(79) Nayak, S.; Lee, H.; Chmielewski, J.; Lyon, L. A. Folate-mediated cell targeting and cytotoxicity using thermoresponsive microgels, *J. Am. Chem. Soc.* **2004**, *126*, 10258-10259.

(80) Murthy, N.; Xu, M. C.; Schuck, S.; Kunisawa, J.; Shastri, N.; Frechet, J. M. J. A macromolecular delivery vehicle for protein-based vaccines: Acid-degradable protein-loaded microgels, *Proc. Natl. Acad. Sci. U. S. A.* **2003**, *100*, 4995-5000.

(81) Soppimath, K. S.; Aminabhavi, T. M.; Dave, A. M.; Kumbar, S. G.; Rudzinski, W. E. Stimulus-responsive "smart" hydrogels as novel drug delivery systems, *Drug Dev. Ind. Pharm.* **2002**, *28*, 957-974.

(82) Debord, J. D.; Lyon, L. A. Thermoresponsive photonic crystals, *J. Phys. Chem. B* **2000**, *104*, 6327-6331.

(83) Senff, H.; Richtering, W. Temperature sensitive microgel suspensions: Colloidal phase behavior and rheology of soft spheres, *J. Chem. Phys.* **1999**, *111*, 1705-1711.

(84) Hellweg, T.; Dewhurst, C. D.; Bruckner, E.; Kratz, K.; Eimer, W. Colloidal crystals made of poly(N-isopropylacrylamide) microgel particles, *Colloid Polym. Sci.* **2000**, *278*, 972-978.

(85) Lyon, L. A.; Debord, J. D.; Debord, S. B.; Jones, C. D.; McGrath, J. G.; Serpe, M. J. Microgel colloidal crystals, *J. Phys. Chem. B* **2004**, *108*, 19099-19108.

(86) Meng, Z.; Cho, J. K.; Debord, S.; Breedveld, V.; Lyon, L. A. Crystallization behavior of soft, attractive microgels, *J. Phys. Chem. B* **2007**, *111*, 6992-6997.

(87) Snowden, M. J.; Chowdhry, B. Z.; Vincent, B.; Morris, G. E. Colloidal copolymer microgels of N-isopropylacrylamide and acrylic acid: pH, ionic strength and temperature effects, *J. Chem. Soc., Faraday Trans.* **1996**, *92*, 5013-5016.

(88) Zhou, S. Q.; Chu, B. Synthesis and volume phase transition of poly(methacrylic acid-co-N-isopropylacrylamide) microgel particles in water, *J. Phys. Chem. B* **1998**, *102*, 1364-1371.

(89) Hirose, Y.; Amiya, T.; Hirokawa, Y.; Tanaka, T. Phase-transition of submicron gel beads, *Macromolecules* **1987**, *20*, 1342-1344.

(90) Jones, C. D.; Lyon, L. A. Synthesis and characterization of multiresponsive core-shell microgels, *Macromolecules* **2000**, *33*, 8301-8306.

(91) Forget, J. L.; Booth, C.; Canham, P. H.; Duggleby, M.; King, T. A.; Price, C. Characterization of poly(styrene-co-divinylbenzene) microgels, *J. Polym. Sci. Polym. Phys.* **1979**, *17*, 1403-1411.

(92) Antonietti, M.; Rosenauer, C. Properties of fractal divinylbenzene microgels, *Macromolecules* **1991**, *24*, 3434-3442.

(93) Lang, P.; Burchard, W.; Wolfe, M. S.; Spinelli, H. J.; Page, L. Structure of PMMA/EGDMA star-branched microgels, *Macromolecules* **1991**, *24*, 1306-1314.

(94) Mura-Kuentz, A.; Riess, G. Synthesis and characterization of poly(methylmethacrylate) microlatexes and microgels, *Macromol. Symp.* **2000**, *150*, 229-234.

(95) Antonietti, M.; Pakula, T.; Bremser, W. Rheology of small spherical polystyrene microgels: A direct proof for a new transport mechanism in bulk polymers besides reptation, *Macromolecules* **1995**, *28*, 4227-4233.

(96) Fritz, G.; Schadler, V.; Willenbacher, N.; Wagner, N. J. Electrosteric stabilization of colloidal dispersions, *Langmuir* **2002**, *18*, 6381-6390.

(97) Bartsch, E.; Kirsch, S.; Lindner, P.; Scherer, T.; Stolken, S. Spherical microgel colloids - Hard spheres from soft matter, *Ber. Bunsenges. Phys. Chem.* **1998**, *102*, 1597-1602.

(98) Heskins, M.; Guillet, J. E. Solution properties of poly(*N*-isopropylacrylamide), *J. Macromol. Sci. Chem.* **1968**, *2*, 1441 - 1455.

(99) Eliassaf, J. Aqueous solutions of poly(*N*-isopropylacrylamide), *J. Appl. Polym. Sci.* **1978**, *22*, 873-874.

(100) Goodwin, J. W.; Ottewill, R. H.; Pelton, R.; Vianello, G.; Yates, D. E. Control of particle size in the formation of polymer latices, *Br. Polym. J.* **1978**, *10*, 173-180.

(101) Kratz, K.; Hellweg, T.; Eimer, W. Effect of connectivity and charge density on the swelling and local structural and dynamic properties of colloidal PNIPAM microgels, *Ber. Bunsenges. Phys. Chem.* **1998**, *102*, 1603-1608.

(102) Ito, S.; Ogawa, K.; Suzuki, H.; Wang, B. L.; Yoshida, R.; Kokufuta, E. Preparation of thermosensitive submicrometer gel particles with anionic and cationic charges, *Langmuir* **1999**, *15*, 4289-4294.

(103) Saunders, B. R.; Crowther, H. M.; Morris, G. E.; Mears, S. J.; Cosgrove, T.; Vincent, B. Factors affecting the swelling of poly(N-isopropylacrylamide) microgel particles: fundamental and commercial implications, *Colloids Surf. A* **1999**, *149*, 57-64.

(104) Kim, K. S.; Kim, M. H.; Cho, S. H. pH- and temperature-sensitive behavior of poly(N-isopropylacrylamide-co-methacrylic acid) microgels, *J. Ind. Eng. Chem.* **2005**, *11*, 736-742.

(105) Sousa, R. G.; Prior-Cabanillas, A.; Quijada-Garrido, I.; Barrales-Rienda, J. M. Dependence of copolymer composition, swelling history, and drug concentration on the loading of diltiazem hydrochloride (DIL.HCl) into poly [(N-isopropylacrylamide)-co-(methacrylic acid)] hydrogels and its release behaviour from hydrogel slabs, *J. Control. Release* **2005**, *102*, 595-606.

(106) Tian, P.; Wu, Q. L.; Lian, K. Preparation of temperature- and pH-sensitive, stimuli-responsive poly(N-isopropylacrylamide-co-methacrylic acid) nanoparticles, *J. Appl. Polym. Sci.* **2008**, *108*, 2226-2232.

(107) Suzuki, D.; Kawaguchi, H. Modification of gold nanoparticle composite nanostructures using thermosensitive core-shell particles as a template, *Langmuir* **2005**, *21*, 8175-8179.

(108) Suzuki, D.; Kawaguchi, H. Stimuli-sensitive core/shell template particles for immobilizing inorganic nanoparticles in the core, *Colloid Polym. Sci.* **2006**, *284*, 1443-1451.

(109) Suzuki, D.; Kawaguchi, H. Hybrid microgels with reversibly changeable multiple brilliant color, *Langmuir* **2006**, *22*, 3818-3822.

(110) Hantzschel, N.; Zhang, F. B.; Eckert, F.; Pich, A.; Winnik, M. A. Poly(N-vinylcaprolactam-co-glycidyI methacrylate) aqueous microgels labeled with fluorescent LaF3 : Eu nanoparticles, *Langmuir* **2007**, *23*, 10793-10800.

(111) Pinkrah, V. T.; Snowden, M. J.; Mitchell, J. C.; Seidel, J.; Chowdhry, B. Z.; Fern, G. R. Physicochemical properties of poly(N-isopropylacrylamide-co-4-vinylpyridine) cationic polyelectrolyte colloidal microgels, *Langmuir* **2003**, *19*, 585-590.

(112) Kim, K. S.; Vincent, B. pH and temperature-sensitive behaviors of poly(4-vinyl pyridine-co-N-isopropyl acrylamide) microgels, *Polym. J.* **2005**, *37*, 565-570.

(113) Pelton, R. H.; Pelton, H. M.; Morphesis, A.; Rowell, R. L. Particle sizes and electrophoretic mobilities of poly(N-isopropylacrylamide) latex, *Langmuir* **1989**, *5*, 816-818.

(114) Blackburn, W. H.; Lyon, L. A. Size-controlled synthesis of monodisperse core/shell nanogels, *Colloid Polym. Sci.* **2008**, *286*, 563-569.

(115) Tam, K. C.; Ragaram, S.; Pelton, R. H. Interaction of surfactants with poly(N-isopropylacrylamide) microgel latices, *Langmuir* **1994**, *10*, 418-422.

(116) Dowding, P. J.; Vincent, B.; Williams, E. Preparation and swelling properties of poly(NIPAM) "minigel" particles prepared by inverse suspension polymerization, *J. Colloid Interface Sci.* **2000**, *221*, 268-272.

(117) Kim, J.; Deike, I.; Dingenouts, N.; Norhausen, C.; Ballauff, M. The volume transition in thermosensitive core-shell latex particles investigated by small-angle X-ray scattering and dynamic light scattering, *Macromol. Symp.* **1999**, *142*, 217-225.

(118) Berndt, I.; Richtering, W. Doubly temperature sensitive core-shell microgels, *Macromolecules* **2003**, *36*, 8780-8785.

(119) Zhang, Y. J.; Guan, Y.; Zhou, S. Q. Synthesis and volume phase transitions of glucose-sensitive microgels, *Biomacromolecules* **2006**, *7*, 3196-3201.

(120) Zhang, Y. J.; Guan, Y.; Zhou, S. Q. Permeability control of glucose-sensitive nanoshells, *Biomacromolecules* **2007**, *8*, 3842-3847.

(121) Binsk, B. P.; Fletcher, P. D. I. Particles adsorbed at the oil-water interface: A theoretical comparison between spheres of uniform wettability and "Janus" particles, *Langmuir* **2001**, *17*, 4708-4710.

(122) Zhang, H.; Tumarkin, E.; Sullan, R. M. A.; Walker, G. C.; Kumacheva, E. Exploring microfluidic routes to microgels of biological polymers, *Macromol. Rapid Commun.* **2007**, *28*, 527-538.

(123) Suzuki, D.; Tsuji, S.; Kawaguchi, H. Janus microgels prepared by surfactant-free pickering emulsion-based modification and their self-assembly, *J. Am. Chem. Soc.* **2007**, *129*, 8088-8089.

(124) Zhang, Z. L.; Glotzer, S. C. Self-assembly of patchy particles, *Nano Lett.* **2004**, *4*, 1407-1413.

(125) Dong, Y.; Ma, Y.; Zhai, T. Y.; Shen, F. G.; Zeng, Y.; Fu, H. B.; Yao, J. N. Silver nanoparticles stabilized by thermoresponsive microgel particles: Synthesis and evidence of an electron donor-acceptor effect, *Macromol. Rapid Commun.* **2007**, *28*, 2339-2345.

(126) Wang, G. Z.; Zhang, Y.; Fang, Y.; Gu, Z. Z. Flower-like SiO_2-coated polymer/Fe_3O_4 composite microspheres of super-paramagnetic properties: Preparation via a polymeric microgel template method, *J. Am. Ceram. Soc.* **2007**, *90*, 2067-2072.

(127) Zhang, J. G.; Xu, S. Q.; Kumacheva, E. Polymer microgels: Reactors for semiconductor, metal, and magnetic nanoparticles, *J. Am. Chem. Soc.* **2004**, *126*, 7908-7914.

(128) Connal, L. A.; Vestberg, R.; Hawker, C. J.; Qiao, G. G. Synthesis of dendron functionalized core cross-linked star polymers, *Macromolecules* **2007**, *40*, 7855-7863.

(129) Blencowe, A.; Tan, J. F.; Goh, T. K.; Qiao, G. G. Core cross-linked star polymers via controlled radical polymerisation, *Polymer* **2009**, *50*, 5-32.

(130) Goh, T. K.; Coventry, K. D.; Blencowe, A.; Qiao, G. G. Rheology of core cross-linked star polymers, *Polymer* **2008**, *49*, 5095-5104.

(131) Read, E. S.; Armes, S. P. Recent advances in shell cross-linked micelles, *Chem. Commun.* **2007**, 3021-3035.

(132) Won, Y.-Y.; Davis, H. T.; Bates, F. S. Giant wormlike rubber micelles, *Science* **1999**, *283*, 960-963.

(133) Zhang, L.; Eisenberg, A. Multiple morphologies of "crew-cut" aggregates of polystyrene-b-poly(acrylic acid) block copolymers, *Science* **1995**, *268*, 1728-1731.

(134) Thurmond, K. B.; Kowalewski, T.; Wooley, K. L. Water-soluble knedel-like structures: The preparation of shell-cross-linked small particles, *J. Am. Chem. Soc.* **1996**, *118*, 7239-7240.

(135) Joralemon, M. J.; O'Reilly, R. K.; Hawker, C. J.; Wooley, K. L. Shell click-crosslinked (SCC) nanoparticles: A new methodology for synthesis and orthogonal functionalization, *J. Am. Chem. Soc.* **2005**, *127*, 16892-16899.

(136) Alvarez-Lorenzo, C.; Concheiro, A. Reversible adsorption by a pH- and temperature-sensitive acrylic hydrogel, *J. Control. Release* **2002**, *80*, 247-257.

(137) Kwon, Y. J.; James, E.; Shastri, N.; Frechet, J. M. J. In vivo targeting of dendritic cells for activation of cellular immunity using vaccine carriers based on pH-responsive microparticles, *Proc. Natl. Acad. Sci. U. S. A.* **2005**, *102*, 18264-18268.

(138) Zhang, H.; Mardyani, S.; Chan, W. C. W.; Kumacheva, E. Design of biocompatible chitosan microgels for targeted pH-mediated intracellular release of cancer therapeutics, *Biomacromolecules* **2006**, *7*, 1568-1572.

(139) Oh, J. K.; Drumright, R.; Siegwart, D. J.; Matyjaszewski, K. The development of microgels/nanogels for drug delivery applications, *Prog. Polym. Sci.* **2008**, *33*, 448-477.

(140) Gan, D. J.; Lyon, L. A. Synthesis and protein adsorption resistance of PEG-modified poly(N-isopropylacrylamide) core/shell microgels, *Macromolecules* **2002**, *35*, 9634-9639.

(141) Nolan, C. M.; Reyes, C. D.; Debord, J. D.; Garcia, A. J.; Lyon, L. A. Phase transition behavior, protein adsorption, and cell adhesion resistance of poly(ethylene glycol) cross-linked microgel particles, *Biomacromolecules* **2005**, *6*, 2032-2039.

(142) Scott, E. A.; Nichols, M. D.; Cordova, L. H.; George, B. J.; Jun, Y. S.; Elbert, D. L. Protein adsorption and cell adhesion on nanoscale bioactive coatings formed from poly(ethylene glycol) and albumin microgels, *Biomaterials* **2008**, *29*, 4481-4493.

(143) Pich, A.; Berger, S.; Ornatsky, O.; Baranov, V.; Winnik, M. A. The influence of PEG macromonomers on the size and properties of thermosensitive aqueous microgels, *Colloid Polym. Sci.* **2009**, *287*, 269-275.

(144) Baskin, J. M.; Bertozzi, C. R. Bioorthogonal click chemistry: Covalent labeling in living systems, *QSAR Comb. Sci.* **2007**, *26*, 1211-1219.

(145) Kolb, H. C.; Finn, M. G.; Sharpless, K. B. Click chemistry: Diverse chemical function from a few good reactions, *Angew. Chem. Int. Ed.* **2001**, *40*, 2004-2021.

(146) Rostovtsev, V. V.; Green, L. G.; Fokin, V. V.; Sharpless, K. B. A stepwise Huisgen cycloaddition process: Copper(I)-catalyzed regioselective "ligation" of azides and terminal alkynes, *Angew. Chem. Int. Ed.* **2002**, *41*, 2596-2599.

(147) Tornoe, C. W.; Christensen, C.; Meldal, M. Peptidotriazoles on solid phase: [1,2,3]-triazoles by regiospecific copper(I)-catalyzed 1,3-dipolar cycloadditions of terminal alkynes to azides, *J. Org. Chem.* **2002**, *67*, 3057-3064.

(148) Kolb, H. C.; Sharpless, K. B. The growing impact of click chemistry on drug discovery, *Drug Discov. Today* **2003**, *8*, 1128-1137.

(149) Huisgen, R. 1,3-Dipolar cycloadditions: Past and future, *Angew. Chem. Int. Ed. Engl.* **1963**, *2*, 565-598.

(150) Bock, V. D.; Hiemstra, H.; van Maarseveen, J. H. Cu-I-catalyzed alkyne-azide "click" cycloadditions from a mechanistic and synthetic perspective, *Eur. J. Org. Chem.* **2006**, 51-68.

(151) Evanoff, D. D.; Hayes, S. E.; Ying, Y.; Shim, G. H.; Lawrence, J. R.; Carroll, J. B.; Roeder, R. D.; Houchins, J. M.; Huebner, C. E.; Foulger, S. H. Functionalization of crystalline colloidal arrays through click chemistry, *Adv. Mater.* **2007**, *19*, 3507-3512.

(152) Evans, C. E.; Lovell, P. A. Click chemistry as a route to surface functionalization of polymer particles dispersed in aqueous media, *Chem. Commun.* **2009**, 2305-2307.

(153) Slater, M.; Snauko, M.; Svec, F.; Frechet, J. M. J. "Click chemistry" in the preparation of porous polymer-based particulate stationary phases for mu-HPLC separation of peptides and proteins, *Anal. Chem.* **2006**, *78*, 4969-4975.

(154) Hawker, C. J.; Wooley, K. L. The convergence of synthetic organic and polymer chemistries, *Science* **2005**, *309*, 1200-1205.

(155) Bhaskar, S.; Roh, K. H.; Jiang, X. W.; Baker, G. L.; Lahann, J. Spatioselective Modification of Bicompartmental Polymer Particles and Fibers via Huisgen 1,3-Dipolar Cycloaddition, *Macromol. Rapid Commun.* **2008**, *29*, 1655-1660.

(156) Ochs, C. J.; Such, G. K.; Stadler, B.; Caruso, F. Low-Fouling, Biofunctionalized, and Biodegradable Click Capsules, *Biomacromolecules* **2008**, *9*, 3389-3396.

(157) Chen, G. J.; Tao, L.; Mantovani, G.; Geng, J.; Nystrom, D.; Haddleton, D. M. A modular click approach to glycosylated polymeric beads: Design, synthesis and preliminary lectin, recognition studies, *Macromolecules* **2007**, *40*, 7513-7520.

(158) Wang, Q.; Chan, T. R.; Hilgraf, R.; Fokin, V. V.; Sharpless, K. B.; Finn, M. G. Bioconjugation by copper(I)-catalyzed azide-alkyne [3+2] cycloaddition, *J. Am. Chem. Soc.* **2003**, *125*, 3192-3193.

(159) Zeng, Q. B.; Li, T.; Cash, B.; Li, S. Q.; Xie, F.; Wang, Q. Chemoselective derivatization of a bionanoparticle by click reaction and ATRP reaction, *Chem. Commun.* **2007**, 1453-1455.

(160) Granick, S.; Kumar, S. K.; Amis, E. J.; Antonietti, M.; Balazs, A. C.; Chakraborty, A. K.; Grest, G. S.; Hawker, C.; Janmey, P.; Kramer, E. J.; Nuzzo, R.; Russell, T. P.; Safinya, C. R. Macromolecules at surfaces: Research challenges and opportunities from tribology to biology, *J. Polym. Sci. Polym. Phys.* **2003**, *41*, 2755-2793.

(161) Ulbricht, M. Membrane separations using molecularly imprinted polymers, *J. Chromatogr. B* **2004**, *804*, 113-125.

(162) Kharlampieva, E.; Sukhishvili, S. A. Hydrogen-bonded layer-by-layer polymer films, *Polym. Rev.* **2006**, *46*, 377-395.

(163) Dimitrov, I.; Trzebicka, B.; Muller, A. H. E.; Dworak, A.; Tsvetanov, C. B. Thermosensitive water-soluble copolymers with doubly responsive reversibly interacting entities, *Prog. Polym. Sci.* **2007**, *32*, 1275-1343.

(164) Lyon, L. A.; Meng, Z. Y.; Singh, N.; Sorrell, C. D.; John, A. S. Thermoresponsive microgel-based materials, *Chem. Soc. Rev.* **2009**, *38*, 865-874.

(165) Schexnailder, P.; Schmidt, G. Nanocomposite polymer hydrogels, *Colloid Polym. Sci.* **2009**, *287*, 1-11.

(166) Nayak, S.; Lyon, L. A. Soft nanotechnology with soft nanoparticles, *Angew. Chem. Int. Ed.* **2005**, *44*, 7686-7708.

(167) Sukhishvili, S. A. Responsive polymer films and capsules via layer-by-layer assembly, *Curr. Opin. Colloid Interface Sci.* **2005**, *10*, 37-44.

(168) Whitesides, G. M.; Mathias, J. P.; Seto, C. T. Molecular self-assembly and nanochemistry: A chemical strategy for the synthesis of nanostructures, *Science* **1991**, *254*, 1312-1319.

(169) Whitesides, G. M.; Grzybowski, B. Self-assembly at all scales, *Science* **2002**, *295*, 2418-2421.

(170) Lehn, J. M. Perspectives in supramolecular chemistry - From molecular recognition towards molecular information processing and self-organization, *Angew. Chem. Int. Ed. Engl.* **1990**, *29*, 1304-1319.

(171) Decher, G. Fuzzy nanoassemblies: Toward layered polymeric multicomposites, *Science* **1997**, *277*, 1232-1237.

(172) Mirkin, C. A.; Letsinger, R. L.; Mucic, R. C.; Storhoff, J. J. A DNA-based method for rationally assembling nanoparticles into macroscopic materials, *Nature* **1996**, *382*, 607-609.

(173) Sun, S. H.; Murray, C. B.; Weller, D.; Folks, L.; Moser, A. Monodisperse FePt nanoparticles and ferromagnetic FePt nanocrystal superlattices, *Science* **2000**, *287*, 1989-1992.

(174) Ulman, A. Formation and structure of self-assembled monolayers, *Chem. Rev.* **1996**, *96*, 1533-1554.

(175) Bong, D. T.; Clark, T. D.; Granja, J. R.; Ghadiri, M. R. Self-assembling organic nanotubes, *Angew. Chem. Int. Ed.* **2001**, *40*, 988-1011.

(176) Grohn, F. Electrostatic self-assembly as route to supramolecular structures, *Macromol. Chem. Phys.* **2008**, *209*, 2295-2301.

(177) Blake, A. J.; Champness, N. R.; Hubberstey, P.; Li, W. S.; Withersby, M. A.; Schroder, M. Inorganic crystal engineering using self-assembly of tailored building-blocks, *Coord. Chem. Rev.* **1999**, *183*, 117-138.

(178) Kotov, N. A. Layer-by-layer self-assembly: The contribution of hydrophobic interactions, *Nanostruct. Mater.* **1999**, *12*, 789-796.

(179) Simard, M.; Su, D.; Wuest, J. D. Use of hydrogen bonds to control molecular aggregation: Self-assembly of three-dimensional networks with large chambers, *J. Am. Chem. Soc.* **1991**, *113*, 4696-4698.

(180) Dusek, K.; Duskov-Smrckova, M. Network structure formation during crosslinking of organic coating systems, *Prog. Polym. Sci.* **2000**, *25*, 1215-1260.

(181) Saatweber, D.; Vogt, B. B. Microgels in organic coatings, *Prog. Org. Coat.* **1996**, *28*, 33-41.

(182) Serpe, M. J.; Jones, C. D.; Lyon, L. A. Layer-by-layer deposition of thermoresponsive microgel thin films, *Langmuir* **2003**, *19*, 8759-8764.

(183) Lawrence, D. B.; Cai, T.; Hu, Z.; Marquez, M.; Dinsmore, A. D. Temperature-responsive semipermeable capsules composed of colloidal microgel spheres, *Langmuir* **2007**, *23*, 395-398.

(184) Antonietti, M.; Hartmann, J.; Neese, M.; Seifert, U. Highly ordered size-dispersive packings of polydisperse microgel spheres, *Langmuir* **2000**, *16*, 7634-7639.

(185) Dinsmore, A. D.; Hsu, M. F.; Nikolaides, M. G.; Marquez, M.; Bausch, A. R.; Weitz, D. A. Colloidosomes: Selectively permeable capsules composed of colloidal particles, *Science* **2002**, *298*, 1006-1009.

(186) Reese, C. E.; Mikhonin, A. V.; Kamenjicki, M.; Tikhonov, A.; Asher, S. A. Nanogel nanosecond photonic crystal optical switching, *J. Am. Chem. Soc.* **2004**, *126*, 1493-1496.

(187) Jones, C. D.; Lyon, L. A. Photothermal patterning of microgel/gold nanoparticle composite colloidal crystals, *J. Am. Chem. Soc.* **2003**, *125*, 460-465.

(188) Gao, J.; Hu, Z. B. Optical properties of N-isopropylacrylamide microgel spheres in water, *Langmuir* **2002**, *18*, 1360-1367.

(189) Debord, J. D.; Eustis, S.; Debord, S. B.; Lofye, M. T.; Lyon, L. A. Color-tunable colloidal crystals from soft hydrogel nanoparticles, *Adv. Mater.* **2002**, *14*, 658-662.

(190) Debord, S. B.; Lyon, L. A. Influence of particle volume fraction on packing in responsive hydrogel colloidal crystals, *J. Phys. Chem. B* **2003**, *107*, 2927-2932.

(191) Meng, Z.; Smith, M. H.; Lyon, L. A. Temperature-programmed synthesis of micron-sized multi-responsive microgels, *Colloid Polym. Sci.* **2009**, *287*, 277-285.

(192) Meng, Z.; Cho, J. K.; Breedveld, V.; Lyon, L. A. Physical aging and phase behavior of multiresponsive microgel colloidal dispersions, *J. Phys. Chem. B* **2009**, *113*, 4590-4599.

(193) Struik, L. C. E. *Physical Aging in Amorphous Polymers and Other Materials*; Elsevier: Amsterdam, 1978.

(194) Cipelletti, L.; Manley, S.; Ball, R. C.; Weitz, D. A. Universal aging features in the restructuring of fractal colloidal gels, *Phys. Rev. Lett.* **2000**, *84*, 2275-2278.

(195) Mueth, D. M.; Crocker, J. C.; Esipov, S. E.; Grier, D. G. Origin of stratification in creaming emulsions, *Phys. Rev. Lett.* **1996**, *77*, 578-581.

(196) Pusey, P. N. *Colloidal suspensions*; In *Liquids, Freezing and Glass Transition*; Hansen, J. P., Levesque, D., Zinn-Justin, J., Eds.; North-Holland: 1989; Vol. 51, p 763-942.

(197) Maret, G. Diffusing-wave spectroscopy, *Curr. Opin. Colloid Interface Sci.* **1997**, *2*, 251-257.

(198) Romer, S.; Scheffold, F.; Schurtenberger, P. Sol-gel transition of concentrated colloidal suspensions, *Phys. Rev. Lett.* **2000**, *85*, 4980-4983.

(199) Knaebel, A.; Bellour, M.; Munch, J. P.; Viasnoff, V.; Lequeux, F.; Harden, J. L. Aging behavior of Laponite clay particle suspensions, *Europhys. Lett.* **2000**, *52*, 73-79.

(200) Bonn, D.; Tanaka, J.; Wegdam, G.; Kellay, H.; Meunier, J. Aging of a colloidal "Wigner" glass, *Europhys. Lett.* **1999**, *45*, 52-57.

(201) Abou, B.; Bonn, D.; Meunier, J. Aging dynamics in a colloidal glass, *Phys. Rev. E* **2001**, *64*, 021510.

(202) Cloitre, M.; Borrega, R.; Leibler, L. Rheological aging and rejuvenation in microgel pastes, *Phys. Rev. Lett.* **2000**, *85*, 4819-4822.

(203) Purnomo, E. H.; van den Ende, D.; Mellema, J.; Mugele, F. Linear viscoelastic properties of aging suspensions, *Europhys. Lett.* **2006**, *76*, 74-80.

(204) Sollich, P.; Lequeux, F.; Hebraud, P.; Cates, M. E. Rheology of soft glassy materials, *Phys. Rev. Lett.* **1997**, *78*, 2020-2023.

(205) Purnomo, E. H.; van den Ende, D.; Mellema, J.; Mugele, F. Rheological properties of aging thermosensitive suspensions, *Phys. Rev. E* **2007**, *76*, 021404.

(206) Purnomo, E. H.; van den Ende, D.; Vanapalli, S. A.; Mugele, F. Glass transition and aging in dense suspensions of thermosensitive microgel particles, *Phys. Rev. Lett.* **2008**, *101*, 238301.

(207) Wang, P.; Song, C. M.; Makse, H. A. Dynamic particle tracking reveals the ageing temperature of a colloidal glass, *Nat. Phys.* **2006**, *2*, 526-531.

(208) Kiefer, J.; Naser, M.; Kamel, A.; Carnali, J. Osmotic deswelling of microgels by linear polyelectrolytes, *Colloid Polym. Sci.* **1993**, *271*, 253-261.

(209) Saunders, B. R.; Vincent, B. Thermal and osmotic deswelling of poly(NIPAM) microgel particles, *J. Chem. Soc., Faraday Trans.* **1996**, *92*, 3385-3389.

(210) Saunders, B. R.; Crowther, H. M.; Vincent, B. Poly[(methyl methacrylate)-co-(methacrylic acid)] microgel particles: Swelling control using pH, cononsolvency, and osmotic deswelling, *Macromolecules* **1997**, *30*, 482-487.

(211) Saunders, B. R.; Vincent, B. Osmotic de-swelling of polystyrene microgel particles, *Colloid Polym. Sci.* **1997**, *275*, 9-17.

(212) Watzlawek, M.; Likos, C. N.; Löwen, H. Phase diagram of star polymer solutions, *Phys. Rev. Lett.* **1999**, *82*, 5289-5292.

(213) Likos, C. N. Effective interactions in soft condensed matter physics, *Phys. Rep. Rev. Sec. Phys. Lett.* **2001**, *348*, 267-439.

(214) Wu, J. Z.; Huang, G.; Hu, Z. B. Interparticle potential and the phase behavior of temperature-sensitive microgel dispersions, *Macromolecules* **2003**, *36*, 440-448.

(215) Wu, J. Z.; Zhou, B.; Hu, Z. B. Phase behavior of thermally responsive microgel colloids, *Phys. Rev. Lett.* **2003**, *90*, 048304.

(216) Gottwald, D.; Likos, C. N.; Kahl, G.; Lowen, H. Phase behavior of ionic microgels, *Phys. Rev. Lett.* **2004**, *92*, 068301.

(217) St. John, A. N.; Breedveld, V.; Lyon, L. A. Phase behavior in highly concentrated assemblies of microgels with soft repulsive interaction potentials, *J. Phys. Chem. B* **2007**, *111*, 7796-7801.

(218) Hoover, W. G.; Ree, F. H. Melting transition and communal entropy for hard spheres, *J. Chem. Phys.* **1968**, *49*, 3609-3617.

(219) Bernal, J. D.; Mason, J. Co-ordination of randomly packed spheres, *Nature* **1960**, *188*, 910-911.

(220) Scott, G. D. Packing of spheres, *Nature* **1960**, *188*, 908-909.

(221) Finney, J. L. Random packings and structure of simple liquids I. The geometry of random close packing, *Proc. Roy. Soc. A* **1970**, *319*, 479-493.

(222) Torquato, S.; Truskett, T. M.; Debenedetti, P. G. Is random close packing of spheres well defined?, *Phys. Rev. Lett.* **2000**, *84*, 2064-2067.

(223) Pusey, P. N.; Vanmegen, W. Phase behaviour of concentrated suspensions of nearly hard colloidal spheres, *Nature* **1986**, *320*, 340-342.

(224) Hoover, W. G.; Ross, M.; Johnson, K. W.; Henderso.D; Barker, J. A.; Brown, B. C. Soft-sphere equation of state, *J. Chem. Phys.* **1970**, *52*, 4931-4941.

(225) Baxter, R. J. Percus-Yevick equation for hard spheres with surface adhesion, *J. Chem. Phys.* **1968**, *49*, 2770-2774.

(226) Jansen, J. W.; Dekruif, C. G.; Vrij, A. Attractions in sterically stabilized silica dispersions. 1. Theory of phase-separation, *J. Colloid Interface Sci.* **1986**, *114*, 471-480.

(227) Jansen, J. W.; Dekruif, C. G.; Vrij, A. Attractions in sterically stabilized silica dispersions. 2. Experiments on phase-separation induced by temperature-variation, *J. Colloid Interface Sci.* **1986**, *114*, 481-491.

(228) Jansen, J. W.; Dekruif, C. G.; Vrij, A. Attractions in sterically stabilized silica dispersions. 3. 2nd virial-coefficient as a function of temperature, as measured by means of turbidity, *J. Colloid Interface Sci.* **1986**, *114*, 492-500.

(229) Jansen, J. W.; Dekruif, C. G.; Vrij, A. Attractions in sterically stabilized silica dispersions. 4. Sedimentation, *J. Colloid Interface Sci.* **1986**, *114*, 501-504.

(230) Jenkins, P.; Snowden, M. Depletion flocculation in colloidal dispersions, *Adv. Colloid Interface Sci.* **1996**, *68*, 57-96.

(231) Palberg, T. Colloidal crystallization dynamics, *Curr. Opin. Colloid Interface Sci.* **1997**, *2*, 607-614.

(232) Arora, A. K.; Tata, B. V. R. Interactions, structural ordering and phase transitions in colloidal dispersions, *Adv. Colloid Interface Sci.* **1998**, *78*, 49-97.

(233) Poon, W. C. K. The physics of a model colloid-polymer mixture, *J. Phys. Condens. Mat.* **2002**, *14*, R859-R880.

(234) Gasser, U. Crystallization in three- and two-dimensional colloidal suspensions, *J. Phys. Condens. Mat.* **2009**, *21*, 203101.

(235) Batchelor, G. K. Effect of Brownian motion on bulk stress in a suspension of sphereical particles, *J. Fluid Mech.* **1977**, *83*, 97-117.

CHAPTER 2

TEMPERATURE-FIXED SYNTHESIS OF MULTI-RESPONSIVE MICROGELS

This chapter describes the synthesis and characterization of multi-responsive cross-linked poly(*N*-isopropylacrylamide-*co*-acrylic acid) (pNIPAm-AAc) microgel particles, which will be used for the aging and phase behavior of colloidal dispersions and synthesis of cross-linker-free pNIPAm-AAc and pNIPAm-based clickable microgels in Chapters 4 and 5. Thermoresponsivity of pNIPAm-AAc microgel particles is due to coil-to-globule transition of *N*-isopropylacrylamide segments at lower critical solution temperature (LCST),[1] also called volume phase transition temperature (VPTT),[1,2] whereas pH-responsivity of pNIPAm-AAc microgel particles is attributed to the change of electrostatic repulsive interaction, hydrogen bonding, hydrophobic interactions between amide and/or carboxylic acid groups and the Donnan equilibrium shift due to osmotic pressure change as environmental pH crossover their pK_a.[3]

2.1 Introduction

2.1.1 One-Pot Copolymerization

Stimuli-responsive microgel particles[4] have received extensive investigation in recent years due to their current and potential applications in coatings,[5] sensors,[6-8] and drug delivery vehicles.[9-12] Most stimuli-responsive homopolymeric microgels are sensitive to only one environment stimulus, which we might termed "mono-responsive" microgels. For instance, poly(*N*-isopropylacrylamide) (pNIPAm) microgels are essentially only responsive to temperature and almost inert to pH and ionic strength;[13-15] whereas poly(acrylic acid) (pAAc) microgels are responsive to pH and ionic strength, but almost inert to temperature.[16] However, multi-responsive microgel systems are required

for the real-world applications such as drug delivery,[9,12,17-24] sensor,[6,7,25] and microreactors.[26] If we assume thermoresponsivity of NIPAm segments are not diminished and pH-responsivity of AAc segments is significant enough by incorporation of less than 20 mol% of AAc, the combination of two monomers NIPAm and AAc into one copolymeric microgel particles is the logical answer to multi-responsive microgel, which is responsive simultaneously to temperature, pH, and ionic strength.[3,27] Therefore, one-pot surfactant-free precipitation polymerization of NIPAm with AAc and cross-linker *N,N*-methylene bisacrylamide (BIS) was conducted at 70 ºC in water for 6 hours to form pNIPAm-AAc multi-responsive microgels,[3] which demonstrated a reduced lower critical solution temperature (LCST), also called volume phase transition temperature (VPTT), in comparison with that of homopolymeric counterpart, pNIPAm microgels.[28] In addition, other anionic monomers, i.e. methacrylic acid (MAAc),[29] and cationic monomers, i.e. 1-vinylimidazole (VIm)[30] and 4-vinylpyridine (VPy),[31] were copolymerized with NIPAm to form multi-responsive microgels as well. Due to the ionizability of AAc and VIm monomers, multi-responsive microgel particles are also called polyelectrolyte microgels.[30] If both cationic and anionic monomers are simultaneously incorporated with NIPAm in microgels, polyampholyte microgels formed with remarkable swelling at both higher and lower temperature.[32] Frisken et al. found that cross-linker-free polymerization of NIPAm with AAc resulted in squishy pNIPAm-AAc multi-responsive microgels.[33] On the other hand, instead of using water as solvent for polymerization, supercritical CO_2 ($scCO_2$) was employed for the precipitation radical polymerization of NIPAm, AAc, and N-vinylpyrrolidone.[34] To transform the fast-responsivity of microgel particles to bulk hydrogel (macrogel), Gupta et al. cross-linked pNIPAm-AAc microgel particles via redox-initiated copolymerization of NIPAm and BIS to form bulk hydrogels with cross-linked microgel particles [35] responding to temperature and/or pH change much faster than conventional bulk hydrogels.[36]

2.1.2 Topological Control of Functionalities

Instead of using random copolymerization of NIPAm and AAc to form microgels, Ballauff et al. adopt a core-shell topology in which polystyrene (pSt) core coated with cross-linked pNIPAm-AAc shell demonstrates continuous volume transition in contrast to the discontinuous volume phase transition (VPT) of pNIPAm-AAc copolymeric microgels.[37] In addition to conventional radical polymerization of NIPAm and AAc on the surface of pSt core, Kawaguchi et al. offered an alternative "Iniferter" approach for grafting pNIPAm-AAc chains on pSt cores. In stead of a discontinuous one-step volume phase transition suggested by Ballauff, Kawaguchi et al. found a two-step volume phase transition of pSt(core)/pNIPAm-AAc(shell) at 0.01M KCl buffer.[38]

Furthermore, Lyon et al. used two-step "seed-feed" polymerization to obtain pNIPAm(core)/pNIPAm-AAc(shell) and pNIPAm-AAc(core) /pNIPAm (shell) core-shell microgel particles with multi-step volume phase transition at pH 6.5 buffer, which was attributed to the restriction effect of shell, inhomogeneity of AAc/NIPAm distribution, and coupling of pNIPAm-AAc and pNIPAm at interfaces.[39-41] Similarly, Khan synthesized pNIPAm(core)/pAAc(shell) microgel particles,[42] and Zhang et al. graft polyethyleneimine (PEI) on surface of pNIPAm-AAc microgels.[43] Hu et al. also used a two-step polymerization to form pNIPAm-AAc microgels with interpenetrating network (IPN) structure, which could self-assemble into ordered structure at temperature lower than LCST[44] or form viscoelastic bulk gel at LCST of pNIPAm-AAc IPN microgels.[45]

Furthermore, to incorporating the biological functionalities, such as folate and NH_2 groups, on the pNIPAm-AAc particle, Lyon et al. used fluorenyl-methoxy-carbonyl (Fmoc)-protected poly(ethylene glycol) (PEG) macromonomer to prepare pNIPAm-AAc-based microgels, and form multifunctional microgels with both carboxylic acid and amine groups followed by deprotection.[46] In addition to chemical modification of microgels, Richtering used layer-by-layer deposition of pNIPAm-AAc, poly(diallyldimethylammonium chloride) (PDADMAC) and poly(sodium 4-

styrenesulfonate) (PSS) to form pNIPAm(core)/ pNIPAm-AAc(shell 1)/PDADMAS (shell 2)/PSS(shell 3) microgels, with charge reversal and strong dependence of particle swelling on the adsorption of each layer on microgel particles.[47] For precise control of spatial distribution of AAc monomers, Janus particles were fabricated via Pickering emulsion approach [48] to control the functionality distribution on the surface of pNIPAm-AAc microgels. Microfluidic approach was employed to form Janus particles as well.[49,50]

2.1.3 Hybridization of Microgel Particles

In fact, a slew of hybridizations of pNIPAm-AAc microgels have been conducted. Vincent et al. synthesized pNIPAm-AAc copolymeric microgel particles for Pb(II) ion adsorption[51], processing aid for alumina powder dispersions,[52] and polyethylene oxide (PEO) uptake and release.[53] Snowden et al. used pNIPAm-AAc microgels for the fabrication of spherical phosphor europium-doped yttrium oxide (Y_2O_3:Eu) particles with diameter smaller than 100nm for field emissive displays (FED's) and cathode ray tube (CRT) applications.[54] Furthermore, hybrid core-shell type nanoparticles with gold core and pNIPAm-AAc shell were obtained for potential applications in targeted drug delivery.[55-58] Similarly, silver nanoparticles (AgNP) are included in pNIPAm-AAc microgels, thus-formed composite microgels demonstrate charge transfer from carbonyl groups to AgNP.[59] Fang, et al. also synthesized composite microgels by deposition of CuS on pNIPAm-AAc microgels to form patterned surface mophologies[60] or by inclusion of Fe_3O_4 nanoparticles to form super-paramagnetic composite microspheres.[61] Li et al. then synthesized CdTe/pNIPAm-AAc hybrid microgels for pH-controllable self-assembly.[62]

2.1.4 Characterization of pNIPAm-AAc Microgel Particles

Many research groups have used a variety of techniques to investigate the thermal and pH responsivity of pNIPAm-AAc microgel particles, especially the volume phase

transition at LCST and pK_a. Saunders et al. found that free polymers induce the de-swelling of pNIPAm-AAc particles due to osmotic de-swelling effect via photon correlation spectroscopy (PCS) and small-angle neutron scattering (SANS).[63] Eimer et al. have also used SANS to determine the influence of cross-linker and charge density on the inhomogeneous local structure and swelling dynamics of pNIPAm-AAc microgels.[27] Kokufuta et al. used potentiometric titration to determine carboxylic acid content of pNIPAm-AAc microgels, and they also claimed that microgels swell through an increase in the net charge density due to the COO^- ions rather than a rise in the osmotic pressure arising from mobile counterions within the microgel boundary.[64] Furthermore, Kokufuta found that apparent dissociation constant (pK_a) increased with increasing degree of dissociation but decreased by addition of NaCl. In addition, Keiding noticed that pK_a was dependent upon the local concentration of AAc residues in microgels albeit independent of overall AAc concentration.[65] Using potentiometric titration and dynamic light scattering, Eimer et al. found that with AAc content higher than 10 wt% in pNIPAm-AAc microgels, two-step phase transition appears at $pH \geq 5$ due to the hydrogen bonding between AAc and NIPAm segments; they also preliminarily investigated the aggregation of pNIPAm-AAc microgels at lower pH and/or higher ionic strength,[66] which was further studied by Makino et al.[67] For random copolymeric pNIPAm-AAc microgel particles, Pelton and Hoare provided a kinetic modeling for copolymerization[68] and a theoretical estimation on the functional group distribution,[69] which could be used to control functional group distribution and thereby tailoring microgel-drug interactions.[70] Their theoretical predication was supported by their electrophoretic[71] and titrimetric[72] characterization of a series of pNIPAm-based microgels.

Stimuli-responsive microgel thin films have been extensively investigated in recent years. Kawaguchi et al. use pNIPAm-AAc self-assembled monolayer (SAM) for surface plasma sensor (SPR) to detect pH and temperature change at different buffer.[73] Hellweg et al. used a spin-coating technique for the fabrication of pNIPAm-AAc thin

films on silicon wafer and observe the thermoresponsivity of microgel films at pH 2 buffer.[74] To understand the multi-responsivity and phase behavior quantitatively, the interaction between pNIPAm-AAc microgel particles and silica surface was further measured via atomic force microscopy(AFM) with silica colloid probe by Jenkins et al.[75] The interaction between microgels and silica probe are not Dejaguin-Landau-Verwey-Overbeek (DLVO)-form[76,77] due to the compression/deformation (softness) of microgels and the presence of "hairy" steric layer composed of dangling polyelectrolyte chains, whose conformations are dictated by the pH and/or ionic strength. Furthermore, *in situ* magnitude cantilever excitation (MAC)-mode AFM was employed to determine the thermal phase transition behavior of single pNIPAm-AAc microgels, showing that Young's modulus of single microgel particles increases approximately 15-fold at volume phase transition temperature (VPTT), corresponding to a transition from a water-swollen soft network to a stiffer deswollen state.[78]

2.1.5 Applications of pNIPAm-AAc Microgel Particles

Furthermore, the real-world applications of microgel particles and their assemblies in drug delivery, diagnostics, and sensors. As for drug delivery, Hu et al. used 6.0 wt% pNIPAm-AAc IPN microgel dispersions to form bulk hydrogel for the release studies.[45] Lynch et al. demonstrated a thin-film of "plum-pudding" gel with two different populations of microgels, pNIPAm-NtBAm (N-tert-butylacrylamide) and pNIPAm-AAc microgels, embedded into a single bulk gel, which could release neutral and cationic hydrophobic fluorescent molecules simultaneously and therefore a multifunctional platform for surface drug delivery.[9]

Instead of using bulk macrogel, Chiu et al. used pNIPAm-AAc microgels for drug delivery system.[79] Similarly, Zhang et al. fabricated pNIPAm-AAc IPN microgels carrying glucosamine for *in vitro* study of the release of insulin, and they found that the release of insulin was faster around tumor cells than normal cells.[24] Vincent found that

the uptake and release of PEO from pNIPAm-AAc microgels were dependent upon the AAc content, pH, molecular weight (MW) of PEO, cross-linking density, and temperature.[53] Huo et al. also pointed out the binding of bovine serum albumin (BSA) with pNIPAm-AAc microgel particles was mainly controlled by pH.[80] Furthermore, Lyon et al. proposed pNIPAm-AAc nanogel with diameter less than 100 nm for targeted drug delivery vehicles.[21] Park et al. used galactosylated pNIPAm-AAc microgels for specific endocytosis by hepatocytes, which demonstrated the potential of pNIPAm-AAc microgels as targeted drug delivery vehicles.[81]

As for biosensors for diagnostics, Lyon et al. have used pNIPAm-AAc microgels to fabricate microlenses for label-free sensing of avidin,[6] anti-biotin,[6] biocytin[82] and to fabricate thin films via layer-by-layer deposition for temperature, pH, and electrolyte-modulated[83] uptake and release of insulin[18,84] and doxorubicin.[85] Lyon et al. also confirmed that bioresponsive microlenses made by pNIPAm-AAc microgels are completely insensitive to simple adsorption via nonspecific protein binding from reconstituted human serum.[86] Zhou et al. conducted functionalization of pNIPAm-AAc microgels with 3-aminophenylboronic acid (APBA) via carbodiimide coupling to make glucose-sensitive microgels.[87,88]

Along with the investigations carried out in Lyon group, this chapter describes the synthesis, purification and characterization of pNIPAm-AAc microgel particles, which will be used in Chapter 4 and 5 for the aging and self-assembly of microgels in closed 3-D system.

2.2 Experimental

2.2.1 Materials

N-Isopropylacrylamide (NIPAm, Acros) was re-crystallized from n-hexanes (J.T. Baker) and dried under vacuum prior to use. Acrylic acid (AAc, Fluka), *N,N'*-methylene

bisacrylamide (BIS, Aldrich) and ammonium persulfate (APS, Sigma) were used as received. All water used throughout this investigation was distilled and deionized to a resistance of at least 18 MΩ·cm (Barnstead E-Pure system) and then filtered through an in-line 0.2-μm filter to remove particulate matter.

2.2.2 Microgel Synthesis, Purification and Lyophilization

The same batch of microgels was used throughout all the experiments presented in this chapter. Multi-responsive pNIPAm-AAc microgels were prepared by APS-initiated surfactant-free radical precipitation copolymerization of monomer NIPAm and comonomer AAc with cross-linker BIS. Isopropyl and carboxyl functional groups on the polymeric side chains were combined for multi-responsivity (temperature and pH). The reactant mixture composed of 84 mol% NIPAm (1.8 g), 15 mol% AAc (0.2 g) and 1 mol% BIS (0.04 g) was made by dissolving the reagents in 100 mL deionized water via ultrasonication. The reactant mixture was charged through an in-line 0.8-μm syringe filter into a 250-mL three-neck round bottom flask. During 60 minutes of N_2 purge, the mixture was heated from 22 to 60 °C and maintained at the same temperature throughout the synthesis. After the temperature of reactant mixture was stabilized and O_2 in reaction vessel was replaced by N_2, 5 mL of 0.078 M APS aqueous solution was added to initiate the copolymerization. The copolymerization was allowed to proceed for 6 h at 60 °C under N_2. The resultant colloidal dispersion was filtered through glass fiber to remove a small amount of coagulum and then transferred to several 10-mL Oak Ridge® polycarbonate centrifuge tubes (Nalgene). After centrifugation at a relative centrifugal force (RCF) of 15,422 × g and 25 °C for 1 hour, the supernatant in each tube was removed. Fresh deionized water was then added into each tube to redisperse microgel pellets via shaking overnight. The centrifugation and redispersion process was repeated four times. After purification, the microgel dispersion was lyophilized at −45 °C under 40 $\times 10^{-3}$ mbar for 72 hours. The freeze-dried product was a hygroscopic white powder.

Note the lyophilization of pNIPAm-AAc microgel dispersions will not have a detrimental effect on the physico-chemical properties, such as polydispersity, re-dispersibility, thermoresponsivity, and pH-responsivity.[89] Furthermore, to examine the synthetic temperature effect on the particle size and yield of pNIPAm-AAc microgels, particles are synthesized at temperature 45, 50, 55, 65, and 70 °C as well to control the particle size. (Refer to Section 2.3.5 for results.)

2.2.3 Aqueous Buffer Preparation

Aqueous buffers were prepared using recipes from buffer calculator developed by R. Beynon at the University of Liverpool.[90] The pH values were measured to ± 0.1 units by a pH meter (pH 430, Corning Corp.) with an Accumet probe (Cole-Palmer). The ionic strength was controlled by adding the appropriate amount of NaCl based on the buffer calculation. Because ionic strength is proportional to the conductivity, the ionic strength of pH buffers was determined by measuring the conductivity of corresponding pH buffers. The conductivity was measured with a Pinnacle 541 conductivity meter (Corning Corp.) with a "3 in 1" Combo with a RJ probe (Corning Corp.). Conductivity values for all aqueous buffers were 1.48 ± 0.20 mS/cm.

2.2.4 Dilute Microgel Dispersion Preparation

The microgel dispersions were prepared by first dispersing approximately 10 mg pNIPAm-AAc powder in 10 g of distilled, de-ionized water and shaking for overnight to obtain an 0.1 wt% dispersion. A 250 μL aliquot of the 0.1 wt% dispersion was then diluted to a concentration of 0.002 wt% and 0.0002 wt% in aqueous buffer for dynamic light scattering and electrophoresis, respectively. For microscopic visualization, the dilute microgel dispersions (0.01 wt%) were introduced into 5.0 × 2.0 × 0.1 mm VITROTUBE™ rectangular capillaries (Fiber Optic Center, Inc.) by capillary force at room temperature, and then sealed with Epoxy Putty™ (ITW Devcon®) resin.

2.2.5 Microgel Characterization

2.2.5.1 Photon Correlation Spectroscopy (Dynamic Light Scattering)

The size of multi-responsive microgel particles was determined via photon correlation spectroscopy (Protein Solutions Inc.) using an irradiation laser with a wavelength of 784 nm. A series of buffer solution with different pH values were prepared for PCS measurement. The dilute (0.001~0.01 wt%) dispersion of pNIPAm-AAc microgels was allowed to equilibrate thermally for at least 30 min before each set of measurements. The schematic diagram of DLS instrument is shown below,

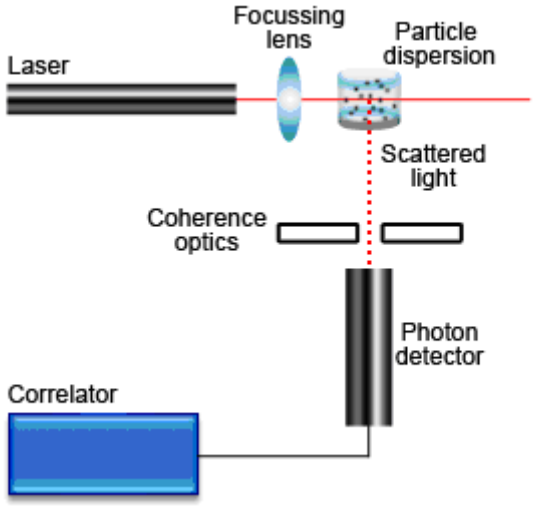

Scheme 2.1 Schematic diagram of a conventional 90º dynamic light scattering instrument from Malvern Instruments Ltd. (http://www.malvern.de/LabGer/technology/dynamic_light_scattering/classical_90_degree_scattering.htm)

The collected intensity-intensity autocorrelation functions $G^{(2)}(\tau,\theta)$ is related to the normalized first-order electric field time correlation function $|g^{(1)}(\tau,\theta)|$ by the Siegert relation[29]

$$G^{(2)}(\tau,\theta) = \langle I(0,\theta)I(\tau,\theta)\rangle = A\left[1+\beta\left|g^{(1)}(\tau,\theta)\right|^2\right] \quad (2\text{-}1)$$

where τ is the delay time, θ the scattering angle, A measured baseline, and β the coherent factor of the detection. For a polydisperse sample, $|g^{(1)}(\tau,\theta)|$ is related to the relaxation rate (Γ) distribution $G(\Gamma)$

$$\left|g^{(1)}(\tau,\theta)\right| = \int_0^\infty G(\Gamma)e^{-\Gamma\tau}d\tau \tag{2-2}$$

The cumulant analysis[91] is used to calculate $G(\Gamma)$ from $|g^{(1)}(\tau,\theta)|$. For a diffusive relaxation at infinite dilution of colloids, the relation rate (Γ) can be expressed as

$$\Gamma = Dq^2 \tag{2-3}$$

where D is the translational diffusion coefficient at $C \rightarrow 0$ and $q \rightarrow 0$. Here q is the scattering vector,

$$q = \frac{4\pi n}{\lambda_0}\sin\left(\frac{\theta}{2}\right) \tag{2-4}$$

with n, λ_0, and θ being the refractive index, irradiation wavelength *in vacuo*, and scattering angle. Therefore, translational diffusion coefficient D is related to the hydrodynamic radius (R_h) by the Stokes-Einstein equation,

$$R_h = \frac{k_B T}{2d\pi\eta_S D} \tag{2-5}$$

where k_B, T, d and η_s are the Boltzmann constant, the absolute temperature, the dimensionality, and the solvent viscosity, respectively. All PCS measurements were carried out at the scattering angle $\theta = 90°$.[29] In the data presented later, each point corresponds to the average of 5 runs, each run including 20 measurements, each measurement having a 10 s integration time.

2.2.5.2 Bright-Field Inverted Optical Video Microscopy

Bright-field images (transmission mode) were obtained with an inverted Olympus IX-71 microscope equipped with a 100× oil immersion objective and Andor™ LUCA electron multiplying charge-coupled device (EMCCD) camera. The sample temperature

was controlled with a temperature stage (Physitemp) as well as an objective heater (Bioptechs) to within ± 0.1 °C. Typically, after thermal equilibration for 60 minutes, the images were recorded at the middle layer of microgel assemblies, ~50 μm away from both upper and lower inner walls to minimize perturbations from the glass surface. Andor™ iQ 3.0 software were used to monitor and record the motion of microgels at a recording rate of 30 frames/s. To enable quantification of particle motion, the microgel positions in an image time series acquired via video microscopy were analyzed using a modified version of the particle tracking code originally developed by Crocker and Grier[92] in the IDL 6.0 (ITT Corporation) programming environment.

A particularly illustrative means for presenting the dynamics of microgel particles in those phases is through a double logarithm plot of the microgel mean squared displacement (*MSD*) versus lag time (τ). The *MSD* of colloidal particles in an ensemble is given by

$$MSD(\tau) = \left\langle \left[r_i(t+\tau) - r_i(t) \right]^2 \right\rangle_{i,t} \tag{2-6}$$

where $r_i(t)$ is the position vector of the ith particle at time t, τ is the lag time, and $\langle\rangle_{i,t}$ indicates the spatial average over the ensemble of particles as well as all starting times t. In the colloidal gas regime, where particle motion is purely diffusive and interactions between particles are minimal, the *MSD* should be proportional to lag time,

$$MSD(\tau) = 2dD\tau \tag{2-7}$$

where d is the dimensionality of the displacement vectors and D is the translational self-diffusion coefficient of microgel particles. Very dilute (0.01 wt%) microgel suspensions were tracked by video microscopy to obtain linear *MSD* vs. τ plots; because dilute

dispersion exhibit unhindered diffusion, the translational self-diffusion coefficient *D* could be extracted from the slope of this plot by using the following equation.

$$D = \frac{dMSD(\tau)}{d\tau} / 2d \tag{2-8}$$

Combining this with the Stokes-Einstein equation (2-5) yields an expression from which the unperturbed hydrodynamic diameter (σ) in the dilute regime can be obtained

$$\sigma = \frac{2k_B T}{\pi \eta_S \frac{dMSD(\tau)}{d\tau}} \tag{2-9}$$

where k_B is Boltzmann constant, T absolute temperature, $\frac{dMSD(\tau)}{d\tau}$ the slope of the linear *MSD* vs. τ plot, and η_s the intrinsic viscosity of solvent.

2.2.5.3 Acid-Base Titration

The solid powder of pNIPAm-AAc (16.8 mg) was dissolved in 10 mL deionized water to obtain pNIPAm-AAc microgel dispersions. Standard NaOH aqueous solution (0.1050 N, Aldrich) was used as a titrant. The pH values were measured to ± 0.01 units by a pH meter (pH 430, Corning Corp.) with an Accumet probe (Cole-Palmer). During the titration, pH was measured as the function of the volume of delivered standard NaOH solution. After each 10 μL of titrant was delivered into the pNIPAm-AAc microgel dispersions, followed by magnetic stirring for approximately 10 minutes, the pH value was stable and recorded. The total volume of standard NaOH solution delivered at equivalence point was used to calculate the carboxyl content of pNIPAm-AAc microgels.

2.2.5.4 Electrophoresis

For a charged particle, moving with respect to the solution phase, the potential at the shear surface, with respect to the bulk solution, is usually referred to as the "zeta (ζ) potential".[93] The following scheme demonstrates the concept of ζ potential.

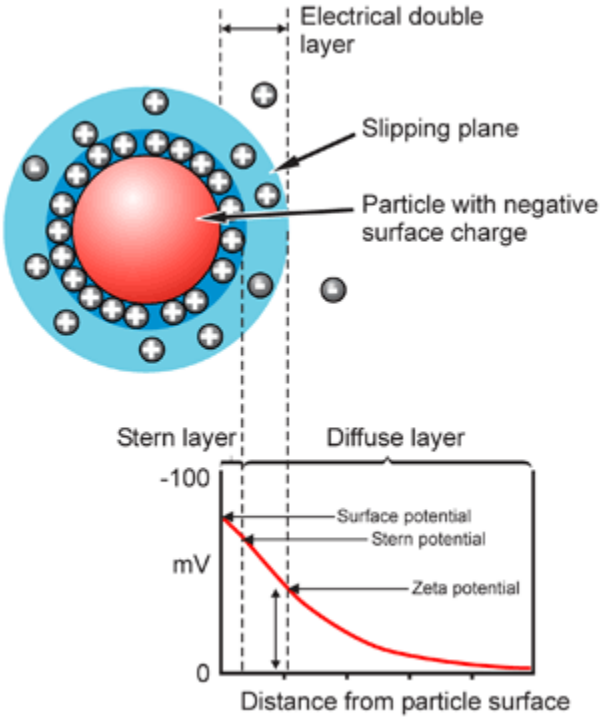

Scheme 2.2 Schematic representation of zeta potential from Malvern Instruments Ltd. (http://www.malvern.com/LabEng/technology/zeta_potential/zeta_potential_LDE.htm)

It is difficult to measure ζ potential directly, and therefore it is estimated indirectly by electrophoresis. In a chamber with parallel oppositely charged electrode, a charged particle is subjected to a uniform electric field E, causing it to move towards the oppositely charged electrode. The particle attains a constant velocity v when the viscous drag force balances the electric force. The velocity v could be used to calculate the electrophoretic mobility μ, which depends on the size, shape, and charge of the particle.

$$v = \mu E \tag{2-10}$$

The electrophoretic mobility μ can be related to the ζ potential using various models.[93] For highly polar solvents such as water, the simplest model relates the zeta potential to the mobility in terms of the viscosity η_s, and the relative permittivity ε_r, of the continuous phase via the Smoluchowski equation,[94]

$$\mu = \frac{\varepsilon_r \varepsilon_0 \zeta}{\eta_s} \tag{2-11}$$

where ε_0 is the permittivity *in vacuo*. The problem then becomes measuring the speed of small particles. The movement of particles can be followed using laser Doppler electrophoresis (LDE). When light is scattered from a moving particle, its frequency will be shifted by an amount depending on the speed and direction of the movement. In the absence of a charge-induced particle flow, the observed frequency broadening is solely due to the Brownian motion of the particles and can be used to calculate the diffusion coefficient and hence hydrodynamic diameter. (Details are shown in Section 2.2.5.1) When an electrical field is applied to a charged particle, its net motion vector becomes a sum of coherent (charge dependant) and incoherent (Brownian motion). The electrical properties of the scattering particle can then be calculated if these terms can be distinguished. In brief, laser Doppler electrophoresis measures small frequency shifts in the scattered light that arise due to the movement of particles in an applied electric field. The frequency shift Δf is equal to

$$\Delta f = \frac{2v\sin(\theta/2)}{\lambda} \tag{2-12}$$

where v is the particle velocity, θ scattering angel, and λ the wavelength of incident light. However, the signal (coherent) to noise (incoherent) ratio becomes progressively smaller for low mobility particles. The charge-induced movement of the particles could be increased, and therefore be more easily measured, by increasing the time they are exposed to the voltage gradient or increasing the magnitude of that gradient. Unfortunately long experiments can lead to an accumulation of particles at one of the electrodes and high voltages can lead to Joule heating—either effect would disrupt measurement. Until recently these limitations made measurement of the charge of low mobility colloids extremely difficult. In phase analysis light scattering (PALS), a laser beam is split, a frequency modulation is applied to a portion of the light and it is then used to generate a scattering pattern from a suspension of particles. The scattered light is recombined with the original (unmodulated) beam. Light scattered from even a stationary

particle by a phase modulated laser beam will have a finite, measurable, Doppler frequency equal to the frequency of the modulation. If the particle moves in the applied voltage gradient, the relative phase will shift, and can be detected by a phase comparator. The phase comparison takes place over many cycles and hence, the frequency shifts can be measured accurately,[95] thereby allowing calculation of ζ potential using Smoluchowski equation.

A Malvern Zetasizer based upon PALS was used to determine the ζ potential of pNIPAm-AAc microgel particles in the very dilute regime (0.0002 wt%) at 20 °C. Before the measurements, the 1-mL pNIPAm-AAc dispersion in designated buffer was thermally equilibrated between parallel electrodes in cuvette for 60 min. Only one run was conducted for each sample, each run containing 20 measurements, each measurement taking 10 s. The ζ potential of pNIPAm-AAc microgels at different pH values was calculated via Smoluchowski equation by software.

2.3 Results and Discussions

2.3.1 Thermoresponsivity

All pNIPAm-AAc microgel particles are thermo- and pH-responsive. For pNIPAm-AAc particles with diameter no more than 2.5 μm, it is possible to determine their size via photo correlation spectroscopy (PCS), also called dynamic light scattering (DLS). (Calculation details are shown in Section 2.2.5.1.) For pNIPAm-AAc particles with diameter above 2.5 μm, particle tracking technique via video microscopy could be used to determine the particle diameter. (Calculation details are shown in Section 2.2.5.2) Figure 2.1 presents the thermo-responsivity of pNIPAm-AAc microgel particles (0.002 wt% of polymer in pH 3.0 buffer). The lower critical solution temperature (LCST) for pNIPAm-AAc microgel particles at pH 3.0 buffer is approximately 30~31 ºC, which is lower than that of pNIPAm microgels (32~33 ºC).[13]

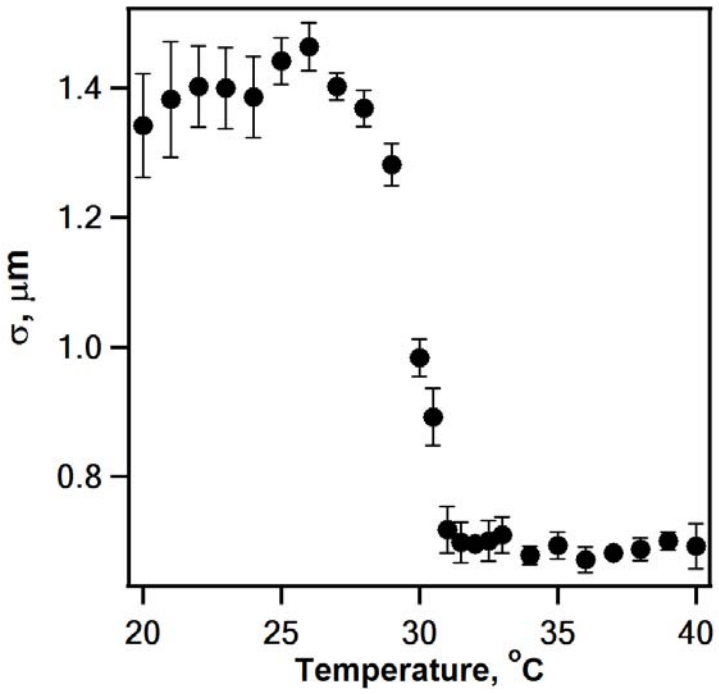

Figure 2.1 The hydrodynamic diameter (σ) of pNIPAm-AAc microgel particles measured by dynamic light scattering at 0.002 wt% in pH 3.0 buffer with temperature ranging from 20 to 40 °C. The LCST is approximately 30~31 ºC.

2.3.2 pH-Responsivity

At pH below pK_a of AAc moieties, the protonation of AAc monomers induce weakly attractive interaction (stickiness) between particles and borosilicate glass surface probably due to hydrogen bonding between carboxyl groups on microgels and hydroxyl groups on glass slides, thereby leading to the irreversible adsorption of pNIPAm-AAc particles on the glass surface in the rectangular capillaries. Figure 2.2 presents the irreversible adsorption of pNIPAm-AAc microgel particles on the glass surface at pH 3.0 buffer.

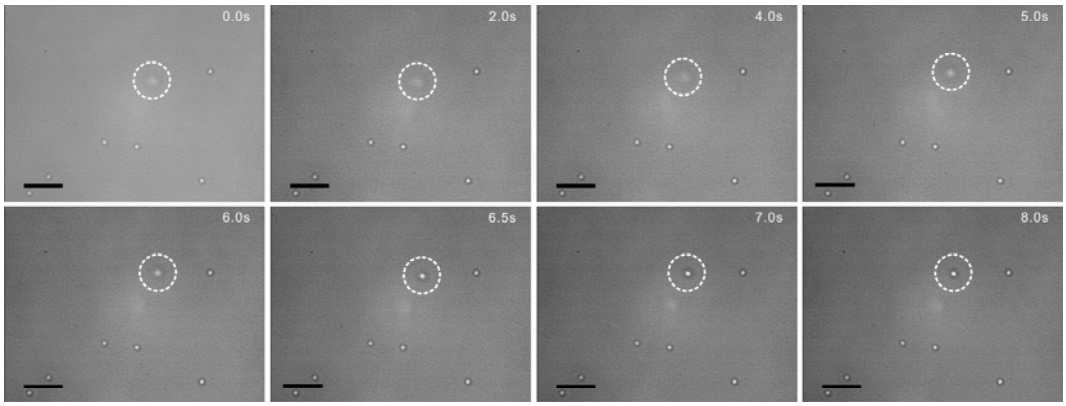

Figure 2.2 Microscopic images of the irreversible adsorption of pNIPAm-AAc microgel particles (0.01 wt% dispersion) to a glass surface (inner surface of a capillary) in a pH = 3.0, I = 10 mM aqueous buffer. The *in situ* recording of the adsorption is a strong evidence of the stickiness of pNIPAm-AAc microgel particles. Note the presence of multiple particles that have already adhered to the glass. Scale bar = 10 μm.

With the increment of pH values of buffer in which pNIPAm-AAc microgel particles are dispersed, the unperturbed hydrodynamic diameter (σ) of particles increase significantly with a size jump at pH close to pK_a (~4.25) of AAc monomers. The increment of pH value leads to the increasing degree of deprotonation of AAc monomers, thereby reducing the hydrogen bonding between carboxylic acid and/or amide groups and increasing the electrostatic repulsion between anionic carboxylate groups and osmotic pressure of microgels. Hence, the average hydrodynamic diameter of pNIPAm-AAc microgel particles increases, thereby reducing the refractive indices of particles and van der Waals attractions between particles. Furthermore, the deprotonation of AAc moieties disrupt the possible hydrogen bonding between carboxyl groups and hydroxyl groups on glass surface of capillaries. Thus at higher pH values such as pH 5.0, no pNIPAm-AAc particles were adsorbed to the inner wall of capillaries. Figure 2.3 demonstrate the increase of unperturbed hydrodynamic diameter of pNIPAm-AAc microgel particles with the increase of pH values under the same ionic strength.

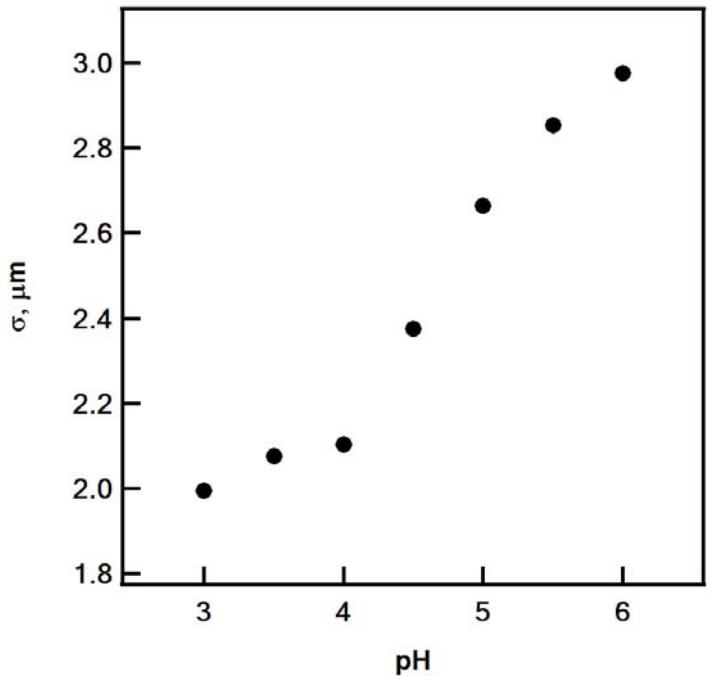

Figure 2.3 The hydrodynamic diameter (σ) of pNIPAm-AAc microgel particles measured by particle tracking via video microscopy at 0.01 wt% in buffers with pH values ranging from 3.0 to 6.0 at 20 °C.

2.3.3 Acid-Base Titration

Acid-base titration was used to determine the amount of AAc in copolymeric microgels based on the neutralization of carboxylic acid by hydroxide. Figure 2.4 demonstrated the acid-base titration curve of pNIPAm-AAc microgel dispersions titrated by standard NaOH aqueous solution (0.0105N). It is noticed that the pH jump from 8.3 up to 8.9 when approximately 1.72 mL standard NaOH solution was delivered to pNIPAm-AAc dispersions. We already know the weight of pNIPAm-AAc polymer powders for preparation of dispersions, so the content of AAc in pNIPAm-AAc powder is calculated as follows,

$$\frac{n_{AAc}}{w_{pNIPAm-AAc}} = \frac{1.72mL \times 0.0105N}{0.0168g} = \frac{0.01806mmol}{0.0168g} = 1.075mmol/g$$

Approximately 77.5 mg of AAc was incorporated in 1 g of pNIPAm-AAc powders via copolymerization, which is lower than the feed ratio, approximately 96.2 mg of AAc in 1

g of pNIPAm-AAc polymer, due to the loss of oligomers, coagulum, and monomers during the polymerization and purification process.

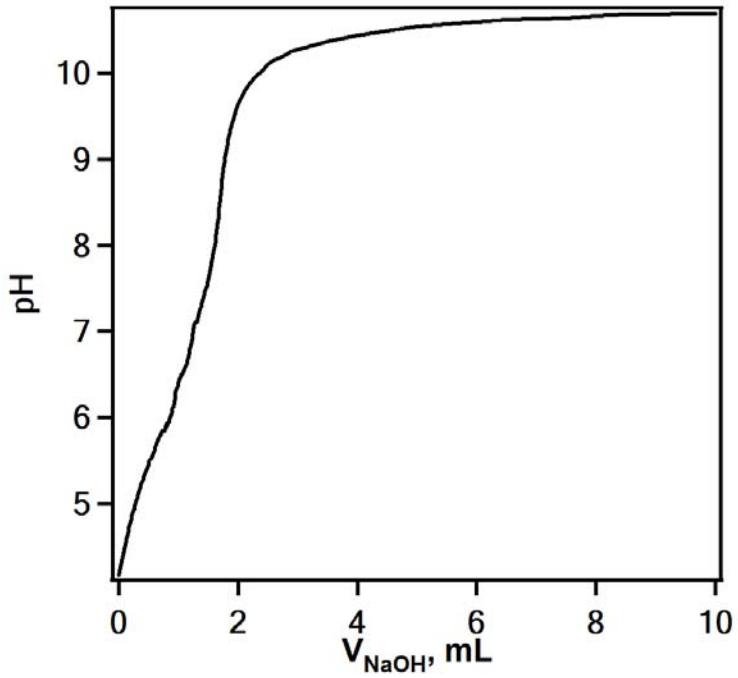

Figure 2.4 The acid-base titration curve of pNIPAm-AAc microgel dispersion (16.8 mg polymer powder dispersed in 10 mL deionized water) titrated by 0.0105 N NaOH standard solution at room temperature. Note that the pH value jumps from 8.3 to 8.9 when the delivered volume of NaOH solution (V_{NaOH}) is approximately 1.72 mL.

2.3.4 Electrophoresis

According to classical DLVO theory,[76,77] the magnitude of the stabilizing force is proportional to surface charge.[93] The measurement of charge properties is clearly important in any attempt to estimate electrostatic interactions between microgel particles. Phase analysis light scattering (PALS) was used to determine the ζ potential of pNIPAm-AAc microgel dispersions at different pH values. Figure 2.5 shows the change of ζ potential with the increase of pH values. Because of the anionic carboxylate and sulfate groups on the surface of pNIPAm-AAc microgel particles, the ζ potential of particles are negative. With the increment of pH, the deprotonation of carboxylic acid leads to more

anionic carboxylate groups, thereby increasing the absolute value of ζ potential. However, when pH reach 5.5, the ζ potential of particles reach a plateau, probably indicating that the majority of carboxylic acid groups have been deprotonated at that pH.

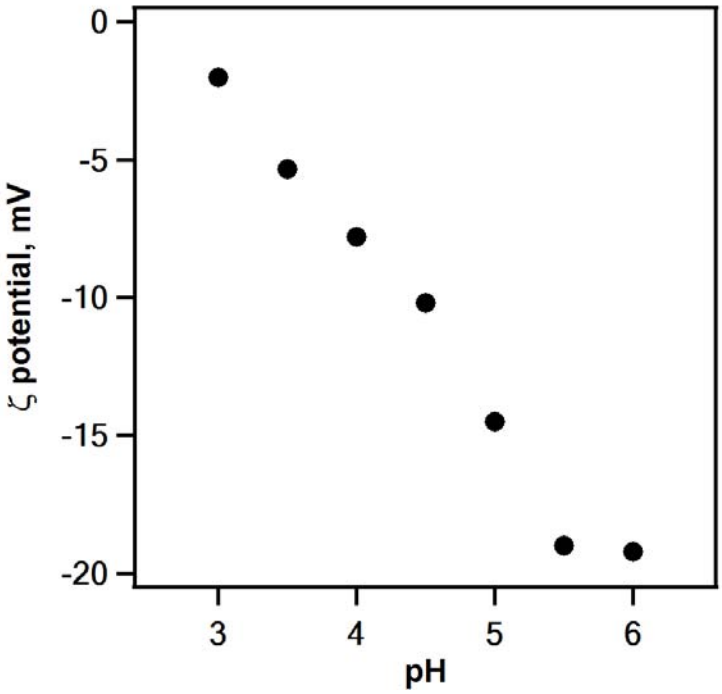

Figure 2.5 The ζ potential of pNIPAm-AAc microgel particles (0.0002 wt%) in buffers from pH 3.0 to 6.0 at 20 ºC. With increasing pH, the absolute value of the ζ potential increases due to deprotonation of AAc units on the microgels.

2.3.5 The Effect of Synthesis Temperature

To explore the effect of temperature during copolymerization on the microgel yield and particle size, the copolymerization of NIPAm and AAc with molar ratio of 85:15 was conducted at temperature including 45, 50, 55, 60, 65, and 70 °C. (The synthesis, purification and lyophilization protocols are referred to Section 2.2.2.) Particle tracking are used to determine the unperturbed hydrodynamic diameter of microgel particles in pH 3.5 buffer. The temperature used for synthesis significantly influences the yield and the diameter of microgel particles. With the increase of temperature for particle

synthesis, pNIPAm-AAc microgel particles become smaller with higher yieldz as shown in Figure 2.6, which agree with other experimental results.[96]

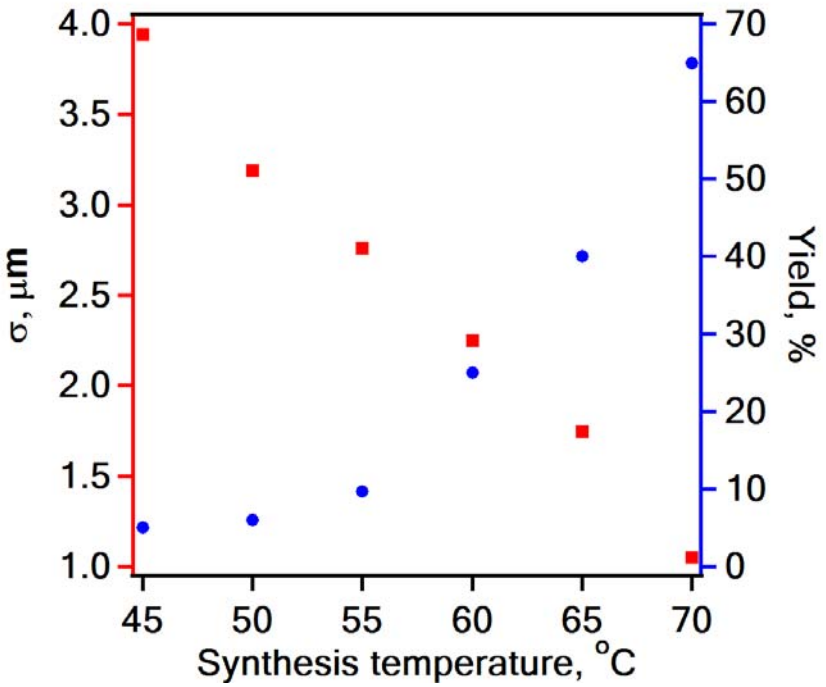

Figure 2.6 The effect of synthesis temperature on the yield and particle size of microgels. The left vertical axis represents the unperturbed hydrodynamic diameter (red filled square, ■) of pNIPAm-AAc microgel particles synthesized at different temperatures, 0.01 wt% in pH 3.5 buffer measured by particle tracking. The right vertical axis represents the overall yield of pNIPAm-AAc microgel powders after lyophilization (blue filled circle, ●) for pNIPAm-AAc synthesis at different temperatures.

2.4 Conclusions

Copolymeric microgels composed of NIPAm and AAc was obtained via one-pot ammonium persulfate-initiated surfactant-free precipitation radical polymerization at fixed temperatures. Copolymeric pNIPAm-AAc microgel particles are both thermo-responsive and pH-responsive. The lower critical solution temperature (LCST) of pNIPAm-AAc microgels is approximately 30~31 °C, lower than that of pNIPAm microgels (32~33 °C). It is clear that when the temperature crosses the LCST of pNIPAm-AAc microgels, the volume of microgel particle decrease approximately 10

folds. In addition to thermoresponsivity, pNIPAm-AAc microgel particles are pH-responsive, with hydrodynamic diameters increasing with pH values, displaying a jump as pH crossover pK_a of AAc moieties. Finally, the synthesis temperature used for copolymerization of NIPAm and AAc is the key factor to dictate both the yield and particle size of particles. Our results show that, with the increase of synthetic temperature, microgel yields increase whereas the size of microgels decreases.

References

(1) Schild, H. G. Poly(*N*-isopropylacrylamide): Experiment, theory and application, *Prog. Polym. Sci.* **1992**, *17*, 163-249.

(2) Pelton, R. Temperature-sensitive aqueous microgels, *Adv. Colloid Interface Sci.* **2000**, *85*, 1-33.

(3) Snowden, M. J.; Chowdhry, B. Z.; Vincent, B.; Morris, G. E. Colloidal copolymer microgels of N-isopropylacrylamide and acrylic acid: pH, ionic strength and temperature effects, *J. Chem. Soc., Faraday Trans.* **1996**, *92*, 5013-5016.

(4) Pichot, C.; Elaissari, A.; Duracher, D.; Meunier, F.; Sauzedde, F. Hydrophilic stimuli-responsive particles for biomedical applications, *Macromol. Symp.* **2001**, *175*, 285-297.

(5) Ishikura, S.; Ishii, K.; Midzuguchi, R. Flow and film properties of coatings containing microgels, *Prog. Org. Coat.* **1988**, *15*, 373-387.

(6) Kim, J.; Nayak, S.; Lyon, L. A. Bioresponsive hydrogel microlenses, *J. Am. Chem. Soc.* **2005**, *127*, 9588-9592.

(7) Lapeyre, V.; Ancla, C.; Catargi, B.; Ravaine, V. Glucose-responsive microgels with a core-shell structure, *J. Colloid Interface Sci.* **2008**, *327*, 316-323.

(8) Ulijn, R. V.; Bibi, N.; Jayawarna, V.; Thornton, P. D.; Todd, S. J.; Mart, R. J.; Smith, A. M.; Gough, J. E. Bioresponsive hydrogels, *Mater. Today* **2007**, *10*, 40-48.

(9) Lynch, I.; de Gregorio, P.; Dawson, K. A. Simultaneous release of hydrophobic and cationic solutes from thin-film "plum-pudding" gels: A multifunctional platform for surface drug delivery?, *J. Phys. Chem. B* **2005**, *109*, 6257-6261.

(10) Murthy, N.; Xu, M. C.; Schuck, S.; Kunisawa, J.; Shastri, N.; Frechet, J. M. J. A macromolecular delivery vehicle for protein-based vaccines: Acid-degradable protein-loaded microgels, *Proc. Natl. Acad. Sci. U. S. A.* **2003**, *100*, 4995-5000.

(11) Lopez, V. C.; Hadgraft, J.; Snowden, M. J. The use of colloidal microgels as a (trans)dermal drug delivery system, *Int. J. Pharm.* **2005**, *292*, 137-147.

(12) Vinogradov, S. V.; Bentham Science Publ Ltd: 2006, p 4703-4712.

(13) Pelton, R. H.; Chibante, P. Preparation of aqueous lattices with *N*-isopropylacrylamide, *Colloids Surf.* **1986**, *20*, 247-256.

(14) Pinkrah, V. T.; Beezer, A. E.; Chowdhry, B. Z.; Gracia, L. H.; Mitchell, J. C.; Snowden, M. J. Thermodynamic considerations of microgel swelling behavior, *Langmuir* **2004**, *20*, 8531-8536.

(15) Arleth, L.; Xia, X. H.; Hjelm, R. P.; Wu, J. Z.; Hu, Z. B. Volume transition and internal structures of small poly(N-isopropylacrylamide) microgels, *J. Polym. Sci. Polym. Phys.* **2005**, *43*, 849-860.

(16) Tuncel, A.; Ecevit, K.; Kesenci, K.; Piskin, E. Nonswellable and swellable ethylene glycol dimethacrylate-acrylic acid copolymer microspheres, *J. Polym. Sci. Polym. Chem.* **1996**, *34*, 45-55.

(17) Qiu, Y.; Park, K. Environment-sensitive hydrogels for drug delivery, *Adv. Drug Deliv. Rev.* **2001**, *53*, 321-339.

(18) Nolan, C. M.; Serpe, M. J.; Lyon, L. A. Pulsatile release of insulin from Layer-by-Layer assembled microgel thin films, *Macromol. Symp.* **2005**, *227*, 285-294.

(19) Das, M.; Zhang, H.; Kumacheva, E. Microgels: Old materials with new applications, *Ann. Rev. Mater. Res.* **2006**, *36*, 117-142.

(20) Zhang, H.; Mardyani, S.; Chan, W. C. W.; Kumacheva, E. Design of biocompatible chitosan microgels for targeted pH-mediated intracellular release of cancer therapeutics, *Biomacromolecules* **2006**, *7*, 1568-1572.

(21) Blackburn, W. H.; Lyon, L. A. Size-controlled synthesis of monodisperse core/shell nanogels, *Colloid Polym. Sci.* **2008**, *286*, 563-569.

(22) Dai, S.; Ravi, P.; Tam, K. C. pH-Responsive polymers: synthesis, properties and applications, *Soft Matter* **2008**, *4*, 435-449.

(23) Oh, J. K.; Drumright, R.; Siegwart, D. J.; Matyjaszewski, K. The development of microgels/nanogels for drug delivery applications, *Prog. Polym. Sci.* **2008**, *33*, 448-477.

(24) Teng, D. Y.; Hou, J. L.; Zhang, X. G.; Wang, X.; Wang, Z.; Li, C. X. Glucosamine-carrying temperature- and pH-sensitive microgels: Preparation, characterization, and in vitro drug release studies, *J. Colloid Interface Sci.* **2008**, *322*, 333-341.

(25) Shipway, A. N.; Katz, E.; Willner, I. Nanoparticle arrays on surfaces for electronic, optical, and sensor applications, *ChemPhysChem* **2000**, *1*, 18-52.

(26) Zhang, J. G.; Xu, S. Q.; Kumacheva, E. Polymer microgels: Reactors for semiconductor, metal, and magnetic nanoparticles, *J. Am. Chem. Soc.* **2004**, *126*, 7908-7914.

(27) Kratz, K.; Hellweg, T.; Eimer, W. Effect of connectivity and charge density on the swelling and local structural and dynamic properties of colloidal PNIPAM microgels, *Ber. Bunsenges. Phys. Chem.* **1998**, *102*, 1603-1608.

(28) Lin, C. L.; Chiu, W. Y.; Lee, C. F. Preparation, morphology, and thermoresponsive properties of poly(N-isopropylacrylamide)-based copolymer microgels, *J. Polym. Sci. Polym. Chem.* **2006**, *44*, 356-370.

(29) Zhou, S. Q.; Chu, B. Synthesis and volume phase transition of poly(methacrylic acid-co-N-isopropylacrylamide) microgel particles in water, *J. Phys. Chem. B* **1998**, *102*, 1364-1371.

(30) Ito, S.; Ogawa, K.; Suzuki, H.; Wang, B. L.; Yoshida, R.; Kokufuta, E. Preparation of thermosensitive submicrometer gel particles with anionic and cationic charges, *Langmuir* **1999**, *15*, 4289-4294.

(31) Routh, A. E.; Vincent, B. Some anomalous effects of sodium ions on the electrophoretic mobility and heteroaggregation of microgel particles, *J. Colloid Interface Sci.* **2004**, *273*, 435-441.

(32) Das, M.; Kumacheva, E. From polyelectrolyte to polyampholyte microgels: comparison of swelling properties, *Colloid Polym. Sci.* **2006**, *284*, 1073-1084.

(33) Gao, J.; Frisken, B. J. Influence of secondary components on the synthesis of self-cross-linked N-isopropylacrylamide microgels, *Langmuir* **2005**, *21*, 545-551.

(34) Cao, L. Q.; Chen, L. P. Influence of reaction parameters on synthesis of temperature-sensitive materials in supercritical carbon dioxide by precipitation polymerization, *Polym. Bull.* **2006**, *57*, 651-659.

(35) Cai, W. S.; Gupta, R. B. Fast-responding bulk hydrogels with microstructure, *J. Appl. Polym. Sci.* **2002**, *83*, 169-178.

(36) Alvarez-Lorenzo, C.; Concheiro, A. Reversible adsorption by a pH- and temperature-sensitive acrylic hydrogel, *J. Control. Release* **2002**, *80*, 247-257.

(37) Kim, J.; Deike, I.; Dingenouts, N.; Norhausen, C.; Ballauff, M. The volume transition in thermosensitive core-shell latex particles investigated by small-angle X-ray scattering and dynamic light scattering, *Macromol. Symp.* **1999**, *142*, 217-225.

(38) Tsuji, S.; Kawaguchi, H. Temperature-sensitive hairy particles prepared by living radical graft polymerization, *Langmuir* **2004**, *20*, 2449-2455.

(39) Jones, C. D.; Lyon, L. A. Synthesis and characterization of multiresponsive core-shell microgels, *Macromolecules* **2000**, *33*, 8301-8306.

(40) Jones, C. D.; Lyon, L. A. Shell-restricted swelling and core compression in poly(N-isopropylacrylamide) core-shell microgels, *Macromolecules* **2003**, *36*, 1988-1993.

(41) Jones, C. D.; Lyon, L. A. Dependence of shell thickness on core compression in acrylic acid modified poly(N-isopropylacrylamide) core/shell microgels, *Langmuir* **2003**, *19*, 4544-4547.

(42) Khan, A. Preparation and characterization of N-isopropylacrylamide/acrylic acid copolymer core-shell microgel particles, *J. Colloid Interface Sci.* **2007**, *313*, 697-704.

(43) Quan, C. Y.; Wei, H.; Sun, Y. X.; Cheng, S. X.; Shen, K.; Gu, Z. W.; Zhang, X. Z.; Zhuo, R. X. Polyethyleneimine modified biocompatible poly(N-isopropylacrylamide)-based nanogels for drug delivery, *J. Nanosci. Nanotechnol.* **2008**, *8*, 2377-2384.

(44) Xia, X. H.; Hu, Z. B. Synthesis and light scattering study of microgels with interpenetrating polymer networks, *Langmuir* **2004**, *20*, 2094-2098.

(45) Zhou, J.; Wang, G. N.; Zou, L.; Tang, L. P.; Marquez, M.; Hu, Z. B. Viscoelastic behavior and in vivo release study of microgel dispersions with inverse thermoreversible gelation, *Biomacromolecules* **2008**, *9*, 142-148.

(46) Singh, N.; Lyon, L. A. Synthesis of multifunctional nanogels using a protected macromonomer approach, *Colloid Polym. Sci.* **2008**, *286*, 1061-1069.

(47) Greinert, N.; Richtering, W. Influence of polyelectrolyte multilayer adsorption on the temperature sensitivity of poly(N-isopropylacrylamide) (PNiPAM) microgels, *Colloid Polym. Sci.* **2004**, *282*, 1146-1149.

(48) Suzuki, D.; Tsuji, S.; Kawaguchi, H. Janus microgels prepared by surfactant-free pickering emulsion-based modification and their self-assembly, *J. Am. Chem. Soc.* **2007**, *129*, 8088-8089.

(49) Zhang, H.; Tumarkin, E.; Sullan, R. M. A.; Walker, G. C.; Kumacheva, E. Exploring microfluidic routes to microgels of biological polymers, *Macromol. Rapid Commun.* **2007**, *28*, 527-538.

(50) Bhaskar, S.; Roh, K. H.; Jiang, X. W.; Baker, G. L.; Lahann, J. Spatioselective Modification of Bicompartmental Polymer Particles and Fibers via Huisgen 1,3-Dipolar Cycloaddition, *Macromol. Rapid Commun.* **2008**, *29*, 1655-1660.

(51) Morris, G. E.; Vincent, B.; Snowden, M. J. Adsorption of lead ions onto N-isopropylacrylamide and acrylic acid copolymer microgels, *J. Colloid Interface Sci.* **1997**, *190*, 198-205.

(52) Greenwood, R.; Kendall, K.; Ritchie, S.; Snowden, M. J. The use of poly (N-isopropylacrylamide) microgels as a multi-functional processing aid for aqueous alumina suspensions, *J. Eur. Ceram. Soc.* **2000**, *20*, 1707-1716.

(53) Bradley, M.; Ramos, J.; Vincent, B. Equilibrium and kinetic aspects of the uptake of poly(ethylene oxide) by copolymer microgel particles of N-isopropylacrylamide and acrylic acid, *Langmuir* **2005**, *21*, 1209-1215.

(54) Martinez-Rubio, M. I.; Ireland, T. G.; Fern, G. R.; Silver, J.; Snowden, M. J. A new application for microgels: Novel method for the synthesis of spherical particles of the Y2O3 : Eu phosphor using a copolymer microgel of NIPAM and acrylic acid, *Langmuir* **2001**, *17*, 7145-7149.

(55) Kim, J. H.; Lee, T. R. Thermo- and pH-responsive hydrogel-coated gold nanoparticles, *Chem. Mat.* **2004**, *16*, 3647-3651.

(56) Kim, J. H.; Lee, T. R. Discrete thermally responsive hydrogel-coated gold nanoparticles for use as drug-delivery vehicles, *Drug Dev. Res.* **2006**, *67*, 61-69.

(57) Kim, J. H.; Lee, T. R. Hydrogel-templated growth of large gold nanoparticles: Synthesis of thermally responsive hydrogel-nanoparticle composites, *Langmuir* **2007**, *23*, 6504-6509.

(58) Dong, Y.; Ma, Y.; Zhai, T. Y.; Zeng, Y.; Fu, H. B.; Yao, J. N. Incorporation of Gold Nanoparticles Within Thermoresponsive Microgel Particles: Effect of Crosslinking Density, *J. Nanosci. Nanotechnol.* **2008**, *8*, 6283-6289.

(59) Dong, Y.; Ma, Y.; Zhai, T. Y.; Shen, F. G.; Zeng, Y.; Fu, H. B.; Yao, J. N. Silver nanoparticles stabilized by thermoresponsive microgel particles: Synthesis and

evidence of an electron donor-acceptor effect, *Macromol. Rapid Commun.* **2007**, *28*, 2339-2345.

(60) Yang, J. X.; Fang, Y.; Bai, C. L.; Hu, D. D.; Zhang, Y. CuS-poly (N-isopropylacrylamide-co-acrylic acid) composite microspheres with patterned surface structures: preparation and characterization, *Chin. Sci. Bull.* **2004**, *49*, 2026-2032.

(61) Wang, G. Z.; Zhang, Y.; Fang, Y.; Gu, Z. Z. Flower-like SiO_2-coated polymer/Fe_3O_4 composite microspheres of super-paramagnetic properties: Preparation via a polymeric microgel template method, *J. Am. Ceram. Soc.* **2007**, *90*, 2067-2072.

(62) Li, J.; Liu, B.; Li, J. H. Controllable self-assembly of CdTe/poly(N-isopropylacrylamide acrylic acid) microgels in response to pH stimuli, *Langmuir* **2006**, *22*, 528-531.

(63) Saunders, B. R.; Crowther, H. M.; Morris, G. E.; Mears, S. J.; Cosgrove, T.; Vincent, B. Factors affecting the swelling of poly(N-isopropylacrylamide) microgel particles: fundamental and commercial implications, *Colloids Surf. A* **1999**, *149*, 57-64.

(64) Suzuki, H.; Wang, B. L.; Yoshida, R.; Kokufuta, E. Potentiometric titration behaviors of a polymer and gel consisting of N-isopropylacrylamide and acrylic acid, *Langmuir* **1999**, *40*, 4283-4288.

(65) Christensen, M. L.; Keiding, K. Study of the compositional heterogeneity in poly (N-isopropylacrylamide-acrylic acid) microgels by potentiometric titration experiments, *Colloids Surf. A* **2005**, *252*, 61-69.

(66) Kratz, K.; Hellweg, T.; Eimer, W. Influence of charge density on the swelling of colloidal poly(N-isopropylacrylamide-co-acrylic acid) microgels, *Colloids Surf. A* **2000**, *170*, 137-149.

(67) Makino, K.; Kado, H.; Ohshima, H. Aggregation behavior of poly(N-isopropylacrylamide) microspheres, *Colloids Surf. B* **2001**, *20*, 347-353.

(68) Hoare, T.; McLean, D. Multi-component kinetic modeling for controlling local compositions in thermosensitive polymers, *Macromol. Theory Simul.* **2006**, *15*, 619-632.

(69) Hoare, T.; Pelton, R. Functional group distributions in carboxylic acid containing poly(N-isopropylacrylamide) microgels, *Langmuir* **2004**, *20*, 2123-2133.

(70) Hoare, T.; Pelton, R. Impact of microgel morphology on functionalized microgel-drug interactions, *Langmuir* **2008**, *24*, 1005-1012.

(71) Hoare, T.; Pelton, R. Electrophoresis of functionalized microgels: morphological insights, *Polymer* **2005**, *46*, 1139-1150.

(72) Hoare, T.; Pelton, R. Titrametric characterization of pH-induced phase transitions in functionalized microgels, *Langmuir* **2006**, *22*, 7342-7350.

(73) Jeenanong, A.; Kawaguchi, H. Effect of pH and temperature on the behavior of microgel in SPR sensor, *Colloids Surf. A* **2008**, *315*, 232-240.

(74) Schmidt, S.; Motschmann, H.; Hellweg, T.; von Klitzing, R. Thermoresponsive surfaces by spin-coating of PNIPAM-co-PAA microgels: A combined AFM and ellipsometry study, *Polymer* **2008**, *49*, 749-756.

(75) Woodward, N. C.; Snowden, M. J.; Chowdhry, B. Z.; Jenkins, P.; Larson, I. Measurement of the interaction forces between poly(N-isopropylacrylamide-acrylic acid) microgel and silica surfaces by colloid probe microscopy, *Langmuir* **2002**, *18*, 2089-2095.

(76) Derjaguin, B. V.; Landau, L. D. Theory of stability of strongly charged lyophobic sols and adhesion of strongly charged particles in solution of electrolytes, *Acta Physicochim. URSS* **1941**, *14*, 633-662.

(77) Verwey, E. J. W.; Overbeek, H. N. W. *Theory of the stability of lyophobic colloids*; Elsevier: Amsterdam, 1948.

(78) Wiedemair, J.; Serpe, M. J.; Kim, J.; Masson, J. F.; Lyon, L. A.; Mizaikoff, B.; Kranz, C. In-situ AFM studies of the phase-transition behavior of single thermoresponsive hydrogel particles, *Langmuir* **2007**, *23*, 130-137.

(79) Lee, C. F.; Lin, C. C.; Chiu, W. Y. Thermosensitive and control release behavior of poly (N-isopropylacrylamide-co-acrylic acid) latex particles, *J. Polym. Sci. Polym. Chem.* **2008**, *46*, 5734-5741.

(80) Huo, D. X.; Li, Y. N.; Qian, Q. W.; Kobayashi, T. Temperature-pH sensitivity of bovine serum albumin protein-microgels based on cross-linked poly(N-isopropylacrylamide-co-acrylic acid), *Colloids Surf. B* **2006**, *50*, 36-42.

(81) Choi, S. H.; Yoon, J. J.; Park, T. G. Galactosylated poly(N-isopropylacrylamide) hydrogel submicrometer particles for specific cellular uptake within hepatocytes, *J. Colloid Interface Sci.* **2002**, *251*, 57-63.

(82) Kim, J. S.; Singh, N.; Lyon, L. A. Displacement-induced switching rates of bioresponsive hydrogel microlenses, *Chem. Mat.* **2007**, *19*, 2527-2532.

(83) Nerapusri, V.; Keddie, J. L.; Vincent, B.; Bushnak, I. A. Swelling and deswelling of adsorbed microgel monolayers triggered by changes in temperature, pH, and electrolyte concentration, *Langmuir* **2006**, *22*, 5036-5041.

(84) Nolan, C. M.; Serpe, M. J.; Lyon, L. A. Thermally modulated insulin release from microgel thin films, *Biomacromolecules* **2004**, *5*, 1940-1946.

(85) Serpe, M. J.; Yarmey, K. A.; Nolan, C. M.; Lyon, L. A. Doxorubicin uptake and release from microgel thin films, *Biomacromolecules* **2005**, *6*, 408-413.

(86) Kim, J.; Singh, N.; Lyon, L. A. Influence of ancillary binding and nonspecific adsorption on bioresponsive hydrogel microlenses, *Biomacromolecules* **2007**, *8*, 1157-1161.

(87) Zhang, Y. J.; Guan, Y.; Zhou, S. Q. Synthesis and volume phase transitions of glucose-sensitive microgels, *Biomacromolecules* **2006**, *7*, 3196-3201.

(88) Zhang, Y. J.; Guan, Y.; Zhou, S. Q. Permeability control of glucose-sensitive nanoshells, *Biomacromolecules* **2007**, *8*, 3842-3847.

(89) Agbugba, C. B.; Hendriksen, B. A.; Chowdhry, B. Z.; Snowden, M. J. The redispersibility and physico-chemical properties of freeze-dried colloidal microgels, *Colloids Surf. A* **1998**, *137*, 155-164.

(90) Beynon, R. Buffer Calculator *http://www.liv.ac.uk/buffers*, 2008

(91) Koppel, D. E. Analysis of macromolecular polydispersity in intensity correlation spectroscopy: The method of cumulants, *J. Chem. Phys.* **1972**, *57*, 4814-4820.

(92) Crocker, J. C.; Grier, D. G. Methods of digital video microscopy for colloidal studies, *J. Colloid Interface Sci.* **1996**, *179*, 298-310.

(93) Hunter, R. J. *Foundations of Colloid Science*; 2nd ed.; Oxford University Press: Oxford, Great Britain, 2001.

(94) Smoluchowski, M. v. *Handbuch der Electrizität und des Magnetismus*; Barth: Leipzig, 1921; Vol. 2.

(95) Vanapalli, S.; Coupland, J. N. Characterization of food colloids by phase analysis light scattering, *Food Hydrocolloids* **2000**, *14*, 315-317.

(96) Goodwin, J. W.; Ottewill, R. H.; Pelton, R.; Vianello, G.; Yates, D. E. Control of particle size in the formation of polymer latices, *Br. Polym. J.* **1978**, *10*, 173-180.

CHAPTER 3

TEMPERATURE-PROGRAMMED SYNTHESIS OF LARGE MULTI-RESPONSIVE MICROGELS

This chapter describes the synthesis and characterization of large multi-responsive pNIPAm-AAc microgel particles with hydrodynamic diameter ranging from 2.5 to 5 μm via temperature-ramp synthesis protocols, and the part of this chapter is excerpted from my paper published in Colloid and Polymer Science.[1] The correlation of reaction temperature with hydrodynamic diameter and yield of microgel particles has been presented in Chapter 2. Inspired by synthesis temperature-particle size correlation, the temperature-programmed approach was employed for pNIPAm-AAc microgel synthesis to increase particle size while maintaining high yield and low polydispersities.

3.1 Introduction

Microgel particles, similar to their hard-sphere counterparts, can be used as a soft-sphere model for the investigation of colloidal dispersions. Particle size control in free radical precipitation polymerization may be accomplished by changing a variety of reaction conditions, including the solvent composition,[2] monomer/comonomer concentration,[3] and degree of cross-linking.[2,4-6] It has been shown that the reaction temperature will dictate particle size in literature. For instance, the surfactant-free precipitation polymerization of thermo/pH responsive poly(*N*-isopropylacrylamide-*co*-acrylic acid) (pNIPAm-AAc) microgels at ~70 °C typically produces particles with diameters of 1 μm or lower.[7,8] The addition of surfactant may further reduce particle size to the sub-100 nm range, resulting in particles often referred to as nanogels.[9] Although 250 nm to 2.5 μm particles (minigels) may be obtained via inverse emulsion polymerization, fairly high polydispersities often result.[10-12] Alternatively, very large polymeric beads (5 to 100 μm) may be synthesized through suspension polymerization.[13]

The direct observation of colloidal dispersions requires that the colloidal particles with a diameter much larger than the size of pixels. However, most microgels have a

diameter close or slightly larger than pixel size (< 2 μm),[7,14] making the imaging of the dynamics of microgels quite difficult, if not impossible. On the other hand, if particle size is too large (> 5 μm), the sedimentation of particles due to gravitational field could complicate the dynamics of particles.[15] Thus the synthetic protocol of microgels for microscopic imaging requires controlling the resultant size of the particles while maintaining low size polydispersities. Therefore, we need to make colloidal particles with a size from 2 to 5 μm, which not only fill the size gap for microgel particles, but also provide microgel particles with the size suitable for microscopic imaging.[1]

3.2 Experimental

3.2.1 Materials

All reagents, materials, and water were purchased and/or prepared as previously described in the Chapter 2, Section 2.2.1 unless otherwise specified.

3.2.2 Microgel Synthesis, Purification, and Lyophilization

3.2.2.1 Temperature-Programmed Synthesis of Large pNIPAm-AAc Microgels

Microgels composed of pNIPAm-AAc with a size from 2 to 5 μm were synthesized via temperature-ramp surfactant-free radical precipitation polymerization. In a typical synthesis, the monomers NIPAm (1.8 g) and AAc (0.2 g), and the cross-linker BIS (0.06 g) were dissolved in 100 mL of distilled, deionized water and filtered through an in-line 0.8-μm filter to remove particulate matter. Deionized water (25 mL) was used to transfer and wash throughout filtration. After delivering the monomer solution to a 250 mL three-neck round-bottom flask via a 20-mL syringe through an in-line 0.8-μm filter, the flask was equipped with a thermometer, condenser/N_2 outlet, stir bar, and a N_2 inlet. The reaction system was purged with N_2 for 1 hour while equilibrating to a temperature of 45 °C. The monomer solution (125-mL volume) was then maintained at 45 °C for 15 min at a stir rate of 450 rpm. A 5 mL aliquot of a 0.078 M aqueous solution of the initiator APS was delivered to the monomer solution via a 5-mL syringe with an in-line

0.8-μm filter to initiate the polymerization. Immediately following initiation, a temperature ramp from 45 °C to 65 °C was applied to the solution at a ramp rate of 30 °C/hr. Following completion of the ramp, the polymerization was allowed to proceed overnight at 65 °C. After polymerization, the resulting turbid reaction product was filtered through glass wool to remove a small amount of coagulum.

3.2.2.2 Purification and Lyophilization of pNIPAm-AAc microgel particles

The purification and lyophilization of large pNIPAm-AAc microgel particles are referred to Chapter 2, Section 2.2.2. The solid yield is approximately 72%.

3.2.3 Preparation of Microgel Dispersions

3.2.3.1 Preparation of Dilute Microgel Dispersions for Video Particle Tracking

The preparation of dilute microgel dispersions for video particle tracking is referred to Chapter 2, Section 2.2.3.

3.2.3.2 Preparation of Concentrated Microgel Dispersions for Video Particle Tracking

The microgel dispersions were prepared by first dispersing pNIPAm-AAc powder in deionized water and shaking for one week to form ~0.1 wt% suspensions in conical 2.5-mL centrifuge tubes (VWR). After centrifugation at a RCF of 15,422 × g for 1 hour, the aliquot was removed, then the designated aqueous buffer was added and the microgel pellets were re-dispersed in the buffer via shaking for 48 hours. After another centrifugation to remove buffer aliquot, the designated amount of the aqueous buffer was added to the pellets adjust the weight concentration of microgel dispersions, followed by shaking for another 48 hours.

3.2.3.3 Preparation of Dilute Microgel Dispersions for Dynamic Light Scattering

The buffer used for dynamic light scattering is the same as above. The microgel dispersions were prepared by first dispersing approximately 10 mg pNIPAm-AAc

powder in 10 g of distilled, de-ionized water and shaking for overnight to obtain an 0.1 wt% dispersion. A 25 μL aliquot of the 0.1 wt% dispersion was then added into 2.47 mL aqueous buffer to get 0.001 wt% (10 ppm) dispersion in a 4-mL transparent polymethyl methacrylate cuvette for dynamic light scattering (DLS). Note that the upper limit of particle diameter for DLS measurement is about 2.5 μm; particles with diameter larger than 2.5 μm do not give an autocorrelation function that can be statistically correlated with the diffusion coefficient. This is largely due to the low number density of particles in the scattering volume, which results in a significant contribution to the scattering signal from number density fluctuations.[16] Furthermore, the concentration of microgel particles is also critical. If the concentration of microgel particles is too low (~1 ppm), the scattered light intensity fluctuates with number density instead of the translational diffusion of particles. On the other hand, if the concentration of microgel particles is too high (> 100 ppm), multiple scattering of irradiation and hydrodynamic interaction between particles bias the particle size larger than the real value.[16]

3.2.4 Video Particle Tracking via Optical Microscopy

The operation of optical microscopy and algorithm for the calculation of unperturbed hydrodynamic diameter of pNIPAm-AAc microgel particles are referred to Chapter 2, Section 2.2.5.2.

3.2.5 Dynamic Light Scattering (DLS)

The DLS operation and calculation details are referred to Chapter 2, Section 2.2.5.1.

3.3 Results and Discussion

Generally, the large microgel particles are colloidally stable in a buffer with wide pH range due to the electrosteric interactions between particles[17] even though they are fairly sticky to the glass surface.[18] In the particle tracking approach, digital video

microscopy was used to obtain a series of images with temporal and spatial information of microgel particles diffusing in the focus plane. To balance the irreversible attachment of particles on the inner wall of borosilicate rectangular capillaries with the thermal equilibrium of particles in the bulk dispersions, images were acquired 30 minutes after sample preparation. The microscopy images and trajectories of large pNIPAm-AAc microgel particles are shown in Figure 3.1.

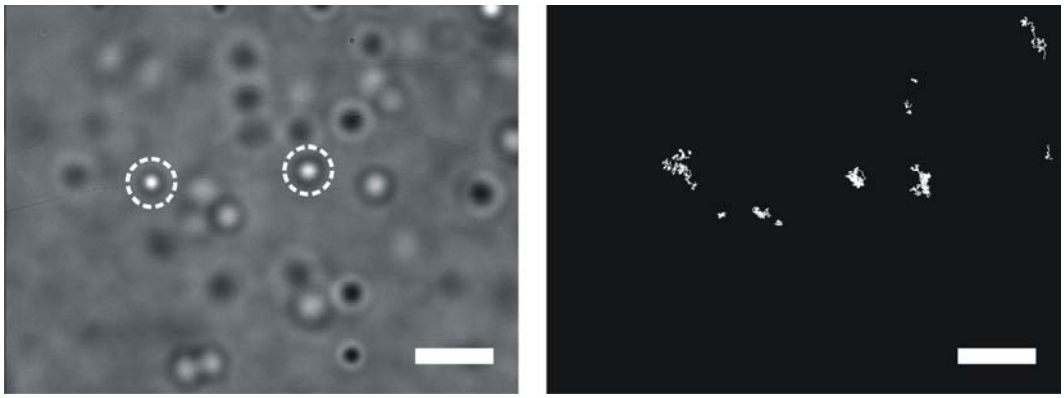

Figure 3.1 Digital microscopy images and particle trajectories for large pNIPAm-AAc microgel particles (0.01 wt% polymer in pH 3.5 buffer). The microscopy image and particle trajectories for large pNIPAm-AAc particles are displayed in left and right side of the panels, respectively. The particles on the focus plane of microscope are circled by dashed lines. Note that particles moving out of the focal plane are excluded from analysis with IDL routines by setting the brightness threshold. The sizes of large pNIPAm-AAc particles are approximately 3.0 ± 0.2 μm, based upon particle tracking and the Stokes-Einstein equation. Scale bar = 10 μm.

The dark spots with bright corona on the microscopy images are corresponding to microgel particles above the focus plane, whereas the pale bright spots with gray corona represent particles below the focus plane. The brightest spots (circled by dashed lines) represent microgel particles in the focus plane. The mismatch between particle trajectories and the microscope images is attributed to the motion of some particles in and out of the focal plane over the course of the particle tracking. The trajectories of these particles are purely diffusive and no interaction between particles is observed in these dilute microgel dispersions. The particle sizes can be extracted by the particle tracking algorithm combined with Stokes-Einstein equation shown in Chapter 2, which gives a

hydrodynamic diameter of approximately 3.0 ± 0.2 μm for large pNIPAm-AAc microgels (in pH 3.5 buffer at 20.0 °C) whereas dynamic light scattering does not give a reasonable measurement of particle size for such large microgel particles.

Figure 3.2 shows the change of average particle size versus pH. Our characterization utilized particle tracking routines for *in situ* determination of the hydrodynamic diameters of larger microgel particles in aqueous buffers. It was not possible to determine pH responsivity by PCS since particle number densities within the scattering volume change drastically for such large sizes at 20 °C. As a result, the scattering intensities by PCS do not statistically correlate with the diffusion coefficients and hydrodynamic diameters of particles could not be determined.

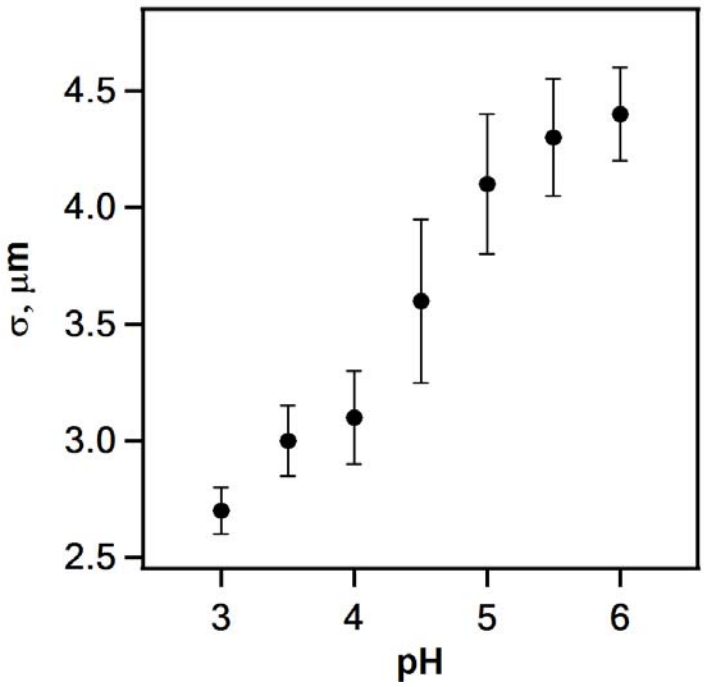

Figure 3.2 The hydrodynamic diameter (σ) versus pH for large pNIPAm-AAc microgels with 0.01 wt% in aqueous buffer at 20 ºC. The polydispersities of measured hydrodynamic diameters are shown as error bars, and size polydispersities are approximately 10%. Note that the average particle size increases drastically at a pH close to the pK_a value of the AAc monomer (pK_a = 4.25).

A notable exception was for measurements made at pH 3.0. In pH 3.0 buffer at 20 °C, tracking algorithms resulted in a calculated hydrodynamic diameter of approximately 2.7 ± 0.2 μm, slightly larger than particle size measured by PCS, 2.5 ± 0.2 μm. The error bars in Figure 2 represent the measured polydispersity, which is below 10%. Furthermore, particle diameters increase from 2.7 μm at pH 3.0 to 4.4 μm at pH 6.0, representing a volume increase of > four fold throughout the pH ramp. The pH-responsive swelling behavior is due to the deprotonation of AAc segments at higher pH values, which leads to the increase of electrostatic repulsion between carboxylate anions and the increase of osmotic pressure inside microgel particles, thereby swelling the polymeric networks.[19,20] It is known that small pNIPAm-AAc microgel particles with diameters below 1 μm display a similar pH responsivity to those observed here.[8,21]

Figure 3.3 shows the temperature-responsivity of large pNIPAm-AAc microgel particles in pH 3.0 buffer.[7,22] Because the particle size in this case is slightly below 2.5 μm, we found that PCS could reliably be used to determine the *in situ* size of microgel particles from 20 to 40 °C.[18]

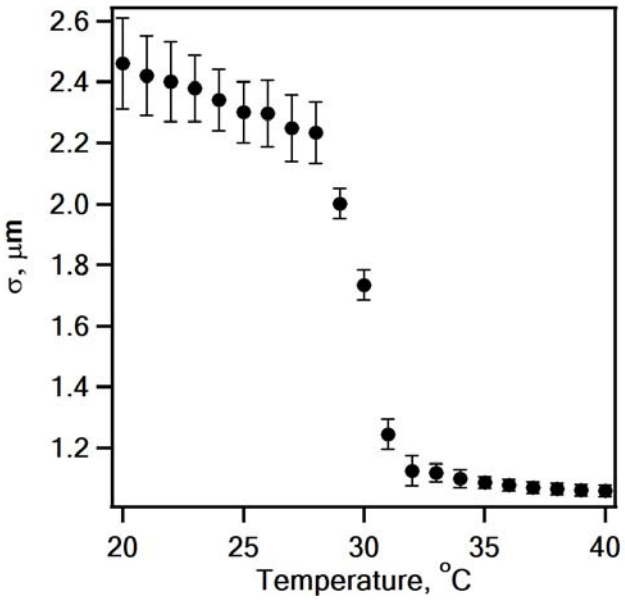

Figure 3.3 The temperature-dependent hydrodynamic diameter of large pNIPAm-AAc microgels with 0.001 wt% in pH 3.0 buffer. The hydrodynamic diameter was measured

by photon correlation spectroscopy with a programmed temperature ramp from 20 to 40 °C. The error bars represent the size polydispersities, which are below 10%. Note that the VPTT of microgel particles is approximately 30 °C, as described in the literature for similar polymer compositions.[8]

The error bars represent the polydispersities, which again are below 10%. The volume phase transition temperature (VPTT) of pNIPAm-AAc microgels is approximately 30 °C, at which the size of particles decreased from 2.2 μm down to approximately 1.2 μm, corresponding to the well known volume phase transition of pNIPAm.[10] The VPTT of these large pNIPAm-AAc microgel particles is slightly lower than that of smaller pNIPAm-AAc microgels (31 °C) synthesized previously in our group.[7,18,23] This is likely due to the fact that the particles described here are ~15 mol% AAc as opposed to the 10 mol% particles synthesized previously; it is known that with increasing AAc content in copolymer, the VPTT of pNIPAm-AAc microgels decreases.[21] It should be noted, however, that AAc incorporation is not required to obtain these particle sizes.

Owing to their excellent monodispersity, these particles can also self-assemble into colloidal crystals. The transmission-mode microscopy image and trajectories of colloidal crystals assembled from a 2.0 wt% dispersion of large pNIPAm-AAc microgels in pH 3.5 buffer are shown in Figure 3.4.

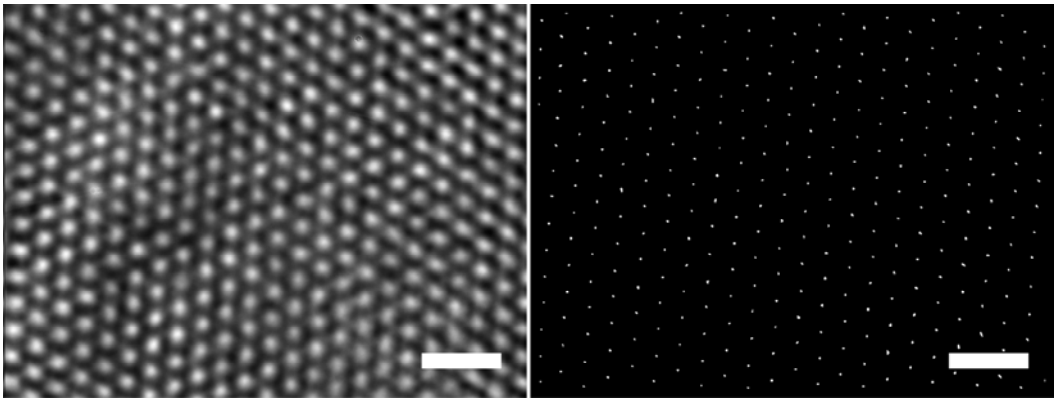

Figure 3.4 Digital microscopy image and particle trajectories for large pNIPAm-AAc microgels assembled into colloidal crystals at 20 ºC (2.0 wt% in pH 3.5 buffer). Note that

the size of the particles as determined from radial distribution analyses is smaller than 3.0 μm, probably due to an osmotic deswelling effect observed previously.[24] Scale bar = 10 μm.

The left panel is the microscopy image of the middle layer of colloidal crystals of microgel particles. The right panel represents the trajectories of microgel particles in the focus plane. Based upon the particle positions in microscopy image series, the radial distribution function *g(r)* could be obtained. (IDL routines are referred to Appendix A) The first peak of radial distribution function, i.e. center-to-center distance between closest neighbor particles, corresponds to the *in situ* average hydrodynamic diameter of particles in colloidal crystals.[25] The particle size calculated from Figure 3.4, 2.8 ± 0.1 μm, is smaller than that calculated from the data in Figure 3.2, 3.0 ± 0.2 μm, probably due to an osmotic deswelling effect observed previously in such colloidal assemblies.[24,26] The above results suggest that the larger pNIPAm-AAc microgel particles show similar crystallization behavior to their smaller counterparts, which have reported previously.[1,18,27-34] The aging and phase behavior of pNIPAm-AAc microgel dispersions will be extensively tackled in Chapters 4 and 5.

3.4 Hypothesis of Large Particle Formation

Whereas we have not to this point undertaken a detailed mechanistic study of this synthetic approach, there are a number of conclusions that can be drawn from these data and from previous polymerization studies. Generally, the temperature used for pNIPAm-based microgel particle synthesis is ~70 °C, where resulting particle size characterizations reveal hydrodynamic diameters of 800 nm or smaller in pH 3.0 buffer.[2,7,8,22,35] The size of microgel particles obtained by this scheme may be further influenced by changing a variety of reaction conditions, including the solvent composition,[2] monomer/comonomer concentration,[3] and degree of cross-linking.[2,4,5] We have shown that precipitation polymerization reactions at lower temperatures (such as 60 °C) results in an increase in particle size up to 1.5 μm in pH 3.0 buffer.[18] However, when

we decreased the reaction temperature further (e.g. to 50 °C), an excessive amount of coagulum formed instead of a monodisperse colloid.[36] Given the phase separating nature of the reaction, it was clear that temperature plays a critical role in the control of particle size if other parameters of polymerization, such as total monomer concentration, comonomer/monomer/cross-linker/initiator/ ratio, stirring speed, degas time, and flow rate of N_2, are fixed. To obtain monodisperse microgel particles with diameters larger than 2.5 μm with relatively high yield, we developed a new strategy for the precipitation polymerization.

When reaction temperature reaches 45 °C, persulfate anions decompose to form primary radicals,[37] which subsequently attack monomers to form oligomeric radical chains (< 3 monomer units). When the oligomeric radical chains reach a critical length (> 5 monomer units) at a temperature higher than the LCST of pNIPAm-AAc segments (30 °C in this study), they collapse to form thermodynamically unstable nuclei with a radical trapped in or on their surface for further reaction.[38] This stage is known as nucleation, forming a population of collapsed precursor particles. Because the decomposition rate of initiator is decreased at lower temperatures,[37] reaction temperatures below conventional initiation temperatures (< 60-70 °C) may reduce the oligomeric radical concentration, thereby lowering the abundance of collapsed nuclei. This lower nuclei concentration likely favors particle growth mechanisms that do not involve appreciable nuclei aggregation, due to the relatively low possibility for bimolecular termination of two radicals on different nuclei. Furthermore, immediately after initiation the monomer concentration in the reaction mixture is higher than later stages. The lower nuclei concentration combined with higher monomer concentration at initial reaction times ensures a higher propagation rate than initiation rate, which favors the growth of nuclei with similar speed in early polymerization stages to achieve low polydispersities.[38] As the reaction proceeds and monomer is consumed, the monomer concentration decreases, thereby decreasing the propagation rate. To compensate for this decrease in propagation

rate (due to monomer consumption), the reaction temperature is ramped up from 45 to 65 °C. This ramp increases the propagation rate constant and also results in the increased decomposition of persulfate, thereby generating more radicals.

After approximately 40 minutes of polymerization, the temperature ramp is completed at 65 °C and the majority of monomers were likely converted to oligomeric radicals, nuclei, and precursor particles.[22] Therefore, the nucleation stage is replaced by the growth of the nuclei/particles via monomer addition, nuclei absorption, and nuclei aggregation.[3,22] At this elevated temperature (65 °C), growth on the nuclei/precursor particles becomes more favorable than nucleation due to much lower monomer concentration and stronger van der Waals attraction between nuclei and/or precursor radicals than nucleation stage. Because of the electrostatic repulsive interactions arising from the sulfate end groups, microgel particles are stabilized from coagulation while still capturing oligomeric radicals and unstable nuclei, thereby precluding any secondary nucleation from unstable nuclei.[39]

3.5 Conclusions

By introducing a temperature ramp in the early stage of the surfactant-free radical precipitation copolymerization, the mean size of the resultant multi-responsive microgel particles has been increased significantly while maintaining a low polydispersity (≤ 10%) and high yield (> 70%). The larger microgel particles demonstrate similar thermal and pH responsivity to their smaller counterparts of similar composition in Chapter 2. We have demonstrated that the mean diameter of pNIPAm-AAc microgel particles can swell from 2.5 to 4.5 μm by increasing the pH. Furthermore, these larger particles can self-assemble to colloidal crystals as their smaller counterparts as well. This synthetic scheme may be promising for producing other monodisperse, thermoresponsive microgel particles for applications as microlenses, imaging, and drug delivery vehicles.

References

(1) Meng, Z.; Smith, M. H.; Lyon, L. A. Temperature-programmed synthesis of micron-sized multi-responsive microgels, *Colloid Polym. Sci.* **2009**, *287*, 277-285.

(2) Kawaguchi, H.; Kawahara, M.; Yaguchi, N.; Hoshino, F.; Ohtsuka, Y. Hydrogel microspheres.1. Preparation of monodisperse hydrogel microspheres of sub-micron or micron size, *Polym. J.* **1988**, *20*, 903-909.

(3) Kawaguchi, H.; Yamada, Y.; Kataoka, S.; Morita, Y.; Ohtsuka, Y. Hydrogel microspheres. 2. Precipitation copolymerization of acrylamide with comonomers to prepare monodisperse hydrogel microspheres, *Polym. J.* **1991**, *23*, 955-962.

(4) Martinez, V. S.; Alvarez, L. P.; Hernaez, E.; Herrero, T.; Katime, I. Synthesis, characterization, and influence of synthesis parameters on particle sizes of a new microgel family, *J. Polym. Sci. Polym. Chem.* **2007**, *45*, 3833-3842.

(5) Hazot, P.; Chapel, J. P.; Pichot, C.; Elaissari, A.; Delair, T. Preparation of poly(N-ethyl methacrylamide) particles via an emulsion/precipitation process: The role of the crosslinker, *J. Polym. Sci. Polym. Chem.* **2002**, *40*, 1808-1817.

(6) Diaz-Camacho, F.; Lopez-Morales, S.; Vivaldo-Lima, E.; Saldivar-Guerra, E.; Vera-Graziano, R.; Alexandrova, L. Effect of regime of addition of initiator on TEMPO-mediated polymerization of styrene, *Polym. Bull.* **2004**, *52*, 339-347.

(7) Jones, C. D.; Lyon, L. A. Synthesis and characterization of multiresponsive core-shell microgels, *Macromolecules* **2000**, *33*, 8301-8306.

(8) Snowden, M. J.; Chowdhry, B. Z.; Vincent, B.; Morris, G. E. Colloidal copolymer microgels of N-isopropylacrylamide and acrylic acid: pH, ionic strength and temperature effects, *J. Chem. Soc., Faraday Trans.* **1996**, *92*, 5013-5016.

(9) Blackburn, W. H.; Lyon, L. A. Size-controlled synthesis of monodisperse core/shell nanogels, *Colloid Polym. Sci.* **2008**, *286*, 563-569.

(10) Hirose, Y.; Amiya, T.; Hirokawa, Y.; Tanaka, T. Phase-transition of submicron gel beads, *Macromolecules* **1987**, *20*, 1342-1344.

(11) Dowding, P. J.; Vincent, B.; Williams, E. Preparation and swelling properties of poly(NIPAM) "minigel" particles prepared by inverse suspension polymerization, *J. Colloid Interface Sci.* **2000**, *221*, 268-272.

(12) Park, T. G.; Hoffman, A. S. Estimation of temperature-dependent pore-size in poly(N-isopropylacrylamide) hydrogel beads, *Biotechnol. Prog.* **1994**, *10*, 82-86.

(13) Ugelstad, J.; Berge, A.; Ellingsen, T.; Schmid, R.; Nilsen, T. N.; Mork, P. C.; Stenstad, P.; Hornes, E.; Olsvik, O. Preparation and application of new monosized polymer particles, *Prog. Polym. Sci.* **1992**, *17*, 87-161.

(14) Blackburn, W. H.; Lyon, L. A. Size-controlled synthesis of monodisperse core/shell nanogels, *Colloid Polym. Sci.* **2008**, *286*, 563-569.

(15) Mueth, D. M.; Crocker, J. C.; Esipov, S. E.; Grier, D. G. Origin of stratification in creaming emulsions, *Phys. Rev. Lett.* **1996**, *77*, 578-581.

(16) Pecora, R. *Dynamic Light Scattering*; Plenum Press: New York, 1985.

(17) Fritz, G.; Schadler, V.; Willenbacher, N.; Wagner, N. J. Electrosteric stabilization of colloidal dispersions, *Langmuir* **2002**, *18*, 6381-6390.

(18) Meng, Z.; Cho, J. K.; Debord, S.; Breedveld, V.; Lyon, L. A. Crystallization behavior of soft, attractive microgels, *J. Phys. Chem. B* **2007**, *111*, 6992-6997.

(19) Dai, S.; Ravi, P.; Tam, K. C. pH-Responsive polymers: synthesis, properties and applications, *Soft Matter* **2008**, *4*, 435-449.

(20) Tan, B. H.; Tam, K. C. Review on the dynamics and micro-structure of pH-responsive nano-colloidal systems, *Adv. Colloid Interface Sci.* **2008**, *136*, 25-44.

(21) Kratz, K.; Hellweg, T.; Eimer, W. Influence of charge density on the swelling of colloidal poly(N-isopropylacrylamide-co-acrylic acid) microgels, *Colloids Surf. A* **2000**, *170*, 137-149.

(22) Zhou, S. Q.; Chu, B. Synthesis and volume phase transition of poly(methacrylic acid-co-N-isopropylacrylamide) microgel particles in water, *J. Phys. Chem. B* **1998**, *102*, 1364-1371.

(23) Serpe, M. J.; Lyon, L. A. Optical and acoustic studies of pH-dependent swelling in microgel thin films, *Chem. Mat.* **2004**, *16*, 4373-4380.

(24) Tan, B. H.; Tam, K. C.; Lam, Y. C.; Tan, C. B. Osmotic compressibility of soft colloidal systems, *Langmuir* **2005**, *21*, 4283-4290.

(25) Hansen, J. P.; McDonald, I. R. *Theory of Simple Liquids*; 4th ed.; Elsevier: Amsterdam, 2006.

(26) Saunders, B. R.; Vincent, B. Thermal and osmotic deswelling of poly(NIPAM) microgel particles, *J. Chem. Soc., Faraday Trans.* **1996**, *92*, 3385-3389.

(27) Senff, H.; Richtering, W. Temperature sensitive microgel suspensions: Colloidal phase behavior and rheology of soft spheres, *J. Chem. Phys.* **1999**, *111*, 1705-1711.

(28) Debord, J. D.; Lyon, L. A. Thermoresponsive photonic crystals, *J. Phys. Chem. B* **2000**, *104*, 6327-6331.

(29) Hellweg, T.; Dewhurst, C. D.; Bruckner, E.; Kratz, K.; Eimer, W. Colloidal crystals made of poly(N-isopropylacrylamide) microgel particles, *Colloid Polym. Sci.* **2000**, *278*, 972-978.

(30) Debord, J. D.; Eustis, S.; Debord, S. B.; Lofye, M. T.; Lyon, L. A. Color-tunable colloidal crystals from soft hydrogel nanoparticles, *Adv. Mater.* **2002**, *14*, 658-662.

(31) Gao, J.; Hu, Z. B. Optical properties of N-isopropylacrylamide microgel spheres in water, *Langmuir* **2002**, *18*, 1360-1367.

(32) Debord, S. B.; Lyon, L. A. Influence of particle volume fraction on packing in responsive hydrogel colloidal crystals, *J. Phys. Chem. B* **2003**, *107*, 2927-2932.

(33) Lyon, L. A.; Debord, J. D.; Debord, S. B.; Jones, C. D.; McGrath, J. G.; Serpe, M. J. Microgel colloidal crystals, *J. Phys. Chem. B* **2004**, *108*, 19099-19108.

(34) Mohanty, P. S.; Richtering, W. Structural ordering and phase behavior of charged microgels, *J. Phys. Chem. B* **2008**, *112*, 14692-14697.

(35) Pelton, R. Temperature-sensitive aqueous microgels, *Adv. Colloid Interface Sci.* **2000**, *85*, 1-33.

(36) Downey, J. S.; McIsaac, G.; Frank, R. S.; Stöver, D. H. Poly(divinylbenzene) microspheres as an intermediate morphology between microgel, macrogel, and coagulum in cross-linking precipitation polymerization, *Macromolecules* **2001**, *34*, 4534-4541.

(37) Kolthoff, I. M.; Miller, I. K. The chemistry of persulfate. I. The kinetics and mechanism of decomposition of the persulfate ion in aqueous medium, *J. Am. Chem. Soc.* **1951**, *73*, 3055-3059.

(38) Wu, X.; Pelton, R. H.; Hamielec, A. E.; Woods, D. R.; McPhee, W. The kinetics of poly(N-isopropylacrylamide) microgel latex formation, *Colloid Polym. Sci.* **1994**, *272*, 467-477.

(39) Duracher, D.; Elaissari, A.; Pichot, C. Preparation of poly(N-isopropylmethacrylamide) latexes: Kinetic studies and characterization, *J. Polym. Sci. Polym. Chem.* **1999**, *37*, 1823-1837.

CHAPTER 4

AGING OF MICROGEL DISPERSIONS

This chapter describes the physical aging of concentrated dispersions containing pNIPAm-AAc microgels in aqueous buffer, and part of this chapter is excerpted from my paper published in Journal of Physical Chemistry B.[1] The aging of microgel dispersions is characterized by the video optical microscopy, in which the time series of images are analyzed by particle tracking routines in IDL programming environment. Our results confirm that pNIPAm-AAc microgel dispersion age over time by showing that the slow-down of particle dynamics and increase of particle size after evolution. The slow-down of dynamics is the universal feature of aging system,[2-4] whereas the swelling of particles is unique to microgel dispersions.[1,5] In addition, crystallization and glass transition are convoluted with aging process, which will be discussed in next chapter.

4.1 Introduction

Physical aging is typically associated with the non-thermodynamic state of amorphous solids, especially polymeric glassy materials below the glass transition temperature.[6] Since the last decade, the aging of disordered metastable systems[3,4] and ordered crystalline systems[7,8] has stimulated in a series of investigations on the fundamental principles of physical aging.[9] Common approaches to probe the physical aging of colloids are light scattering[3,8] and rheology,[4,10] wherein the structure, dynamics and response functions of the system are monitored over time. Optical microscopy[11,12] with dynamic particle tracking routines was also recently employed to probe aging of colloidal systems.

We have noticed that the phase behavior of microgel dispersions immediately after sample preparation is completely different from that of microgel assemblies long after preparation, which we believe is the evidence of aging in microgel dispersions. In

this chapter, we employ video optical microscopy[13] with particle tracking algorithms[14] to better understand the complex evolution of structure and dynamics in microgel dispersions. In particular, we have monitored the evolution of mean square displacement (*MSD*) and radial distribution function (*g(r)*) of pNIPAm-AAc microgel particles in aqueous dispersions as a function of age of these dispersions under quiescent conditions in a closed system. To illustrate the evolution of attractive interparticle interactions between pNIPAm-AAc microgels, we further measured the influence of aging on the thermostability of microgel assemblies. By investigating the dynamics, structure, and thermal stability of these dispersions, and the time evolution of these behaviors, the fundamental details of the aging process and the inter-particle potentials responsible for aging is being elucidated.

4.2 Experimental

4.2.1 Materials

All reagents, materials, and water were purchased and/or prepared as previously described in the Chapter 2, Section 2.2.1, unless otherwise specified.

4.2.2 Microgel Synthesis, Purification and Lyophilization

The synthesis, purification, and lyophilization of microgel particles used in this chapter are referred to Chapter 2, Section 2.2.2.

4.2.3 Microgel Dispersion Preparation

The preparation of microgel dispersions for particle tracking is referred to Chapter 2, Section 2.2.3 and 2.2.4.

4.2.4 Microgel Aging Sample Preparation

The dispersions were introduced into 5.0 × 2.0 × 0.1 mm VITROTUBE™ rectangular capillaries (Fiber Optic Center, Inc.) by capillary force at room temperature,

and then sealed with Epoxy Putty™ (ITW Devcon®) resin. The dispersions were then allowed to age at room temperature for set periods of time prior to measurements being performed. Note that if the weight concentration is too high to flow easily at room temperature, slight heat was employed to fluidize the microgel dispersions for their introduction to the capillaries. It's suggested that the sample should be used for particle tracking measurements no later than three months after preparation due to inevitable solvent evaporation through the resin, which increases the volume fraction and dehydrates aged sample finally.

4.2.5 Tracking Microgel Particles by Video Optical Microscopy

Particle tracking by video microscopy and data analysis algorithms via IDL routines are referred to Chapter 2, Section 2.2.5.2.

4.3 Results and Discussion

4.3.1 Microscopic Dynamics during Aging

It is quite surprising to notice that pNIPAm-AAc microgel dispersions, almost diffusive immediate after preparation, eventually form a crystalline or glassy phase after evolving for a period of time. Due to the obvious optical difference between the fresh sample and aged sample, we start to track the evolution of macroscopic appearance and microscopic dynamics of microgel particles in the closed system. We used photography and video microscopy to describe the time-dependent phase behavior of pNIPAm-AAc microgel dispersions. Perhaps the observation via naked eye gives the first impression of aging behavior of microgel dispersions. Figure 4.1 shows a photograph comparing the appearance of new and aged samples; the left capillary holds a 1-day-old pNIPAm-AAc microgel dispersion (2.0 wt% polymer in pH 3.5 buffer), whereas the right capillary holds an aged (27 days old) dispersion (2.0 wt% polymer in pH 3.5 buffer). The aged sample

clearly shows iridescence under white light illumination due to Bragg diffraction from the colloidal crystalline lattice.

Figure 4.1. The aging of pNIPAm-AAc microgel samples at 20.0 °C as visualized on the macroscopic scale. Both microgel samples contain 2.0 wt% polymer in a pH 3.5 buffer after aging for different periods [left: 1 day (fluid), right: 27 days (crystal)]. The samples were photographed against a white grid to aid in photographic focusing.

Whereas the slow assembly of colloids is not in and of itself surprising, the detailed dynamics and pathway of the assembly are suggestive of an extremely complex colloidal system. Indeed, very surprising results obtained from this system illustrate just how different the physics are from those of repulsive hard sphere particles. The complexity of the system can be understood phenomenologically by considering the additional energetic terms that must be considered in microgel dispersions as compared with traditional hard spheres. Whereas hard spheres possess a fixed volume, which dictates the length scales over which they interact, microgels can swell and collapse to minimize the free energy of the assembly. For example, we and others have shown in the case of purely repulsive microgels that when the number density of microgels is increased, the microgels condense to occupy a smaller volume in order to accommodate the additional particles.[15-17] This phenomenon is physically similar to the osmotic deswelling of gels in the presence of linear polymer,[18] and to the conformational changes observed for linear polymers as the concentration of polymer is increased (e.g. moving from the dilute to the semi-dilute regime).[19] From these examples, it is clear that the behavior of microgel dispersions must be interpreted both in terms of their colloidal and

polymer solution properties. The solvation, conformation, elasticity, and topology of the polymer chains will contribute to the observed colloidal behavior, as all of these factors will dictate how the microgel volume and particle-particle interactions change as a function of microgel concentration, solution conditions, and external stimuli (e.g. temperature). The picture becomes even more complex when weakly attractive interactions are introduced. Now as the particle concentration (volume fraction) is increased, those interactions must influence not only how the microgels assemble with each other, but also how the microgels swell or collapse in order to minimize the free energy of the system. For example, one could imagine conditions under which the entropic cost associated with swelling the microgels could be compensated for by enthalpic gain from attractive polymer-polymer interactions. Under conditions where the pairwise interactions are weak relative to the thermal energy (k_BT), such microgel swelling would be particularly important in the stabilization of an assembly, since multibody interactions would be required to overcome Brownian forces. In the results below, we illustrate a wide range of behaviors wherein the delicate interplay between the colloidal and polymer energy scales produce complexity that is not observable in the hard sphere domain.

Examples of the complexity in the system are evident in the optical microscopy images and the particle trajectories shown in Figure 4.2. A microgel sample buffered at pH 3.0 with an effective volume fraction of 40% is a fluid immediately after preparation. (All calculations of effective volume fractions hereinafter are shown in Appendix of this chapter.) This is expected, as the sample lies below the canonical freezing point for hard-sphere colloids (~0.494). However, after 53 days the sample has evolved to form a highly ordered crystalline phase wherein the particles appear to be in contact with one another, which should not be possible for a simple repulsive dispersion. This result is an apparent example of the case discussed above, where the ability of the microgels to swell permits the evolution of a close-packed phase from a non-close-packed one. On the other hand, if

the effective volume fraction of a sample at the same pH is 74% (the packing limit for hard spheres), the sample again is a fluid immediately after preparation. This result is extremely surprising, given the fact that the diffusion of hard spheres is so frustrated at this packing fraction that such concentrations are typically not possible in dispersions due to particle jamming; close packed hard sphere assemblies are typically formed by more specialized approaches such as slow solvent evaporation.[20] After 53 days, this sample has completely crystallized to form a close packed structure, thereby aligning with our preconceived notions of the colloidal phase behavior. In this case, the initial state is illustrative of the previously described osmotic deswelling effect,[16,21] wherein the microgels deswell in order to accommodate their neighbors. Despite these phenomenological descriptions, these data illustrate some key questions that need to be addressed experimentally: (1) How can "packed" samples behave as fluids when first prepared, and how can more dilute samples form crystals? (2) What is the pathway by which microgel dispersions age and what can the pathway tell us about the evolution of the interparticle forces? (3) How do temperature, volume fraction, and pH influence sample aging, and the initial and final states?

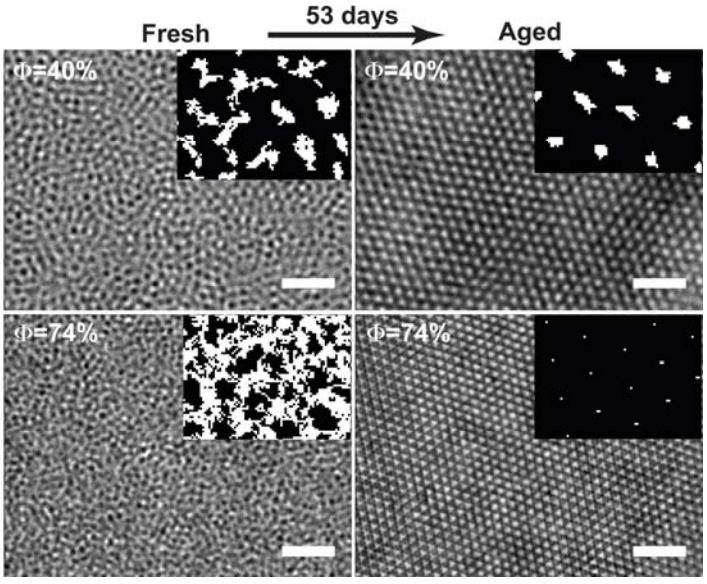

Figure 4.2 Microscopic phase behavior of pNIPAm-AAc microgel dispersions at pH 3.0 and 20 °C. The effective volume fractions of the pNIPAm-AAc microgels are displayed on the top-left of each image. The top-right inset in each image shows the particle trajectories over ~10 s of observation. Trajectories are magnified 4× relative to the images for ease of trajectory visualization. All scale bars represent 10 μm.

The data presented in Figure 4.2, are representative of all samples observed between pH 3 and 4.5 with effective volume fractions between ~0.35 and 0.74. These samples begin as diffusive fluids immediately after preparation, and equilibrate to colloidal crystals or crystal/glass mixed phases after aging at room temperature for ~1 month.[22] At pH 3.5, the aging process is quite slow and crystallization is favored over a broad range of volume fractions (*vide infra*), thereby making this a suitable experimental condition for detailed investigations of the aging-convoluted crystallization dynamics; we will therefore focus on experiments at pH 3.5 for the detailed aging studies shown here. Note, however, that qualitatively similar behavior is observed for all microgel samples that we have observed to undergo aging from fluids to glasses or crystals.

More detailed observation of these samples via bright-field video optical microscopy permits direct determination of the dispersions' structures and the particle dynamics. The brightfield micrographs and trajectories (inset) for a 2.0 wt% polymer in pH 3.5 buffer at different timepoints are displayed in Figure 4.3. Note that the inset trajectory maps are magnified 4 × relative to the brightfield images for easier visualization of the trajectories. The microgel dispersions are fluid-like immediately after sample preparation (1-day and 5-day data), with diffuse trajectories and no evidence of spatial order. Eventually the samples display crystalline order and caged trajectories, which are illustrated here by the 11 day and 27 day data. Note that even after formation of the ordered phase, the particle dynamics continue to evolve, with the particle trajectories becoming more constrained with aging (11 vs. 27 day data).

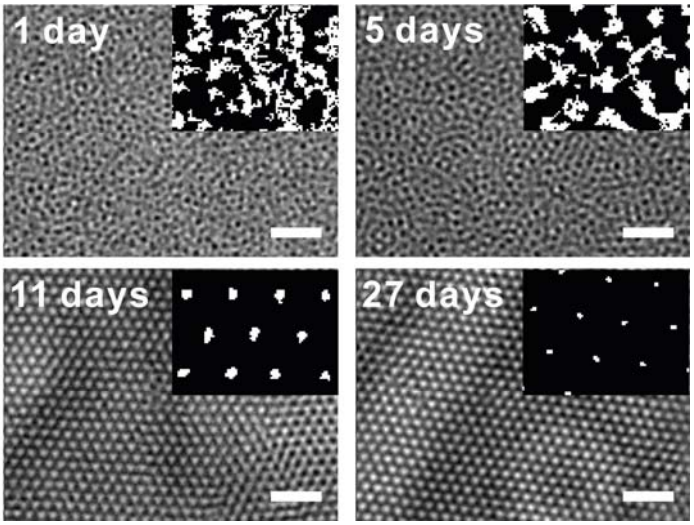

Figure 4.3 Microscopic images and trajectories (inset, ~10 s of observation) of pNIPAm-AAc microgel samples (2.0 wt% polymer in pH 3.5 buffer) at different ages (not in the same spot) and 20.0 °C, the aging times are indicated on all microscopic images. Trajectories are magnified 4 × relative to the images for ease of trajectory visualization. Scale bar = 10 μm.

In addition to the direct visualization of particle dynamics and spatial organization, the microscopy data can offer a quantitative assessment of the particle diffusion. To illustrate this, a double logarithm plot of the particles' mean square displacement (*MSD*) versus lag time (τ) as a function of the number of days after preparation is shown in Figure 4.4a (2.0 wt%, pH 3.5). The *MSD* of microgel particles in an ensemble is given as follows:

$$MSD(\tau) = \left\langle \left[\vec{r}_i(t+\tau) - \vec{r}_i(t)\right]^2 \right\rangle_{i,t} \tag{4-1}$$

where $\vec{r}_i(t)$ is the position vector of the i^{th} particle at time t, τ is the lag time, and $\langle\rangle_{i,t}$ indicates the spatial average over the ensemble of particles as well as all starting times t. In the colloidal gas regime, where particle motion is purely diffusive and interactions between particles are negligible, the *MSD* should be proportional to lag time,

$$MSD(\tau) = 2dD\tau \tag{4-2}$$

where d is the dimensionality of the displacement vectors and D is the translational self-diffusion coefficient of microgel particles. In general, the *MSD* of colloidal particles scales with lag time,

$$MSD(\tau) \propto \tau^{\beta} \tag{4-3}$$

where the scaling parameter β is the slope in a double logarithmic plot of $MSD(\tau)$ versus τ. Generally, $\beta = 1$ for Brownian diffusive motion, whereas β values between 0 and 1 denote sub-diffusive behavior. In these studies, β was obtained by regression analysis of $MSD(\tau)$ versus τ plots over the range $\tau = 0.1$ to 1 s.

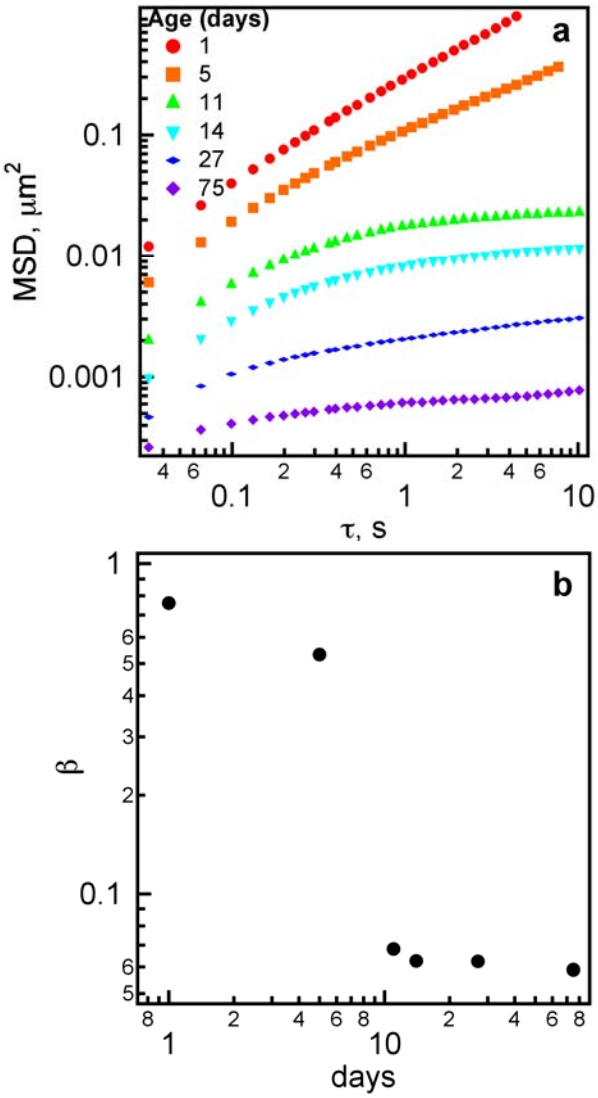

Figure 4.4 (a) Mean square displacement (*MSD*) versus lag time (τ) of pNIPAm-AAc microgel particles (2.0 wt% polymer in pH 3.5 buffer) at different ages and 20.0 °C. (b) The power of the lag time versus the age of pNIPAm-AAc the microgel dispersion. $MSD \propto \tau^{\beta}$, where β is the power of lag time.

The *MSD* plots in Figure 4a and the β values in Figure 4.4b illustrate a marked slowing of particle motion with sample aging; one day after sample preparation, the colloidal dispersion shows nearly diffusive fluid behavior with $\beta = 0.76$. As the sample ages, the maximum *MSD* of the samples at long lag time decreases along with a decrease in the magnitude of β. These data also illustrate that the initial aging is fairly rapid, with the 1-day old sample showing a *MSD* of > 1 μm^2 at a lag time of 10 s (determined via extrapolation), whereas the 5-day old sample shows a *MSD* of ~0.14 μm^2 at 10 s. Thus, during the first 5 days of aging, the maximum particle displacement decreases by about 90%, with the sample progressing from a fast, diffusive fluid to a slow, sub-diffusive fluid. When these microgel dispersions were aged for over 7 days, crystallization occurred, with the crystallites initially coexisting with a fluid phase (data not shown). After aging for 11 days, a macroscopic crystalline phase had fully formed, which was observed through the appearance of sample iridescence, as shown in Figure 4.1. At this point, *MSD* analysis shows the appearance of a plateau, indicating the formation of permanent cage around the particles, as opposed to the transient cages observed in the fluid phase. However, even in the crystalline phase, the microgel assemblies still age with time, which is manifest by the continual slowing of the dynamics with sample aging. The plot of β versus aging time *t* (Figure 4.4b) provides semi-quantitative representation for the aging of these dispersions.[11] As illustrated by the images shown in Figures 4.2 and 4.3 and microscopic dynamics shown in Figure 4.4, the structure of microgel assemblies evolves as the dynamics of the particles slow down. In addition to the slow down of dynamics during the aging process, microgel particles swell as the result of aging.

4.3.2 Microscopic Structure during Aging

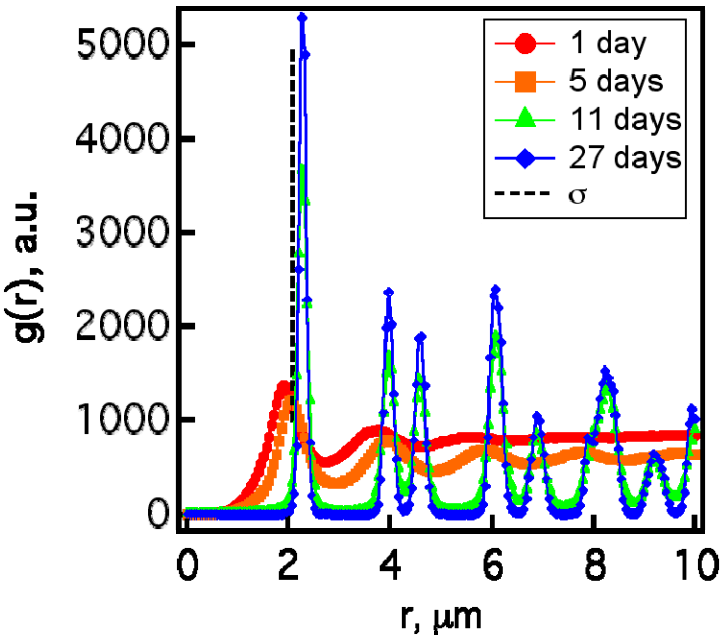

Figure 4.5 The radial distribution function, *g(r)*, for 2.0 wt% pNIPAm-AAc microgel dispersions at pH 3.5 as a function of aging time. Note that the first *g(r)* peak for the fluid phases (1 day and 5 days after preparation) corresponds to the hydrodynamic diameter of microgel particles, whereas the first peak for crystalline phase (11 days and 27 days after preparation) corresponds to the lattice constant of colloidal crystals. The black vertical dashed line corresponds to the unperturbed hydrodynamic diameter of the microgels determined in the dilute limit.

Figure 4.5 illustrates this in terms of the radial distribution function (*g(r)*) for pNIPAm-AAc microgel assemblies (2.0 wt% polymer in pH 3.5 buffer) as a function of the number of days after sample preparation. In general, the first peak in the *g(r)* plot for an attractive fluid phase is equal to the diameter of particles,[23,24] whereas for a crystalline phase the first peak represents the mean particle center-to-center distance.[25] One day after sample preparation, the *g(r)* plot has relatively weak structure, with only the first two peaks being easily identified. In very dilute (0.01 vol%) dispersions at pH 3.5, the pNIPAm-AAc microgel particles have an unperturbed hydrodynamic diameter of 2.1 μm (from particle tracking microrheology). However, in the freshly prepared 2.0 wt% microgel sample, the inter-particle distance is only about 1.9 μm, as determined from the first peak in the *g(r)* plot. The particle size in the dispersion is presumably smaller than

the unperturbed hydrodynamic diameter measured in highly dilute conditions (2.1 μm) because of the previously observed osmotic deswelling of the microgels,[15,16] which occurs when the polymer concentration is increased beyond the dilute regime.[26] In this case, osmotic deswelling significantly decreases the actual volume fraction of the microgels from 56% to 41% (All calculations of actual volume fractions hereinafter are shown in Appendix of this chapter.), which is too dilute to produce long-range crystalline order for inter-particle interactions that are dominated by mutual volume exclusion only.

These data also suggest that the particle size increases with aging even in the fluid phase, which is evident from the fact that the apparent particle size after 5-days of aging is slightly larger than that observed after 1 day. After 10 days, the microgel particles self-assembled into colloidal crystals, which are clearly observed in the *g(r)* plots by a dramatic increase in structure at larger values of *r*. After aging for 27 days, the inter-particle distance has increased to 2.3 μm, which is slightly greater than the hydrodynamic diameter determined under dilute conditions (2.1 μm) probably due to the evolution of a net attractive interaction between particles during aging. Whereas the changes occurring at the molecular scale that result in the observed aging of our assemblies is still not clear, it seems likely that the decrease in particle dynamics over such long times is the result of a slow progression to a system with strongly attractive inter-particle interactions. As we have suggested before,[17,22] it may be the case that the microgel particles swell due to the formation of multiple inter-particle hydrogen bonds between the protonated carboxylic acid groups and/or amide groups, which decreases configurational entropy of polymeric chains while increasing the enthalpic contribution to particle assembly.[1,17,22] With the pairwise interactions between the particles being apparently very weak, as evidenced by the lack of aggregation in the dispersions, it is likely that multi-body interactions are required to form the crystalline assembly.[27] The rearrangement of polymeric segments on multiple neighboring particles (particle swelling and interdigitation) to optimize both the number and orientation of the hydrogen bonds, and concomitant multi-body interactions

between particles may favor particle swelling in order to minimize the local free Gibbs energy.[1,22]

4.3.3 Age-dependent Thermostability

Our speculation that attractive inter-particle interaction potentials might drive the phase transition with aging can conceivably be probed in a more direct manner. For example, colloidal interaction potentials have been measured directly via optical tweezers,[28] total internal reflection microscopy,[29,30] and atomic force microscopy[31] techniques. Herein we use the thermostability of the colloidal assemblies as an indirect *in situ* indicator of inter-particle interaction between pNIPAm-AAc microgel particles in the context of their instantaneous phase behavior and their aging history. Reports by Richtering,[32] Hu,[33,34] and Lyon[15] have illustrated that for purely repulsive microgel crystals, melting will occur at temperature slightly below the intrinsic LCST of homopolymeric pNIPAm microgel particles comprising the assembly. As the temperature is raised, the microgels deswell enough to drive the volume fraction of the assembly from the crystalline region of the phase diagram to the fluid region. Therefore, the thermal stability of a microgel dispersion should report on the inter-particle interactions, with the assembly becoming more thermally stable if multi-body inter-particle attractive interactions are present; the additional enthalpic contribution to the assembly will represent an additional energetic barrier that must be overcome to drive assembly melting.

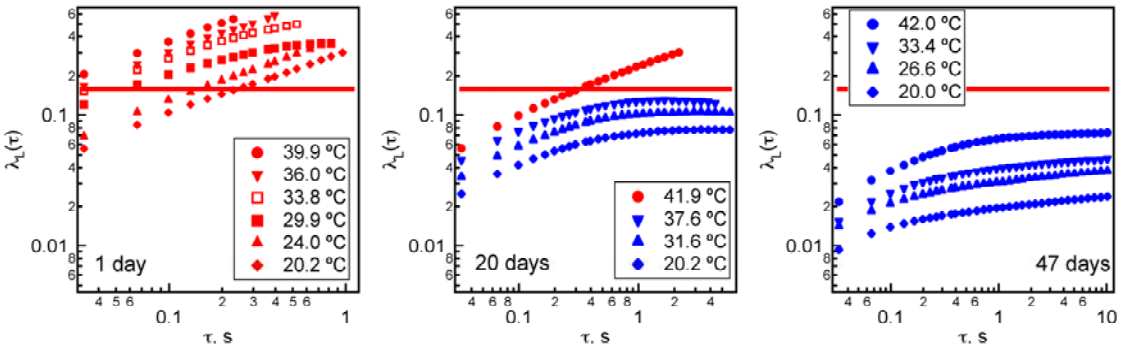

Figure 4.6 Age-dependent thermostability of 2.0 wt% pNIPAm-AAc microgel dispersions in pH 3.5 buffer. Red symbols indicate fluid microgel dispersions, whereas

blue symbols represent crystalline behavior. The age of each sample is indicated on each Lindemann parameter ($\gamma_L(\tau)$) versus lag time (τ) plot. The horizontal red line in each frame is the critical Lindemann parameter for crystal melting ($\gamma_L^{max} = 0.16$).

Figure 4.6 presents the thermal melting behavior of 2.0 wt% pNIPAm-AAc microgel dispersions in pH 3.5 buffer as a function of sample age. We quantitatively assess crystal melting using the phenomenological Lindemann criterion. The quasi-2D time-dependent Lindemann parameter is defined as

$$\gamma_L(\tau) = \frac{\sqrt{MSD(\tau)}}{r} \tag{4-4}$$

where r is the ensemble-averaged center-to-center distance between particles.[1,22,35,36] The quasi-2D Lindemann parameter is a measurement of time-dependent positional fluctuations of microgel particles relative to the crystal lattice spacing. From the data presented in Figure 4.6, the thermal stability of microgel dispersions clearly increases with the age. For all aged samples, the temperature increase leads to the accelerated dynamics of microgel particles. However, microgel particles' dynamics are dissimilar in different ages if we compared the maximum Lindemann parameters with the critical melting Lindemann parameters. After 1 day of sample aging, the time-dependent Lindemann parameter $\gamma_L(\tau)$ is roughly linear with lag time, and at all temperatures from 20 °C up to 39.9 °C, the maximum Lindemann parameters are greater than critical melting Lindemann parameter (0.16 for an FCC lattice). For the 1-day old sample, it is interesting to notice that there is a marked decrease in the particle dynamics when temperature is raised to 30 °C. This arises from weak, transient particle aggregation, where the hydrophobic interaction between the deswollen microgels begins to dominate over electrosteric repulsion. However, when temperature continues to increase up to 36 °C, the thermal energy of particles dominates over inter-particle attractions, thereby

resulting in a recovery of diffusive behavior. After 20 days of aging, the microgel dispersion is largely crystalline with some regions of fluid coexistence. At this point the crystalline phase displays melting at approximately 40 °C as shown in Figure 4.6. Note that this temperature is far above the LCST of pNIPAm-AAc microgels at this pH (~31 °C), reflecting the onset of attractive inter-particle interactions. The 47-day aged sample, which is completely crystallized, is not observed to melt even when the temperature is raised to 42 °C, which is the highest temperature our instrument allows. Indeed, the particles are still strongly caged and appear to be in close contact with one another, with the maximum Lindemann parameter being nearly 10-fold lower than the melting value, reflecting an extremely stable assembly. These data clearly indicate that the aging process is associated with the evolution of attractive interactions between neighboring microgel particles.

4.4 Conclusions

In this chapter, we have directly observed aging during the self-assembly of pNIPAm-AAc microgel particles in a closed system. During this aging process, the microgel dynamics slow down, the microgel diameters increase, and the mean interaction potential between particles become more attractive, which stabilize the thus-formed colloidal crystals against thermal melting. Our results also suggest that the crystallization process is convolved with aging, where the slowing dynamics of the dispersion is synergistic with crystallization due to an increase in particle volume fraction with time. Even after crystallization of microgel particles, the slower of particle dynamics indicates that the aging is still going on. Additionally, although the molecular origins of aging are not yet clear, our data suggest that microgel dispersions evolve due to a slow

reconfiguration of the system from one that is dominated by intra-particle (polymer-polymer) interactions to multi-body inter-particle interactions.

Appendix: Calculation of Effective and Actual Volume Fractions

Due to the swellability of microgel particles, the estimation of volume fraction of soft microgels is not as straightforward as their hard sphere counterparts. Only cryo-electron microscopy[37] can be used to precisely determine the *in situ* size of microgels. Due to the limited availability and cost of cryo-electron microscopy, our group used dynamic light scattering combined with particle tracking to determine microgel particle size in dilute, semi-dilute dispersions and colloidal crystals as well. The following calculation algorithms are therefore used for the estimation of volume fractions of microgel dispersions.

The effective volume fraction for microgel dispersions is calculated as shown below,

$$\Phi_{eff} = \frac{0.74}{(r/\sigma)^3} \tag{4A-1}$$

where Φ_{eff} is effective volume fraction, r average center-to-center distance between closest neighboring particles (from the first peak of $g(r)$ versus r plot),[24] and σ average unperturbed hydrodynamic diameter of particles, used to calculate all volume fractions spam from liquid phase to crystalline phase. The above scheme will be used for the volume fraction calculation in Chapter 5.

However, we have already noticed that the actual volume fraction for the same sample changes over aging in this Chapter. Therefore, we have to derive the actual volume fraction of liquid state and crystalline state for the same sample which can age over time. Thus we use the following scheme to calculate actual volume fractions for the same sample in different phases,

i) For crystalline phase assuming FCC or HCP packing: $\Phi_C = \frac{0.74}{(r/\sigma_C)^3}$ (4A-2)

where r is center-to-center distance between closest neighboring particles, σ_C the hydrodynamic diameter of particles in crystalline phase obtained from $\sigma_C = r - \sqrt{MSD_{\max}}$ if we assume particles in this case are hard-sphere like, here $MSD_{\max}$ is the maximum mean square displacement of particles in crystalline cage.

ii) For glassy phase: $\Phi_G = \frac{0.65}{(r/\sigma_G)^3}$ (4A-3)

where r is center-to-center distance between closest neighboring particles, σ_G the hydrodynamic diameter of particles in glassy phase obtained from $\sigma_G = r - \sqrt{MSD_{\max}}$ if we assume particles in this case are hard-sphere like, here $MSD_{\max}$ is the maximum mean square displacement of particles in cages in glassy phase.

Herein we only consider the case in which the fluid phase finally aged to crystalline phase. Due to the constant number density for the same sample, we could use the following calculation to determine the actual volume fraction Φ_L for fluid phase,

$$\Phi_L = \frac{\Phi_C}{(r/\sigma_L)^3} \quad (4A\text{-}4)$$

where Φ_C is shown above, and σ_L is hydrodynamic diameter of particles in concentrated dispersions obtained from the first peak of *g(r)-r* plot. Note for aging cases in which particles are swollen, the effective volume fraction lies in between the actual fluid-phase volume fraction and actual crystalline-phase volume fraction of the same sample, $\Phi_L < \Phi_{eff} < \Phi_C$. Whereas particles are compressed in aging process, the effective volume fraction is larger than both crystalline-phase volume fraction and liquid-phase volume fraction, $\Phi_L < \Phi_C < \Phi_{eff}$

Reference

(1) Meng, Z.; Cho, J. K.; Breedveld, V.; Lyon, L. A. Physical aging and phase behavior of multiresponsive microgel colloidal dispersions, *J. Phys. Chem. B* **2009**, *113*, 4590-4599.

(2) Bonn, D.; Tanaka, J.; Wegdam, G.; Kellay, H.; Meunier, J. Aging of a colloidal "Wigner" glass, *Europhys. Lett.* **1999**, *45*, 52-57.

(3) Cipelletti, L.; Manley, S.; Ball, R. C.; Weitz, D. A. Universal aging features in the restructuring of fractal colloidal gels, *Phys. Rev. Lett.* **2000**, *84*, 2275-2278.

(4) Cloitre, M.; Borrega, R.; Leibler, L. Rheological aging and rejuvenation in microgel pastes, *Phys. Rev. Lett.* **2000**, *85*, 4819-4822.

(5) Purnomo, E. H.; van den Ende, D.; Vanapalli, S. A.; Mugele, F. Glass transition and aging in dense suspensions of thermosensitive microgel particles, *Phys. Rev. Lett.* **2008**, *101*, 238301.

(6) Struik, L. C. E. *Physical Aging in Amorphous Polymers and Other Materials*; Elsevier: Amsterdam, 1978.

(7) Kegel, W. K.; Dhont, J. K. G. "Aging" of the structure of crystals of hard colloidal spheres, *J. Chem. Phys.* **2000**, *112*, 3431-3436.

(8) Martelozzo, V. C.; Schofield, A. B.; Poon, W. C. K.; Pusey, P. N. Structural aging of crystals of hard-sphere colloids, *Phys. Rev. E* **2002**, *66*, 021408.

(9) Cipelletti, L.; Ramos, L.; Manley, S.; Pitard, E.; Weitz, D. A.; Pashkovski, E. E.; Johansson, M. Universal non-diffusive slow dynamics in aging soft matter, *Faraday Discuss.* **2003**, *123*, 237-251.

(10) Purnomo, E. H.; van den Ende, D.; Mellema, J.; Mugele, F. Rheological properties of aging thermosensitive suspensions, *Phys. Rev. E* **2007**, *76*, 021404.

(11) Wang, P.; Song, C. M.; Makse, H. A. Dynamic particle tracking reveals the ageing temperature of a colloidal glass, *Nat. Phys.* **2006**, *2*, 526-531.

(12) Courtland, R. E.; Weeks, E. R. Direct visualization of ageing in colloidal glasses, *J. Phys. Condens. Mat.* **2003**, *15*, S359-S365.

(13) Inoué, S.; Spring, K. R. *Video Microscopy: The Fundamentals*; 2nd ed.; Plenum Press: New York, 1997.

(14) Crocker, J. C.; Grier, D. G. Methods of digital video microscopy for colloidal studies, *J. Colloid Interface Sci.* **1996**, *179*, 298-310.

(15) St. John, A. N.; Breedveld, V.; Lyon, L. A. Phase behavior in highly concentrated assemblies of microgels with soft repulsive interaction potentials, *J. Phys. Chem. B* **2007**, *111*, 7796-7801.

(16) Tan, B. H.; Tam, K. C.; Lam, Y. C.; Tan, C. B. Osmotic compressibility of soft colloidal systems, *Langmuir* **2005**, *21*, 4283-4290.

(17) Debord, S. B.; Lyon, L. A. Influence of particle volume fraction on packing in responsive hydrogel colloidal crystals, *J. Phys. Chem. B* **2003**, *107*, 2927-2932.

(18) Saunders, B.; Vincent, B. Osmotic deswelling of microgel particles in the presence of free polymer, *Prog. Colloid Polym. Sci.* **1997**, *105*, 11-15.

(19) Heo, Y.; Larson, R. G. Universal scaling of linear and nonlinear rheological properties of semidilute and concentrated polymer solutions, *Macromolecules* **2008**, *41*, 8903-8915.

(20) Tsuji, S.; Kawaguchi, H. Colored thin films prepared from hydrogel microspheres, *Langmuir* **2005**, *21*, 8439-8442.

(21) Saunders, B. R.; Vincent, B. Osmotic de-swelling of polystyrene microgel particles, *Colloid Polym. Sci.* **1997**, *275*, 9-17.

(22) Meng, Z.; Cho, J. K.; Debord, S.; Breedveld, V.; Lyon, L. A. Crystallization behavior of soft, attractive microgels, *J. Phys. Chem. B* **2007**, *111*, 6992-6997.

(23) Pusey, P. N. *Colloidal suspensions*; In *Liquids, Freezing and Glass Transition*; Hansen, J. P., Levesque, D., Zinn-Justin, J., Eds.; North-Holland: 1989; Vol. 51, p 763-942.

(24) Hansen, J. P.; McDonald, I. R. *Theory of Simple Liquids*; 4th ed.; Elsevier: Amsterdam, 2006.

(25) Israelachvili, J. N. *Intermolecular and Surface Forces*; 2nd ed.; Academic Press: London, UK, 1991.

(26) Kiefer, J.; Naser, M.; Kamel, A.; Carnali, J. Osmotic deswelling of microgels by linear polyelectrolytes, *Colloid Polym. Sci.* **1993**, *271*, 253-261.

(27) Wu, J. Z.; Bratko, D.; Blanch, H. W.; Prausnitz, J. M. Effect of three-body forces on the phase behavior of charged colloids, *J. Chem. Phys.* **2000**, *113*, 3360-3365.

(28) Grier, D. G. Optical tweezers in colloid and interface science, *Curr. Opin. Colloid Interface Sci.* **1997**, *2*, 264-270.

(29) Prieve, D. C. Measurement of colloidal forces with TIRM, *Adv. Colloid Interface Sci.* **1999**, *82*, 93-125.

(30) Prieve, D. C.; Frej, N. A. Total internal reflection microscopy: a quantitative tool for the measurement of colloidal forces, *Langmuir* **1990**, *6*, 396-403.

(31) Ducker, W. A.; Senden, T. J.; Pashley, R. M. Direct measurement of colloidal forces using an atomic force microscope, *Nature* **1991**, *353*, 239-241.

(32) Senff, H.; Richtering, W. Temperature sensitive microgel suspensions: Colloidal phase behavior and rheology of soft spheres, *J. Chem. Phys.* **1999**, *111*, 1705-1711.

(33) Wu, J. Z.; Huang, G.; Hu, Z. B. Interparticle potential and the phase behavior of temperature-sensitive microgel dispersions, *Macromolecules* **2003**, *36*, 440-448.

(34) Wu, J. Z.; Zhou, B.; Hu, Z. B. Phase behavior of thermally responsive microgel colloids, *Phys. Rev. Lett.* **2003**, *90*, 048304.

(35) Alsayed, A. M.; Islam, M. F.; Zhang, J.; Collings, P. J.; Yodh, A. G. Premelting at defects within bulk colloidal crystals *Science* **2005**, *309*, 1207-1210.

(36) Saija, F.; Prestipino, S.; Giaquinta, P. V. Evaluation of phenomenological one-phase critieria for the melting and freezing of softly repulsive particles, *J. Chem. Phys.* **2006**, *124*, 244504.

(37) Crassous, J. J.; Ballauff, M.; Drechsler, M.; Schmidt, J.; Talmon, Y. Imaging the volume transition in thermosensitive core-shell particles by cryo-transmission electron microscopy, *Langmuir* **2006**, *22*, 2403-2406.

CHAPTER 5

PHASE DIAGRAM OF MICROGEL DISPERSIONS

This chapter describes the pH-tunable phase behavior of pNIPAm-AAc microgel dispersions, and part of this chapter is excerpted from my papers published in Journal of Physical Chemistry B.[1,2] The synthesis and purification of pNIPAm-AAc microgel particles has been presented in Chapter 2. As well as the preparation protocol of microgel dispersions in designated buffers, the video microscopy and the particle tracking routines will be described for the dynamics, trajectories, and structure of microgel dispersions. From the data obtained from video microscopy, we can infer the phase diagram of pNIPAm-AAc microgel dispersions at different pH values. Combined with aging phenomena discussed in Chapter 4, the results presented in this chapter could shed light on the correlation between interparticle interactions and phase behavior of microgel dispersions.

5.1 Introduction

Colloidal particles can be thought of as "big atoms"[3] in a continuous medium that mimic the interactions, thermodynamics, and dynamics of atoms or molecules in gas, liquid, and solid phases.[4-6] Theoretical methodologies to estimate the pair interactions of charge stabilized colloidal particles were originally developed by Derjaguin, Landau,[7] Verwey and Overbeek[8] (DLVO theory). Furthermore, Kirkwood[9] and McMillan[10] developed a coarse-graining framework in which the correlation of equilibrium properties of colloidal dispersions with effective pair potentials is used to calculate the phase behavior and structure of colloidal assemblies. In these theoretical treatments, colloidal particles are categorized by the shape of their interparticle pair potential curve, wherein the interactions can be classified as hard spheres,[11,12] sticky hard spheres,[13] and soft

spheres.[14] In general, as the volume fraction of colloidal particles is increased, their Brownian dynamics slow from being diffusive to sub-diffusive due to the formation of transient 'cages', which eventually become permanent cages as the particle density increases.[15] When the volume fraction of monodispersed hard-sphere particles, such as sterically stabilized poly(methyl methacrylate) (pMMA),[12] interacting via short-range repulsive potentials reaches the canonical crystallization volume fraction (~0.494), the particles self-assemble into a crystalline phase in order to maximize their local free volume (i.e., entropically driven assembly).[16] If the volume fraction is increased further, the colloidal system can be forced into a disordered, out of equilibrium phase from which it cannot escape on accessible experimental timescales; this kinetically-trapped phase is commonly referred to as being jammed[17] or glassy.[18]

In contrast to hard spherical particles, microgel is a micrometer- or sub-micrometer-sized particle composed of a cross-linked polymer network swollen in a good solvent,[19] wherein the degree of swelling is governed by the network elasticity,[20] polymer solubility,[21] and the solution osmotic pressure.[22] Of the microgels that are extremely sensitive to environmental conditions and most heavily investigated are those based on poly(*N*-isopropylacrylamide) (pNIPAm) because of the dramatic volume phase transition (VPT) that occurs in such particles near the lower critical solution temperature (LCST) of the polymer.[23,24] Poly(*N*-isopropylacrylamide) (pNIPAm)-based microgels[25] have emerged as potentially useful model soft spheres[4] due to the tunability of their softness and volume as a function of temperature.[26] It has been shown that monodisperse pNIPAm microgels can self-assemble into colloidal crystalline phases,[26-28] which have been applied to sensing,[29] for photonics,[27,30] and in the study of fundamental issues in condensed matter physics.[26,31,32] Soft repulsive interactions arising from repulsion between coronas around pNIPAm particles[21] and the deformability of pNIPAm particles[20] confer to pNIPAm colloidal dispersions the ability to exhibit richer phase behavior than hard sphere colloids.[26,31-33] The temperature-induced volume phase transition of pNIPAm

also provides a relatively simple experimental variable with which the effective volume fraction occupied by the microgels in dispersion can be modulated.[34]

Furthermore, the incorporation of acrylic acid (AAc) moieties into pNIPAm particles adds pH- and ionic strength-tunability,[35,36] giving rise to even more complex phase behavior [1,2,33], in that ionic strength, pH, temperature, and medium composition have been found to affect the pair interactions of these colloidal particles.[1,2,33,36] Our groups[1,2,33] and others[26,34,37] have illustrated that the phase behavior of pNIPAm-AAc microgel dispersions with modulated soft interactions can be very different from that of repulsive hard spheres due to a significant degree of complexity associated with soft interaction potentials,[32,37] and the ability to use external triggers such as pH[36,38] and temperature[31-33] to modulate both the interactions and the volume fraction of the spheres, thereby manipulating the phase behavior of pNIPAm-AAc colloids. As described in Chapter 4, the addition of this co-monomer also imparts tremendous complexity to the system: aging convoluted with phase transition for microgel dispersions.[2]

5.2 Experimental

5.2.1 Materials

All reagents, materials, and water were purchased and/or prepared as previously described in the Chapter 2, Section 2.2.1, unless otherwise specified.

5.2.2 Microgel Synthesis, Purification and Lyophilization

The synthesis, purification, and lyophilization of microgel particles used in this chapter are referred to Chapter 2, Section 2.2.2

5.2.3 Microgel Dispersion Sample Preparation

Aqueous buffers were prepared using recipes from buffer calculator developed by R. Beynon at the University of Liverpool.[39] The microgel dispersions were prepared by

first dispersing approximately 10 mg pNIPAm-AAc powder in 10 g of de-ionized water and shaking for one week to obtain a 0.1 wt% dispersion. For dynamic light scattering and phase analysis light scattering, a 250 μL aliquot of the 0.1 wt% dispersion was then diluted to a concentration of 0.01 wt% in aqueous buffer. For video microscopy and particle tracking, after centrifugation of the 0.1 wt% dispersion at a RCF of 15,422 × g for 1 hour, the supernatant was removed. The designated aqueous buffer was then added to the pellets, and the microgels were re-dispersed in the buffer via shaking for 48 hours. After another centrifugation to remove buffer aliquot, the designated amount of the aqueous buffer was added to adjust the weight concentration of microgel dispersions, followed by shaking for another 48 hours. The dispersions were introduced into 5.0 × 2.0 × 0.1 mm VITROTUBE™ rectangular capillaries (Fiber Optic Center, Inc.) by capillary force at room temperature, and then sealed with Epoxy Putty™ (ITW Devcon®) resin. Note that the weight concentrations of dispersions are fairly low so that the dispersions could flow. If the dispersions are too viscous, they should be heated to elevate temperature (~40 ºC) for good fluidity. Note samples are prepared for all available pH values (3.0, 3.5, 4.0, 4.5, 5.0, 5.5, 6.0) and weight concentrations.

5.2.4 Microgel Dispersions Characterization

5.2.4.1 Photon Correlation Spectroscopy (Dynamic Light Scattering)

The operation and calculation details for dynamic light scattering are referred to Chapter 2, Section 2.2.5.1.

5.2.4.2 Bright-Field Inverted Optical Video Microscopy

The operation and algorithm for the dynamics of pNIPAm-AAc microgel particles are referred to Chapter 2, Section 2.2.5.2.

5.3 Results and Discussions

5.3.1 Cluster of Microgel Particles

The irreversible adsorption of pNIPAm-AAc microgel particles on inner wall of rectangular capillaries is shown in Figure 2.2 in Chapter 2, Section 2.3.2. It is also noticed that microgels could form dimer, trimer, tetramer,…, which is another evidence for the stickiness of pNIPAm-AAc particles. In fact, the aggregation of microgel paricles into oligomeric cluster is also regarded as a certain type of self-assembly.[40] Figure 5.1 shows the oligomeric cluster of pNIPAm-AAc microgel particles in pH 3.0 buffer.

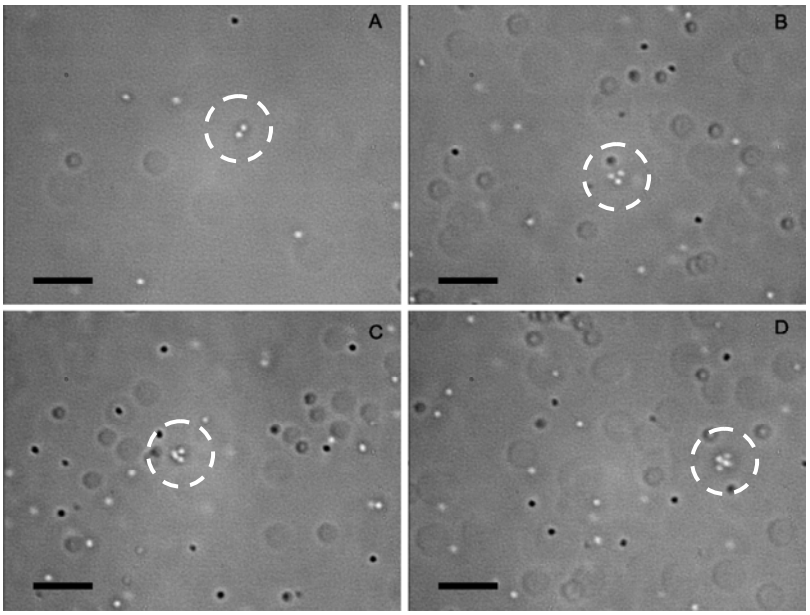

Figure 5.1 Microscopy images of the oligomeric clusters of pNIPAm-AAc microgel particles (0.04 wt % dispersion) approximately 50 μm from the glass surfaces in a pH = 3.0, I = 10 mM aqueous buffer. Dimer, trimer, tetramer, and hexamer are displayed in panel A, B, C, and D, respectively. The *in situ* recording of the oligomeric clusters (circled in each panel) is another strong evidence of the stickiness of pNIPAm-AAc microgel particles. Note the presence of multiple particles that are in (white) or out of (black) focus plane. Scale bar = 10 μm.

5.3.2 pH-Tunable Colloidal Phase Behaviors

As diffusive fluid immediately after sample preparation, pNIPAm-AAc microgel dispersions at some weight percentage range could form sub-diffusive fluid, crystalline, and glassy state after weeks of aging (described in Chapter 4). During the aging, as we have suggested before, it may be the case that the microgel particles swell due to the formation of multiple interparticle hydrogen bonds between the protonated carboxylic acid groups and/or amide groups, which decreases configurational entropy of polymeric chains while increasing the enthalpic contribution to particle assembly.[1,2,32,33] With the pairwise interactions between the particles being apparently very weak, it is likely that multi-body interactions are required to form the crystalline assembly. The rearrangement of polymeric segments on multiple neighboring particles (particle swelling and interdigitation) to optimize both the number and orientation of the hydrogen bonds, and concomitant multi-body interactions between particles may favor particle swelling in order to minimize the local Gibbs free energy.[1,2,33]

As suggested above, the large magnitude of swelling that occurs as a function of pH should result in dispersion phase behavior that is similarly pH dependent. At lower pH values, since each particle occupies a smaller volume, it is expected that pNIPAm-AAc particles will assemble into colloidal crystals or glasses at higher weight fractions than those at higher pH values, where the particle volume is greater. This is clearly seen in Figures 5.2 and 5.3, which illustrate the progression of phase behavior at pH 3.0 (Figure 5.2) and pH 5.0 (Figure 5.3) as a function of polymer (microgel) weight fraction following ~30 days of aging.

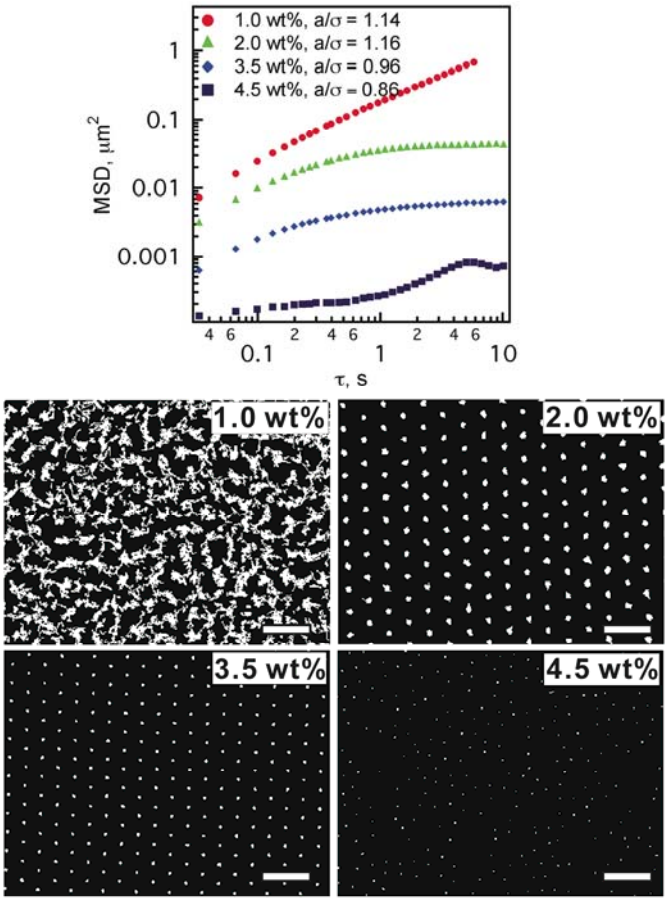

Figure 5.2 Concentration-dependent phase behavior of microgels at pH 3.0 and 20 °C, approximately 30 days after sample preparation. The double logarithm plot of *MSD* vs. τ is shown on the top panel, and the weight concentrations with corresponding r/σ are indicated in the legend. Note that center-to-center distance to hydrodynamic diameter ratio, r/σ, can be used to estimate the volume fraction in crystalline and glassy phase using equation (5-14). The bottom panels contain the trajectories of microgel assemblies over ~10 s of observation for weight percentages from 1.0 wt% to 4.5 wt%. Scale bar = 5 μm.

Figure 5.2 presents the double logarithm plot of *MSD* vs. τ for pNIPAm-AAc microgels at pH 3.0 and 20 °C with increasing concentration. As the concentration of particles is increased, the dispersion progresses through a typical fluid → crystal → glass transition.[12,41] At 0.5 wt%, the microgel dispersion remains in the fluid phase even after aging, where $\beta \approx 1$ indicating diffusive motion. When the microgel concentration reaches 1.5 wt%, the microgels form a crystalline phase and the *MSD* reaches a plateau after an

initial increase, indicating the microgels are caged in fixed lattice sites. When the particle concentration is raised above 4.0 wt%, the microgels are compressed together in a confined arrangement and tend to form a random glassy phase. Under these conditions, microgel diffusion is too frustrated to form an ordered crystalline lattice. Note that polycrystalline and crystal-glass coexistence phases are observed in some high concentration samples; for simplicity, we will refer to samples that are largely frozen in a disordered configuration as 'glassy'.

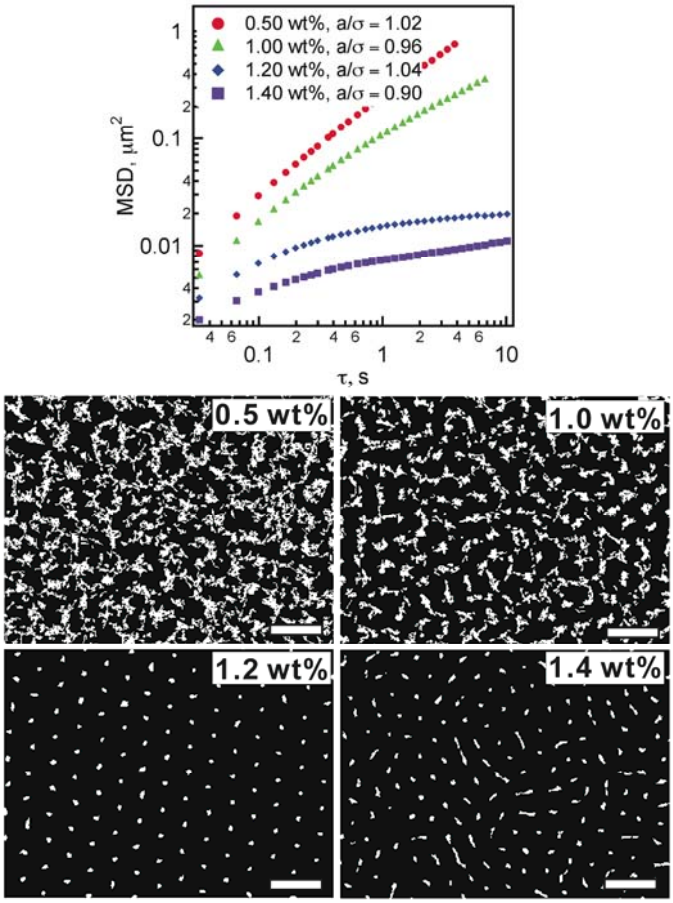

Figure 5.3 Concentration-dependent phase behavior of microgels at pH 5.0 and 20 °C, approximately 30 days after sample preparation. The top panel is the double logarithm plot of *MSD* vs. τ, and the weight concentrations with corresponding r/σ are indicated in the legend. The bottom panel contains the trajectories over ~10 s of observation for microgel assemblies at weight percentages from 0.5 wt% to 1.4 wt%. Scale bar = 5 μm.

Analogous phase transitions are observed for microgel dispersions at pH 5.0, albeit at very different weight concentrations. As shown in Figure 5.3, at 0.5 wt % the

sample is in a fluid phase, as was observed for the pH 3.0 sample. A subtle curvature is observed in the 0.5 wt% *MSD* plot at long lag times, suggesting that the microgel motion is slightly sub-diffusive even at very low concentration. At 1.0 wt% the particle motion slows down, the *MSD* plot shows more pronounced curvature, and the trajectories are clearly less diffusive than the 0.5 wt% sample. Increasing the concentration to 1.2 wt% results in the assembly of the microgels into a crystalline phase in which the *MSD* reaches a plateau after initial increase. A further increase in microgel concentration to 1.4 wt% results in a partially disordered glassy/crystalline sample with even lower maximum *MSD* in longer lag time. The data presented in Figures 5.2 and 5.3 are representative of the expected phenomenon: swelling of microgel particles with increasing pH results in transitions to crystalline and glassy states at lower wt% values.

5.3.3 Phase Diagram of Microgel Dispersions

To place these observations in an experimental framework commensurate with previous work on hard sphere packing,[12,42] it is necessary to express the microgel concentration in terms of volume fraction, which is the typical control parameter used for hard spheres. Due to the extreme amount of solvent swelling observed in pNIPAm-AAc microgels,[43] it is difficult to directly determine the volume fraction from the weight fraction, since the density of the individual microgels varies with concentration and pH, and is difficult to measure directly.[26] It is also difficult to measure the diameters of microgel particles precisely in situ via direct optical microscopic imaging due to the diffraction limit.[44] We and others[26,32,33] have previously addressed this by extrapolating packing fractions from shift factors obtained in the dilute regime via rheological measurements on dispersions. However, this approach is likely to be valid only in the case of purely repulsive hard spheres, which, given the results presented above, clearly is not an appropriate assumption for the system under study. Therefore, we only use the rheology method for samples that remain in the fluid regime after aging, in which the

volume fraction can be estimated by multiplying the weight fraction with the appropriate shift factor for each pH.[26] In the crystalline and glassy phases, the volume fraction is represented as the ratio of the average microgel center-to-center distance (r) in concentrated dispersions to the unperturbed microgel hydrodynamic diameter in dilute dispersions (σ). The average center-to-center distance (r) was obtained from the first peak in the radial distribution function $g(r)$, which was obtained via analysis of the microscopy images. From these data, one can determine the effective volume fraction in the crystalline and glassy phases, since it is known that the volume fraction for closest packing is 0.740 ($\sqrt{2}\pi/6$) in a face-centered cubic (FCC) or hexagonal close packed (HCP) lattice. If we assume the crystalline packing of microgel particles is FCC, the effective volume fraction of microgels (Φ_{eff}) will scale with r/σ by

$$\Phi_{eff} = \frac{0.740}{(r/\sigma)^3} \tag{5-1}$$

Therefore, for hard spheres the freezing transition at $\Phi_F = 0.494$, corresponds to $(r/\sigma)_F = 1.14$, whereas the melting transition at $\Phi_M = 0.545$, corresponds to $(r/\sigma)_M = 1.11$. It is critical to note that for hard spheres, r/σ can never be less than 1, since rigid particles cannot be compressed, whereas for soft spheres such as pNIPAm-AAc microgels, r/σ can have values much less than unity because of the intrinsic compressibility of microgels. Thus, by the above treatment, the effective volume fraction of microgels can be greater than 0.740 when $r/\sigma < 1$, equivalent to compression of all microgel particles. It is also noteworthy to mention that for random closest packing, as would be found in a Bernal glass, the maximum volume fraction is 0.65.[45,46] Therefore, for systems that are either completely glassy or display glass-crystal coexistence, the volume fraction will lie between 0.65 and 0.74, and equation (5-1) will overestimate the effective volume fraction. Furthermore, we have never observed any evidence of particle deformation from a spherical shape; the actual close packing limit is therefore not being expected to much higher than 0.74.

Given this approach, the experimentally determined phase diagram for pNIPAm-AAc microgel suspensions following ~30 days of aging is displayed in Figure 5.4, in which the left vertical axis represents r/σ, and the right vertical axis denotes the effective volume fraction Φ_{eff}. At each pH value (with constant ionic strength), a series of microgel dispersions with increasing weight fractions were prepared, and the microgel dynamics were recorded as described previously to construct the phase diagram. In line with the more detailed data in Figures 5.2 and 5.3, the phase diagram shows that a decrease in r/σ (increase in volume fraction) at a fixed pH is accompanied by a fluid → crystal → glass transition, similar to the phase behavior for repulsive hard spheres[12,42] and simple pNIPAm colloids.[26,41] However, the similarity to hard spheres is not quantitative when considering the canonical phase transitions for that system.

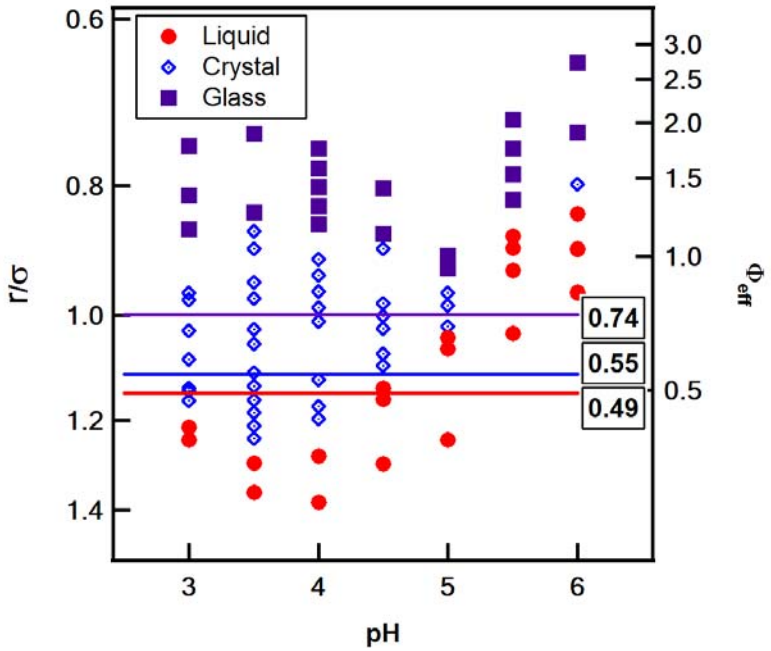

Figure 5.4 The phase diagram of pNIPAm-AAc microgels as a function of pH and volume fraction after ~30 days of aging. The volume fraction of microgels in suspension is scaled by the ratio between the center-to-center distance between nearest neighboring microgels (r) and the unperturbed hydrodynamic diameter of the microgels (σ) as a function of pH. The red closed circles represent the fluid phase, blue diamonds represent the crystalline phase, and magenta squares represent the glassy phase. The red, blue and magenta horizontal lines represent the hard sphere freezing, melting and maximum packing volume fractions, respectively.

The typical phase boundaries are superimposed onto the experimental data in Figure 5.4 ($\Phi_F = 0.494$, $\Phi_M = 0.545$, and $\Phi_{max} = 0.74$); by and large, the observed transitions for the microgel dispersions are very different from those found for hard spheres. For example, at very low effective volume fractions ($\Phi_{eff} = 0.40$, corresponding to $r/\sigma = 1.22$) crystallization was observed at pH 3.0, 3.5, and 4.0 after aging. Conversely, dispersions remained fluid-like at pH 5.5 and 6.0 even above the close-packing limit ($r/\sigma = 1$). These values are also very dissimilar from those measured for simple pNIPAm colloids, for which crystallization has been observed for $\Phi_{eff} = 0.56$-0.63.[26,41] The general trend displayed in Figure 5.4 is that the pNIPAm-AAc microgels apparently crystallize at much lower Φ_{eff} values under acidic conditions (pH < pK_a), and are too compressible to form crystals at higher pH values (pH > pK_a), along with fluid-like mobility at high packing fractions. As we suggested in previous publications,[1,33] one possible explanation for this odd phase behavior centers around the AAc moieties on the pNIPAm-AAc microgels. For example, in the case of pH 3.0, only 5% of AAc moieties are ionized, and the Coulombic repulsion and internal osmotic pressure of microgel particles are thus much smaller than at higher pH values. Because of the moderate ionic strength, which was kept constant at 10 mM in all samples, the Debye-Hückel screening length is rather short with an estimated value of ~3 nm. Under these conditions, carboxylic acid-carboxylic acid and carboxylic acid-amide hydrogen bonding between dangling chains tethered on pNIPAm-AAc particles should be maximized, thereby potentially resulting in a net attractive interaction at short particle separations. Conversely, as the pH is increased, the degree of AAc deprotonation increases, not only causing microgel swelling, but also an increased Coulombic repulsion between particles, at least over short distances. Apparently, under these conditions crystallization is frustrated and the dispersions remain fluid up to very high effective volume fractions. Similar effects have been observed for highly charged, ultrasoft microgels by Weitz and co-workers.[47] In those experiments, mechanical particle deformation was invoked as the main mechanism by which the

particles diffused by each other in concentrated dispersions. Whereas we cannot precisely determine if this is occurring for our microgel dispersions by microscopy due to limited optical resolution, we do not see strong evidence for particle deformation from the optical microscopy. It may be the case, however, that transient deformation allows particle motion to be diffusive even at high concentrations.

5.3.4 pH-Tunable Thermostablity of Microgel Assemblies

The net attractive interaction between pNIPAm-AAc microgel particles after aging was probably due to carboxylic acid-carboxylic acid, carboxylic acid-amide, and amide-amide hydrogen bonding.[48] The unique phase behavior of microgel dispersions result from the convolution of aging and phase transition.[2] Although direct methods for quantifying pair interaction between particles are available,[49,50] to account for multi-body interaction *in situ*, we use particle tracking to assess the melting temperature of pNIPAm-AAc colloidal crystals. To quantitatively assess crystal melting, we use the phenomenological Lindemann criterion. The quasi-2D time-dependent Lindemann parameter is defined as

$$\gamma_L(\tau) = \frac{\sqrt{MSD(\tau)}}{r} \tag{5-2}$$

where r is the ensemble-averaged center-to-center distance between nearest neighboring particles.[51,52] The quasi-2D Lindemann parameter is a measurement of time-dependent positional fluctuations of microgel particles relative to the crystal lattice spacing.[51] We quantitatively assess crystal melting using the phenomenological Lindemann criterion. If the maximum Lindemann parameter of microgels in hexagonal assemblies at longer lag time is over 0.16, the microgel assemblies melted.[51,52] For purely repulsive pNIPAm particles, we and others have report that pNIPAm colloidal crystals melt at temperature lower than the LCST of pNIPAm microgels.[26,32,34] Here we presume that if microgel size is the function of environmental temperature, when temperature crossover LCST of

pNIPAm microgel, the volume of microgel will decrease drastically so that the effective volume fraction of pNIPAm dispersions become less than the canonical melting volume fraction (Φ_M), thereby melting the colloidal crystals. Therefore, the thermal stability of a microgel dispersion should report on the interparticle interactions, with the assembly becoming more thermally stable if multi-body interparticle attractive interactions are present; the additional enthalpic contribution to the assembly will represent an additional energetic barrier that must be overcome to drive assembly melting. As shown below, pNIPAm-AAc microgel assemblies show thermal behavior completely different from their pNIPAm counterparts.

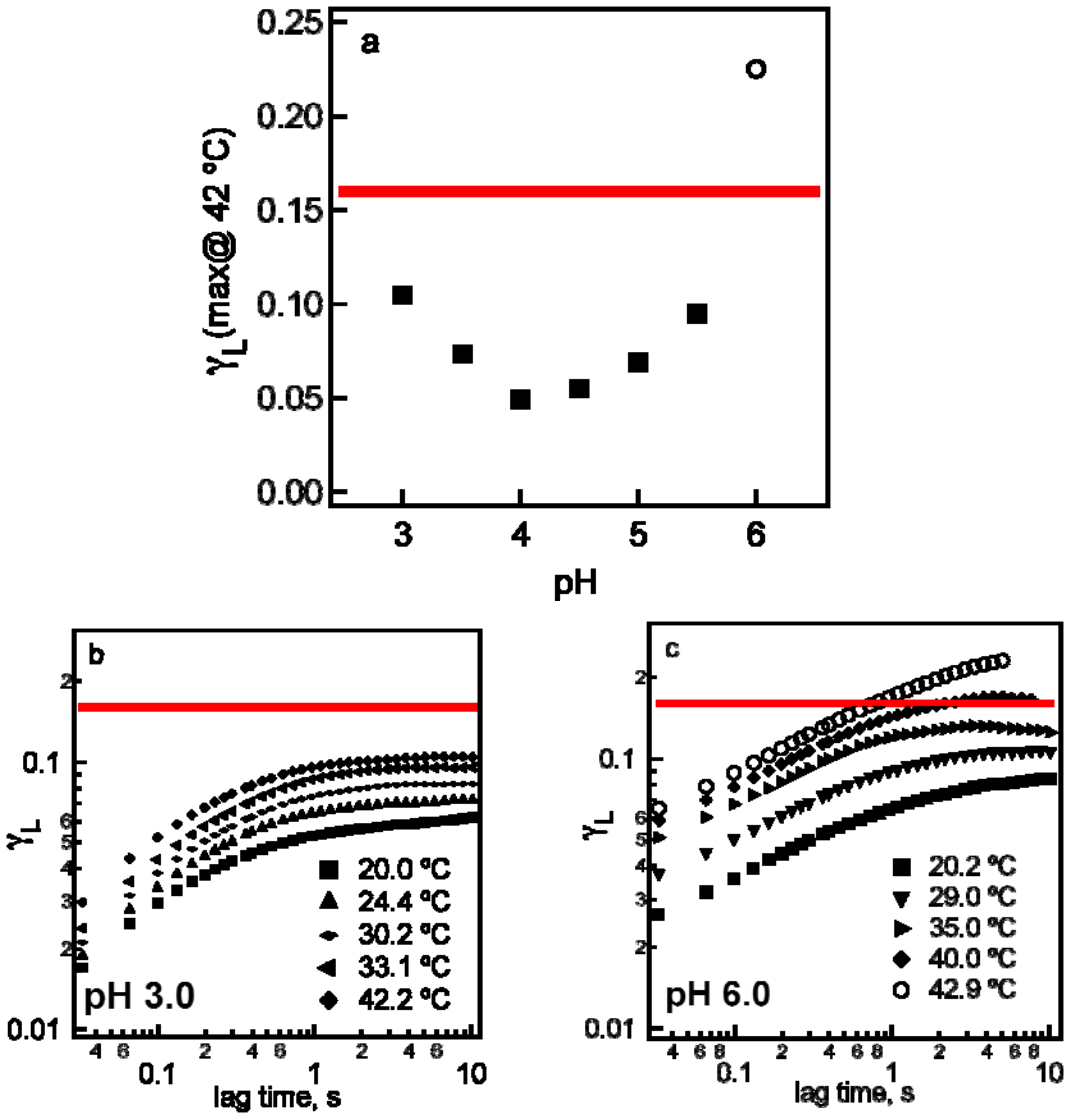

Figure 5.5 (a) The maximum time-dependent Lindemann parameter ($\gamma_L^{max@42C}$) of pNIPAm-AAc microgels at 42.0 °C from pH 3.0 to 6.0. The weight percentage for each pH is: 2.0 wt% for pH 3.0, 3.5, 4.0, and 4.5, 1.2 wt% for pH 5.0, 1.1% for pH 5.5 and 6.0. (b,c) The time-dependent Lindemann parameter [$\gamma_L(\tau)$] of pNIPAm-AAc microgels at different temperatures at pH 3.0 (b) and pH 6.0 (c). The horizontal red lines represent the critical Lindemann parameter, 0.16, which is the melting point of FCC or HCP-type crystals. Closed symbols represent solid phase samples, whereas open symbols represent fluid phases.

Figure 5.5a shows the maximum Lindemann parameter ($\gamma_L^{max@42C}$) measured at a temperature of 42 °C for pNIPAm-AAc dispersions as a function of pH. Note that this temperature represents the upper limit for our objective heater; direct microscopic observation of melting in all samples with accurate temperature control is not possible on our current equipment due to this limitation. In this figure, we show the results obtained for dispersions with weight fractions near the lower limit for crystallization at each pH value. Thus, these data represent the "weakest" assemblies formed at each pH. The thick red line represents the critical Lindemann parameter for FCC lattice melting, $\gamma_L^c = 0.16$. We observe that the $\gamma_L^{max@42C}$ values for pNIPAm-AAc crystals from pH 3.0 to 5.5 are well below the critical Lindemann parameter for melting. The only sample that melts below 42 °C is the one formed at pH 6.0, for which melting of the pNIPAm-AAc assembly and the formation of fluid phase is quantitatively confirmed by the maximum Lindemann parameter of 0.23 at 42 °C. The time-dependent Lindemann parameters of dispersions at different temperatures in pH 3.0 and pH 6.0 buffers are shown in Figures 5.5b and 5.5c, respectively. For colloidal crystals at pH 3.0, the particle motion remains caged even at temperatures much higher than the intrinsic volume phase transition temperature (VPTT) of pNIPAm-AAc microgels at this pH (~31 °C). As was discussed above, the marked thermostability of the pNIPAm-AAc colloidal crystals suggests that significant enthalpic, attractive interparticle interactions exist in these microgel assemblies. These presumably can be attributed to hydrogen bonding[48] and/or hydrophobic interactions at temperature above the VPTT.[53] In Figure 5.5c, the time-

dependent Lindemann values are also shown for a caged pNIPAm-AAc dispersion (1.4 wt%) at pH 6.0. In this case, the assembly actually melts at a temperature of ~40 °C, which is lower than the intrinsic VPTT of pNIPAm-AAc microgels at this pH (~50 °C).[54] This sub-LCST melting behavior is typical for microgel crystals with purely repulsive interactions, as described previously.[26,32,34] Thus, in contrast to the other data shown in Figure 5.5, the thermally induced melting of the pNIPAm-AAc crystalline phase at pH 6.0 suggests that repulsive interactions dominate at this pH, where hydrogen bonding is frustrated by AAc deprotonation. Together, these data suggest that the pH tunability of these microgel dispersions arises not only from particle volume changes, but also from modulation of the interparticle interactions, which evolve slowly, presumably due to a subtle competition between inter- and intraparticle chain-chain interactions.

5.4 Conclusions

As described in Chapter 4 and 5, for pNIPAm-AAc microgel dispersions, particularly in semi-dilute or concentrated regime, aging is convoluted with phase transition. The interparticle attractive interaction, probably due to hydrogen bonding at temperature lower than LCST and pH below pK_a of AAc, evolves with the swelling of microgel particles in the dispersion during the aging process. Thus formed pNIPAm-AAc microgel assemblies are thermodynamically more stable than their pNIPAm counterparts. The thermostability of pNIPAm-AAc assemblies after aging suggests that attractive interactions are at work. When the pH of suspension medium is lower than the AAc pK_a, the pNIPAm-AAc microgel particles form colloidal crystals at effective volume fractions as low as 40% (pH 3.0), which is probably due to hydrogen bonding and/or multi-body interactions between particles. Due to the delicate balance between repulsive and attractive interactions between particles, the formation of colloidal crystals becomes more favored when the pH is close to the AAc pK_a, at which point the effective volume fraction for crystallization spans from 40% to over 100% (indicating the compression of

particles under dense packing conditions). On the other hand, when the pH is above the AAc pK_a, the deprotonated AAc segments do not form hydrogen bonds efficiently, thereby shutting down a source of attractive interactions. It also appears that under these conditions, the pNIPAm-AAc particles are so deformable that crystallization is frustrated and the dispersion prefers to remain fluid even at very high packing fractions (> 100%). Together, these results illustrate the incredibly rich physics and dynamic nature found in this colloidal system. Despite the extensive amount of experimentation carried out in these studies, it is likely that we have only scratched the surface, and that deeper studies of these phenomena will produce additional observations that speak to the complex interplay between the colloidal and polymer energetics.

REFERENCES

(1) Meng, Z.; Cho, J. K.; Debord, S.; Breedveld, V.; Lyon, L. A. Crystallization behavior of soft, attractive microgels, *J. Phys. Chem. B* **2007**, *111*, 6992-6997.

(2) Meng, Z.; Cho, J. K.; Breedveld, V.; Lyon, L. A. Physical aging and phase behavior of multiresponsive microgel colloidal dispersions, *J. Phys. Chem. B* **2009**, *113*, 4590-4599.

(3) Poon, W. Colloids as big atoms, *Science* **2004**, *304*, 830-831.

(4) Saunders, B. R.; Vincent, B. Microgel particles as model colloids: theory, properties and applications, *Adv. Colloid Interface Sci.* **1999**, *80*, 1-25.

(5) Nayak, S.; Lyon, L. A. Soft nanotechnology with soft nanoparticles, *Angew. Chem. Int. Ed.* **2005**, *44*, 7686-7708.

(6) Das, M.; Zhang, H.; Kumacheva, E. Microgels: Old materials with new applications, *Ann. Rev. Mater. Res.* **2006**, *36*, 117-142.

(7) Derjaguin, B. V.; Landau, L. D. Theory of stability of strongly charged lyophobic sols and adhesion of strongly charged particles in solution of electrolytes, *Acta Physicochim. URSS* **1941**, *14*, 633-662.

(8) Verwey, E. J. W.; Overbeek, H. N. W. *Theory of the stability of lyophobic colloids*; Elsevier: Amsterdam, 1948.

(9) Kirkwood, J. G. Statisical mechanics of fluid mixtures, *J. Chem. Phys.* **1935**, *3*, 300-313.

(10) McMillan, W. G. J.; Mayer, J. E. The statistical thermodynamics of multicomponent systems, *J. Chem. Phys.* **1945**, *13*, 276-305.

(11) Hoover, W. G.; Ree, F. H. Melting transition and communal entropy for hard spheres, *J. Chem. Phys.* **1968**, *49*, 3609-3617.

(12) Pusey, P. N.; Vanmegen, W. Phase behaviour of concentrated suspensions of nearly hard colloidal spheres, *Nature* **1986**, *320*, 340-342.

(13) Baxter, R. J. Percus-Yevick equation for hard spheres with surface adhesion, *J. Chem. Phys.* **1968**, *49*, 2770-2774.

(14) Hoover, W. G.; Ross, M.; Johnson, K. W.; Henderso.D; Barker, J. A.; Brown, B. C. Soft-sphere equation of state, *J. Chem. Phys.* **1970**, *52*, 4931-4941.

(15) Weeks, E. R.; Weitz, D. A. Properties of cage rearrangements observed near the colloidal glass transition, *Phys. Rev. Lett.* **2002**, *89*, 095704.

(16) Yodh, A. G.; Lin, K.-H.; Crocker, J. C.; Dinsmore, A. D.; Verma, R.; Kaplan, P. D. Entropically driven self-assembly and interaction in suspension, *Philos. Trans. Roy. Soc. A* **2001**, *359*, 921-937.

(17) Torquato, S.; Stillinger, F. H. Multiplicity of generation, selection, and classification procedures for jammed hard-particle packings, *J. Phys. Chem. B* **2001**, *105*, 11849-11853.

(18) Kegel, W. K.; van Blaaderen, A. Direct observation of dynamical heterogeneities in colloidal hard-sphere suspensions, *Science* **2000**, *287*, 290-293.

(19) Pelton, R. Temperature-sensitive aqueous microgels, *Adv. Colloid Interface Sci.* **2000**, *85*, 1-33.

(20) Kiminta, D. M. O.; Luckham, P. F.; Lenon, S. The rheology of deformable and thermoresponsive microgel particles, *Polymer* **1995**, *36*, 4827-4831.

(21) Bartsch, E.; Kirsch, S.; Lindner, P.; Scherer, T.; Stolken, S. Spherical microgel colloids - Hard spheres from soft matter, *Ber. Bunsenges. Phys. Chem.* **1998**, *102*, 1597-1602.

(22) Tan, B. H.; Tam, K. C.; Lam, Y. C.; Tan, C. B. Osmotic compressibility of soft colloidal systems, *Langmuir* **2005**, *21*, 4283-4290.

(23) Heskins, M.; Guillet, J. E. Solution properties of poly(*N*-isopropylacrylamide), *J. Macromol. Sci. Chem.* **1968**, *2*, 1441-1455.

(24) Murray, M.; Rana, F.; Haq, I.; Cook, J.; Chowdhry, B. Z.; Snowden, M. J. Colloidal microgel systems: phase transition properties in aqueous solution of poly(N-isopropylacrylamide), *J. Chem. Soc., Chem. Commun.* **1994**, 1803-1804.

(25) Pelton, R. H.; Chibante, P. Preparation of aqueous lattices with *N*-isopropylacrylamide, *Colloids Surf.* **1986**, *20*, 247-256.

(26) Senff, H.; Richtering, W. Temperature sensitive microgel suspensions: Colloidal phase behavior and rheology of soft spheres, *J. Chem. Phys.* **1999**, *111*, 1705-1711.

(27) Debord, J. D.; Lyon, L. A. Thermoresponsive photonic crystals, *J. Phys. Chem. B* **2000**, *104*, 6327-6331.

(28) Hellweg, T.; Dewhurst, C. D.; Bruckner, E.; Kratz, K.; Eimer, W. Colloidal crystals made of poly(N-isopropylacrylamide) microgel particles, *Colloid Polym. Sci.* **2000**, *278*, 972-978.

(29) Kim, J.; Nayak, S.; Lyon, L. A. Bioresponsive hydrogel microlenses, *J. Am. Chem. Soc.* **2005**, *127*, 9588-9592.

(30) Reese, C. E.; Mikhonin, A. V.; Kamenjicki, M.; Tikhonov, A.; Asher, S. A. Nanogel nanosecond photonic crystal optical switching, *J. Am. Chem. Soc.* **2004**, *126*, 1493-1496.

(31) Wu, J. Z.; Huang, G.; Hu, Z. B. Interparticle potential and the phase behavior of temperature-sensitive microgel dispersions, *Macromolecules* **2003**, *36*, 440-448.

(32) St. John, A. N.; Breedveld, V.; Lyon, L. A. Phase behavior in highly concentrated assemblies of microgels with soft repulsive interaction potentials, *J. Phys. Chem. B* **2007**, *111*, 7796-7801.

(33) Debord, S. B.; Lyon, L. A. Influence of particle volume fraction on packing in responsive hydrogel colloidal crystals, *J. Phys. Chem. B* **2003**, *107*, 2927-2932.

(34) Wu, J. Z.; Zhou, B.; Hu, Z. B. Phase behavior of thermally responsive microgel colloids, *Phys. Rev. Lett.* **2003**, *90*, 048304.

(35) Snowden, M. J.; Chowdhry, B. Z.; Vincent, B.; Morris, G. E. Colloidal copolymer microgels of N-isopropylacrylamide and acrylic acid: pH, ionic strength and temperature effects, *J. Chem. Soc., Faraday Trans.* **1996**, *92*, 5013-5016.

(36) Kratz, K.; Hellweg, T.; Eimer, W. Effect of connectivity and charge density on the swelling and local structural and dynamic properties of colloidal PNIPAM microgels, *Ber. Bunsenges. Phys. Chem.* **1998**, *102*, 1603-1608.

(37) Watzlawek, M.; Likos, C. N.; Löwen, H. Phase diagram of star polymer solutions, *Phys. Rev. Lett.* **1999**, *82*, 5289-5292.

(38) Kokufuta, E.; Wang, B.; Yoshida, R.; Khokhlov, A. R.; Hirata, M. Volume phase transition of polyelectrolyte gels with different charge distributions, *Macromolecules* **1998**, *31*, 6878-6884.

(39) Beynon, R. Buffer Calculator *http://www.liv.ac.uk/buffers/buffercalc.html*, 2006

(40) Zhang, Z. L.; Glotzer, S. C. Self-assembly of patchy particles, *Nano Lett.* **2004**, *4*, 1407-1413.

(41) Gao, J.; Hu, Z. B. Optical properties of N-isopropylacrylamide microgel spheres in water, *Langmuir* **2002**, *18*, 1360-1367.

(42) Pusey, P. N. *Colloidal suspensions*; In *Liquids, Freezing and Glass Transition*; Hansen, J. P., Levesque, D., Zinn-Justin, J., Eds.; North-Holland: 1989; Vol. 51, p 763-942.

(43) Zhou, S. Q.; Chu, B. Synthesis and volume phase transition of poly(methacrylic acid-co-N-isopropylacrylamide) microgel particles in water, *J. Phys. Chem. B* **1998**, *102*, 1364-1371.

(44) Baumgartl, J.; Bechinger, C. On the limits of digital video microscopy, *Europhys. Lett.* **2005**, *71*, 487-493.

(45) Bernal, J. D. The Bakerian Lecture, 1962. The Structure of Liquids, *Proc. Roy. Soc. A* **1964**, *280*, 299-322.

(46) Scott, G. D.; Kilgour, D. M. The density of random close packing of spheres, *J Phys. D: Appl. Phys.* **1969**, *2*, 863-866.

(47) Cho, E. C.; Kim, J. W.; Fernandez-Nieves, A.; Weitz, D. A. Highly responsive hydrogel scaffolds formed by three-dimensional organization of microgel nanoparticles, *Nano Lett.* **2008**, *8*, 168-172.

(48) Keerl, M.; Smirnovas, V.; Winter, R.; Richtering, W. Interplay between hydrogen bonding and macromolecular architecture leading to unusual phase behavioir in thermosensitive micirogels, *Angew. Chem. Int. Ed.* **2008**, *47*, 338-341.

(49) Grier, D. G. Optical tweezers in colloid and interface science, *Curr. Opin. Colloid Interface Sci.* **1997**, *2*, 264-270.

(50) Prieve, D. C. Measurement of colloidal forces with TIRM, *Adv. Colloid Interface Sci.* **1999**, *82*, 93-125.

(51) Alsayed, A. M.; Islam, M. F.; Zhang, J.; Collings, P. J.; Yodh, A. G. Premelting at defects within bulk colloidal crystals *Science* **2005**, *309*, 1207-1210.

(52) Saija, F.; Prestipino, S.; Giaquinta, P. V. Evaluation of phenomenological one-phase critieria for the melting and freezing of softly repulsive particles, *J. Chem. Phys.* **2006**, *124*, 244504.

(53) Ishida, N.; Kobayashi, M. Interaction forces measured between poly(N-isopropylacrylamide) grafted surface and hydrophobic particle, *J. Colloid Interf. Sci.* **2006**, *297*, 513-519.

(54) Kratz, K.; Hellweg, T.; Eimer, W. Influence of charge density on the swelling of colloidal poly(N-isopropylacrylamide-co-acrylic acid) microgels, *Colloids Surf. A* **2000**, *170*, 137-149.

CHAPTER 6

CLICKABLE MULTI-RESPONSIVE MCIROGELS

FOR CHEMO-LIGATION

This chapter describes the synthesis, purification and characterization of clickable microgels, poly(*N*-isopropylacrylamide-*co*-acrylic acid-*co*-3-azido-2-hydroxypropyl methacrylate) (pNIPAm-AAc-AzHPMA) and poly(*N*-isopropylacrylamide-*co*-acrylic acid-*co*-propargyl acrylate) (pNIPAm-AAc-PA), and clickable fluorophores, fluorescein propargyl thiourea (FPTU) and 5-azidofluorescein (AzF). The click reaction between clickable microgels and clickable fluorophores is then performed to demonstrate the advantage of click reaction for chemo-ligation of microgel particles in aqueous phase. The simultaneous and two-step click reaction and EDC (1-ethyl-3-(3-dimethylamino-propyl)- carbodiimide hydrochloride) coupling were performed to confirm the orthogonality of click reaction to other ligation techniques, such as EDC coupling. Note that this chapter is excerpted from my paper submitted to Journal of American Chemical Society.

6.1 Introduction

6.1.1 Literature Review

Microgels are micrometer or sub-micrometer sized polymeric networks swollen in good solvent,[1,2] and are called hydrogel microparticles[3] or hydrogel microspheres[4] if the dispersant is water. Solvent occupies the majority of the volume within microgels, as the interactions between the polymer and the solvent dominate over interactions between polymeric chains.[2] However, external stimuli can trigger an abrupt shift towards the dominance of polymer-polymer over polymer-solvent interactions. A classic illustration of this effect is observed in polymers displaying a lower critical solution temperature

(LCST), above which the polymer desolvates in an entropically-driven phase transition.[5,6] The most extensively investigated thermoresponsive microgels are composed of poly(N-isopropylacrylamide) (pNIPAm), which displays an LCST at approximately 31 ºC.[2,6-8] Furthermore, the co-polymerization of acidic or basic co-monomers yields microgels that exhibit not only temperature- but also pH- and ionic strength-responsivity.[9,10] As a result of there properties, stimuli-responsive microgel systems have been used as targeted drug delivery vehicles since the last decade.[11-16] Our group attempted to load microgel/nanogels with biomacromolecules, such as peptides,[17,18] siRNA,[15] and drugs, such as Doxorubisin,[19] via electrostatic interaction/osmotic pressure.[15,17,18] Furthermore, to facilitate the targeted drug delivery, routine bioconjugation techniques, such as EDC (1-ethyl-3-(3-dimethylamino-propyl)- carbodiimide hydrochloride) coupling of carboxylic acid and amine[20,21] and Michael addition between maleimide and thiol,[22] were used to introduce the ligands on the surface of microgel/nanogel particles. However, the synthesis of such vehicles can be compromised when the targeting moieties and therapeutics possess functionalities that are cross-reactive or do not permit controlled, high-yield coupling to the microgel carrier. To circumvent this problem, the chemical handles should possess chemical orthogonality: not only be chemically inert to common functionalities and reactions in biological environments, but also react rapidly with complementary functionalities under ambient conditions and in aqueous media without interference from other functional groups. Bioorthogonal click reactions,[23] especially Cu(I)-catalyzed azide-terminal alkyne 1,3-dipolar cycloadditions,[24,25] meet the above criteria and therefore represent a good choice for functionalization of microgel particles.

Click reactions are by definition easy and robust to perform, generate products in high yield with little or no byproducts, and tolerate O_2, H_2O, or even physiological conditions.[26] Click chemistry, especially Cu(I)-catalyzed[24,25] 1,3-dipolar Huisgen[27] cycloaddition of azide and terminal alkyne, due to the very narrow reaction profile of azides and alkynes in biological environments, offer bioorthogonality[23,28] to any naturally

occurred functionalities, such as mercapto, hydroxy, carboxy, and amino groups.[29] Whereas metal-free click reactions have recently been developed,[23,28,30] Cu(I)-catalyzed azide-terminal alkyne cycloaddition is most extensively investigated reaction for bioorthogonal conjugation of macromolecules.[31,32] In addition to dendrimers[33] and polymers,[31,32] this click reaction has also been executed on the microgel particles[34-37] and biological nanoparticles.[38,39] Hawker and Wooley prepared shell-cross-linked (SCK) nanoparticles via a click reaction.[40] The Frechet group developed a "two-step" polymerization-azidation process to fabricate azido-containing polymer beads for HPLC separation.[37] The Foulger group has prepared alkynyl-containing latex particles to stabilize colloidal crystals.[35] However, none of these papers demonstrated azido-containing microgel particles in a "one-pot" polymerization process. In the present study, we demonstrate a one-pot, multi-feed synthesis of microgel particles with either azido or terminal alkynyl groups on poly(*N*-isopropylacrylamide-co-acrylic acid) (pNIPAm-AAc) microgel particles. Furthermore, the click reaction between microgel-based azide and terminal alkyne groups with alkynyl- and azido-containg fluorophores confirms the validity of the click reaction on microgel carriers. Additionally, the demonstration of a simultaneous click reaction and a 1-ethyl-3-(3-(dimethylamino)propyl) carbodiimide hydrochloride (EDC) coupling reaction[20] confirms the orthogonality of click reaction to functionalities such as hydroxyl, carboxyl, and amino groups.

6.1.2 Experimental Design

To achieve the azido-containing microgel synthesis, we used glycidyl methacrylate as precursor co-monomer in one-pot, multi-feed copolymerization with *in situ* ring-opening conversion of the epoxy group to an azidohydrin.[41,42] Although the conversion of glycidyl methacrylate (GMA) to 3-azido-2-hydroxypropyl methacrylate (AzHPMA) has been reported previously, those approaches required either a polymeric phase-transfer catalyst in water[43] or samarium chloride hexahydrate catalyst in DMF.[44] In

our approach, no specific phase-transfer catalyst or organic solvent was used for azidation of the microgels during polymerization. Furthermore, the one-pot synthesis of azido-containing clickable microgels eliminated the complications involved with synthesis and purification of AzHPMA.[43,44] The one-pot, three-stage copolymerization of NIPAm, AAc, and GMA with NaN3 is shown in Scheme 1. For all schemes below, carboxylic acid groups for EDC coupling are denoted by red, whereas azido and alkynyl groups for the click reactions are denoted by purple and blue, respectively.

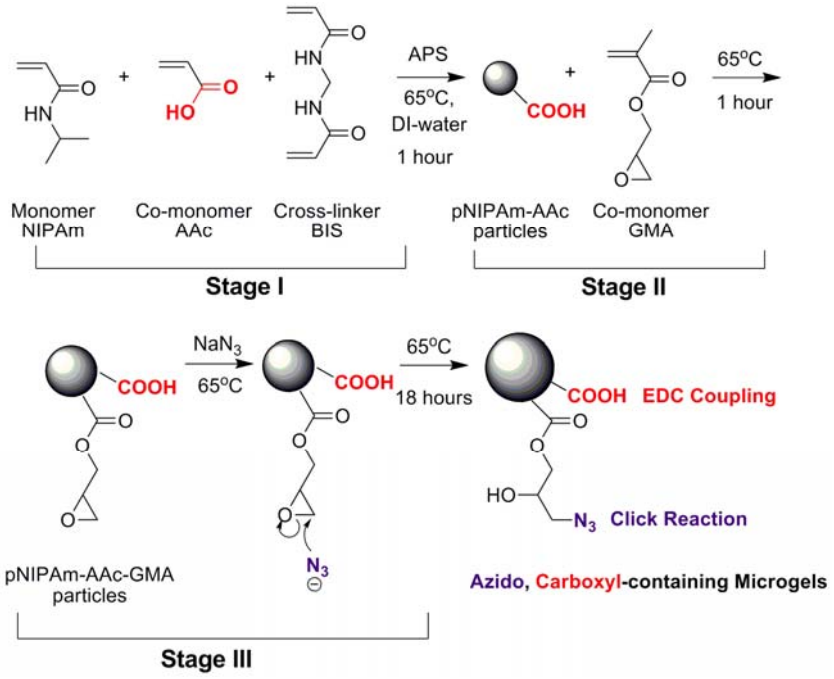

Scheme 6.1 One-pot, three-stage synthesis of azido and carboxylic acid-containing, multi-responsive, clickable microgels **1** (See Chart 6.1).

Scheme 6.1 contains three synthetic stages. Stage I consists of the copolymerization of NIPAm, AAc, and BIS initiated by APS in deionized (DI) water at 65 ºC for an hour. Stage II consists of the addition of GMA to the microgel copolymerization mixture. The late addition of GMA was performed to circumvent phase segregation of hydrophobic GMA into the core of pNIPAm-based microgels.[45] After another hour of copolymerization, Stage III was started with the addition of NaN_3 to the

copolymerization mixture for the azidation of the GMA moieties *in situ*. Note that the amount of NaN_3 added was divided into several portions to avoid an abrupt ionic strength increase, which induces the rapid coagulation of microgels at elevated temperature. The *in situ* azidation of GMA did not inhibit the copolymerization process if the NaN_3 was added 2 hours after initiation. Under these conditions, it is not known whether the azidation occurs before or after GMA co-polymerization with NIPAm or AAc, although given the late addition of NaN_3 it is likely that the majority of the azidohydrin formation occurs after GMA incorporation into the microgel. The detailed mechanism of this polymerization is currently under further investigation in our group.

Similarly, we also used propargyl acrylate (PA) as co-monomer in a one-pot, two-stage, multi-feed approach for the preparation of alkynyl-containing microgels, which is shown in Scheme 6.2. To avoid phase separation of PA into the microgel core, we also delayed the addition of PA until 1 hour after the initiation. Note that the reaction time required for high conversion is longer for PA copolymerizations, which is likely due to its relatively slow propagation rate.[35]

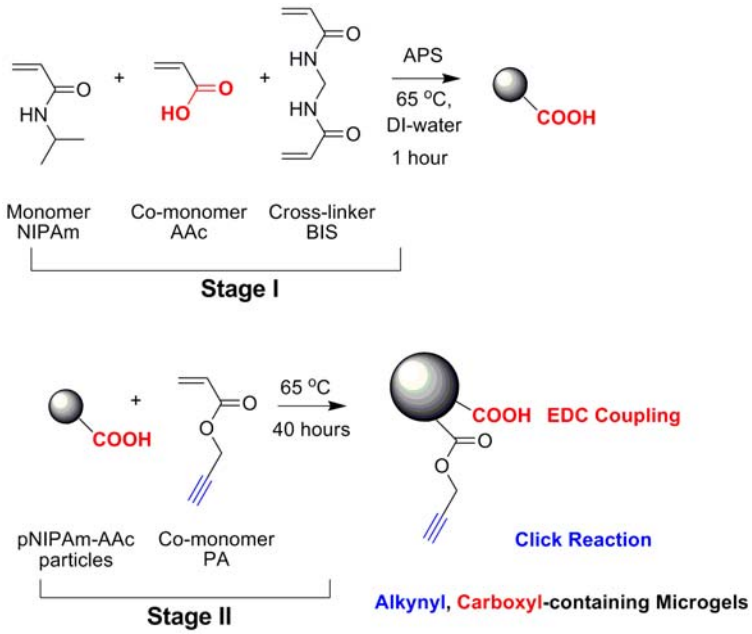

Scheme 6.2 One-pot, two-stage synthesis of alkynyl and carboxylic acid-containing multi-responsive, clickable microgels **2** (See Chart 6.1).

To examine the click reaction between microgels and fluorescent dyes, the "clickable" fluorophores, fluorescein propargyl thiourea (FPTU **4**, Chart 6.1) and 5-azidofluorescein (AzF **3**, Chart 6.1) were synthesized and purified in our laboratory. Furthermore, to test the orthogonality of click reaction to EDC coupling between carboxylic acid groups on microgels and fluorescent dyes with amino groups, tetramethylrhodamine-5,6-carboxamide cadeverine (TMRC **5**, Chart 6.1) was used. The chemical functionalities on the two clickable microgels and the structures of the fluorophores are shown in Chart 6.1.

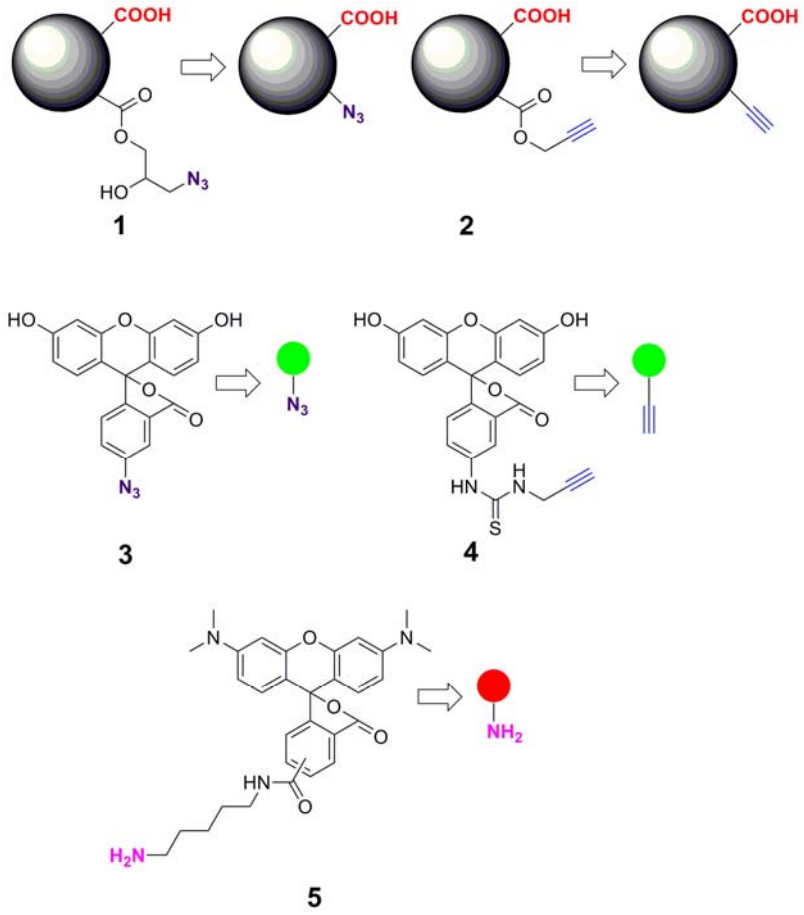

Chart 6.1 Chemical structures of azido- and alkynyl, carboxyl-containing microgels (**1** and **2**) and azido-, alkynyl, and amino-functionalized fluorophores (**3**, **4** and **5**).

Epifluorescence microscopy was used to determine if click reactions or EDC coupling occurs between functional microgels and fluorophores with complementary functionalities. The click reaction between azide microgel **1** and alkyne fluorophore **4** was performed with Cu(I) catalysis in aqueous media at ambient temperature. The EDC coupling between the carboxylic acid groups on microgel **1** with amino groups on fluorophore **5** was performed simultaneously with the click reaction to test orthogonality of click reaction. Similarly, the click reaction of alkyne microgel **2** with azide fluorophore **3** with Cu(I) catalysis and EDC coupling of microgel **2** with fluorophore **5** were also performed simultaneously. All microgel-fluorophore ligations were allowed to proceed in pH 5.0 aqueous buffer at ambient temperature. The one-pot click reaction + EDC coupling between microgel **1** and dyes **4** and **5** or between microgel **2** and dyes **3** and **5** are shown in Scheme 6.3. The one-pot, simultaneous ligation of **1** with **4** and **5**, gave rise to microgel **6**. Similarly, the one-pot, simultaneous ligation microgel **2** with **3** and **5** gave rise to microgel **7**. After reaction with the fluorophores, the resultant microgels were cleaned extensively by a centrifugation-redispersion procedure to remove residual Cu(I) species and nonspecifically adsorbed fluorophores. (Details in Experimental, Section 6.2.4.2.1)

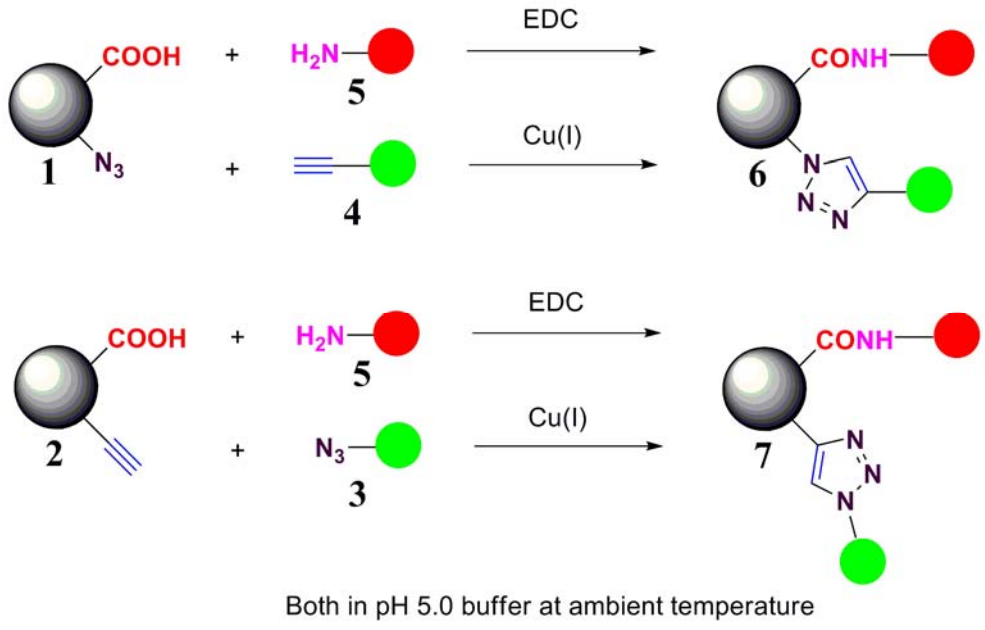

Scheme 6.3 One-pot click reaction and EDC coupling of clickable microgels with fluorophores with complementary functionalities in pH 5.0 buffer at ambient temperature.

To compare with the simultaneous ligation method, two-step ligations of microgels **1** and **2** were also performed. Azido and carboxylic acid-containing microgel **1**, can either first click with **4** followed by EDC coupling with **5** or first EDC couple with **5** followed by clicking with **4**. Alkynyl and carboxylic acid-containing microgel **2**, can also click with **3** and EDC couple with **5** in a similar manner. The two-step chemo-ligations of fluorophores on multiresponsive clickable microgels are illustrated in Scheme 6.4.

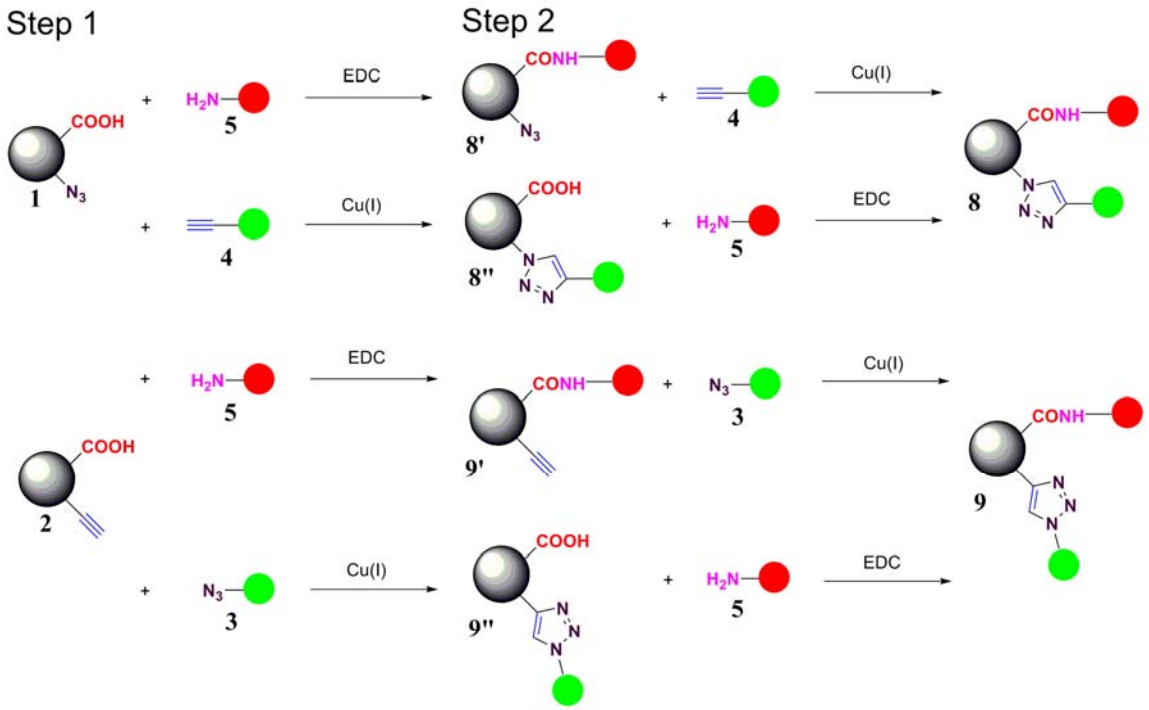

Scheme 6.4 Two-step coupling to clickable microgels **1** and **2** with fluorophores in pH 5.0 buffer at ambient temperature.

The fluorescently labeled microgels produced in Steps 1 (**8'**, **8"**, **9'**, and **9"**) and 2 (**8** and **9**), were purified for fluorescence microscopy. Similar purification protocols were used for microgels after ligation in each step. (Details are shown in Experimental, Section

6.2.4.2.2.) After purification, microgel dispersions **8** and **9** were dropped and dried on the cleaned glass slides.

To further illustrate the fidelity of these coupling reactions, control experiments were designed to examine the reactivity of azido/alkynyl groups with amino groups and the orthogonality of click reactions to EDC coupling. To minimize the cross-reactivity, monofunctional microgels pNIPAm-AAc **10**, pNIPAm-AzHPMA **11**, and pNIPAm-PA **12** for control experiments were synthesized as shown in Scheme 6.5. Note the synthesis of pNIPAm-AAc microgels **10** was conducted at fairly low temperature, thereby giving particles with relatively larger size, which is shown in Scheme 6.5 and 6.6. Then the control experiments will answer the following questions as shown in Scheme 6.6: I) As for carboxyl groups, are they reacted with alkynyl or azido groups in the presence of Cu(I)? Furthermore, are they reacted with amino groups in the absence of EDC? II) As for azido groups, are they reacted with alkynyl groups without Cu(I)-catalysis? Or are they reacted with themselves with Cu(I)-catalysis? Or are they reacted with amino groups in the presence of Cu(I) or EDC? III) As for alkynyl groups, are they reacted with azido groups without Cu(I)-catalysis? Or are they reacted with themselves with Cu(I)-catalysis? Or are the reacted with amino groups in the presence of Cu(I) or EDC? (Experimental details are shown in Experimental, Section 6.2.4.3.)

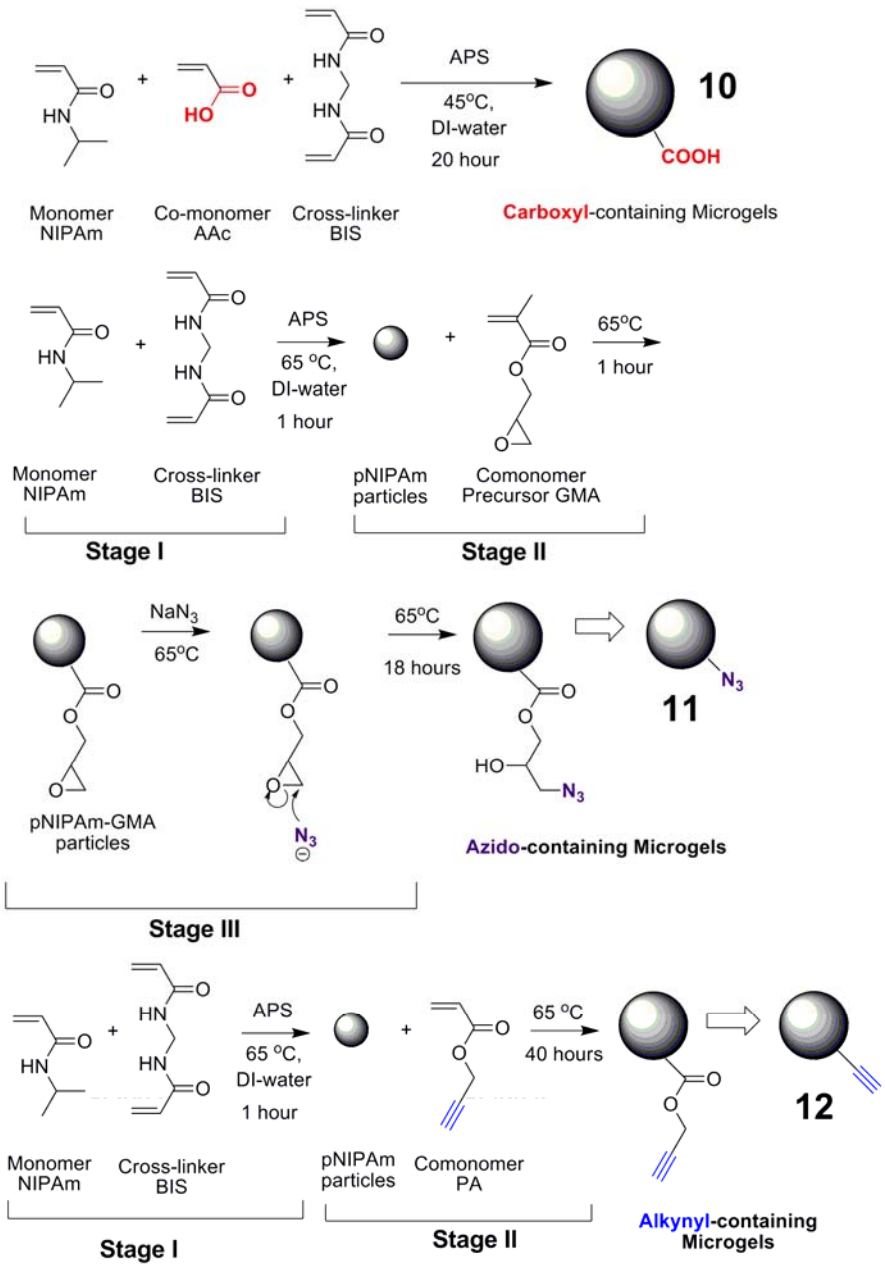

Scheme 6.5 Syntheses of microgels pNIPAm-AAc **10**, pNIPAm-AzPMA **11**, and pNIPAm-PA **12** for control experiments. Note the experimental details are shown in Section 6.2.3.2.

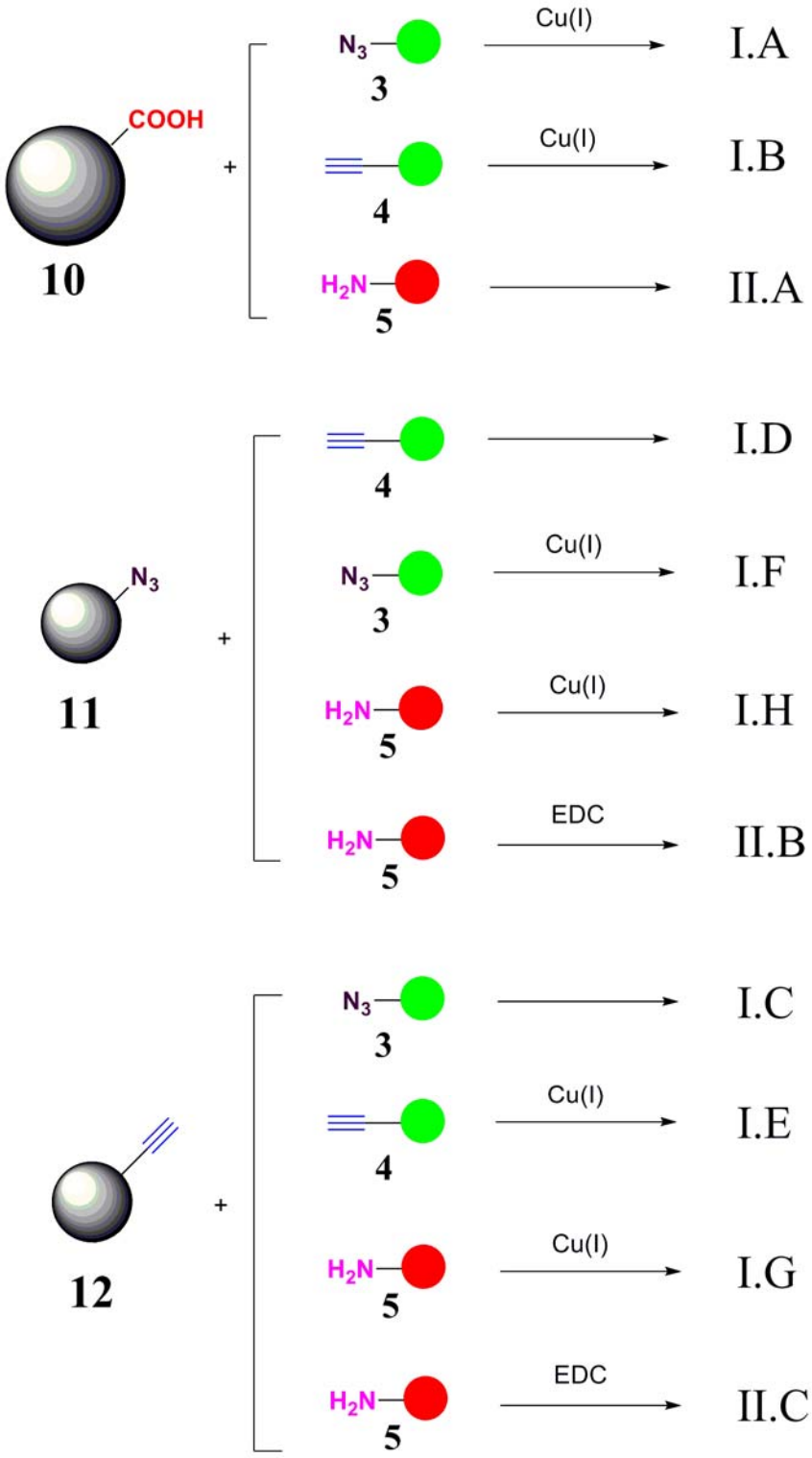

Scheme 6.6 Control experiments designed to examine the orthogonality of Cu(I)-catalyzed azido-alkyne click reactions to EDC coupling on microgels.

6.2 Experimental

6.2.1 Clickable Fluorophores

6.2.1.1 Materials

Fluorescein isothiocyanate I (FITC-I, Acros), propargyl amine (PAm, Acros), 5-aminofluorescein (AmF, TCI), sodium nitrate ($NaNO_2$, Alfa Aesar), HCl (0.5 M, Fisher), sodium azide (NaN_3, Acros), dimethylformamide (DMF, EMD), triethylamine (TEA, EMD), methanol (BDH), and methylene chloride (BDH) were all used without further purification. Sodium tetraborate decahydrate ($Na_2B_4O_7.10H_2O$, Fisher) was used to prepare Borax buffer.[46] Silica gel (Natland, 100-200 mesh) was used for column chromatographic purification of crude product. All water used in the synthesis and purification are deionized water with a resistivity of 18MΩ·cm.

6.2.1.2 Synthesis and Column Chromatographic Purification of Fluorophores

*6.2.1.2.1 Synthesis and Column Chromatographic Purification of Fluorescein Propargyl Thiourea (FPTU **4**)*

The synthetic and purification protocol is based upon the combination of available references.[47,48] Approximately 38.3 mg of sodium tetraborate decahydrate was dissolved in 100 mL deionized water to prepare 0.01 M Borax buffer. The pH value of Borax buffer was 9.2 ± 0.1. Then 80 μL propargyl amine (PAm) (1.2 mmol) was dissolved in approximately 10 mL Borax buffer. Approximately 180.6 mg of fluorescein isothiocyanate I (FITC-I) (0.53 mmol) was dissolved in 60 mL Borax buffer. The reaction start by transferring 10 mL PAm buffer solution into 60 mL FITC-I buffer solution under magnetic stirring at room temperature. The reaction was allowed to proceed for 48 hours. The reaction mixture was purified by column chromatography with silica gel as stationary phase and CH_2Cl_2/MeOH (95:5 v/v) as mobile phase. After dried in vacuum oven at room temperature, the dark yellow solid powder was obtained with the yield of 63%.

*6.2.1.2.2 Synthesis and Column Chromatographic Purification of 5-Azidofluorescein (AzF **3**)*

The synthetic protocol is a revised version of available reference.[49] Of 5-amino-fluorescein (AmF), 368.6 mg (1.06 mmol) were dissolved in 20 ml of methanol. Dissolve 409.9 mg of sodium nitrite in 10 mL deionized water. Sodium nitrite solution was then added into AmF methanol solution under vigorous stirring in three-neck round bottom flask within ice bath, followed by the slowly dripping addition of 10 ml of a 0.5 M solution of hydrochloric acid. After NO stopped evolving from the stirred reaction, 0.5 g of solid sodium azide in 10 mL aqueous solution was added under stirring in an open flask, in a well ventilated hood (Caution: Hydrazoic acid is very toxic). After nitrogen stopped evolving from the stirred mixture, the mixture was filtered through Whatman qualitative filter paper and the solvents removed under vacuum. Approximately 20 mL of 0.5 M HCl solution were added to the residue and the resulting precipitate was washed extensively with cold water. After re-dissolving precipitate in DMF, the reaction product was purified by column chromatography with silica gel as stationary phase and CH_2Cl_2/acetone (80:20 v/v) as mobile phase. After dried in vacuum oven at room temperature, the brown-yellow solid powder was obtained with the yield of 74%.

6.2.1.3 Fluorescene Spectrophotometry

A steady-state fluorescence spectrophotometer (Photon Technology International) equipped with a Model 814 PMT photon-counting detector was used to record absorption of irradiation and emission of fluorescence of 1 μM fluorophore aqueous solution at controlled temperature. The temperature was controlled using a PE 60 Temperature Controller and Peltier Stage (Linkam Scientific Instruments Ltd., Surrey, UK). The slit widths were set to a bandwidth of 1 nm and the excitation and emission monochromators were set to approximately 400-500 nm and 500-600 nm, respectively. The solution

temperature was measured with a platinum resistor immersed in the solution; the temperature accuracy was ± 0.1 °C, as specified by the manufacturer.

6.2.2 Clickable Microgels for Click Reaction and EDC Coupling

6.2.2.1 Materials

The monomers *N*-isopropylacrylamide (NIPAm, TCI) was purified by recrystallization from n-hexane (J. T. Baker). Glycidyl methacrylate (GMA, Fluka), sodium azide (NaN_3, Acros), propargyl acrylate (PA, Polysciences), acrylic acid (AAc, Fluka), *N,N'*-methylene bisacrylamide (BIS, Aldrich) and ammonium persulfate (APS, Aldrich) were used as received. Water for polymerizations, purification, and dispersion preparations was distilled, de-ionized to a resistivity of 18 MΩ•cm (Barnstead E-Pure system), and filtered through an in-line 0.8-μm filter to remove particulate matter.

6.2.2.2 One-Pot Multi-Stage Synthesis and Purification of Clickable Microgels

*6.2.2.2.1 Synthesis and Purification of pNIPAm-AAc-AzHPMA **1***

The 250 mL three-neck round-bottom flask equipped with N_2 inlet and outlet, condenser, and thermometer was charged with 95 mL aqueous solution containing 2.045 g (18 mmol) NIPAm (monomer), 0.072 g (1 mmol) AAc (co-monomer) and 0.031 g (1 mmol) BIS (cross-linker) through syringe with an in-line 0.8-μm filter. The reaction mixture was heated up to 50 °C and bubbled with N_2 for an hour before the addition of APS solution (0.023 g, 0.1 mmol, in 5 mL de-ionized water). After addition of APS, the copolymerization was allowed to proceed for 60 minutes. The reaction mixture became turbid due to the formation of microgel particles at temperature higher than their lower critical solution temperature (LCST). Then the temperature was set to ramp from 50 °C up to 65 °C with a ramp rate of 30 °C/hr. After 60 minutes, add 5 mL acetone solution

containing 0.143 g (1 mmol) GMA (co-monomer precursor containing epoxy group) through syringe with an in-line 0.8-μm filter. A 5 mL aqueous solution containing 0.098 g (1.5 mmol) NaN_3 (modifier for azidation of epoxy group) was also added dropwise through syringe with an in-line 0.8-μm filter in several portions. When the temperature of reaction mixture reached 65 °C, the copolymerization was allowed to proceed for 20 hours. After copolymerization, the reaction mixture was allowed to filter through glass fiber to remove coagulum, followed by centrifugation at a radial centrifugal force (RCF) of 15, 422 × g to separate residual monomers, soluble oligomers, and residual APS and NaN_3. After centrifugation, the supernatant was removed and the pellet was re-dispersed in fresh de-ionized water and allowed to shake for overnight. The centrifugation-redispersion process were repeated four times before lyophilization at – 49 °C under 40×10^{-3} mbar for 72 hours. The product was hygroscopic white powder.

*6.2.2.2.2 Synthesis and Purification of pNIPAm-AAc-PA **2***

The 250 mL three-neck round-bottom flask equipped with N_2 inlet and outlet, condenser, and thermometer was charged with 95 mL aqueous solution containing 2.045 g (18 mmol) NIPAm (monomer), 0.072 g (1 mmol) AAc (co-monomer) and 0.031 g (1 mmol) BIS (cross-linker) through syringe with an in-line 0.8-μm filter. The reaction mixture was heated up to 50 °C and bubbled with N_2 for an hour before the addition of APS solution (0.023 g, 0.1 mmol, in 5 mL de-ionized water). After addition of APS, the copolymerization was allowed to proceed for 60 minutes. The reaction mixture became turbid due to the formation of microgel particles at temperature higher than their lower critical solution temperature (LCST). Then the temperature was set to ramp from 50 °C up to 65 °C with a ramp rate of 30 °C/hr. After 60 minutes, add 5 mL acetone solution

containing 0.110 g (1 mmol) PA (co-monomer containing acetylene group) through syringe with an in-line 0.8-μm filter. When the temperature of reaction mixture reached 65 °C, the copolymerization was allowed to proceed for 40 hours. After copolymerization, the reaction mixture was allowed to filter through glass fiber to remove large coagulum, followed by centrifugation at a force of 15, 422 × g to separate residual monomers, soluble oligomers, and residual APS. After centrifugation, the supernatant was removed and the pellet was re-dispersed in fresh de-ionized water and allowed to shake for overnight. The centrifugation-redispersion process were repeated four times before lyophilization at – 49 °C under 40×10^{-3} mbar for 72 hours. The product was hygroscopic white powder.

6.2.2.3 Characterization of Clickable Microgels

6.2.2.3.1 Photon Correlation Spectroscopy

The theoretical background and operation protocol are referred to Chapter 2, Section 2.2.5.1 in this dissertation.

6.2.2.3.2 Attenuated Total Reflectance-Fourier Transform Infrared Spectroscopy (ATR-FTIR)

As shown in Scheme 6.7, an attenuated total reflection accessory operates by measuring the changes that occur in a totally internally reflected infrared beam when the beam comes into contact with a sample.[50] An infrared beam is directed onto an optically dense crystal with a high refractive index at a certain angle. This internal reflectance creates an evanescent wave that extends beyond the surface of the crystal into the sample held in contact with the crystal. This evanescent wave protrudes only a few microns (0.5 - 5 μm) beyond the crystal surface and into the sample. In regions of the infrared spectrum

where the sample absorbs energy, the evanescent wave will be attenuated or altered. The attenuated energy from each evanescent wave is passed back to the IR beam, which then exits the opposite end of the crystal and is passed to the detector in the IR spectrometer. The system then generates an infrared spectrum.

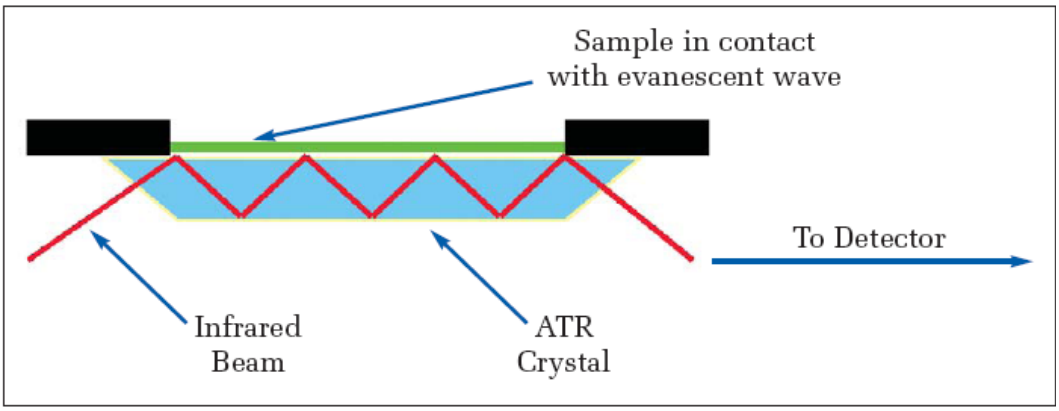

Scheme 6.7 The schematic diagram of attenuated total reflection accessory mount on ATR-FTIR instrument, where the green thick line represent unknown sample, red line IR beam, and blue invert trapezoid ATR crystal.

At room temperature, approximately 25 mg of polymeric solid was put on the ATR crystal (diamond is used as ATR crystal) of Thermo Electron Nicolet 4700 FT-IR instrument. The software OMNIC 7.0 was used to set the resolution to 1 cm^{-1} and scanning range from 500 to 4000 cm^{-1}. After background scanning in air, the sample was mounted on the ATR crystal for sample scanning. The resulting data were saved as SPA and CSV formats for data analysis.

6.2.3 Microgels for Control Experiments

6.2.3.1 Materials

All reagents used here are referred to Section 6.2.2.1

6.2.3.2 One-Pot Multi-Stage Synthesis of Microgels for Control Experiments

*6.2.3.2.1 Synthesis of pNIPAm-AAc **10** Microgels for Control Experiments.*

The monomers NIPAm (1.8 g, 15.9 mmol), AAc (0.2 g, 2.78 mmol), and the cross-linker BIS (0.04 g, 0.259 mmol) were dissolved in 100 mL of distilled, deionized water and filtered through an in-line 0.8-μm filter to remove particulate matter. Deionized water (25 mL) was used to transfer and wash throughout filtration. After delivering the monomer solution to a 250 mL three-neck round-bottom flask via a 20-mL syringe with an in-line 0.8-μm filter, the flask was equipped with a thermometer, condenser/N_2 outlet, stir bar, and a N_2 inlet. The reaction system was purged with N_2 for 1 hour while equilibrating to a temperature of 45 °C. The monomer solution (115-mL volume) was then maintained at 45 °C for 15 min at a stir rate of 450 rpm. A 5 mL aliquot of a 0.044 M aqueous solution of the initiator APS was delivered to the monomer solution via a 5-mL syringe with an in-line 0.8-μm filter to initiate the polymerization. The polymerization was allowed to proceed 20 hours at 45 °C. After polymerization, the resulting turbid reaction product was filtered through glass wool to remove a large amount of coagulum. Microgels were purified by centrifugation to separate unreacted monomers, oligomers, and initiator from the microgels. The synthesis product was separated at a RCF of 15, 422 × g for 1 hour, followed by removal of the supernatant and re-dispersion of microgel pellets by shaking with fresh deionized water. The centrifugation and re-dispersion process was repeated four times. After purification, the microgel dispersion was lyophilized at –42 °C under 40×10^{-3} mbar for 48-72 hours. The freeze-dried product was a hygroscopic white powder.

*6.2.3.2.2 Synthesis of pNIPAm-AzHPMA **11** Microgels for Control Experiments.*

A 250 mL three-neck round-bottom flask equipped with N_2 inlet and outlet, condenser, and thermometer was charged with 95 mL aqueous solution containing 2.158 g (19 mmol) NIPAm (monomer) and 0.031 g (2 mmol) BIS (cross-linker) through syringe with an in-line 0.8-μm filter. The reaction mixture was heated to 65 °C and bubbled with N_2 for an hour before the addition of APS solution (0.023 g, 0.1 mmol, in 5

mL deionized water). After addition of APS, the copolymerization was allowed to proceed for 60 minutes. The reaction mixture became turbid due to the formation of microgel particles. Then a 5 mL acetone solution containing 0.143 g (1 mmol) GMA was added via syringe with a 0.8-μm filter; the reaction was allowed to proceed for another one hour. A 5-mL aqueous solution containing 0.098 g (1.5 mmol) NaN_3 was added dropwise via syringe with an in-line 0.8-μm filter. When the temperature of the reaction mixture stabilized at 65 °C, the copolymerization was allowed to proceed for 18 hours. After copolymerization, the reaction mixture was filtered through glass wool to remove coagulum, followed by centrifugation at a force of 15,422 × g to separate residual monomers, soluble oligomers, and residual APS and NaN_3. After centrifugation, the supernatant was removed and the pellet was re-dispersed in fresh deionized water and allowed to shake overnight. The centrifugation-redispersion process were repeated four times before lyophilization at – 49 °C under 40×10^{-3} mbar for 72 hours. The product was hygroscopic white powder.

*6.2.3.2.3 Synthesis of pNIPAm-PA **12** Microgels for Control Experiments.*

A 250 mL three-neck round-bottom flask equipped with N_2 inlet and outlet, condenser, and thermometer was charged with 95 mL aqueous solution containing 2.159 g (19 mmol) NIPAm (monomer) and 0.031 g (2 mmol) BIS (cross-linker) through syringe with a 0.8-μm filter. The reaction mixture was heated to 50 °C and bubbled with N_2 for an hour before the addition of APS solution (0.023 g, 0.1 mmol, in 5 mL deionized water). After addition of APS, the copolymerization was allowed to proceed for 60 minutes. The reaction mixture became turbid due to the formation of microgel particles. Then the temperature was set to ramp from 50 °C up to 65 °C with a ramp rate of 30 °C/hr. After 60 minutes, a 5 mL acetone solution containing 0.110 g (1 mmol) PA was added via syringe with an in-line 0.8-μm filter. When the temperature of the reaction mixture stabilized at 65 °C, the copolymerization was allowed to proceed for 40 hours.

After copolymerization, the reaction mixture was filtered through glass fiber to remove large coagulum, followed by centrifugation at a RCF of 15,422 × g to separate residual monomers, soluble oligomers, and residual APS. After centrifugation, the supernatant was removed and the pellet was re-dispersed in fresh deionized water and allowed to shake for overnight. The centrifugation-redispersion process were repeated four times before lyophilization at –49 °C under 40×10^{-3} mbar for 72 hours. The product was hygroscopic white powder.

6.2.4 Click Reaction and EDC Coupling (Including Control Experiments)

To test the orthogonality of Cu(I)-catalyzed azide-terminal alkyne click reaction to EDC coupling of carboxylic acid and amine groups, both azido-/alkynyl-containing fluorophore and amino-containing fluorophore was used to reacted with alkynyl-/azido- and carboxylic acid-containing microgels. It is expected that complementary clickable functional groups, azide and terminal alkyne, only cross-coupling with each other under catalysis of Cu(I) in aqueous phase at room temperature. Fluorophores, fluorescein and tetramethylrhodamine, was used to trace the reaction product: if green fluorescence was detected under blue light (450-490 nm) excitation, click reaction occurred between clickable fluoresceins and microgels with complementary clickable functionalities; if red fluorescence was detected under green light (510-560 nm) excitation, EDC coupling occurred between tetramethylrhodamine 5,6-carboxamide cadavarine (TMRC) with carboxyl-containing microgels.

6.2.4.1 Materials

Azido-containing cross-linked pNIPAm-AAc-AzHPMA **1** microgels, Alkynyl-containing cross-linked pNIPAm-AAc-PA **2** microgels, 5-azidofluorescein (AzF **3**), and fluorescein propargyl thiourea (FPTU **4**) were synthesized and purified in our lab. Tetramethylrhodamine-5,6-carboxamide cadaverine (TMRC **5**, Molecular Probes), 1-

ethyl-3-(3-dimethylaminopropyl)-carbodiimide hydrochloride (EDC, Sigma), sodium ascorbate (Sigma), copper(II) sulfate pentahydrate ($CuSO_4$•$5H_2O$, Aldrich) were used as received.

6.2.4.2 Click Reaction and EDC Coupling

6.2.4.2.1 Simultaneous Click Reaction and EDC Coupling

A. Simultaneous click reaction and EDC coupling of multi-responsive clickable microgels, pNIPAm-AAc-AzHPMA **1** with FPTU **4** and TMRC **5**, respectively

Approximately 20 mg of microgel **1** solid powders, in which approximately 8 μmol of azido and 15 μmol carboxylic acid groups presented based upon feed ratio, were dissolved in 10 mL de-ionized water. Then 2.0 mg sodium ascorbate (10 μmol) was dissolved in 2 mL de-ionized water, which was subsequently added into microgel dispersions. After that, 2.5 mL 0.01 mg/mL **4** solution (0.05 μmol) in water/ethanol (50:50) and 100 μL of 0.1mg/mL **5** (0.02 μmol) in DMF solution were added into microgel dispersions followed by adding 1.9 mg EDC (10 μmol) solid and 10 mL de-ionized water. After N_2 bubbling for 5 min, 50 μL 0.1 M $CuSO_4$ (5 μmol) solution was added to initiate click reaction. The reaction was allowed to proceed at room temperature for 18 hours. The product mixture was centrifuged at a relative centrifugal force (RCF) of 15,422 × g for 1 hr at 25 °C, followed by removal of supernatant, a 0.1 M sodium citrate buffer was added to chelate Cu(I) residue in the reaction mixture. After shaking overnight, the second centrifugation was performed at a RCF of 15,422 × g for 1 hr at 25 °C, followed by removal of supernatant; ethanol was added to remove residual free **4** and **5**. After shaking overnight, the third centrifugation was performed at a RCF of 15,422 × g

for 1 hr at 25 °C, followed by removal of supernatant; de-ionized water was added to the pellet to form dilute microgel **6** dispersions.

B. Simultaneous click reaction and EDC coupling of multi-responsive clickable microgels, pNIPAm-AAc-PA **2** with AzF **3** and TMRC **5**, respectively.

Approximately 20 mg of microgel **2** solid powders, in which approximately 8 μmol of alkynyl and 15 μmol carboxylic acid groups presented based upon feed ratio, were dissolved in 10 mL de-ionized water. Then 2.0 mg sodium ascorbate (10 μmol) was dissolved in 2 mL de-ionized water, which was subsequently added into microgel dispersions. After that, 250 μL 0.04 mg/mL **3** solution (0.02 μmol) in water/ethanol (50:50) and 100 μL of 0.1 mg/mL **5** (0.02 μmol) in DMF solution were added into microgel dispersions followed by adding 1.9 mg EDC (10 μmol) solid and 10 mL de-ionized water. After N_2 bubbling for 5 min, 50 μL 0.1 M $CuSO_4$ (5 μmol) solution was added to initiate click reaction. The reaction was allowed to proceed at room temperature for 18 hours. The product mixture was centrifuged at a relative centrifugal force (RCF) of 15,422 × g for 1 hr at 25 °C, followed by removal of supernatant, a 0.1 M sodium citrate buffer was added to chelate Cu(I) residue in the reaction mixture. After shaking overnight, the second centrifugation was performed at a RCF of 15,422 × g for 1 hr at 25 °C, followed by removal of supernatant; ethanol was added to remove residual free **3** and **5**. After shaking overnight, the third centrifugation was performed at a RCF of 15,422 × g for 1 hr at 25 °C, followed by removal of supernatant; de-ionized water was added to the pellet to form dilute microgel **7** dispersions.

6.2.4.2.2 Two-Step Click Reaction and EDC Coupling

A. Click reaction between multi-responsive clickable microgels, azido-containing pNIPAm-AAc-AzHPMA **1**, and alkynyl-containing fluorophore, FPTU **4**, followed by EDC coupling between carboxyl-containing clicked microgels **8"** and amino-containing fluorophore, TMRC **5**.

Approximately 20 mg of microgel **1** solid powders, in which approximately 8 μmol of azido group presented based upon feed ratio, was dissolved in 10 mL de-ionized water. Then 2.0 mg sodium ascorbate (10 μmol) was dissolved in 2 mL de-ionized water, which was subsequently added into microgel dispersions. After that, 2.5 mL 0.01 mg/mL FPTU **4** solution (0.05 μmol) in water/ethanol (50:50) was added into microgel dispersions followed by N_2 bubbling for 5 min. After N_2 purge, 50 μL 0.1 M $CuSO_4$ (5 μmol) solution was added to initiate click reaction. The color of reaction mixture changed from yellow-greenish to brownish immediately after addition of $CuSO_4$. The click reaction was allowed to proceed at room temperature for 18 hours. The product mixture was centrifuged at a relative centrifugal force (RCF) of 15,422 × g for 1 hr at 25 °C, followed by removal of supernatant, a 0.1 M sodium citrate buffer was added to chelate Cu(I) residue in the reaction mixture. After shaking overnight, the second centrifugation was performed at a RCF of 15,422 × g for 1 hr at 25 °C, followed by removal of supernatant; ethanol was added to remove residual free **4**. After shaking overnight, the third centrifugation was performed at a RCF of 15,422 × g for 1 hr at 25 °C, followed by removal of supernatant; de-ionized water was added to the pellet to form dilute microgel **8"** dispersions.

Approximately half of above formed clicked microgel **8"** dispersions (10 mL), in which approximately 7.5 μmol of carboxylic acid group was presented, was used for EDC coupling. Then 50 μL of 0.1 mg/mL TMRC **5** (0.01 μmol) in DMF solution was added to microgel dispersions, followed by adding 1 mg EDC (5 μmol) solid and 5 mL de-ionized water. The EDC coupling reaction was allowed to proceed at room

temperature for 18 hours. After reaction, the reaction mixture was centrifuged at a relative centrifugal force (RCF) of 15,422 × g for 1 hr at 25 °C, followed by removal of supernatant; DMF was added to remove residual free **5**. After shaking overnight, the second centrifugation was performed at a relative centrifugal force (RCF) of 15,422 × g for 1 hr at 25 °C, followed by removal of supernatant, de-ionized water was added to the pellet to form dilute microgel **8** dispersions.

B. EDC coupling between multi-responsive carboxylic acid-containing clickable microgels, pNIPAm-AAc-AzHPMA **1**, and amino-containing fluorophore, TMRC **5**, followed by click reaction between azido-containing coupled microgels **8'** and alkynyl-containing fluorophore, FPTU **4**.

Approximately 20 mg of microgel solid powders, in which approximately 15 μmol of carboxylic acid group presented based upon feed ratio, was dissolved in 10 mL de-ionized water. Then 100 μL of 0.1 mg/mL TMRC **5** (0.02 μmol) in DMF solution was added to microgel dispersions, followed by adding 2 mg EDC (10 μmol) solid and 10 mL de-ionized water. The EDC coupling reaction was allowed to proceed at room temperature for 18 hours. After reaction, the reaction mixture was centrifuged at a relative centrifugal force (RCF) of 15,422 × g for 1 hr at 25 °C, followed by removal of supernatant; DMF was added to remove residual free **5**. After shaking overnight, the second centrifugation was performed at a relative centrifugal force (RCF) of 15,422 × g for 1 hr at 25 °C, followed by removal of supernatant, de-ionized water was added to the pellet to form dilute microgel **8'** dispersions.

Approximately half of above formed coupled microgel **8'** dispersions (10 mL), in which approximately 4 μmol of azido group was presented, was used for click reaction. Then 1.0 mg sodium ascorbate (5 μmol) was dissolved in 1 mL de-ionized water, which was subsequently added into microgel dispersions. After that, 1.25 mL 0.01 mg/mL

FPTU **4** solution (0.025 μmol) in water/ethanol (50:50) was added into microgel dispersions followed by N_2 bubbling for 5 min. After N_2 purge, 25 μL 0.1 M $CuSO_4$ (2.5 μmol) solution was added to initiate click reaction. The color of reaction mixture changed from yellow-greenish to brownish immediately after the addition of $CuSO_4$. The click reaction was allowed to proceed at room temperature for 18 hours. The product mixture was centrifuged at a relative centrifugal force (RCF) of 15,422 × g for 1 hr at 25 °C, followed by removal of supernatant, a 0.1 M sodium citrate buffer was added to chelate Cu(I) residue in the reaction mixture. After shaking overnight, the second centrifugation was performed at a RCF of 15,422 × g for 1 hr at 25 °C, followed by removal of supernatant; ethanol was added to remove residual free **4**. After shaking overnight, the third centrifugation was performed at a RCF of 15,422 × g for 1 hr at 25 °C, followed by removal of supernatant; de-ionized water was added to the pellet to form dilute microgel **8** dispersions.

C. Click reaction between multi-responsive alkynyl-containing clickable microgels, pNIPAm-AAc-PA **2**, and azido-containing clickable fluorophore, AzF **3**, followed by EDC coupling between carboxylic acid-containing clicked microgels **9"** and amino-containing fluorophore, TMRC **5**.

Approximately 20 mg of microgel **2** solid powders, in which approximately 8 μmol of alkynyl group presented based upon feed ratio, was dissolved in 10 mL de-ionized water. Then 2.0 mg sodium ascorbate (10 μmol) was dissolved in 2 mL de-ionized water, which was subsequently added into microgel dispersions. After that, 250 μL 0.04 mg/mL AzF **3** solution (0.02 μmol) in water/ethanol (50:50) was added into microgel dispersions followed by N_2 bubbling for 5 min. After N_2 purge, 50 μL 0.1 M $CuSO_4$ (5 μmol) solution was added to initiate click reaction. The color of reaction mixture changed from yellow-greenish to brownish immediately after addition of $CuSO_4$.

The click reaction was allowed to proceed at room temperature for 18 hours. The product mixture was centrifuged at a relative centrifugal force (RCF) of 15,422 × g for 1 hr at 25 °C, followed by removal of supernatant, a 0.1 M sodium citrate buffer was added to chelate Cu(I) residue in the reaction mixture. After shaking overnight, the second centrifugation was performed at a RCF of 15,422 g for 1 hr at 25 °C, followed by removal of supernatant; ethanol was added to remove residual free **3**. After shaking overnight, the third centrifugation was performed at a RCF of 15,422 × g for 1 hr at 25 °C, followed by removal of supernatant; de-ionized water was added to the pellet to form dilute microgel **9”** dispersions.

Approximately half of above formed clicked microgel **9”** dispersions (10 mL), in which approximately 7.5 μmol of carboxylic acid group was presented, was used for EDC coupling. Then 50 μL of 0.1 mg/mL TMRC **5** (0.01 μmol) in DMF solution was added to microgel dispersions, followed by adding 1 mg EDC (5 μmol) solid and 5 mL de-ionized water. The EDC coupling reaction was allowed to proceed at room temperature for 18 hours. After reaction, the reaction mixture was centrifuged at a relative centrifugal force (RCF) of 15,422 × g for 1 hr at 25 °C, followed by removal of supernatant; DMF was added to remove residual free **5**. After shaking overnight, the second centrifugation was performed at a relative centrifugal force (RCF) of 15,422 × g for 1 hr at 25 °C, followed by removal of supernatant, de-ionized water was added to the pellet to form dilute microgel **9** dispersions.

D. EDC coupling between multi-responsive carboxylic acid-containing clickable microgels, pNIPAm-AAc-PA **2**, and amino-containing fluorophore, TMRC **5**, followed by click reaction between alkynyl-containing coupled microgels and alkynyl-containing clickable fluorophore, AzF **3**.

Approximately 20 mg of microgel solid powders, in which approximately 15 μmol of carboxylic acid group presented based upon feed ratio, was dissolved in 10 mL de-ionized water. Then 100 μL of 0.1 mg/mL TMRC **5** (0.02 μmol) in DMF solution was added to microgel dispersions, followed by adding 2 mg EDC (10 μmol) solid and 10 mL de-ionized water. The EDC coupling reaction was allowed to proceed at room temperature for 18 hours. After reaction, the reaction mixture was centrifuged at a relative centrifugal force (RCF) of 15,422 × g for 1 hr at 25 °C, followed by removal of supernatant; DMF was added to remove residual free **5**. After shaking overnight, the second centrifugation was performed at a relative centrifugal force (RCF) of 15,422 × g for 1 hr at 25 °C, followed by removal of supernatant, de-ionized water was added to the pellet to form dilute microgel **9'** dispersions.

Approximately half of above formed coupled microgel **9'** dispersions (10 mL), in which approximately 4 μmol of alkynyl group was presented, was used for click reaction. Then 1.0 mg sodium ascorbate (5 μmol) was dissolved in 1 mL de-ionized water, which was subsequently added into microgel dispersions. After that, 125 μL 0.04 mg/mL AzF **3** solution (0.01 μmol) in water/ethanol (50:50) was added into microgel dispersions followed by N_2 bubbling for 5 min. After N_2 purge, 25 μL 0.1 M $CuSO_4$ (2.5 μmol) solution was added to initiate click reaction. The color of reaction mixture changed from yellow-greenish to brownish immediately after the addition of $CuSO_4$. The click reaction was allowed to proceed at room temperature for 18 hours. The product mixture was centrifuged at a relative centrifugal force (RCF) of 15,422 × g for 1 hr at 25 °C, followed by removal of supernatant, a 0.1 M sodium citrate buffer was added to chelate Cu(I) residue in the reaction mixture. After shaking overnight, the second centrifugation was performed at a RCF of 15,422 × g for 1 hr at 25 °C, followed by removal of supernatant; ethanol was added to remove residual free **3**. After shaking overnight, the third centrifugation was performed at a RCF of 15,422 × g for 1 hr at 25 °C, followed by

removal of supernatant; de-ionized water was added to the pellet to form dilute microgel dispersions.

6.2.4.3 Control Experiments

*6.2.4.3.1 Orthogonality of Click Reaction to Carboxyl Groups on pNIPAm-AAc **10** Microgels*

This series of control reaction is used to examine if carboxylic acid groups on pNIPAm-AAc **10** microgels react with azido- or alkynyl-containing fluorophores in the presence of Cu(I).

I.A. Reaction of pNIPAm-AAc **10** with AzF **3** in the presence of Cu(I)

Approximately 20 mg of microgel **10** solid powders, in which approximately 27 μmol carboxylic acid groups presented based upon feed ratio, was dissolved in 10 mL deionized water. Then 2.0 mg sodium ascorbate (10 μmol) was dissolved in 2 mL de-ionized water, which was subsequently added into microgel dispersions. After that, 1.0 mL 0.04 mg/mL AzF **3** solution (0.12 μmol) in water/ethanol (50:50) solution were added into microgel dispersions followed by adding 50 μL 0.1 M $CuSO_4$ (5 μmol) solution was added to initiate click reaction. The reaction was allowed to proceed at room temperature for 20 hours. The reaction mixture was dialyzed against deionized water for 2 weeks with daily replenishment of water.

I.B. Reaction of pNIPAm-AAc **10** with FPTU **4** in the presence of Cu(I)

Approximately 20 mg of microgel **10** solid powders, in which approximately 27 μmol carboxylic acid groups presented based upon feed ratio, was dissolved in 10 mL deionized water. Then 2.0 mg sodium ascorbate (10 μmol) was dissolved in 2 mL de-ionized water, which was subsequently added into microgel dispersions. After that, 1.0 mL 0.01 mg/mL FPTU **4** solution (0.03 μmol) in water/ethanol (50:50) solution were added into microgel dispersions followed by adding 50 μL 0.1 M $CuSO_4$ (5 μmol)

solution was added to initiate click reaction. The reaction was allowed to proceed at room temperature for 20 hours. The purification protocol is the same as described above.

6.2.4.3.2 Click Reaction between Alkynyl and/or Azido Groups

This series of control reactions is used to examine the essential role of Cu(I) in click reaction between azido-containing fluorescein and alkynyl-containing microgels and *vice versa*.

I.C. Reaction of pNIPAm-AzHPMA **11** with FPTU **4** without Cu(I)-catalysis

Approximately 20 mg of microgel **11** solid powders, in which approximately 9.5 μmol of alkynyl groups presented based upon feed ratio, was dissolved in 10 mL deionized water. Then 1 mL 0.01 mg/mL FPTU **4** solution (0.02 μmol) in water/ethanol (50:50) solution was added into microgel dispersions under magnetic stirring. The reaction was allowed to proceed at room temperature for 20 hours. The purification protocol is the same as described above.

I.D. Reaction of pNIPAm-PA **12** with AzF **3** without Cu(I)-catalysis

Approximately 20 mg of microgel **12** solid powders, in which approximately 8.8 μmol of alkynyl groups presented based upon feed ratio, was dissolved in 10 mL deionized water. Then 250 μL 0.04 mg/mL AzF **3** solution (0.03 μmol) in water/ethanol (50:50) solution was added into microgel dispersions under magnetic stirring. The reaction was allowed to proceed at room temperature for 20 hours. The purification protocol is the same as described above.

I.E. Reaction of pNIPAm-PA **12** with FPTU **4** in the presence of Cu(I)

Approximately 20 mg of microgel **12** powder, in which approximately 8.8 μmol of alkynyl groups was present based upon the feed ratio, was dissolved in 10 mL deionized water. Then 2.0 mg sodium ascorbate (10 μmol) was dissolved in 2 mL deionized water, which was subsequently added into microgel dispersions. After that, 1.0 mL 0.01 mg/mL solution of FPTU **4** (0.02 μmol) in water/ethanol (50:50) was added into

microgel dispersions followed by N_2 bubbling for 5 min. After N_2 purge, 50 μL 0.1 *M* $CuSO_4$ (5 μmol) solution was added to initiate reaction. The reaction was allowed to proceed at room temperature for 20 hours. The purification protocol is the same as described above.

I.F. Reaction of pNIPAm-AzPMA **11** with AzF **3** in the presence of Cu(I)

Approximately 20 mg of microgel **11** powder, in which approximately 9.5 μmol of azido was present based upon the feed ratio, was dissolved in 10 mL deionized water. Then 2.0 mg sodium ascorbate (10 μmol) was dissolved in 2 mL deionized water, which was subsequently added into microgel dispersions. After that, 250 μL 0.04 mg/mL solution of AzF **3** (0.02 μmol) in water/ethanol (50:50) was added into the dispersion followed by N_2 bubbling for 5 min. After N_2 purge, 50 μL 0.1 *M* $CuSO_4$ (5 μmol) solution was added to initiate click reaction. The reaction was allowed to proceed at room temperature for 20 hours. The purification protocol is the same as described above.

6.2.4.3.3 Click Reaction between Alkynyl or Azido with Amino Functionalities

I.G. Reaction of pNIPAm-PA **12** with TMRC **5** in the presence of Cu(I)

Approximately 20 mg of microgel **12** powder, in which approximately 8.8 μmol of alkynyl groups was present based upon the feed ratio, was dissolved in 10 mL deionized water. Then 100 μL of 0.1 mg/mL solution of TMRC **5** (0.02 μmol) in DMF was added into the dispersion. After that, 2.0 mg sodium ascorbate (10 μmol) was dissolved in 2 mL deionized water, which was subsequently added into the dispersion followed by N_2 bubbling for 5 min. After N_2 purge, 50 μL 0.1 *M* $CuSO_4$ (5 μmol) solution was added to initiate reaction. The reaction was allowed to proceed at room temperature for 20 hours. The purification protocol is the same as described above.

I.H. Reaction of pNIPAm-AzPMA **11** with TMRC **5** under Cu(I) catalysis

Approximately 20 mg of microgel **11** powder, in which approximately 9.5 μmol of azido was present based upon the feed ratio, was dissolved in 10 mL deionized water.

Then 100 μL of 0.1 mg/mL solution of TMRC **5** (0.02 μmol) in DMF was added into the dispersion. After that, 2.0 mg sodium ascorbate (10 μmol) was dissolved in 2 mL deionized water, which was subsequently added into the dispersion followed by N_2 bubbling for 5 min. After N_2 purge, 50 μL 0.1 *M* $CuSO_4$ (5 μmol) solution was added to initiate reaction. The reaction was allowed to proceed at room temperature for 20 hours. The purification protocol is the same as described above.

6.2.4.3.4 Coupling of Carboxyl with Amino Groups without EDC

II.A. Reaction of pNIPAm-AAc **10** with TMRC **5** without EDC

Approximately 20 mg of microgel **10** powder, in which approximately 27 μmol carboxylic acid groups was present based upon the feed ratio, was dissolved in 10 mL deionized water. Then 100 μL of 0.1 mg/mL solution of TMRC **5** (0.02 μmol) in DMF was added into the dispersion under magnetic stirring. The reaction was allowed to proceed at room temperature for 20 hours. The purification protocol is the same as described above.

6.2.4.3.5 Orthogonality of EDC Coupling to Clickable Functionalies on Microgels

II.B. Orthogonality of EDC Coupling to Azidohydrin on pNIPAm-AzHPMA **11** Microgels

Approximately 20 mg of microgel **11** solid powders, in which approximately 9.5 μmol of azido groups presented based upon feed ratio, was dissolved in 10 mL deionized water. Then 100 μL of 0.1 mg/mL TMRC **5** (0.02 μmol) in DMF solution were added into microgel dispersions followed by adding 1.9 mg EDC (10 μmol) solid. The reaction was allowed to proceed at room temperature for 20 hours. The purification protocol is the same as described above.

II.C. Orthogonality of EDC Coupling to Alkynyl Groups on pNIPAm-PA **12** Microgels

Approximately 20 mg of microgel **12** solid powders, in which approximately 8.8 μmol of alkynyl groups presented based upon feed ratio, was dissolved in 10 mL deionized water. Then 100 μL of 0.1 mg/mL TMRC **5** (0.02 μmol) in DMF solution were added into microgel dispersions followed by adding 1.9 mg EDC (10 μmol) solid. The reaction was allowed to proceed at room temperature for 20 hours. The purification protocol is the same as described above.

6.2.5 Preparation of Amino-Functionalized Glass Substrates

Glass microscope coverslips (25 × 25mm) were cleaned by sequential sonication in dilute Alconox solution, deionized water, acetone, absolute ethanol, isopropanol, and back in absolute ethanol. Then the slides were placed in a solution of 1% 3-aminopropyltrimethoxysilane (APTMS) and absolute ethanol for 2 hours and stored in absolute ethanol for up to 5 days before use. Before deposition of particles, the coverslips were removed from ethanol and dried under nitrogen.

6.2.6 Preparation of Microgel Dispersion Samples for Fluorescence and Optical Microscopy

Approximately one drop of 0.1 wt% of microgels purified after click reaction and/or EDC coupling was dropped on a dry glass slide by plastic pipette. A gentle stream of N_2 was used to spread the microgel drop over the surface of glass slide. The slide coated with wet microgel dispersions was allowed to dry overnight in a fume hood before microscopic observation.

6.2.7 Epifluorescence Microscopy

Both fluorescence and optical microscopies were conducted on an Olympus IX70 inverted microscope equipped with a high numerical aperture, oil immersion 100 × objective (NA = 1.30). In fluorescence mode, the excitation irradiation was a mercury

lamp filtered by excitation band-pass filters of 450-490 nm (blue) or 510-560 nm (green). Images were captured using a color CCD camera (PixelFly, Cooke Corporation).

6.3 Results and Discussion

6.3.1 Clickable Fluorophores

The alkynyl-containing fluorescein, fluorescein propargyl thiourea (FPTU **4**), and azido-containing fluorescein, 5-azidofluorescein (AzF **3**), are characterized by fluorometry and ^{1}H-NMR. Fluorometry provide the excitation and emission spectrum of fluorophores, whereas ^{1}H-NMR provides the structural information of fluorophores.

6.3.1.1 Fluorescence Spectroscopy and ^{1}H-NMR of Fluorescein Propargyl Thiourea (FPTU **4**)

FPTU **4** demonstrate the fluorescence spectrum in Figure 6.1 below.

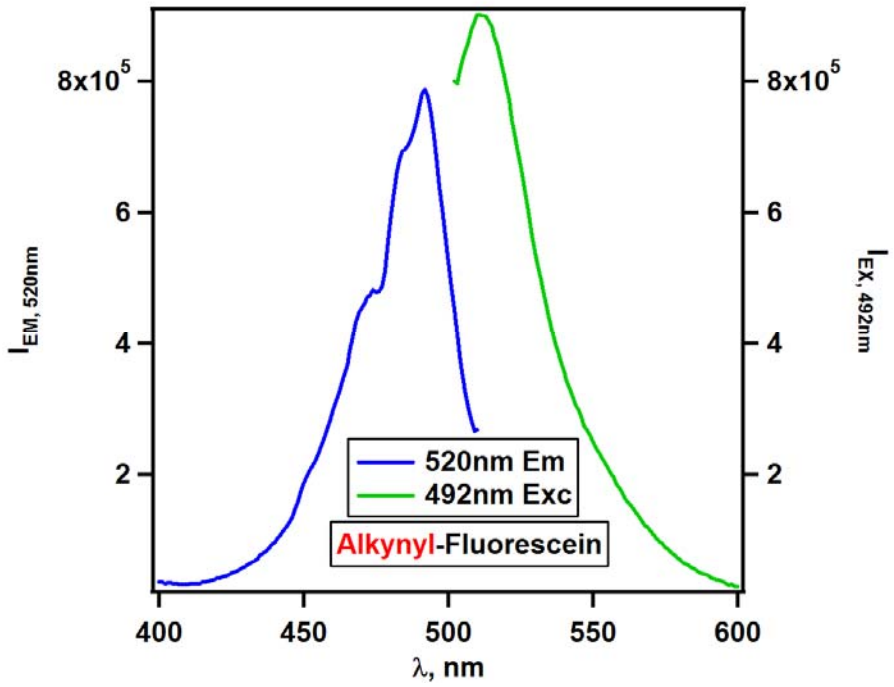

Figure 6.1 The excitation and emission spectrum of alkynyl-containing fluorophore, fluorescein propargyl thiourea (FPTU **4**). The blue curve represents the excitation spectrum of FPTU if the emission wavelength was set at 520 nm, whereas the green curve represents the emission spectrum if the excitation wavelength was set at 492 nm.

The ^{1}H-NMR spectroscopy of FPTU **4** is shown in Figure 6.2 below.

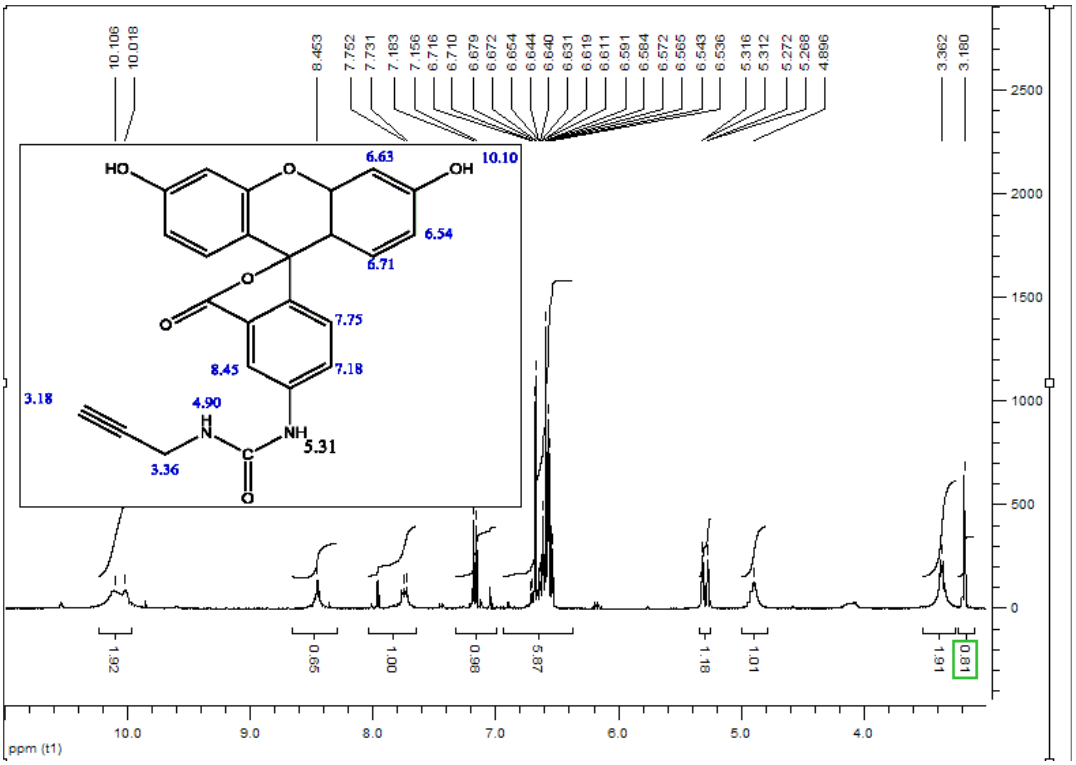

Figure 6.2 The ^{1}H-NMR spectroscopy of FPTU **4**, the inset structure shows the protons corresponding to different chemical shifts.

6.3.1.2 Fluorescence Spectroscopy and ^{1}H-NMR of 5-Azidofluorescein (AzF **3**)

AzF give rise to the following fluorescence spectrum shown in Figure 6.3.

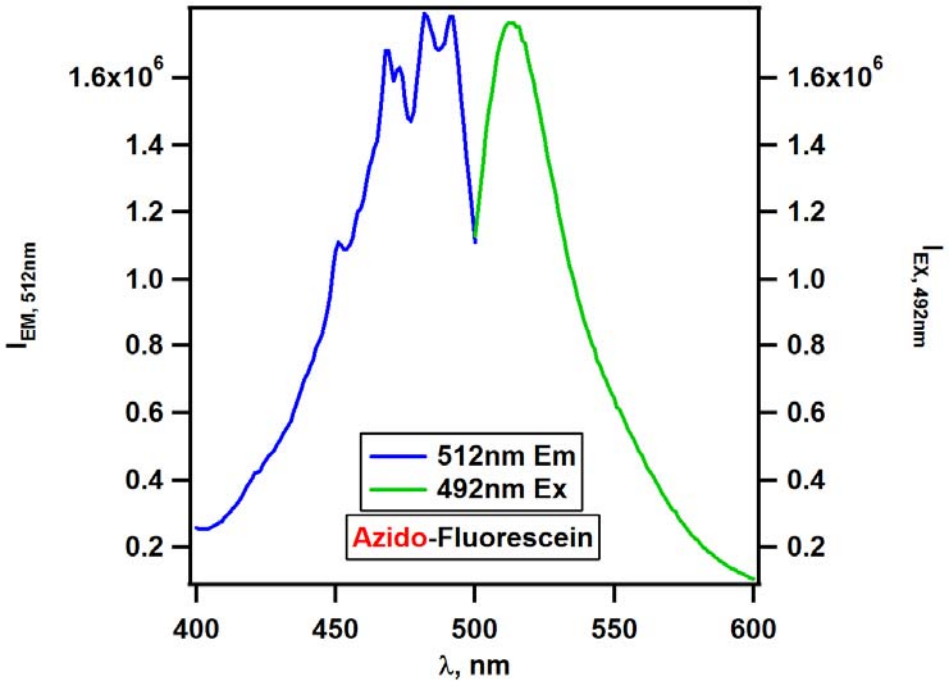

Figure 6.3 The excitation and emission spectrum of azido-containing fluorophore, 5-azidofluorescein (AzF **3**). The blue curve represents the excitation spectrum of AzF if the emission wavelength was set at 512 nm, whereas the green curve represents the emission spectrum if the excitation wavelength was set at 492 nm.

The ^{1}H-NMR spectroscopy of AzF is shown in Figure 6.4 below.

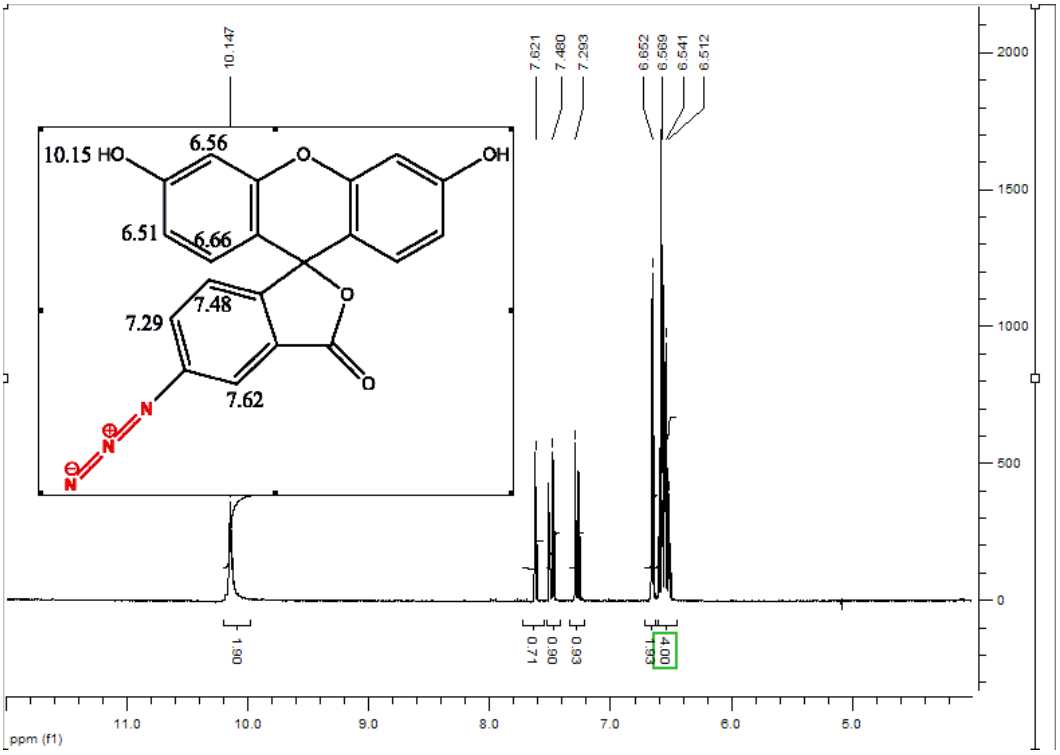

Figure 6.4 The [1]H-NMR spectroscopy of AzF **3**, the inset structure shows the protons corresponding to different chemical shifts.

6.3.2 Clickable Multi-Responsive Microgels

6.3.2.1 Photon Correlation Spectroscopy (PCS)

Clickable multi-responsive azido-containing microgel, pNIPAm-AAc-AzHPMA **1**, and alkynyl-containing microgel, pNIPAm-AAc-PA **2**, show both thermo- and pH-responsivity. Both azido- and alkynyl-containing microgels have hydrodynamic diameter less than 2.5 μm in pH 3.0 buffer, thereby allowing the size characterization via PCS.

6.3.2.1.1 Thermoresponsivity (LCST)

The volume phase transitions of azido-containing and alkynyl-containing microgels, measured by temperature-programmed PCS are shown below. To minimize the convolution of electrostatic repulsion between polymeric chains and microgel particles, the pH 3.0 buffer was used for PCS measurement.

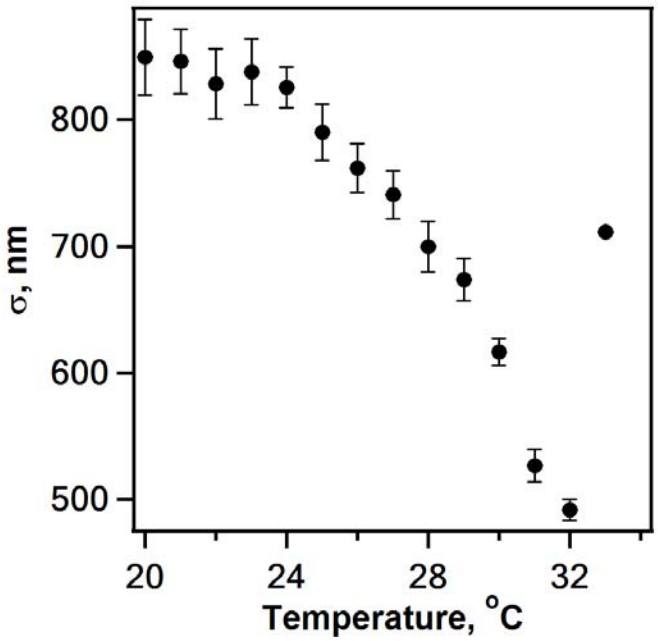

Figure 6.5 The hydrodynamic diameter of pNIPAm-AAc-AzHPMA **1** clickable microgel particles in pH 3.0 buffer (0.001 wt%) versus temperature. Note that crossover 30 ºC, particle size change drastically. Above 32 ºC, particles aggregate so that no scattering data available for the calculation of individual particles.

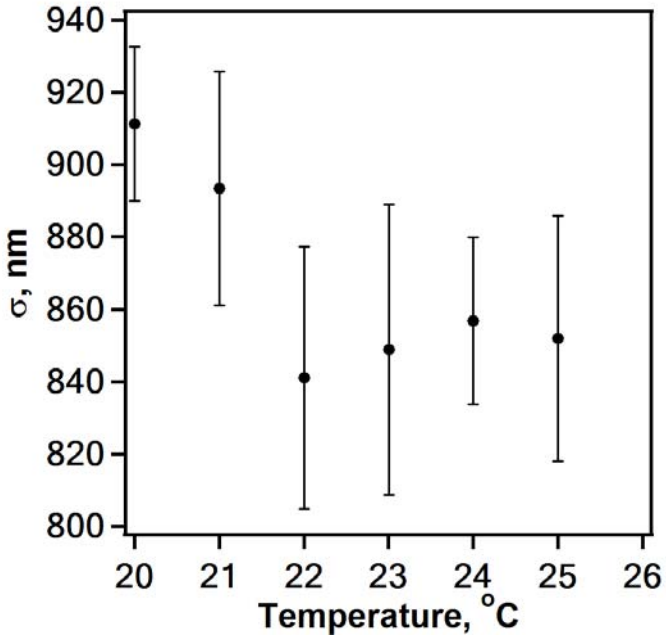

Figure 6.6 The hydrodynamic diameter of pNIPAm-AAc-PA **2** clickable microgel particles in pH 3.0 buffer (0.001 wt%) versus temperature. Note that above 25ºC, particle aggregate so that no scattering data available for the calculation of the size of individual particles.

The clickable pNIPAm-AAc-based microgel particles will form aggregate when temperature reaches some critical point. For azido-containing pNIPAm-AAc-AzHPMA **1** microgel particles, the aggregation temperature is approximately 34 ºC (higher than LCST, ~30 ºC), whereas for alkynyl-containing pNIPAm-AAc-PA **2** microgel particles, the aggregation temperature is approximately 26 ºC (lower than hypothetical LCST).

6.3.2.1.2 pH-Responsivity

Both azido- and alkynyl-containing pNIPAm-AAc-based microgels show pH-responsivity due to either osmotic pressure of charged ions and electrostatic repulsion between carboxylate groups at pH higher than pK_a of AAc moieties or hydrogen bonding between amide and/or carboxylic acid groups at pH lower than pK_a of AAc moieties. The pH-responsive hydrodynamic diameters of both azido- and alkynyl-containing microgels are shown below.

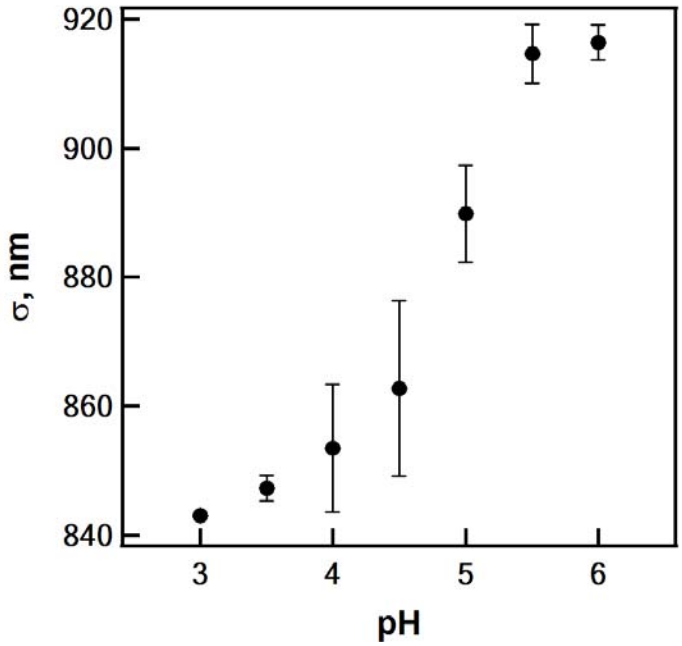

Figure 6.7 The hydrodynamic diameter of pNIPAm-AAc-AzHPMA **1** clickable microgel particles in buffers with pH values from 3.0 up to 6.0 (0.001 wt%) at 20 ºC. Note that crossover pH 5.0, particle size change drastically.

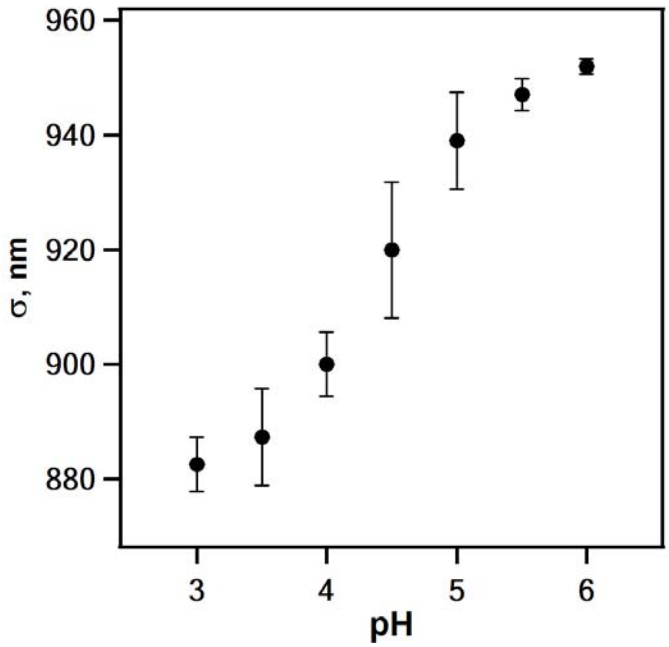

Figure 6.8 The hydrodynamic diameter of pNIPAm-AAc-PA **2** clickable microgel particles in buffers with pH values from 3.0 up to 6.0 (0.001 wt%) at 20 ºC. Note that crossover pH 4.5, particle size change drastically.

6.3.2.2 Attenuated Total Reflectance Fourier Transform Infrared (ATR-FTIR) Spectroscopy

ATR-FTIR spectroscopy was used to determine if azido and alkynyl functional groups exist presumably in azido-containing and alkynyl-containing pNIPAm-AAc-based polymeric solid powders. It is known that azido group shows a symmetric stretching vibration at approximately 2100 cm^{-1}, whereas alkynyl group shows asymmetric stretching vibration at approximately 2160 cm^{-1}. The following ATR-FTIR spectra confirm the existence of azido and alkynyl groups in azido- and alkynyl-containing microgel powders.

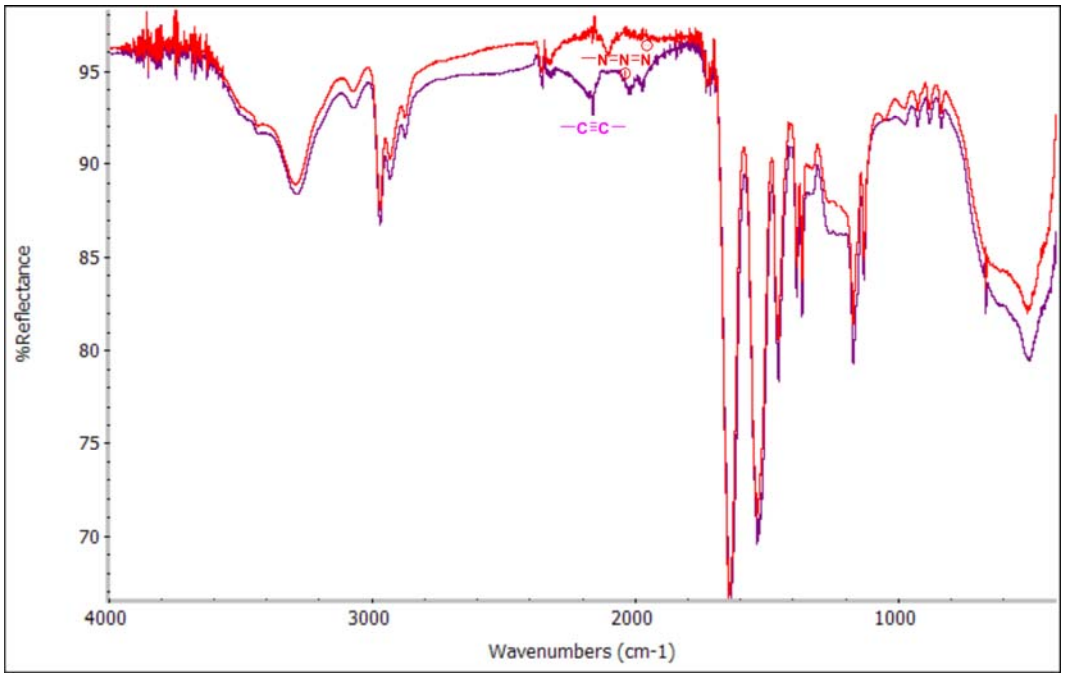

Figure 6.9 The ATR-FTIR spectra of pNIPAm-AAc-AzHPMA **1** (red spectrum) and pNIPAm-AAc-PA **2** (purple spectrum) solid powder. Note the specific IR absorption peak was marked by corresponding functional groups. The IR absorption peaks at 2100 cm^{-1} and 2160 cm^{-1} correspond to azido and alkynyl groups, respectively.

6.3.3 Click Reaction and EDC Coupling

The interference between click reaction and EDC coupling was examined by simultaneous click reaction of azido-containing pNIPAm-AAc-AzHPMA **1** microgels with alkynyl-containing fluorescein, FPTU **4** and EDC coupling of the above carboxy-containing microgels with amino-containing tetramethyrhodamine, TMRC **5**. Similarly, the simultaneous click reaction of alkynyl-containing pNIPAm-AAc-PA microgels **2** with azido-containing fluorescein, AzF **3** and EDC coupling of the above carboxy-containing microgels with amino-containing tetramethyrhodamine, TMRC **5**. Based upon the fluorescence spectra of AzF, FPTU and TMRC, if AzF or FPTU is covalently bonded on microgels, we can observe the green fluorescence if excited at 450-490 nm, whereas if TMRC is covalently bonded on microgels, we can observe the red fluorescence if excited at 510-560 nm. To eliminate the non-specific absorbed fluorophores, ethanol and/or DMF,

which could dissolve both fluorophores, was used to wash the particles extensively. (Refer to Scheme 6.3 in Introduction, details are shown in the Experimental, Section 6.2.4.2.1) After purification, microgel dispersions of **6** and **7** were dried on clean glass slides. The fluorescence microscopy images of microgels **6** and **7** are shown in Figure 6.10; note that for microgel **6**, excitation of **4** yields a somewhat yellow emission color, suggesting either simultaneous excitation of **5** or FRET is occurring in this case. Furthermore, the existence of EDC seems not to impare the catalytic capability of Cu(I) and *vice versa*.

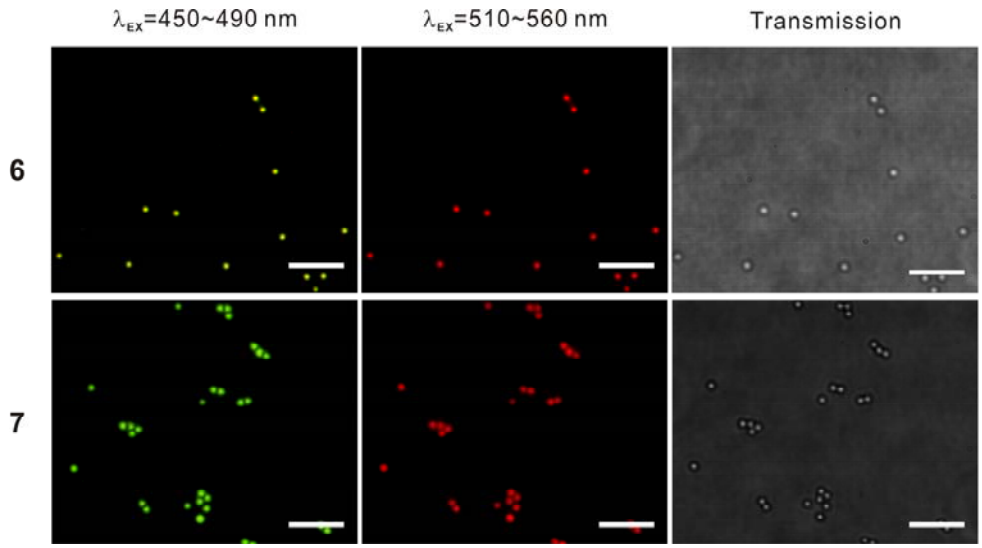

Figure 6.10 Fluorescence and transmission microscopic images of microgels after one-pot simultaneous click reaction and EDC coupling of clickable microgels with fluorophores with complementary functionalities. Top row: Microscopy images of microgel **6**. Bottom row: Microscopy images of microgel **7**. Images in the left and central columns show fluorescence of the microgels excited by irradiation of 450-490 nm and 510-560 nm, respectively. Transmission microscopy images are displayed in the right column. Scale bar = 5 μm

As for two-step reactions containing click reaction and EDC coupling, the fluorescently labeled microgels produced in Steps 1 (**8'**, **8"**, **9'**, and **9"**) and 2 (**8** and **9**), were purified for fluorescence microscopy. Similar purification protocols were used for microgels after ligation in each step. (Refer to Scheme 6.4 in Introduction, details are shown in Experimental, Section 6.2.4.2.2) After purification, microgel dispersions **8** and

9 were coated and dried on the cleaned glass slides. The fluorescence microscopy images of microgels **8** and **9** were shown in Figure 6.11. By comparing the fluorescence microscopy images of microgels after one-pot simultaneous ligation and two-step ligation, it is believed that the catalytic activity of Cu (I) are not significantly impaired by EDC and *vice versa*.[51,52] Additionally, after coupling of TMRC **5**, the fluorescence observed under blue irradiation (450-490 nm) changes from green to yellow, again suggesting either direct excitation of **5** at this wavelength, or that fluorescein-to-rhodamine FRET is occurring. Since the leftmost panels in columns 1 and 4 show some faint evidence of fluorescence, which is likely due to direct excitation of **5**, it is likely that the strong yellow emission observed for **8** and **9** under blue excitation is due to a combination of direct excitation of **5** and FRET. As discussed above, these phenomena are currently being investigated in our group.

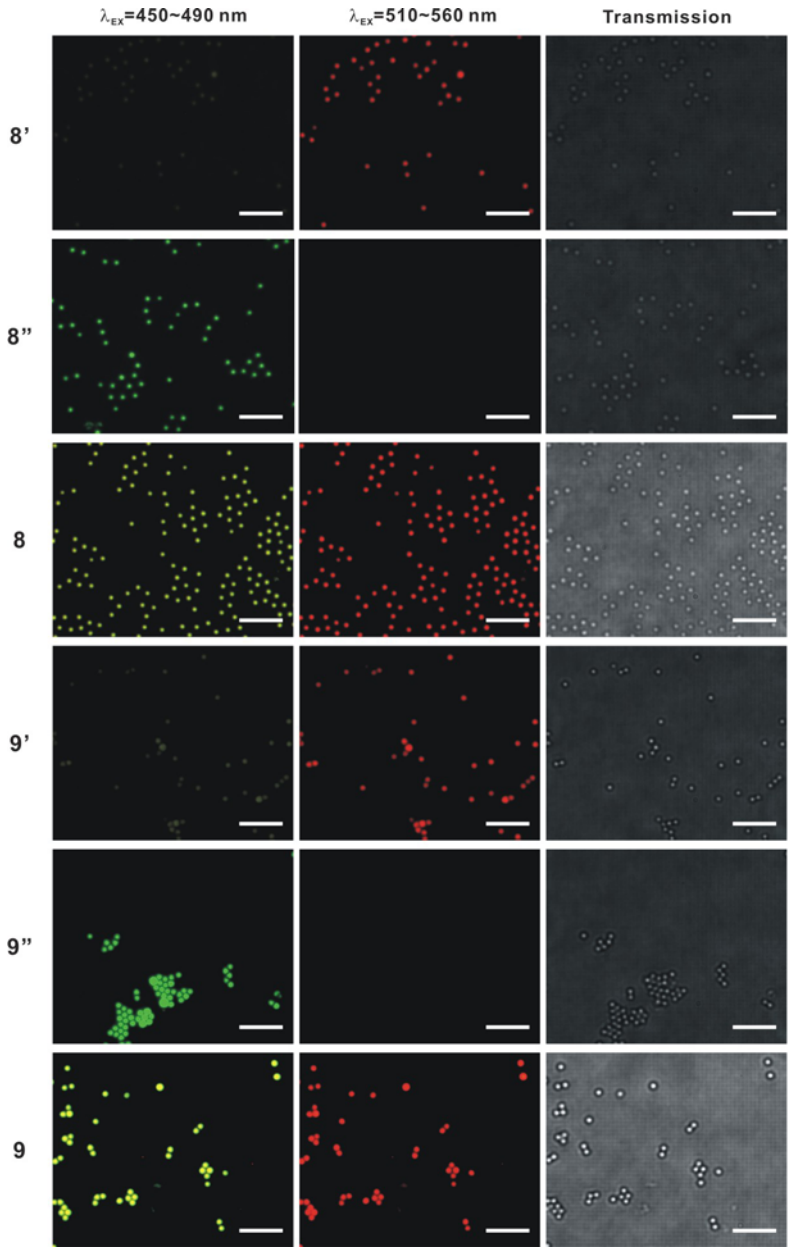

Figure 6.11 Fluorescence and transmission microscopic images of microgels after two-step sequential click reaction and EDC coupling of clickable microgels with fluorophores with complementary functionalities. The top three rows show microscopy images of microgels obtained by either first EDC coupling of azide/carboxylic acid microgel **1** with amino-containing fluorophore **5** (**8'**, row 1) followed by clicking with alkynyl-containing fluorophore **4** (**8**, row 3), or first clicking with **4** (**8"**, row 2) followed by EDC coupling with **5** (not shown, similar to **8**). The bottom three rows show microscopy images of microgels obtained by either first EDC coupling alkyne/carboxylic acid microgel **2** with amino-containing fluorophore **5** (**9',** row 4) followed by clicking with azido-containing fluorophore **3** (**9**, row 6), or first clicking with **3** (**9"**, row 5) followed by EDC coupling with **5** (not shown, similar to **9**). The left and middle columns are fluorescence

microscopy images obtained by the excitation of 450-490 and 510-560 nm, respectively. The right column contains brightfield transmission images. Scale bar = 5 μm

6.3.4 Control Experiments

To further illustrate the fidelity of these coupling reactions, control experiments were designed to examine the reactivity of azido/alkynyl groups with amino groups and the orthogonality of click reactions to EDC coupling. (Detailed experimental designs are documented in Section 6.2.4.3, Schemes 6.5 and 6.6) The epifluorescence microscopy images are shown in Figure 6.12. The control experiments confirmed that the click reaction is orthogonal to other functional groups such as hydroxyl, carboxyl and amino groups. However, some small amount of cross-reactivity is apparently observed during EDC coupling of microgel **11** (azidohydrin-modified) and fluorophore **5**. (Control experiment II.B in Experiment, Section 6.2.4.3) It is likely that this arises from coupling between the alcohol on the azidohydrin and the carboxylic acid moiety[53,54] on the fluorophore (tautomer[55] of the lactone ring). The possible reaction between azidohydrin-containing microgels **11** and amino-containing fluorophore 5 was shown in Scheme 6.8. Despite this slight complication, all other negative controls fail to produce coupled fluorophores, illustrating the robustness of the method for producing multifunctional microgels for orthogonal chemo-ligations.

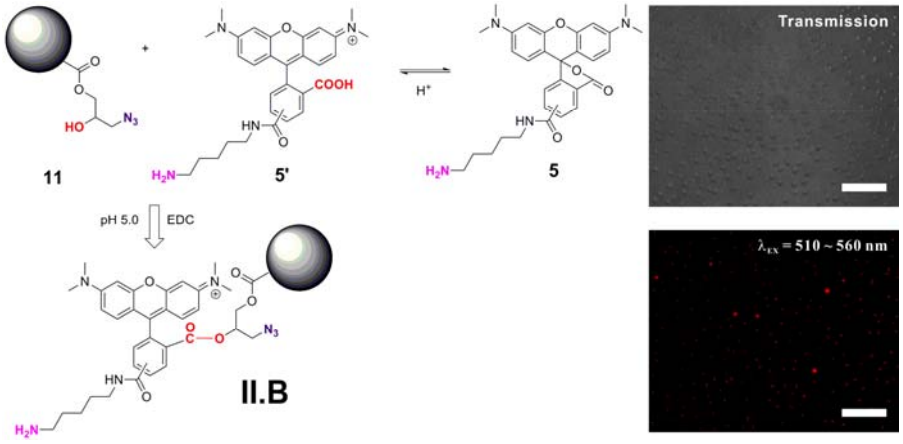

Scheme 6.8 The EDC coupling of azidohydrin-microgel **11** with tautomer of amino-fluorophore TMRC **5** with transmission and fluorescence microscopy images. Scale bar = 10 μm.

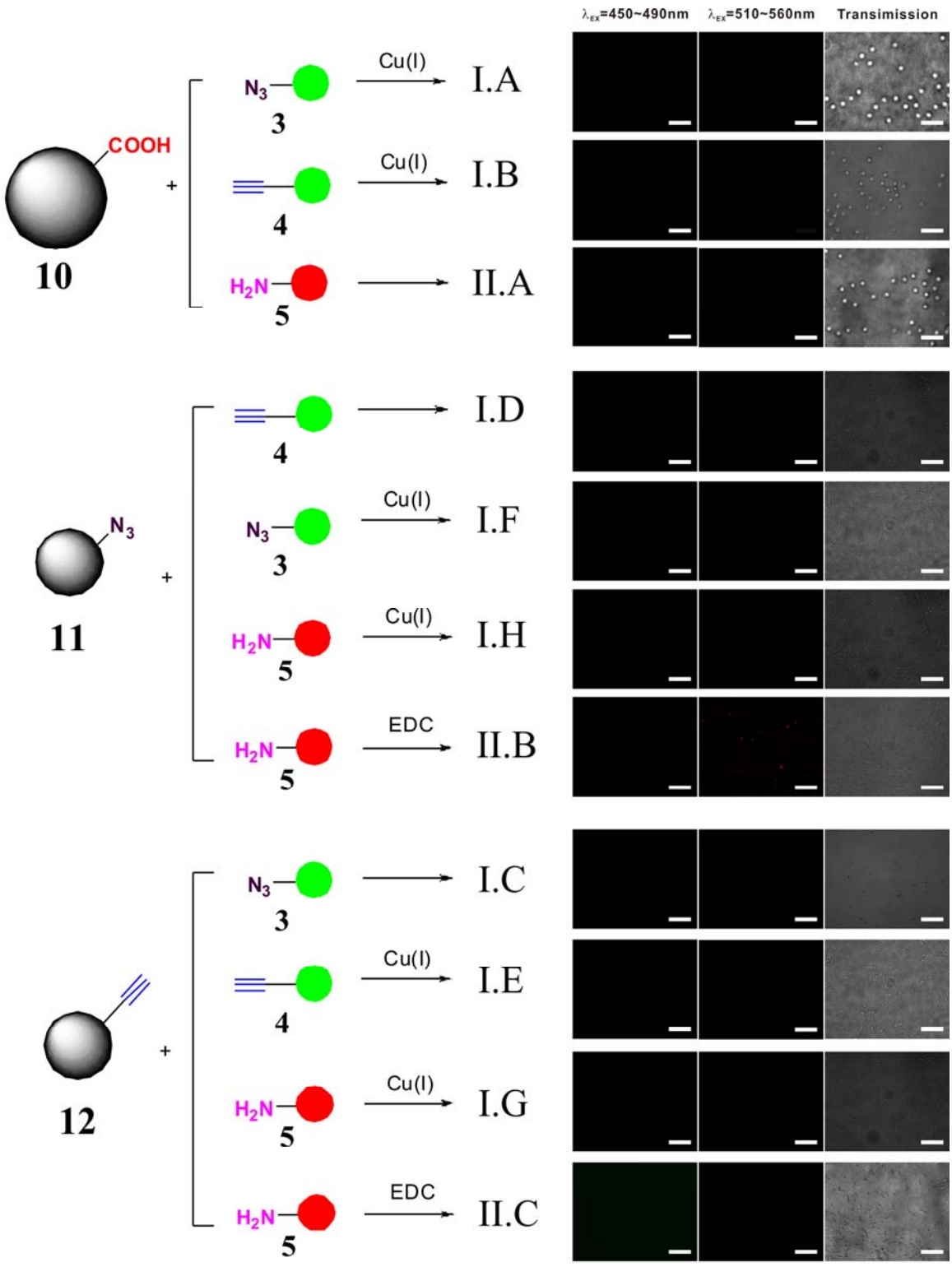

Figure 6.12 Microscopic images (both fluorescence and transmission mode) for all control experiments. Scale bar = 10 μm

6.4 Conclusions

This chapter first describes the one-pot multi-stage synthesis of multi-responsive azido- or alkynyl-containing clickable microgels. Furthermore, this chapter describes the simultaneous and two-step click reaction between pNIPAm-AAc-based clickable microgels and complementary clickable fluorophores and EDC coupling between carboxy-containing pNIPAm-AAc-based microgels and amine-containing fluorophores. It's believed that the click reaction and EDC coupling are orthogonal to each other when conducted simultaneously. However, EDC was found to couple carboxy-containing tautomer of fluorophore, tetramethylrhodamine-5,6-carboxamide cadaverine, and azidohydrin-containing microgel particles. A wide range of control experiments illustrate the excellent specificity of the coupling reactions, suggesting that such particles may be useful for synthesis of bioconjugates not typically attainable using reactions that rely exclusively on biologically prevalent functional groups.

References

(1) Saunders, B. R.; Vincent, B. Microgel particles as model colloids: theory, properties and applications, *Adv. Colloid Interface Sci.* **1999**, *80*, 1-25.

(2) Pelton, R. Temperature-sensitive aqueous microgels, *Adv. Colloid Interface Sci.* **2000**, *85*, 1-33.

(3) Debord, J. D.; Lyon, L. A. Thermoresponsive photonic crystals, *J. Phys. Chem. B* **2000**, *104*, 6327-6331.

(4) Kawaguchi, H. Functional polymer microspheres, *Prog. Polym. Sci.* **2000**, *25*, 1171-1210.

(5) Tanaka, T. Collapse of gels and the critical endpoint, *Phys. Rev. Lett.* **1978**, *40*, 820-823.

(6) Schild, H. G. Poly(*N*-isopropylacrylamide): Experiment, theory and application, *Prog. Polym. Sci.* **1992**, *17*, 163-249.

(7) Heskins, M.; Guillet, J. E. Solution properties of poly(*N*-isopropylacrylamide), *J. Macromol. Sci. Chem.* **1968**, *2*, 1441-1455.

(8) Pelton, R. H.; Chibante, P. Preparation of aqueous lattices with *N*-isopropylacrylamide, *Colloids Surf.* **1986**, *20*, 247-256.

(9) Snowden, M. J.; Chowdhry, B. Z.; Vincent, B.; Morris, G. E. Colloidal copolymer microgels of N-isopropylacrylamide and acrylic acid: pH, ionic strength and temperature effects, *J. Chem. Soc., Faraday Trans.* **1996**, *92*, 5013-5016.

(10) Pinkrah, V. T.; Snowden, M. J.; Mitchell, J. C.; Seidel, J.; Chowdhry, B. Z.; Fern, G. R. Physicochemical properties of poly(N-isopropylacrylamide-co-4-vinylpyridine) cationic polyelectrolyte colloidal microgels, *Langmuir* **2003**, *19*, 585-590.

(11) Murthy, N.; Xu, M. C.; Schuck, S.; Kunisawa, J.; Shastri, N.; Frechet, J. M. J. A macromolecular delivery vehicle for protein-based vaccines: Acid-degradable protein-loaded microgels, *Proc. Natl. Acad. Sci. U. S. A.* **2003**, *100*, 4995-5000.

(12) Kim, J. H.; Lee, T. R. Thermo- and pH-responsive hydrogel-coated gold nanoparticles, *Chem. Mat.* **2004**, *16*, 3647-3651.

(13) Kwon, Y. J.; James, E.; Shastri, N.; Frechet, J. M. J. In vivo targeting of dendritic cells for activation of cellular immunity using vaccine carriers based on pH-responsive microparticles, *Proc. Natl. Acad. Sci. U. S. A.* **2005**, *102*, 18264-18268.

(14) Vinogradov, S. V. Colloidal microgels in drug delivery applications, *Curr. Pharm. Des.* **2006**, *12*, 4703-4712.

(15) Blackburn, W. H.; Lyon, L. A. Size-controlled synthesis of monodisperse core/shell nanogels, *Colloid Polym. Sci.* **2008**, *286*, 563-569.

(16) Vinogradov, S. V. Polymeric nanogel formulations of nucleoside analogs, *Expert Opin. Drug Deliv.* **2007**, *4*, 5-17.

(17) Nolan, C. M.; Serpe, M. J.; Lyon, L. A. Thermally modulated insulin release from microgel thin films, *Biomacromolecules* **2004**, *5*, 1940-1946.

(18) Nolan, C. M.; Serpe, M. J.; Lyon, L. A. Pulsatile release of insulin from Layer-by-Layer assembled microgel thin films, *Macromol. Symp.* **2005**, *227*, 285-294.

(19) Serpe, M. J.; Yarmey, K. A.; Nolan, C. M.; Lyon, L. A. Doxorubicin uptake and release from microgel thin films, *Biomacromolecules* **2005**, *6*, 408-413.

(20) Nakajima, N.; Ikada, Y. Mechanism of amide formation by carbodiimide for bioconjugation in aqueous media, *Bioconjugate Chem.* **1995**, *6*, 123-130.

(21) Nayak, S.; Lee, H.; Chmielewski, J.; Lyon, L. A. Folate-mediated cell targeting and cytotoxicity using thermoresponsive microgels, *J. Am. Chem. Soc.* **2004**, *126*, 10258-10259.

(22) Wang, N.; Dong, A.; Radosz, M.; Shen, Y. Q. Thermoresponsive degradable poly(ethylene glycol) analogues, *J. Biomed. Mater. Res.* **2008**, *84A*, 148-157.

(23) Baskin, J. M.; Bertozzi, C. R. Bioorthogonal click chemistry: Covalent labeling in living systems, *QSAR Comb. Sci.* **2007**, *26*, 1211-1219.

(24) Rostovtsev, V. V.; Green, L. G.; Fokin, V. V.; Sharpless, K. B. A stepwise Huisgen cycloaddition process: Copper(I)-catalyzed regioselective "ligation" of azides and terminal alkynes, *Angew. Chem. Int. Ed.* **2002**, *41*, 2596-2599.

(25) Tornoe, C. W.; Christensen, C.; Meldal, M. Peptidotriazoles on solid phase: [1,2,3]-triazoles by regiospecific copper(I)-catalyzed 1,3-dipolar cycloadditions of terminal alkynes to azides, *J. Org. Chem.* **2002**, *67*, 3057-3064.

(26) Kolb, H. C.; Finn, M. G.; Sharpless, K. B. Click chemistry: Diverse chemical function from a few good reactions, *Angew. Chem. Int. Ed.* **2001**, *40*, 2004-2021.

(27) Huisgen, R. 1,3-Dipolar cycloadditions: Past and future, *Angew. Chem. Int. Ed. Engl.* **1963**, *2*, 565-598.

(28) Agard, N. J.; Baskin, J. M.; Prescher, J. A.; Lo, A.; Bertozzi, C. R. A comparative study of bioorthogonal reactions with azides, *ACS Chem. Biol.* **2006**, *1*, 644-648.

(29) Kolb, H. C.; Sharpless, K. B. The growing impact of click chemistry on drug discovery, *Drug Discov. Today* **2003**, *8*, 1128-1137.

(30) Agard, N. J.; Prescher, J. A.; Bertozzi, C. R. A strain-promoted [3+2] azide-alkyne cycloaddition for covalent modification of blomolecules in living systems, *J. Am. Chem. Soc.* **2004**, *126*, 15046-15047.

(31) Binder, W. H.; Sachsenhofer, R. 'Click' chemistry in polymer and materials science, *Macromol. Rapid Commun.* **2007**, *28*, 15-54.

(32) Hawker, C. J.; Wooley, K. L. The convergence of synthetic organic and polymer chemistries, *Science* **2005**, *309*, 1200-1205.

(33) Wu, P.; Feldman, A. K.; Nugent, A. K.; Hawker, C. J.; Scheel, A.; Voit, B.; Pyun, J.; Frechet, J. M. J.; Sharpless, K. B.; Fokin, V. V. Efficiency and fidelity in a click-chemistry route to triazole dendrimers by the copper(I)-catalyzed ligation of azides and alkynes, *Angew. Chem. Int. Ed.* **2004**, *43*, 3928-3932.

(34) Chen, G. J.; Tao, L.; Mantovani, G.; Geng, J.; Nystrom, D.; Haddleton, D. M. A modular click approach to glycosylated polymeric beads: Design, synthesis and preliminary lectin, recognition studies, *Macromolecules* **2007**, *40*, 7513-7520.

(35) Evanoff, D. D.; Hayes, S. E.; Ying, Y.; Shim, G. H.; Lawrence, J. R.; Carroll, J. B.; Roeder, R. D.; Houchins, J. M.; Huebner, C. E.; Foulger, S. H. Functionalization of crystalline colloidal arrays through click chemistry, *Adv. Mater.* **2007**, *19*, 3507-3512.

(36) Evans, C. E.; Lovell, P. A. Click chemistry as a route to surface functionalization of polymer particles dispersed in aqueous media, *Chem. Commun.* **2009**, 2305-2307.

(37) Slater, M.; Snauko, M.; Svec, F.; Frechet, J. M. J. "Click chemistry" in the preparation of porous polymer-based particulate stationary phases for mu-HPLC separation of peptides and proteins, *Anal. Chem.* **2006**, *78*, 4969-4975.

(38) Zeng, Q. B.; Li, T.; Cash, B.; Li, S. Q.; Xie, F.; Wang, Q. Chemoselective derivatization of a bionanoparticle by click reaction and ATRP reaction, *Chem. Commun.* **2007**, 1453-1455.

(39) Wang, Q.; Chan, T. R.; Hilgraf, R.; Fokin, V. V.; Sharpless, K. B.; Finn, M. G. Bioconjugation by copper(I)-catalyzed azide-alkyne [3+2] cycloaddition, *J. Am. Chem. Soc.* **2003**, *125*, 3192-3193.

(40) O'Reilly, R. K.; Joralemon, M. J.; Hawker, C. J.; Wooley, K. L. Facile syntheses of surface-functionalized micelles and shell cross-linked nanoparticles, *J. Polym. Sci. Polym. Chem.* **2006**, *44*, 5203-5217.

(41) Fringuelli, F.; Piermatti, O.; Pizzo, F.; Vaccaro, L. Ring opening of epoxides with sodium azide in water. A regioselective pH-controlled reaction, *J. Org. Chem.* **1999**, *64*, 6094-6096.

(42) Falk, B.; Crivello, J. V. Synthesis and modification of epoxy- and hydroxy-functional microspheres, *J. Appl. Polym. Sci.* **2005**, *97*, 1574-1585.

(43) Tamami, B.; Mahdavi, H. Synthesis of azidohydrins from epoxides using quaternized amino functionalized cross-linked polyacrylamide as a new polymeric phase-transfer catalyst, *Tetrahedron Lett.* **2001**, *42*, 8721-8724.

(44) Bhaumik, K.; Mali, U. W.; Akamanchi, K. G. High yield regioselective ring opening of epoxides using samarium chloride hexahydrate, *Syn. Comm.* **2003**, *33*, 1603-1610.

(45) Suzuki, D.; Kawaguchi, H. Gold nanoparticle localization at the core surface by using thermosensitive core-shell particles as a template, *Langmuir* **2005**, *21*, 12016-12024.

(46) Bates, R. G.; Bower, V. E. Alkaline solutions for pH control, *Anal. Chem.* **1956**, *28*, 1322-1324.

(47) Maeda, H.; Kawauchi, H. A new method for the determination of N-terminus of peptides chain with fluorescein-isothiocyanate, *Biochem. Biophys. Res. Commun.* **1968**, *31*, 188-192.

(48) Ikeda, M.; Minari, J.; Shimada, N.; Numata, M.; Sakurai, K.; Shinkai, S. Complex formation between cationic beta-1,3-glucan and hetero-sequence oligodeoxynucleotide and its delivery into macrophage-like cells to induce cytokine secretion, *Org. Biomol. Chem.* **2007**, *5*, 2219-2224.

(49) Salic, A.; Mitchison, T. J. A chemical method for fast and sensitive detection of DNA synthesis in vivo, *Proc. Natl. Acad. Sci. U. S. A.* **2008**, *105*, 2415-2420.

(50) PerkinElmer FT-IR Spectroscopy: Attenuated Total Reflectance (ATR), *http://las.perkinelmer.com/content/TechnicalInfo/TCH_FTIRATR.pdf*, 2005

(51) Alleyne, T. A.; Wilson, M. T.; Antonini, G.; Malatesta, F.; Vallone, B.; Sarti, P.; Brunori, M. Investigation of the electron-transfer properties of Cytochrome-C-oxidase covalently cross-linked to Fe-containing or Zn-containing Cytochrome-C, *Biochem. J.* **1992**, *287*, 951-956.

(52) Hayes, C. S.; Setlow, P. Identification of protein-protein contacts between alpha/beta-type small, acid-soluble spore proteins of Bacillus species bound to DNA, *J. Biol. Chem.* **1998**, *273*, 17326-17332.

(53) Tomihata, K.; Ikada, Y. Crosslinking of hyaluronic acid with water-soluble carbodiimide, *J. Biomed. Mater. Res.* **1997**, *37*, 243-251.

(54) Khandare, J.; Minko, T. Polymer-drug conjugates: Progress in polymeric prodrugs, *Prog. Polym. Sci.* **2006**, *31*, 359-397.

(55) Corrie, J. E. T.; Craik, J. S. Synthesis and characterisaation of pure isomers of iodoacetamidotetramethylrhodamine, *J. Chem. Soc. Perkin Trans. 1* **1994**, 2967-2973.

APPENDIX A

IDL ROUTINES FOR PARTICLE TRACKING

A.1 Batch File for Particle Tracking

The following batch processing file in IDL environment was written by Professor Victor Breedveld at the Department of Chemical and Biomolecular Engineering in Georgia Institute of Technology, and I use this IDL routine for particle tracking of all of the data I obtained through video microscopy on Olympus IX71. The resultant data include particle position file, "_p.gdf", particle trajectory file, "_trm.gdf", and mean square displacement file, "_rrm.txt", all of which were used to analyze the dynamics and size of microgel particles in colloidal dispersions.

```
pro batchLyon_IDL56

;batchLyon_IDL56.pro by VB, Oct 2003
;Batch file for particle tracking

;OUTPUT files
;- '*_par.dat': list of parameters used for image anlysis
;- '*_p.gdf': list of particle positions
;- '*_t.gdf': list of particle trajectories
;- '*_trm.gdf': list of particle trajectories after removing average motion
;- '*_r.gdf': mean squared displacement
;- '*_rrm.gdf': mean squared displacement after removing average motion
```

```
;**********************************
;***** CHANGE PARAMETERS BELOW *****
;**********************************
;***** DEFINE FILE ****************
;**********************************
dirname='Drive:\Folder\';***PUT '\' AT END!!!
samplename='Current File Name_'
savename='Saved File Name'
mpp=0.1000  ;*** micron per pixel
Dt=0.033    ;*** timeinterval between frame
;***** IMAGE ANALYSIS *****
;*** pre_track ***
bpmin=2
bpmax=8
feat=17
mcut=20000
;*** particle selection ***
emin=0      ;*** minimum elongation
emax=0.20   ;*** maximum elongation
minsize=10  ;*** minimum size
maxsize=40  ;*** maximum size
;***** TRACKING PARAMETERS *****
maxdisp=3   ;*** Maximum displacement of particle from frame to frame [pixels]
mem=1       ;*** length of interval over which particles must be invisible to be
dropped [# images]
minlen=10   ;*** minimum length of trajectory to be kept [# images]
maxtime_msd=15 ;*** maximum lag time for MSD plot
```

```
;*** WARNING!!!! Do not set too high; program might crash
Nmin=10
;*** minimum number of points in the statistical MSD averages
;************************************
;******** START PROGRAM **************
;************************************
a=read_tiff(dirname+samplename+'t0000.tif')
b=bpass(a,bpmin,bpmax)
device, decomposed=0
window,0,xsize=658,ysize=496, title = 'Original/BPASS image'
flickscl,a,b,/scale
f=feature(b,feat,masscut=mcut)
window,2, xsize = 500, ysize = 350, xpos = 0, ypos = 0, title = 'Elongation Image
#1'
window,3, xsize = 500, ysize = 350, xpos = 510, ypos = 0, title = 'Brightness
Image #1'
window,4, xsize = 500, ysize = 350, xpos = 0, ypos = 370, title = 'Average
Brightness Image #1'
device,decomposed=1
wset,2 & plot,f(3,*),f(4,*), psym=3, xtitle='Size [pix]', ytitle='Elongation'
wset,3 & plot,f(3,*),f(2,*), psym=3, xtitle='Size [pix]', ytitle='Brightness'
wset,4 & plot,f(3,*),f(2,*)/f(3,*)^2, psym=3, xtitle='Size [pix]', ytitle='Ave.
Brightness'
wait,10
device,decomposed=0
xf=fover2d(b,f,radius=4)
f2=eclip(f,[4,emin,emax])
```

```
        f2=eclip(f2,[3,minsize,maxsize])
        xf2=fover2d(b,f2,radius=4)
        window,0,xsize=658,ysize=496, title = 'Features before/after ECLIP'
        flickscl,xf,xf2,/scale
        window,0,xsize=658,ysize=496, title = 'Features after ECLIP'
        flickscl,a,xf2,/scale

        void = dialog_message('Parameter settings OK to proceed with full analysis?',
/quest,title='batchLyon.pro')
        if (void eq 'Yes') then begin
         ;***** WRITE PARAMETERS TO FILE ******
         OPENW,1, dirname+savename+'_par.dat'
         PRINTF,1, 'General Parameters'
         printf,1,mpp,Dt
         printf,1,'Image Analysis Parameters'
         printf,1,bpmin,bpmax,feat,mcut,emin,emax,minsize,maxsize
         printf,1,'Tracking Parameters'
         printf,1,maxdisp,mem,minlen,maxtime_msd,Nmin
         CLOSE,1
         ;************************************
         void = dialog_message('TIFF_PRETRACK needed?',/quest,title='batchLyon.pro')
         if (void eq 'Yes') then begin
          bio_pretrack,dirname,samplename+'*.tif',[bpmin,bpmax,feat,mcut],/quiet
          cutcat_vb,samplename+'*',savename,dir=dirname
          FileN = findfile(dirname+'xys.*')
          file_delete,FileN
         endif
```

```
x=read_gdf(dirname+'cat.'+savename)
x(5,*)=x(5,*)/1000.
x=eclip(x,[4,emin,emax])
x=eclip(x,[3,minsize,maxsize])
count=n_elements(uniq(x(5,*)))
ave_n=n_elements(x(0,*))/count
print,'Average Number of Particles: ' + strcompress(ave_n)
device,decomposed=1
window,2, xsize = 450, ysize = 400, xpos = 0, ypos = 0, title = 'Histogram X
mod 1'
window,3, xsize = 450, ysize = 400, xpos = 460, ypos = 0, title = 'Histogram Y
mod 1'
wset,2 & plot_hist,x(0,*) mod 1
wset,3 & plot_hist,x(1,*) mod 1
wait,10

;**** Write particle positions to file ****
write_gdf,x,dirname+savename+'_p.gdf'
;**** Find and save tracks ****
t=track(x,maxdisp,memory=mem,goodenough=minlen)
mot = motion(t,dim=2)
trm=rm_motion(t,mot,dim=2,smooth=50)
;write_gdf,t,dirname+savename+'_t.gdf'
write_gdf,trm,dirname+savename+'_trm.gdf'
;**** Calculate and save MSD ****
mt=maxtime_msd
;if (mt ge 10.0) then mt=10
```

```
r=msd_vb(t,maxtime=mt,micperpix=mpp,timestep=Dt,erode=2)
w=where(r(6,*) gt Nmin)
r=r(*,w)
rrm=msd_vb(trm,maxtime=mt,micperpix=mpp,timestep=Dt,erode=2)
w=where(rrm(6,*) gt Nmin)
rrm=rrm(*,w)
;write_gdf,r,dirname+savename+'_r.gdf'
;write_text,r,dirname+savename+'_r.txt'
;write_gdf,rrm,dirname+savename+'_rrm.gdf'
write_text,rrm,dirname+savename+'_rrm.txt'
;**** Plot overlay ****
device,decomposed=0
window,0,xsize=658,ysize=496, title = 'All trajectories'
plottr,t,res,/tv,goodenough=minlen,x=658,y=496
;flickscl,res,res
;window,0,xsize=658,ysize=496, title = 'All trajectories on Image #1'
;tot=overlay_traj(a,res)
;flickscl,tot,tot,/scale
;**** Plot MSD graphs ****
;device,decomposed=1
;window,1, xsize = 450, ysize = 400, xpos = 0, ypos = 0, title = 'MSD before
rm_motion'
;window,2, xsize = 450, ysize = 400, xpos = 460, ypos = 0, title = 'MSD after
rm_motion'
;wset,1
;plot,r(0,*),r(5,*),/xlog,/ylog,xtitle='lag time [s]',ytitle='MSD [um^2]',psym=4
;oplot,r(0,*),r(3,*),psym=5
```

```
  ;oplot,r(0,*),r(4,*),psym=6
  ;wset,2
  ;plot,rrm(0,*),rrm(5,*),/xlog,/ylog,xtitle='lag time [s]',ytitle='MSD
[um^2]',psym=4
  ;oplot,rrm(0,*),rrm(3,*),psym=5
  ;oplot,rrm(0,*),rrm(4,*),psym=6
endif
;*** END OF PROGRAM ******
end
```

A.2 Using "_p.gdf" File to Derive Radial Distribution Function

The batch file in A.1 could generate a particle position file with the format of "_p.gdf", which could therefore be used to derive radial distribution function *g(r)* using the following IDL routines.

```
pro batch_g2

dirname='Drive:\Folder\ '
samplename='Filem Name'
a=read_gdf(dirname+samplename+'_p.gdf')
b=ericgr2d(a, rmin=0.0, rmax=100.0, deltar=1)
write_text, b, dirname+samplename+'_1_g2.txt'
write_jpeg, dirname+samplename+'_1_g2.jpg', tvrd()

end
```

The IDL routine “ericgr2d” was written by Professor Eric Weeks at Department of Physics in Emory University, adopted by Jae Kyu Cho at Department of Chemical and Biomolecular Engineering at Georgia Institute of Technology.

A.3 Using “_trm.gdf” to Generate Particle Trajectory Images

The batch file in A.1 could generate a particle position file with the format of “_trm.gdf”, which could therefore be used to generate particle trajectory images using the following IDL routines.

```
pro batch_traj

dirname='Dirve:\Folder\' ;***NEEDS \ to run properly
samplename='File Name'
tarray=read_gdf(dirname+samplename+'_trm.gdf')
plottr,tarray,res,goodenough=10,/tv,x=658,y=496
outputfilename=dirname+samplename+'_trm.tif'
write_tiff,outputfilename,res

end
```

This batch file is revised by Zhiyong Meng, adopted from the routine originally written by Jae Kyu Cho.

APPENDIX B

MULTI-FUNCTIONAL FILM COMPOSED OF CLICKABLE MICROGELS

B.1 Introduction

Microgel films are first made by organic[1] or aqueous[2] microgel dispersions used for paints and coating technology.[3-7] Specifically, Langmuir-Blodgett films could be prepared by various microgels.[8-10] However, all the aforementioned films are not stimuli-responsive. To enhance the environmental responsivity, thin films made of stimuli-responsive microgels, especially thermoresponsive poly(*N*-isopropylacrylamide) (pNIPAm) microgels, were developed recently. The first stimuli-responsive microgel film was prepared by photo-initiated cross-linking of pNIPAm microgels with NIPAm and *N,N'*-methylenebisacrylamide (BIS) on vinyl-functionalized glass slides.[11] Thus formed "plum-pudding gels" were used for drug delivery, in which two different microgel populations were employed to release two distinct drugs.[12] However, the photopolymerization process of matrix-embedded microgels is quite time-consuming. Layer-by-layer (LbL) technique was then developed to improve the efficacy and robustness of fabrication process. Electrostatic interaction is the obvious option for LbL assembly of polyelectrolyte microgels.[13] With a polycation, polyallylamine hydrochloride, as a glue, anionic poly(*N*-isopropylacrylamide-*co*-acrylic acid) (pNIPAm-AAc) microgels were assembled on the amino-functionalized glass slides via a LbL approach.[14] Due to its pH-dependent swelling-deswelling behavior,[15] pNIPAm-AAc microgel films were used for controlled protein[16,17] and drug[18] release. Furthermore, by incorporating poly(ethylene glycol) (PEG)-diacrylate as cross-linker into pNIPAm microgels, the non-specific protein and/or cell binding problem of pNIPAm microgel LbL thin films was minimized.[19] In addition to electrostatic attraction, hydrogen bonding is another force to

form microgel thin films form polar but neutral polymeric microgels via LbL approach.[20] LbL technique allows the control of thickness of microgel assemblies by counting the total number of layers. Furthermore, other conventional approaches, such as solvent evaporation,[21] spin coating,[22] and electrochemical deposition,[23] could also be used for the preparation of microgel thin films. Some of microgel thin films are at least partially crystalline due to the self-assembly of microgels on the substrate, which demonstrates the iridescence.[21,24] On the other hand, microgels formed on the glass substrate also act as microlense arrays, which could be used as biosensors.[25,26] For more details, the readers are referred to some excellent reviews covering the nanostructure materials made of microgels via self-assembly.[27-29] All the above thin-film fabrication techniques are actually passive adsorption of microgel particles on the substrates.

Recently, our group has developed an active deposition approach for microgel thin film fabrication, which involves the centrifugation of microgel dispersions onto an amino-functionalized glass slides with or without EDC coupling. Furthermore, "clickable" microgel particles and "clickable" fluorophores equipped with azido or alkynyl groups were synthesized in our group. (Chapter 6) If the clickable fluorophores, which click with microgels with complementary functionalities, emit different fluorescent light, we could visualize the distribution of microgels with different clickable functionalities via epifluorescence microscopy. Therefore, it is possible to use fluorescent dyes to demonstrate the functionalities of microgels adsorbed on glass substrate. In this section, the multi-functional thin films prepared by centrifugation of clickable microgels will be presented, and the click reaction will be employed to demonstrate multi-functionality of the microgel thin films.

B.2 Experimental

B.2.1 Materials

The "clickable" fluorescent dyes, 5-azidofluorescine (AzF) and 5/6-propargyl tetramethylrhodamine carboxamide (PTMRC), were prepared in our laboratory, whereas the amino-containing fluorophore, lucifer yellow cadaverine (LYC, Invitrogen) was used as received. The "clickable" carboxyl-containing microgels, pNIPAm-AAc-AzMPA and pNIPAm-AAc-PA, were prepared in our laboratory as well. Sodium ascorbate (Sigma), 1-ethyl-3-(3-dimethylaminopropyl)-carbodiimide hydrochloride (EDC, Sigma), 5/6-carboxyltetramethylrhodamine (CTMRA, AnaSpec), N-hydroxysuccinimide (NHS, Aldrich), propargylamine (PAm, Acros), 3-aminopropyltrimethoxysilane(APTMS), pure ethanol(EtOH, EMD), and copper(II) sulfate pentahydrate ($CuSO_4 \bullet 5H_2O$, Aldrich) were used as received. MES pH 6.0 buffer was prepared for NHS-enhanced EDC coupling reaction.

B.2.2 Preparation of pNIPAm-AAc Microgels with/without Clickable Functionalities

The preparation of clickable pNIPAm-AAc-based microgels is referred to Chapter 6, Section 6.2.2, whereas the preparation of pNIPAm-AAc microgels is referred to Chapter 2.

B.2.3 Preparation of Clickable Fluorophores

The preparation of 5-azidofluorescein (AzF) is referred to Chapter 6, Section 6.2.1.2.2. The preparation of 5/6-propargyl tetramethylrhodamine carboxamide (PTMRC) from 5/6-carboxyl tetramethylrhodamine (CTMRA) and propargylamine (PAm) catalyzed by NHS and EDC is described as follows. Approximately 10.5 mg (19.8 mmol) of CTMRA and 13.6 mg (197.5 mmol) of PAm were dissolved in a 10 mL MES pH 6.0 buffer within an amber vial. Then 53.3 mg (278 μmol) of EDC and 5.6 mg (48.7 μmol) of NHS were added into reaction mixture. The reaction was allowed to proceed at room

temperature under magnetic stirring for 20 hours. After reaction, the reaction mixture was lyophilized at –49 ºC under 40 × 10^{-3} mbar for 48 hours. The freeze-dried crude product was then dissolved in DMF, which was purified via column chromatographic purification with acetone/MeOH (60/40, v/v) as mobile phase and silica gel (Natland, 100-200 mesh) as stationary phase. The purified product solution was allowed to dry in vacuum oven at room temperature under 30 torr for over 72 hours. The product is dark-red solid powder. All microgels and fluorophores used in Appendix B are shown in Chart B.1.

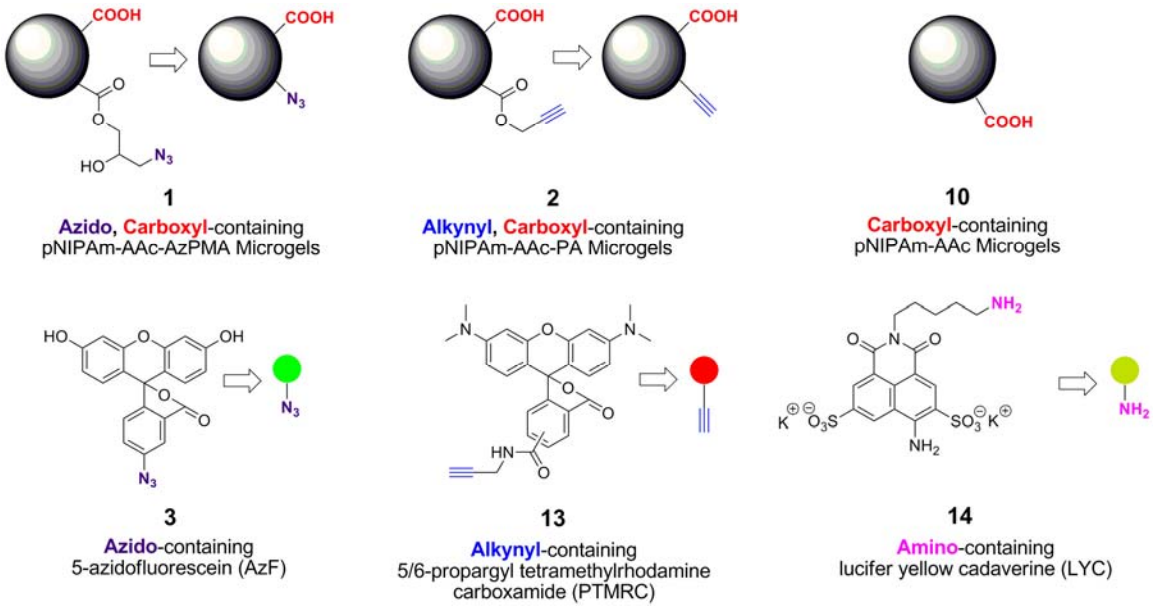

Chart B.1 The chemical structure of microgels forming multi-functional films and fluorophores reacting with functional microgels

B.2.4 Preparation of Amino-Functionalized Glass Substrates

The preparation of amino-functionalized glass substrate is referred to Chapter 6, Section 6.2.5. Note for active deposition of microgel particles via centrifugation, 22 × 22 mm glass slides are supposed to be used.

B.2.5 Preparation of Multi-Functional Films via Centrifugation

Add appropriate amount (shown later in Results and Discussion) of 0.1 wt% microgel dispersions in the 6-well cell culture plate (Greiner-BioOne CellStar®),

followed by add appropriate amount (shown later in Preliminary Results and Discussion) of pH 5.0 buffer. The 22 × 22 mm amino-functionalized glass slides were put in the microgel dispersions (0.01 wt% in pH 5.0 buffer) and then centrifuged under 2,250 × g for 15 min at 25 ºC. After shaking with EDC and NHS in water for overnight, the Multi-functional films are ready for click reaction and EDC coupling.

B.2.6 Reaction of Multi-Functional Films with Fluorescent Dyes

B.2.6.1 Reaction of Multi-Functional Films made of One Type of Microgels with Fluorophores with Complementary Functionalities

The reaction of multi-functional films made of pNIPAm-AAc-AzPMA, or pNIPAm-AAc-PA, or pNIPAm-AAc with fluorophores containing complementary functionalities are shown in Scheme B.1

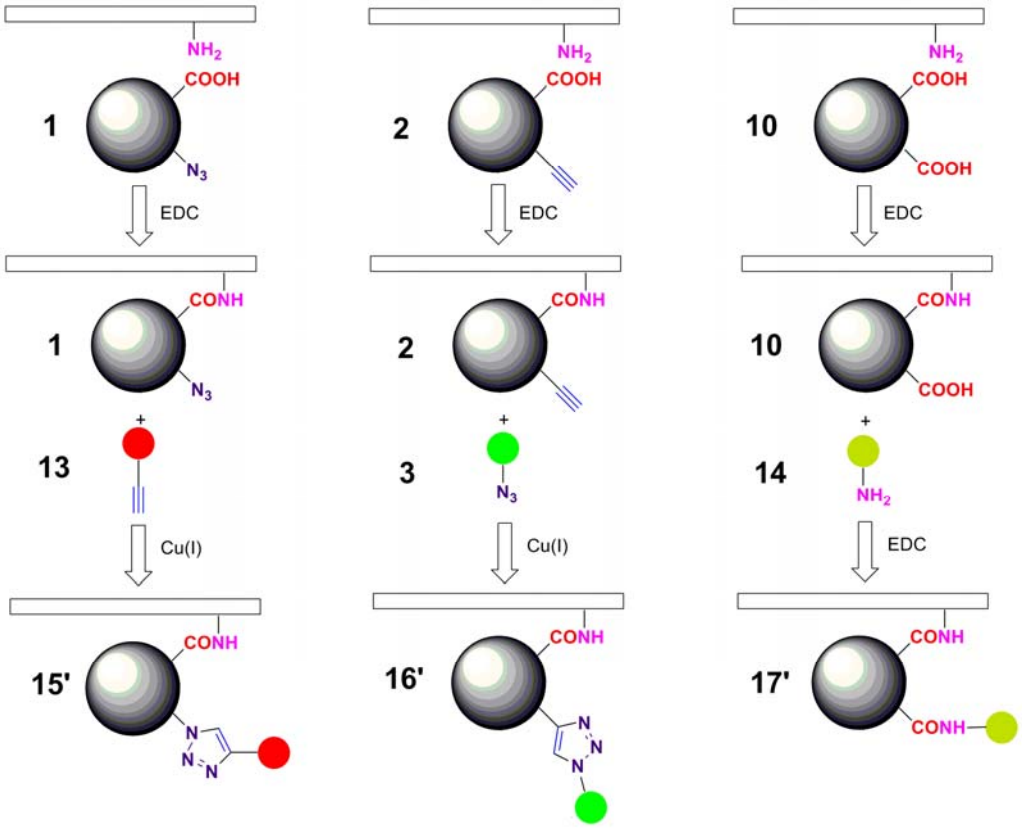

Scheme B.1 Reaction of multi-functional films composed of one type of microgels with fluorescent dyes with complementary functionalities. The left and central columns demonstrate Cu(I)-catalyzed reaction of pNIPAm-AAc-AzPMA **1** microgels and pNIPAm-AAc-PA **2** microgels with PTMRC **13** and AzF **3**, respectively, whereas the right column demonstrates EDC coupling between pNIPAm-AAc microgels **10** and LYC **14**. The resulting images are shown in Table 1, row 1, 2 and 3. Note the slabs tethered with amino groups on the top are amino-functionalized glass slides.

*B.2.6.1.1 Cu(I)-Catalyzed Click Reaction of pNIPAm-AAc-AzPMA **1** microgels with PTMRC **13**.*

Approximately 3.6 mL of pH 5.0 acetate buffer and 0.4 mL of 0.1 wt% of pNIPAm-AAc-AzPMA **1** microgel dispersions was delivered into one well of 6-well cell culture plate (Greiner-BioOne CellStar®) followed by swirling to homogenize the diluted 0.01 wt% microgel **1** dispersions. Then a clean amino-functionalized 22 × 22 mm glass slide was introduced into the bottom of that well. After centrifugation with a RCF of 2, 250 × g for 15 minutes at 25 ºC, the glass slide covered by microgels **1** was then transfer to a clean well containing 2.5 mL of fresh pH 5.0 acetate buffer in the culture plate. Then 1 mg (5.22 μmol) of EDC solid and 0.316 mg (2.75 μmol) of NHS solid was added into the buffer followed by shaking overnight. The EDC coupling between carboxyl groups on microgels **1** and amino groups on glass substrate built up the covalent bonds between microgels **1** and glass substrate. After EDC coupling, the glass slide covalently bound with microgels **1** was then transferred to another clean well containing 2.5 mL of fresh pH 5.0 buffer in the culture plate. Approximately 10 μL of 0.01 M PTMRC **13** aqueous solution and 0.457 mg (2.31 μmol) of sodium ascorbate powder was delivered to the buffer. After N_2 bubbling for 5 minutes, 50 μL of 0.1 mM $CuSO_4$ aqueous solution was delivered to the buffer to initiate click reaction of azido-containing pNIPAm-AAc-AzPMA **1** microgels (covalently binding on glass substrate) with alkynyl-containing PTMRC **13**. The reaction mixture became yellow-brownish approximately 10 minutes after starting reaction. The reaction was allowed to proceed for 18 hours. After click

reaction, the reaction mixture became clear again, and the glass substrate covered with microgels **15'** was rinsed thoroughly by deionized water before transferring to clean well containing deionized water. After dried by N_2 blow, the glass slide covered with microgels **15'** is ready for epifluorescence microscopy.

*B.2.6.1.2 Cu(I)-Catalyzed Click Reaction of pNIPAm-AAc-PA **2** Microgels with AzF **3**.*

Approximately 3.6 mL of pH 5.0 acetate buffer and 0.4 mL of 0.1 wt% of pNIPAm-AAc-PA **2** microgel dispersions was delivered into one well of 6-well cell culture plate (Greiner-BioOne CellStar®) followed by swirling to homogenize the diluted 0.01 wt% microgel **2** dispersions. Then a clean amino-functionalized 22 × 22 mm glass slide was introduced into the bottom of that well. After centrifugation with a RCF of 2, 250 × g for 15 minutes at 25 ºC, the glass slide covered by microgels **2** was then transfer to a clean well containing 2.5 mL of fresh pH 5.0 acetate buffer in the culture plate. Then 1 mg (5.22 μmol) of EDC solid and 0.316 mg (2.75 μmol) of NHS solid was added into the buffer followed by shaking overnight. The EDC coupling between carboxyl groups on microgels **2** and amino groups on glass substrate built up the covalent bonds between microgels **2** and glass slide. After EDC coupling, the glass slide covalently bound with microgels **2** was then transferred to another clean well containing 2.5 mL of fresh pH 5.0 buffer in the culture plate. Approximately 10 μL of 0.11 mM AzF **3** aqueous solution and 0.457 mg (2.31 μmol) of sodium ascorbate powder was delivered to the buffer. After N_2 bubbling for 5 minutes, 50 μL of 0.1 M $CuSO_4$ aqueous solution was delivered to the buffer to initiate click reaction of alkynyl-containing pNIPAm-AAc-PA **2** microgels (covalently binding on glass substrate) with azido-containing AzF **3**. The reaction mixture became brownish approximately 10 minutes after starting reaction. The reaction was allowed to proceed for 18 hours. After click reaction, the reaction mixture became slightly blue, and the glass substrate covered with microgels **16'** was rinsed thoroughly by deionized water before transferring to clean well containing deionized water. After

dried by N_2 blow, the glass slide covered with microgels **16'** is ready for fluorescence microscopy.

*B.2.6.1.3 EDC Coupling of pNIPAm-AAc **10** Microgels with LYC **14***

Approximately 3.6 mL of pH 5.0 acetate buffer and 0.4 mL of 0.1 wt% of pNIPAm-AAc **10** microgel dispersions was delivered into one well of 6-well cell culture plate (Greiner-BioOne CellStar®) followed by swirling to homogenize the diluted 0.01 wt% microgel **10** dispersions. Then a clean amino-functionalized 22 × 22 mm glass slide was introduced into the bottom of that well. After centrifugation with a RCF of 2, 250 × g for 15 minutes at 25 ºC, the glass slide covered by microgels **10** was then transfer to a clean well containing 2.5 mL of fresh pH 5.0 acetate buffer in the culture plate. Then 1 mg (5.22 μmol) of EDC solid and 0.316 mg (2.75 μmol) of NHS solid was added into the buffer followed by shaking overnight. The EDC coupling between carboxyl groups on microgels **10** and amino groups on glass substrate built up the covalent bonds between microgels **10** and glass slide. After EDC coupling, the glass slide covalently bound with microgels **1** was then transferred to another clean well containing 2.5 mL of fresh pH 5.0 buffer in the culture plate. Approximately 10 μL of 0.29 mM YLC **14** aqueous solution and 1 mg (5.22 μmol) of EDC solid and 0.316 mg (2.75 μmol) of NHS solid was delivered to the buffer to initiate EDC coupling of carboxyl-containing pNIPAm-AAc **10** microgels (covalently binding on glass substrate) with amino-containing YLC **14**. The reaction was allowed to proceed for 18 hours. After EDC coupling, the glass substrate covered with microgels **17'** was rinsed thoroughly by deionized water before transferring to clean well containing deionized water. After dried by N_2 blow, the glass slide covered with microgels **17'** is ready for fluorescence microscopy.

<u>B.2.6.2 Reaction of Multi-Functional Films made of Multiple Types of Microgels with Multiple Fluorophores</u>

The reaction of multi-functional films made of pNIPAm-AAc-AzPMA, and/or pNIPAm-AAc-PA, and/or pNIPAm-AAc with fluorophores containing complementary functionalities are shown in Scheme B.2. Due to the possible click reaction between clickable fluorophores, the ligations of clickable fluorophores on clickable microgels have to be performed sequentially.

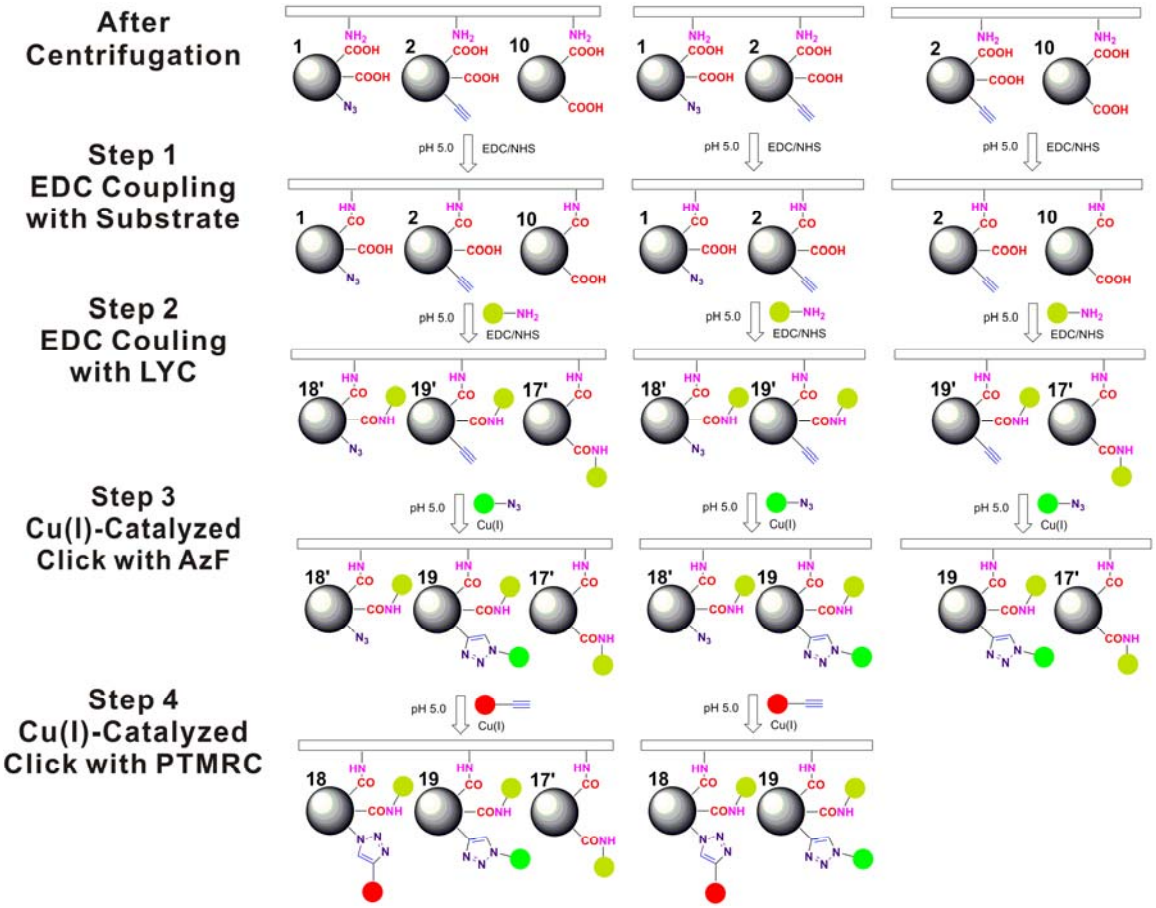

Scheme B.2 The multi-step sequential reactions of multi-functional films composed of two or three types of functional microgels with fluorescent dyes with complementary functionalities. The left, central and right columns represent glass slides covered by microgels **1** + **2** + **10**, **1** + **2**, and **2** + **10**, respectively. After centrifugation, EDC coupling between carboxyl groups on all microgels and amino groups on glass substrates are performed. Then steps 2, 3, and 4 demonstrate microgels undergo EDC coupling with amino-containing LYC, Cu(I)-catalyzed click with azido-containing AzF, and Cu(I)-catalyzed click with alkynyl-containing PTMRC sequentially.

*B.2.6.2.1 Sequential Reactions of Multi-Functional Films of pNIPAm-AAc-AzPMA **1**, pNIPAm-AAc-PA **2**, and pNIPAm-AAc **10** microgels with LYC **14**, AzF **3**, and PTMRC **13***

Approximately 2.8 mL of pH 5.0 acetate buffer, 0.4 mL of 0.1 wt% of pNIPAm-AAc-AzPMA **1** microgel, 0.4 mL of 0.1 wt% of pNIPAm-AAc-PA **2** microgel, and 0.4 mL of 0.1 wt% of pNIPAm-AAc **10** microgel dispersions was delivered into one well of 6-well cell culture plate (Greiner-BioOne CellStar®) followed by swirling to homogenize the diluted 0.01 wt% microgel dispersions. Then a clean amino-functionalized 22 × 22 mm glass slide was introduced into the bottom of that well. After centrifugation with a RCF of 2, 250 × g for 15 minutes at 25 ºC, the glass slide covered by microgels **1**, **2** and **10** was then transfer to a clean well containing 2.5 mL of fresh pH 5.0 acetate buffer in the culture plate. Then 1 mg (5.22 μmol) of EDC solid and 0.316 mg (2.75 μmol) of NHS solid was added into the buffer followed by shaking overnight. The EDC coupling between carboxyl groups on microgels **1**, **2** and **10** and amino groups on glass substrate built up the covalent bonds between microgels **1**, **2** and **10** and glass slide. After EDC coupling, the glass slide covalently bound with microgels **1**, **2** and **10** was then transferred to another clean well containing 2.5 mL of fresh pH 5.0 buffer in the culture plate. Approximately 10 μL of 0.29 mM YLC **14** aqueous solution and 1 mg (5.22 μmol) of EDC solid and 0.316 mg (2.75 μmol) of NHS solid was delivered to the buffer to initiate EDC coupling of carboxyl-containing microgels **1**, **2** and **10** (covalently binding on glass substrate) with amino-containing YLC **14**. The reaction was allowed to proceed for 18 hours. After EDC coupling, the glass substrate covered with microgels **18'**, **19'** and **17'** was rinsed thoroughly by deionized water before transferring to clean well containing 2.5 mL of fresh pH 5.0 buffer in the culture plate. Then approximately 10 μL of 0.11 mM AzF **3** aqueous solution and 0.457 mg (2.31 μmol) of sodium ascorbate powder was delivered to the buffer. After N_2 bubbling for 5 minutes, 50 μL of 0.1 M $CuSO_4$ aqueous solution was delivered to the buffer to initiate click reaction of alkynyl-containing microgels **19'** (covalently binding on glass substrate) with azido-containing AzF **3**. The reaction mixture became brownish approximately 10 minutes after starting reaction. The reaction was allowed to proceed for 18 hours. After the first click reaction,

the reaction mixture became slightly blue, and the glass substrate covered with microgels **18'**, **19** and **17'**was rinsed thoroughly by deionized water before transferring to clean well containing 2.5 mL of fresh pH 5.0 buffer in the culture plate. Approximately 10 μL of 0.01 M PTMRC **13** aqueous solution and 0.457 mg (2.31 μmol) of sodium ascorbate powder was delivered to the buffer. After N_2 bubbling for 5 minutes, 50 μL of 0.1 mM $CuSO_4$ aqueous solution was delivered to the buffer to initiate click reaction of azido-containing microgels **18'** (covalently binding on glass substrate) with alkynyl-containing PTMRC **13**. The reaction mixture became yellow-brownish approximately 10 minutes after starting reaction. The reaction was allowed to proceed for 18 hours. After the second click reaction, the reaction mixture became clear again, and the glass substrate covered with microgels **18, 19 and 17'** was rinsed thoroughly by deionized water before transferring to clean well containing deionized water. After dried by N_2 blow, the glass slide covalently bonding with microgels **18**, **19** and **17'** is ready for fluorescence microscopy.

*B.2.6.2.2 Sequential Reactions of Multi-Functional Films of pNIPAm-AAc-AzPMA **1** and pNIPAm-AAc-PA **2** with LYC **14**, PTMRC **13**, and AzF **3***

Approximately 3.2 mL of pH 5.0 acetate buffer, 0.4 mL of 0.1 wt% of pNIPAm-AAc-AzPMA **1** microgel and 0.4 mL of 0.1 wt% of pNIPAm-AAc-PA **2** microgel dispersions was delivered into one well of 6-well cell culture plate (Greiner-BioOne CellStar®) followed by swirling to homogenize the diluted 0.01 wt% microgel **1** and **2** dispersions. Then a clean amino-functionalized 22 × 22 mm glass slide was introduced into the bottom of that well. After centrifugation with a RCF of 2, 250 × g for 15 minutes at 25 ºC, the glass slide covered by microgels **1** and **2** was then transfer to a clean well containing 2.5 mL of fresh pH 5.0 acetate buffer in the culture plate. Then 1 mg (5.22 μmol) of EDC solid and 0.316 mg (2.75 μmol) of NHS solid was added into the buffer followed by shaking overnight. The EDC coupling between carboxy groups on microgels

1 and **2** and amino groups on glass substrate built up the covalent bonds between microgels **1** and **2** and glass slide. After EDC coupling, the glass slide covalently bound with microgels **1** and **2** was then transferred to another clean well containing 2.5 mL of fresh pH 5.0 buffer in the culture plate. Approximately 10 μL of 0.29 mM YLC **14** aqueous solution and 1 mg (5.22 μmol) of EDC solid and 0.316 mg (2.75 μmol) of NHS solid was delivered to the buffer to initiate EDC coupling of carboxyl-containing microgels **1** and **2** (covalently binding on glass substrate) with amino-containing YLC **14**. The reaction was allowed to proceed for 18 hours. After EDC coupling, the glass substrate covered with microgels **18'** and **19'** was rinsed thoroughly by deionized water before transferring to clean well containing 2.5 mL of fresh pH 5.0 buffer in the culture plate. Then approximately 10 μL of 0.11 mM AzF **3** aqueous solution and 0.457 mg (2.31 μmol) of sodium ascorbate powder was delivered to the buffer. After N_2 bubbling for 5 minutes, 50 μL of 0.1 M $CuSO_4$ aqueous solution was delivered to the buffer to initiate click reaction of alkynyl-containing microgels **19'** (covalently binding on glass substrate) with azido-containing AzF **3**. The reaction mixture became brownish approximately 10 minutes after starting reaction. The reaction was allowed to proceed for 18 hours. After the first click reaction, the reaction mixture became slightly blue, and the glass substrate covered with microgels **18'** and **19** was rinsed thoroughly by deionized water before transferring to clean well containing 2.5 mL of fresh pH 5.0 buffer in the culture plate. Approximately 10 μL of 0.01 M PTMRC **13** aqueous solution and 0.457 mg (2.31 μmol) of sodium ascorbate powder was delivered to the buffer. After N_2 bubbling for 5 minutes, 50 μL of 0.1 mM $CuSO_4$ aqueous solution was delivered to the buffer to initiate click reaction of azido-containing microgels **18'** (covalently binding on glass substrate) with alkynyl-containing PTMRC **13**. The reaction mixture became yellow-brownish approximately 10 minutes after starting reaction. The reaction was allowed to proceed for 18 hours. After the second click reaction, the reaction mixture became clear again, and the glass substrate covered with microgels **18** and **19** was rinsed thoroughly by deionized

water before transferring to clean well containing deionized water. After dried by N_2 blow, the glass slide covalently bonding with microgels **18** and **19** is ready for fluorescence microscopy.

*B.2.6.2.3 Sequential Reactions of Multi-Functional Films of pNIPAm-AAc-PA **2** and pNIPAm-AAc **10** with LYC **14** and AzF **3***

Approximately 3.2 mL of pH 5.0 acetate buffer, 0.4 mL of 0.1 wt% of pNIPAm-AAc-PA **2** microgel and 0.4 mL of 0.1 wt% of pNIPAm-AAc **10** microgel dispersions was delivered into one well of 6-well cell culture plate (Greiner-BioOne CellStar®) followed by swirling to homogenize the diluted 0.01 wt% microgel **2** and **10** dispersions. Then a clean amino-functionalized 22 × 22 mm glass slide was introduced into the bottom of that well. After centrifugation with a RCF of 2, 250 × g for 15 minutes at 25 ºC, the glass slide covered by microgels **2** and **10** was then transfer to a clean well containing 2.5 mL of fresh pH 5.0 acetate buffer in the culture plate. Then 1 mg (5.22 μmol) of EDC solid and 0.316 mg (2.75 μmol) of NHS solid was added into the buffer followed by shaking overnight. The EDC coupling between carboxyl groups on microgels **2** and **10** and amino groups on glass substrate built up the covalent bonds between microgels **2** and **10** and glass slide. After EDC coupling, the glass slide covalently bound with microgels **2** and **10** was then transferred to another clean well containing 2.5 mL of fresh pH 5.0 buffer in the culture plate. Approximately 10 μL of 0.29 mM YLC **14** aqueous solution and 1 mg (5.22 μmol) of EDC solid and 0.316 mg (2.75 μmol) of NHS solid was delivered to the buffer to initiate EDC coupling of carboxyl-containing microgels **2** and **10** (covalently binding on glass substrate) with amino-containing YLC **14**. The reaction was allowed to proceed for 18 hours. After EDC coupling, the glass substrate covered with microgels **19'** and **17'** was rinsed thoroughly by deionized water before transferring to clean well containing 2.5 mL of fresh pH 5.0 buffer in the culture plate. Then approximately 10 μL of 0.11 mM AzF **3** aqueous solution and 0.457 mg (2.31 μmol) of

sodium ascorbate powder was delivered to the buffer. After N_2 bubbling for 5 minutes, 50 μL of 0.1 M $CuSO_4$ aqueous solution was delivered to the buffer to initiate click reaction of alkynyl-containing microgels **19'** (covalently binding on glass substrate) with azido-containing AzF **3**. The reaction mixture became brownish approximately 10 minutes after starting reaction. The reaction was allowed to proceed for 18 hours. After the first click reaction, the reaction mixture became slightly blue, and the glass substrate covered with microgels **19** and **17'**was rinsed thoroughly by deionized water before transferring to clean well containing deionized water. After dried by N_2 blow, the glass slide covered with microgels **19** and **17'** is ready for fluorescence microscopy.

B.2.7 Observation of Multi-Functional Films via Fluorescence Microscopy

Both fluorescence and optical microscopies were conducted on an Olympus IX70 inverted microscope equipped with a high numerical aperture, oil immersion 100 × objective (NA = 1.30). In fluorescence mode, the excitation irradiation was a mercury lamp filtered by excitation band-pass filters of 450-490 nm (blue) or 510-560 nm (green). Images were captured using a color CCD camera (PixelFly, Cooke Corporation).

B.3 Preliminary Results and Discussion

Table B.1 demonstrates the results of reaction of microgels adsorbed on the glass slides with fluorescent dyes via EDC coupling and/or click reaction.

Table B.1 The chemo-ligation of multi-functional films composed of one type of functional microgels with fluorescent dyes with complementary functionalities. The top three rows of images demonstrate the chemo-ligation of multi-functional films made of one type of microgels, left: pNIPAm-AAc-AzPMA (containing azido + carboxyl groups), center: pNIPAm-AAc-PA (containing alkynyl + carboxyl groups), right: pNIPAm-AAc (containing carboxyl groups), in which row 1 and 2 represent fluorescence microscopy images of microgel films excited at wavelength of 450-490 nm and 510-560 nm, respectively, and row 3 transmission microscopy images. The bottom three rows of images demonstrate the chemo-ligation of multi-functional films made of multiple type of microgels, left: three microgels with azido + alkynyl + carboxyl groups, center: two microgels with azido + alkynyl + carboxyl groups, right: two microgels with alkynyl +

carboxyl groups, in which row 4 and 5 represent fluorescence microscopy images of microgel films excited at wavelength of 450-490 nm and 510-560 nm, respectively, and row 6 transmission microscopy images. Scale bar = 10 μm

Multi-Functional Surface of One Type of Microgels	pNIPAm -AAc-AzPMA (**COOH + N_3**) + **PTMRC (C≡CH)** Cu(I)-Click	pNIPAm-AAc-PA (**COOH + C≡CH**) + **AzF (N_3)** Cu(I)-Click	pNIPAm-AAc (**COOH**) + **LYC (NH_2)** EDC Coupling
1 λ_{EX} = 450-490 nm		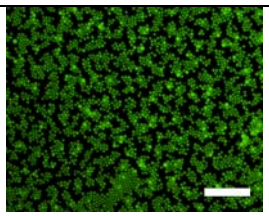	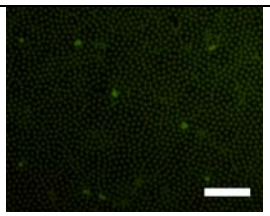
2 λ_{EX} = 510-560 nm	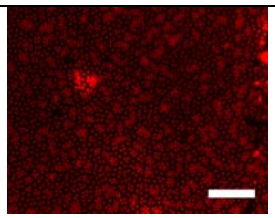		
3 Transmission	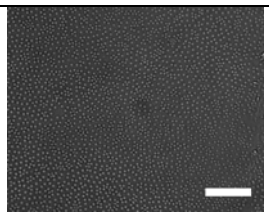	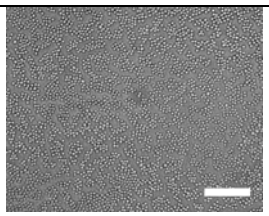	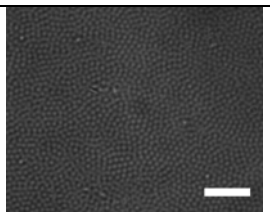
Multi-Functional Surface of Multiple Types of Microgels	pNIPAm-AAc-AzPMA (**COOH + N_3**) pNIPAm-AAc-PA (**COOH + C≡CH**) pNIPAm-AAc (**COOH**)	pNIPAm-AAc-AzPMA (**COOH + N_3**) pNIPAm-AAc-PA (**COOH + C≡CH**)	pNIPAm-AAc-PA (**COOH + C≡CH**) pNIPAm-AAc (**COOH**)
Reactions	1. **LYC (NH_2)** EDC Coupling 2. **AzF (N_3)**	1. **LYC (NH_2)** EDC Coupling 2 **AzF (N_3)**	1. **LYC (NH_2)** EDC Coupling 2. **AzF (N_3)**

	Cu(I)-Click 3. **PTMRC (C≡CH)** Cu(I)-Click	Cu(I)-Click 3. **PTMRC(C≡CH)** Cu(I)-Click	Cu(I)-Click
4 λ_{EX} = 450-490 nm	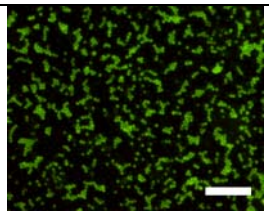	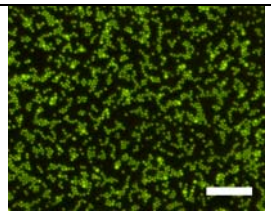	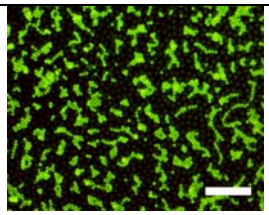
5 λ_{EX} = 510-560 nm	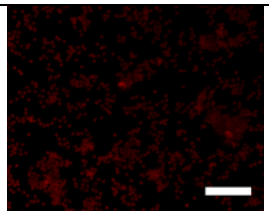	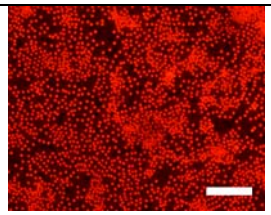	
6 Transmission	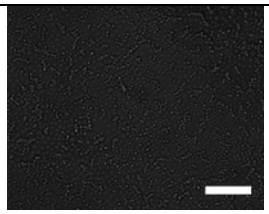	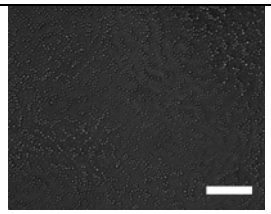	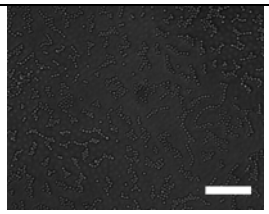

From the microscopic images presented above, it's quite clear that the particles with different functionalities can react with fluorophores containing complementary functionalities in an orthogonal manner. To illustrate this, let's take the bottom central column for closer examination in Figure B.1: both alkynyl-containing pNIPAm-AAc-PA and azido-containing pNIPAm-AAc-AzPMA microgel particles were actively deposited on the amino-functionalized glass surface via centrifugation, followed by EDC coupling with lucifer yellow cadaverine (LYC) and click reaction with 5-azidofluorescein (AzF) and 5,6-propargyl tetramethylrhodamine carboxamide (PTMRC) sequentially. Deionized water rinse was used before, between, and after two sequential click reactions. The yellow-greenish microgels shown in the top panel of Figure B.1 represent fluorescence from AzF ligated on pNIPAm-AAc-PA microgels, whereas the red microgels shown in the bottom panel represent fluorescence from PTMRC ligated on pNIPAm-AAc-AzPMA

microgels. On the other hand, the pale yellow microgels shown in the top panel of Figure B.1 represent fluorescence from LYC attached on pNIPAm-AAc-AzPMA microgels, whereas the pale red microgels shown in the bottom panel represent fluorescence from LYC attached on pNIPAm-AAc-PA microgels.

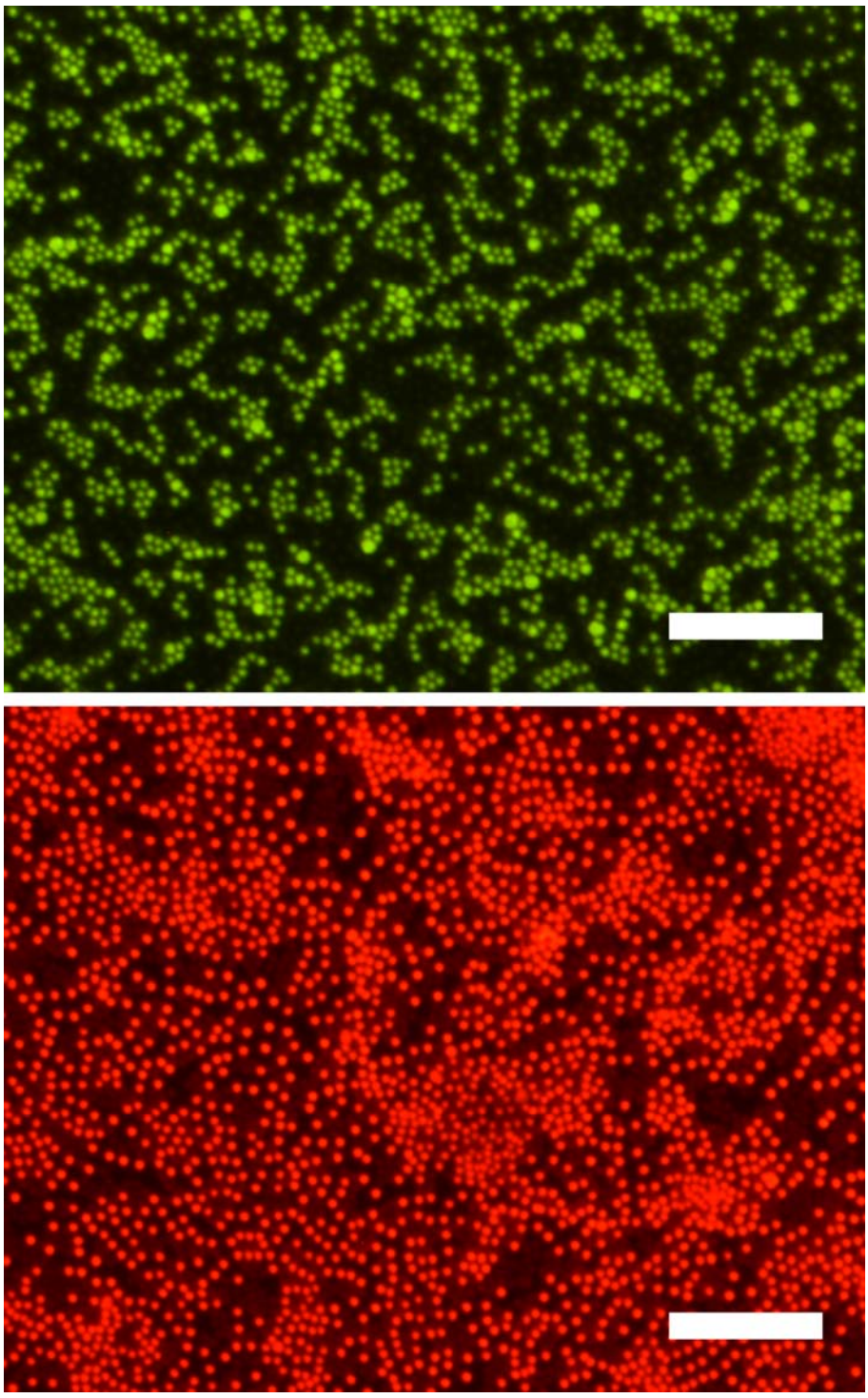

Figure B.1 Fluorescence microscopy images of multi-functional film made of clickable pNIPAm-AAc-AzPMA **1** and pNIPAm-AAc-PA **2** microgels, after clicking with PTMRC **13** and AzF **3**, respectively. Note before click reaction, the film was EDC coupled with YLC **14**. Scale bar = 10 μm.

By overlapping the above two fluorescence images together, we obtain Figure B.2.

Figure B.2 shows that yellow-greenish particles (alkynyl-containing pNIPAm-AAc-PA **2** microgels) and red particles (azido-containing pNIPAm-AAc-AzPMA **1** microgels). The multi-functional films are pseudo-monolayer of microgels adsorbed on amino-functionalized glass substrate. Note that yellow particles are also observable, which might be due to the addition of fluorescence from both particles at the same location.

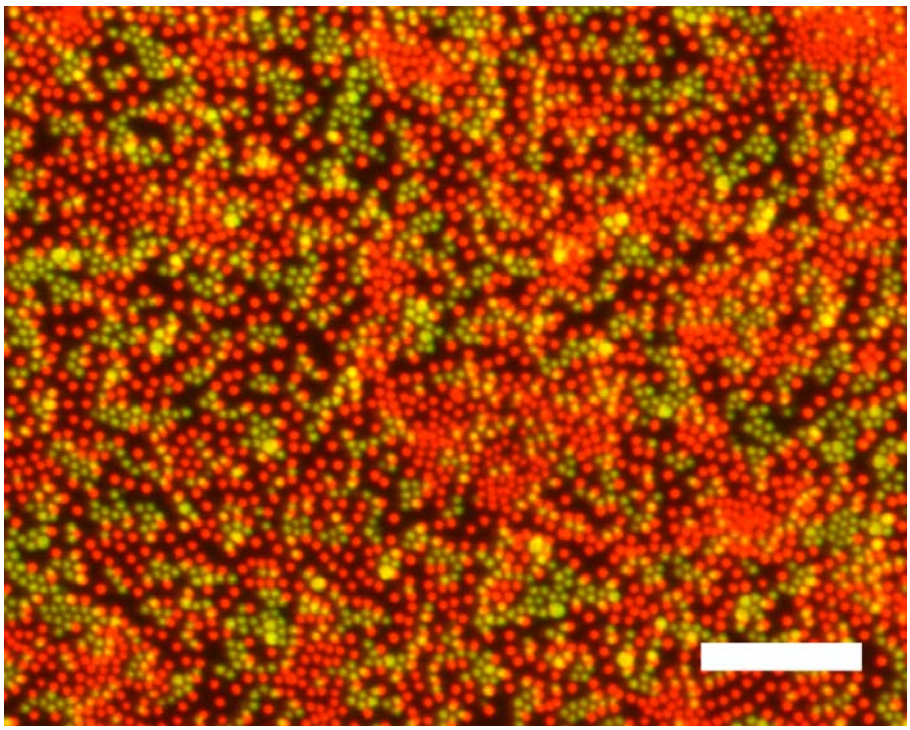

Figure B.2 Overlapped fluorescence microscopy images of multi-functional film made of clickable pNIPAm-AAc-AzPMA **1** (red) and pNIPAm-AAc-PA **2** (yellow-greenish) microgels, after clicking with PTMRC **13** and AzF **3**, respectively. Note before click reaction, the film was EDC coupled with YLC **14**. Scale bar = 10 μm.

B.4 Conclusions

This section presents a preliminary study of fabrication and characterization of multi-functional films on amino-functionalized glass substrates via active deposition (centrifugation). It is noticed that the Cu(I)-catalyzed click reaction between alkynyl and azido functionalities and EDC coupling between carboxyl and amino functionalities are orthogonal to each other except the cross-reaction situation identified in Chapter 6.

Furthermore, the multi-functional microgel films can also be used as a sensor to determine if clickable biomolecules or cells with complementary functionalities in the solution flowing over the films.

APPENDIX C ULTRATHIN FILMS COMPOSED OF CROSS-LINKER-FREE SQUISHY MICROGEL NANODISKS

C.1 Introduction

Ultrathin films are films with a thickness of nanometer scale, which can be metal,[30] inorganic,[31] organic,[32] polymeric,[33] or hybrid[34,35] materials. Ultrathin films of organic and polymeric materials are particularly interesting because they allow the fabrication of nanostrcutured molecular assemblies with tailored architecture and functionalities. Langmuir-Blodgett technique,[36] organic molecular beam deposition/epitaxy,[37] self-assembled monolayer (SAM),[32] and Layer-by-Layer (LbL) assembly[33] as fabrication approaches of ultrathin films were extensively reviewed. Our group first prepared thin films of stimuli-responsive pNIPAm-based microgels via seed-polymerization in matrix[11] and Layer-by-Layer[14] (LbL) approaches. It's well known that ultrathin microgel films are excellent surface drug release vehicles.[16-18,29] In contrast to passive adsorption, active adsorption such as centrifugation[38] and spin coating[39] has been developed to manipulate the thickness and structure of ultrathin films. Recently we have been noticing that an ultrathin film with a thickness of approximately 8 nm can be made of extremely soft (squishy) microgels via active deposition of them on glass substrates. Furthermore, we noticed that the diameter of adsorbed squishy microgels on the glass substrate is almost the same as their diameter in bulk dispersions, and the microgels form "nanodisks" on glass substrate tiled to each other. The squishy microgels are pNIPAm-based particles prepared via APS-initiated surfactant-free radical precipitation polymerization without adding external cross-linker such as BIS.[40-42] The synthesis of cross-linker-free pNIPAm-AAc microgel particles is shown in Scheme C.1.

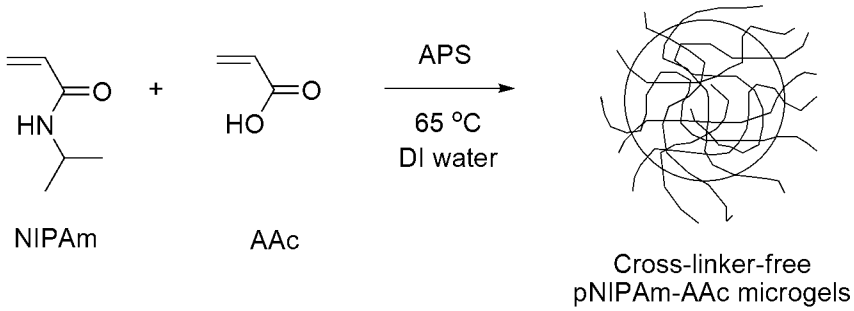

Scheme C.1 Synthesis of cross-linker-free pNIPAm-AAc microgel at 65 ºC

C.2 Experimental

C.2.1 Materials

N-Isopropylacrylamide (NIPAm, TCI) was re-crystallized from hexanes (J.T. Baker) and dried under vacuum prior to use. Acrylic acid (AAc, Fluka), ammonium persulfate (APS, Sigma), 1-ethyl-3-(3-dimethylaminopropyl)-carbodiimide hydrochloride (EDC, Sigma), and N-hydroxysuccinimide (NHS, Aldrich) were used as received. Amino-functionalized glass slides (22 × 22 mm) were prepared in our laboratory. (Refer to Chapter 6, Section 6.2.5 for details). The pH 3.0 formate buffer, pH 4.0 formate buffer, and pH 5.0 acetate buffer were prepared in our laboratory for active deposition. All water used throughout this investigation was distilled and deionized to a resistivity of at least 18 MΩ·cm (Barnstead E-Pure system) and then filtered through an in-line 0.2-μm filter to remove particulate matter.

C.2.2 Synthesis, Purification and Lyophilization of Cross-Linker-Free Microgels

Cross-linker-free microgels were prepared by ammonium persulfate (APS)-initiated surfactant-free radical precipitation copolymerization of monomer *N*-isopropylacrylamide (NIPAm) and comonomer acrylic acid (AAc). The reactant mixture composed of 84 mol% NIPAm (1.8 g) and 15 mol% AAc (0.2 g) was made by dissolving the reagents in 100 mL deionized water via ultrasonication. The reactant mixture was

then filtered through an in-line 0.8 μm syringe filter into a 250 mL three-neck round bottom flask. During 60 minutes of N_2 purge, the mixture was heated from 22 to 65 °C and maintained at the same temperature throughout the synthesis. After the temperature of reactant mixture was stabilized and O_2 in reaction vessel was replaced by N_2, 5 mL of 0.078 M APS was added to initiate the copolymerization. The copolymerization was allowed to proceed for 18 hours at 65 °C under N_2. The resultant colloidal dispersion was filtered through glass fiber to remove a small portion of coagulum and then transferred to dialysis tubes (Spectra, MWCO = 10 kDa) and sealed for dialysis against deionized water. The dialysis was allowed to proceed for 3 weeks with water replenishing every day. After purification, the microgel dispersion was lyophilized at −45 °C under 40×10^{-3} mbar for 72 hours. The freeze-dried product was a hygroscopic white powder. Note that centrifugation-redispersion of microgel particles to remove water-soluble impurities such as initiator residue and oligomers could also be performed, however, the redispersion of microgel pellets in deionized water should be done in 4 ºC to facilitate the process. If the cross-linker-free microgel pellets were redispersed at room temperature, the pellets will not completely redispersed even after months of shaking.

C.2.3 Preparation of Cross-Linker-Free Microgel Dispersions

The microgel dispersions were prepared by first dispersing approximately 10 mg cross-linker-free pNIPAm-AAc powder in 10 g of distilled, de-ionized water and shaking for 48 hours to obtain an 0.1 wt % dispersion.

C.2.4 Preparation of Ultrathin Films via Centrifugal Deposition of Dilute Cross-Linker-Free Microgel Dispersions

Add 0.6 mL 0.1 wt% cross-linker-free microgel dispersions in the one well of 6-well cell culture plate (Greiner-BioOne CellStar®), followed by add 5.4 mL pH 3.0 buffer. The 22 × 22 mm amino-functionalized glass slide were put in the microgel

dispersions (0.01 wt % in pH 3.0 buffer) and then centrifuged under 2, 250 × g for 15 min at 25 ºC. After centrifugation, 1 mg (5.22 μmol) of EDC solid and 0.316 mg (2.75 μmol) of NHS solid were added to that well followed by shaking for overnight to covalently bond pNIPAm-AAc fluorescent particles on the glass slide. Note the procedures are the same for active deposition of microgels in pH 4.0 and 5.0 buffer.

C.2.5 Observation of Microgel Ultrathin Films via Atomic Force Microscopy

AFM data were taken both in air and in aqueous buffer in Non-Contact mode on an Asylum Research MFP3D. Imaging and analysis was performed with the Asylum Research MFP3D software running in IgorPro (WaveMetrics, Inc., Lake Oswego, OR) that was provided with the instrument. A NanoWorld aluminum-coated carbon nitride cantilever (The force constant = 42 N/m and resonance frequency = 320 kHz in air) was used for imaging in air, whereas an Asylum Research iDrive cantilever (The force constant = 0.09 N/m and resonant frequency = 32 kHz in air) was used in aqueous buffer. The imaging area is 20 × 20 or 10 × 10 μm^2 with a resolution of 512 × 512 $pixels^2$ for each image.

C.3 Preliminary Results and Discussion

The AFM images of dried cross-linker-free microgel films actively deposited on amino-functionalized glass substrates at different pH values are demonstrate in Figure C.1. It's noticed that with the increase of pH values, the diameters of "nanodisks" increase significantly, and the defects between "nanodisks" increase as well. Furthermore, for cross-linker-free microgel films at pH 3.0 and 4.0 buffer, the central area of each "nanodisk" formed by microgel particle is darker than the edge of "nanodisk", indicating that the "nanodisk" is blood-cell like with a collapsed center surrounded by edge networks. The "nanodisk" film is clearly a monolayer of pNIPAm-AAc microgels on glass substrate. Note that some bright spots in the AFM images are salt crystals due to the

evaporation of buffer solution. Because cross-linker-free pNIPAm-AAc microgel ultrathin films give a pseudo-defect-free monolayer at pH 3.0 buffer after active deposition of squishy particles on glass substrate, we then compare the morphology of the ultrathin films fabricated at pH 3.0 in the air and aqueous buffer.

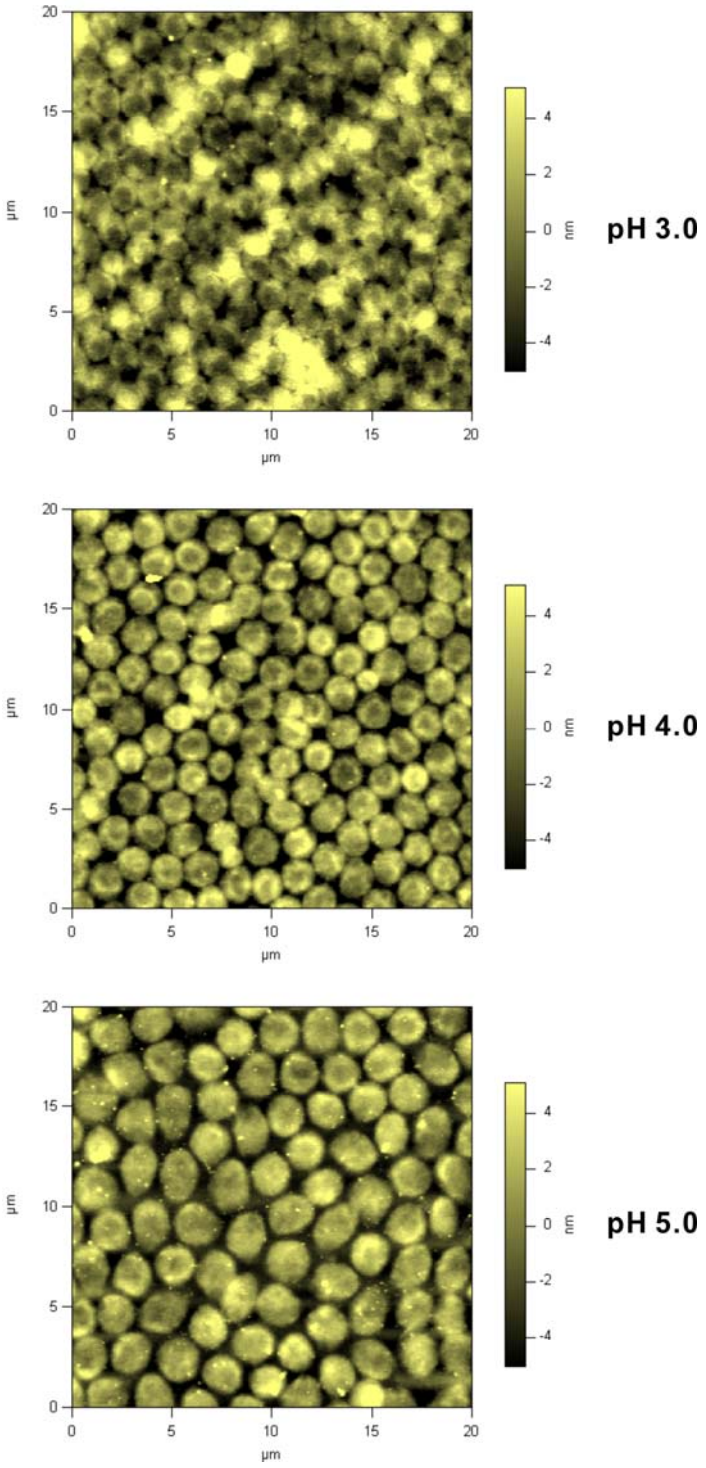

Figure C.1 The AFM images of cross-linker-free pNIPAm-AAc microgel ultrathin films fabricated by centrifugation of 0.01 wt% microgel dispersions at pH 3.0, 4.0 and 5.0 buffers.

Figure C.2 demonstrates the AFM images of wet and dry ultrathin films fabricated by centrifugation of 0.01 wt% of cross-linker-free pNIPAm-AAc microgel dispersions in pH 3.0 buffer. The height of nanodiscks in wet condition is approximately 20 nm, which is higher than that of nanodisks in dry condition, ~8 nm.

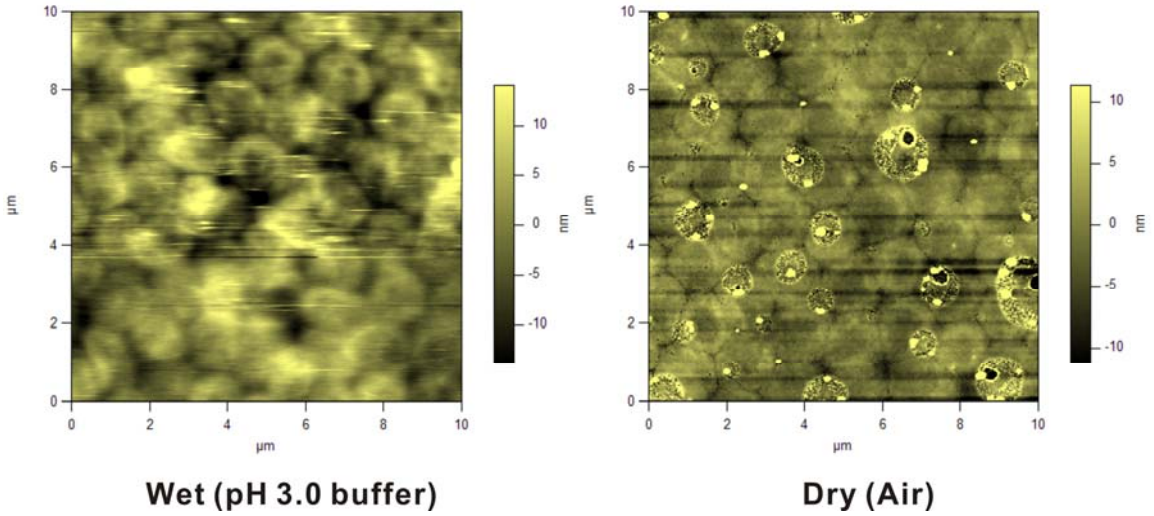

Figure C.2 The AFM images of cross-linker-free pNIPAm-AAc nanodisks on glass substrate in aqueous buffer (left panel) and air (right panel). Note that the dried sample has a lot of salt spots.

C4. Conclusions

Cross-linker-free pNIPAm-AAc microgel dispersions could form ultrathin films via active deposition in pH buffers. The ultrathin film is composed of pNIPAm-AAc "nanodisks". The ultrathin film might have potential applications as surface modifier, surface drug release vehicles, and biosensor. The in-depth investigation is currently ongoing in our laboratory.

REFERENCES

(1) Saatweber, D.; Vogt-Birnbrich, B. Microgels in organic coatings, *Prog. Org. Coat.* **1996**, *28*, 33-41.

(2) Nakayama, Y. Polymer blend systems for water-borne paints, *Prog. Org. Coat.* **1998**, *33*, 108-116.

(3) Ishikura, S.; Ishii, K.; Midzuguchi, R. Flow and film properties of coatings containing microgels, *Prog. Org. Coat.* **1988**, *15*, 373-387.

(4) Yagi, T.; Saito, K.; Ishikura, S. Coatings containing microgels. 2. Moisture vapor permeable coatings, *Prog. Org. Coat.* **1992**, *21*, 25-35.

(5) Padget, J. C. Polymers for water-based coatings. A systematic overview, *J. Coat. Technol.* **1994**, *66*, 89-105.

(6) Ishii, K. Synthesis of microgels and their application to coatings, *Colloid Surf. A* **1999**, *153*, 591-595.

(7) Dusek, K.; Duskov-Smrckova, M. Network structure formation during crosslinking of organic coating systems, *Prog. Polym. Sci.* **2000**, *25*, 1215-1260.

(8) Shen, J. C.; Zhang, X.; Zhang, R. F. A new kind of amphiphilic polymer — reversed duckweed type Langmuir-Blodgett film, *Thin Solid Films* **1992**, *210*, 625-627.

(9) Zhang, R. F.; Zhang, X.; Li, H. B.; Zhao, B.; Shen, J. C. A highly ordered polymeric Langmuir-Blodgett film, *Polym. Bull.* **1996**, *36*, 227-232.

(10) Zhao, B.; Li, H. B.; Zhang, X.; Shen, J. C.; Ozaki, Y. Infrared study on molecular orientation and phase transition in Langmuir-Blodgett films of an amphiphilic microgel copolymer with the branching of octadecyl groups, *J. Phys. Chem. B* **1998**, *102*, 6515-6520.

(11) Nayak, S.; Debord, S. B.; Lyon, L. A. Investigations into the deswelling dynamics and thermodynamics of thermoresponsive microgel composite films, *Langmuir* **2003**, *19*, 7374-7379.

(12) Lynch, I.; de Gregorio, P.; Dawson, K. A. Simultaneous release of hydrophobic and cationic solutes from thin-film "plum-pudding" gels: A multifunctional platform for surface drug delivery?, *J. Phys. Chem. B* **2005**, *109*, 6257-6261.

(13) Glinel, K.; Dejugnat, C.; Prevot, M.; Scholer, B.; Schonhoff, M.; Klitzing, R. V. Responsive polyelectrolyte multilayers, *Colloid Surf. A* **2007**, *303*, 3-13.

(14) Serpe, M. J.; Jones, C. D.; Lyon, L. A. Layer-by-layer deposition of thermoresponsive microgel thin films, *Langmuir* **2003**, *19*, 8759-8764.

(15) Serpe, M. J.; Lyon, L. A. Optical and acoustic studies of pH-dependent swelling in microgel thin films, *Chem. Mat.* **2004**, *16*, 4373-4380.

(16) Nolan, C. M.; Serpe, M. J.; Lyon, L. A. Thermally modulated insulin release from microgel thin films, *Biomacromolecules* **2004**, *5*, 1940-1946.

(17) Nolan, C. M.; Serpe, M. J.; Lyon, L. A. Pulsatile release of insulin from Layer-by-Layer assembled microgel thin films, *Macromol. Symp.* **2005**, *227*, 285-294.

(18) Serpe, M. J.; Yarmey, K. A.; Nolan, C. M.; Lyon, L. A. Doxorubicin uptake and release from microgel thin films, *Biomacromolecules* **2005**, *6*, 408-413.

(19) Nolan, C. M.; Reyes, C. D.; Debord, J. D.; Garcia, A. J.; Lyon, L. A. Phase transition behavior, protein adsorption, and cell adhesion resistance of poly(ethylene glycol) cross-linked microgel particles, *Biomacromolecules* **2005**, *6*, 2032-2039.

(20) Kharlampieva, E.; Kozlovskaya, V.; Tyutina, J.; Sukhishvili, S. A. Hydrogen-bonded multilayers of thermoresponsive polymers, *Macromolecules* **2005**, *38*, 10523-10531.

(21) Tsuji, S.; Kawaguchi, H. Colored thin films prepared from hydrogel microspheres, *Langmuir* **2005**, *21*, 8439-8442.

(22) Schmidt, S.; Motschmann, H.; Hellweg, T.; von Klitzing, R. Thermoresponsive surfaces by spin-coating of PNIPAM-co-PAA microgels: A combined AFM and ellipsometry study, *Polymer* **2008**, *49*, 749-756.

(23) Bunsow, J.; Johannsmann, D. Electrochemically produced responsive hydrogel films: Influence of added salt on thickness and morphology, *J. Colloid Interface Sci.* **2008**, *326*, 61-65.

(24) Zhou, J.; Wang, G. N.; Marquez, M.; Hu, Z. B. The formation of crystalline hydrogel films by self-crosslinking microgels, *Soft Matter* **2009**, *5*, 820-826.

(25) Kim, J.; Nayak, S.; Lyon, L. A. Bioresponsive hydrogel microlenses, *J. Am. Chem. Soc.* **2005**, *127*, 9588-9592.

(26) Lapeyre, V.; Ancla, C.; Catargi, B.; Ravaine, V. Glucose-responsive microgels with a core-shell structure, *J. Colloid Interface Sci.* **2008**, *327*, 316-323.

(27) Wong, J. E.; Richtering, W. Layer-by-layer assembly on stimuli-responsive microgels, *Curr. Opin. Colloid Interface Sci.* **2008**, *13*, 403-412.

(28) Lyon, L. A.; Meng, Z. Y.; Singh, N.; Sorrell, C. D.; John, A. S. Thermoresponsive microgel-based materials, *Chem. Soc. Rev.* **2009**, *38*, 865-874.

(29) Sukhishvili, S. A. Responsive polymer films and capsules via layer-by-layer assembly, *Curr. Opin. Colloid Interface Sci.* **2005**, *10*, 37-44.

(30) Campbell, C. T. Ultrathin metal films and particles on oxide surfaces: Structural, electronic and chemisorptive properties, *Surf. Sci. Rep.* **1997**, *27*, 1-111.

(31) Chambers, S. A. Epitaxial growth and properties of thin film oxides, *Surf. Sci. Rep.* **2000**, *39*, 105-180.

(32) Ulman, A. Formation and structure of self-assembled monolayers, *Chem. Rev.* **1996**, *96*, 1533-1554.

(33) Decher, G. Fuzzy nanoassemblies: Toward layered polymeric multicomposites, *Science* **1997**, *277*, 1232-1237.

(34) Coronado, E.; Mingotaud, C. Hybrid organic/inorganic Langmuir-Blodgett films. A supramolecular approach to ultrathin magnetic films, *Adv. Mater.* **1999**, *11*, 869-872.

(35) Pyun, J.; Jia, S. J.; Kowalewski, T.; Patterson, G. D.; Matyjaszewski, K. Synthesis and characterization of organic/inorganic hybrid nanoparticles: Kinetics of surface-initiated atom transfer radical polymerization and morphology of hybrid nanoparticle ultrathin films, *Macromolecules* **2003**, *36*, 5094-5104.

(36) Tredgold, R. H. *Order in Thin Organic Films*; Cambridge University Press: Cambridge, 1994.

(37) Forrest, S. R. Ultrathin Organic Films Grown by Organic Molecular Beam Deposition and Related Techniques, *Chem. Rev.* **1997**, *97*, 1793-1896.

(38) Volegova, I. A.; Cherevatenko, A. E.; Godovsky, Y. K. Visualization of temperature-induced changes in two-layer morphology of ultrathin films of a poly(ethylene oxide)-block-poly(arylene sulfone oxide), *Polym. Sci. Ser. A* **2005**, *47*, 984-994.

(39) Ogawa, M. Formation of novel oriented transparent films of layered silica-surfactant nanocomposites, *J. Am. Chem. Soc.* **1994**, *116*, 7941-7942.

(40) Gao, J.; Frisken, B. J. Cross-linker-free N-isopropylacrylamide gel nanospheres, *Langmuir* **2003**, *19*, 5212-5216.

(41) Gao, J.; Frisken, B. J. Influence of reaction conditions on the synthesis of self-cross-linked N-isopropylacrylamide microgels, *Langmuir* **2003**, *19*, 5217-5222.

(42) Gao, J.; Frisken, B. J. Influence of secondary components on the synthesis of self-cross-linked N-isopropylacrylamide microgels, *Langmuir* **2005**, *21*, 545-551.

VITA

ZHIYONG MENG

MENG was born in Luzhou, Sichuan Province, CHINA in September 1974. He attended ex-Changjiang Middle School (now Luzhou Experimental School) before being admitted in ex-Chengdu University of Science and Technology (now Sichuan University) by waiving the National Higher Education Matriculation Examination of CHINA in 1992. He received a B.Eng. in Polymer Materials Science and Engineering from Sichuan University, Chengdu, Sichuan Province, CHINA in 1996 and a M.Sc. in Polymer Chemistry and Physics from Peking University, Beijing, CHINA in 1999 before joining the University of Toronto, where he obtained his M.A.Sc. in Polymer Materials Engineering. Before coming to Georgia Tech to pursue a doctorate in Polymer Chemistry, he enjoyed a short industrial career in CIBA Vision Corporation (A Novartis Company) for the development of soft contact lens. He is currently working on poly(*N*-isopropylacrylamide) (pNIPAm)-based microgel systems under the supervision of Professor L. Andrew Lyon and will get his Ph.D. in July 2009. When he is not working on his research, he enjoys jogging, surfing internet, calligraphy, and GO chess.